Structural identification and quantification of β-amyloid polypeptide-ligand interactions using affinity-mass spectrometric methods

Dissertation
zur Erlangung des akademischen Grades
eines Doktors der Naturwissenschaften
an der Universität Konstanz

vorgelegt von

Gabriela Ioana Paraschiv

an der

Universität Konstanz

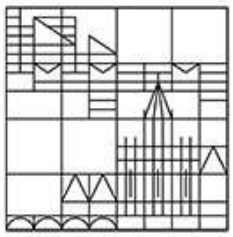

Fachbereich Chemie

Tag der mündlichen Prüfung:

01. August 2012

1. Referent: Prof. Dr. Dr. h. c. Przybylski, Michael

2. Referent: Prof. Dr. Welte, Wolfram

"*Jede neue Wahrheit durchläuft drei Stufen: Zunächst wird sie lächerlich gemacht, dann heftig bekämpft und schließlich gilt sie als selbstverständlich.“*
„All truth passes through three stages: First, it is ridiculous, Second is violently opposed, Third, it is accepted as being self-evident.“

Arthur Schopenhauer (1788-1860)

I dedicate this work to my wonderful parents Elena and Aurel Paraschiv, and especially to my loving husband Sergiu and my daughters Sofie Amalia and Rebecca Ioana.

The present work has been performed in the time from March 2005 to November 2008 and from January 2010 to June 2011 in the Laboratory of Analytical Chemistry and Biopolymer Structure Analysis, Department of Chemistry of the University of Konstanz, under the supervision of Prof. Dr. Dr. h. c. Michael Przybylski.

Special thanks to:

Prof. Dr. Dr. h. c. Michael Przybylski for giving me the opportunity to work in his group, for the very interesting research topic and discussions concerning my work and for his entire support;

Prof. Dr. Wolfram Welte, for writing the second evaluation of the dissertation;

Prof. Dr. Serge Muyldermans and Dr. Cecile Vincke for providing the single chain llama anti-Aβ antibodies employed in epitope identification;

Dr. Paulina Czaplewska and Dr. Aneta Szymanska for providing human Cystatin C protein employed in this work and for interesting scientific discussions;

Gleichstellungsrat, University of Konstanz for the financial support;

All former and present members of the group for the nice and inspiring atmosphere, for scientific discussions and interesting advices during my work;

Last but not least I wish to thank and to express my deep gratitude to my family and all my friends, for supporting and encouraging me during this time and to my loving, understanding husband Sergiu for his encouragement, support and his trust in me.

This dissertation has been published in part, and presented at the following conferences:

Publications:

1 Juszczyk, P.*, **Paraschiv, G**.*, Szymanska, A., Kolodziejczyk, A, Rodziewicz-Motowidlo, S., Grzonka, Z., Przybylski, M. (2009) Binding epitopes and interaction structure of the neuroprotective protease inhibitor cystatin C with β-amyloid revealed by proteolytic excision-mass spectrometry and molecular docking simulation. *J. Med. Chem.,* 8(11), 1263-1269.
* Both with equal collaboration

2 **Paraschiv, G.**, Vincke, C., Czaplewska, P., Manea, M., Muyldermans, S. Przybylski, M. (2012) Fibril-inhibiting epitope and binding affinity of single chain llama anti-β-amyloid antibodies revealed by proteolytic excision affinity- mass spectrometry – *J. Mol. Recognition* in press.

3 Stefanescu, R., Iacob, R.E., Damoc, E.N., Marquardt, A., Amstalden, E., Manea, M., Perdivara, I., Maftei, M., **Paraschiv, G.**, and Przybylski, M. (2007) Mass spectrometric approaches for elucidation of antigen–antibody recognition structures in molecular immunology. *Eur. J. Mass Spectrom.,* 13(1), 69-75.

4 Pimenova, T., Meier, L., Roschitzki, B. , **Paraschiv, G.**, Przybylski, M., Zenobi, R. (2009) Polystyrene beads as an alternative support material for epitope identification of a prion-antibody interaction using proteolytic excision–mass spectrometry. *Anal. Bioanal. Chem,* 395, 1395–1401.

5 Śladewska, A., Szymańska, A., Kordalska, M., Lewandowska, A.S., **Paraschiv, G.**, Przybylski, M., Czaplewska, P. (2011) Identification of the epitope for anti-cystatin C antibody. *J. Mol. Recognition*, 24(4), 687-699.

Conference presentations:

1 **Paraschiv, G.,** Czaplewska, P., Przybylski, M. **(2011**) Affinity binding and interaction structure of the neuroprotective protease inhibitor cystatin C with Alzheimer's β-amyloid peptide. *AD/PD Conference*, Barcelona.

2 **Paraschiv, G.,** Czaplewska, P., Przybylski, M. **(2011)** Affinity mass spectrometric approaches for the elucidation of the interaction structure of the neuroprotective protease inhibitor cystatin C with Alzheimer's β-amyloid peptide. *2nd RSMS*, Timisoara.

3 **Paraschiv, G**., Juszczyk, P., Iurascu, M., Vincke, C., Muyldermans, S., Szymanska, A., Grzonka, Z., Przybylski, M. **(2008)** Structure identification and binding affinities of neuroprotective β-amyloid (Aβ) epitopes recognized by a single-chain llama anti-Aβ-antibody and the protease inhibitor cystatin. *European peptide symposium*, Helsinki.

4 **Paraschiv, G**., Juszczyk, P., Vincke, C., Muyldermans, S., Szymanska, A., Grzonka, Z.,and Przybylski, M. **(2008)** Mass spectrometric identification and immunoananlytical characterization of a β-amyloid epitope peptide recognized by single chain llama anti-Aβ antibody and human Cystatin C. *3rd ESF Conference on Functional Genomics and Disease*, Innsbruck.

5 Juszczyk, P., Szymańska, A., Kołodziejczyka, A.S., Rodziewicz-Motowidło, S., Grzonka, Z., **Paraschiv, G.**, Przybylski, M. **(2008)** Human β-amyloid-Cystatin C interaction structure revealed by epitope-excision high resolution mass spectrometry. *2nd European Conference on Chemistry for Life Sciences*, Wrocław.

6 **Paraschiv, G**., Juszczyk, P., Vincke, C., Muyldermans, S., Przybylski, M **(2007)** Epitope identification of llama single chain anti-β amyloid antibodies using proteolytic epitope extraction- and excision- mass spectrometry. *2nd European Conference on Chemistry for Life Sciences*, Wrocław.

7 Stefanescu R., Iacob R., Manea M., Tian X., Perdivara I., Maftei M., **Paraschiv G.**, McLaurin J., St. George-Hyslop P., Przybylski M. **(2007)** Epitope identification and structure determination of Aβ-specific antibodies upon Aβ-Immunisation using High-Resolution Mass Spectrometry. *8th International Conference AD/PD*, Salzburg, Austria.

8 **Paraschiv G.**, Juszczyk P., Vincke C., Muyldermans S., Przybylski M. **(2007)** Epitope Identification of llama single chain anti-β-amyloid antibodies using proteolytic epitope extraction- and excision- mass spectrometry. *55th ASMS Conference on Mass Spectrometry and Allied Topics*, Indianapolis, USA.

TABLE OF CONTENTS

1 INTRODUCTION

1.1 Molecular interactions of proteins

Molecular interactions take place between two partner molecules, such as proteins, nucleic acids, lipids, carbohydrates [1-3]. Examples of molecular interactions in which proteins are involved are protein-protein interactions (PPI) [4, 5], protein-ligand interactions [6, 7], enzymatic turnover [8] and antibody-antigen interactions [9].

1.1.1 Antibody – antigen interactions

Antibodies, also called immunoglobulins are glycoproteins occurring in blood or in other body fluids and are classified into five distinct isotypes (IgA, IgD, IgE, IgG and IgM). An IgG type-antibody structure consists of two types of polypeptide chains, two identical heavy (H) and two identical light chains (L) (Figure 1a) linked by disulphide bridges and non-covalent interactions [10]. The amino terminal regions of the heavy and light chains (VH and VL) contain each around 110 amino acids and have variable and homologous amino acid sequences. The variable regions V_H and V_L contain three hypervariable or complementarity-determining regions (CDR1, CDR2 and CDR3), which form a single surface located at the end of each variable domain. The CDRs determine the sequence and conformation of the antigen binding structure, called paratope, and confer the recognition and the binding affinity of the antibodies for their target antigens [11]. The constant region of heavy chain, named C_H1, C_H2 and C_H3 and the constant half of the light chain, termed C_L, have homologous amino acid sequences that belong to one of the classes: κ and λ for light chains and μ, δ, γ, ε and α for heavy chains [12].

A major function of an antibody is to bind to pathogens and it generally recognizes only a small region on the surface of an antigen called antigenic determinant or epitope. The epitopes are classified on the basis of their interaction with the antibody into linear and discontinuous epitopes. The linear epitope involves a single segment of the polypeptide-chain that binds to the antibody [13]. The discontinuous epitope contains some segments of the protein that are discontinuous in the amino acid sequence of the antigen, but all segments are involved in binding with the antibody.

The epitope-paratope interaction can be seen in the three dimensional structure of the antibody-antigen complex [14-16].

The characterization of an antibody-antigen complex (Figure 1b) represents a major step in understanding the antibody specificity and it is essential for the application of antibodies in clinical diagnosis and therapy [17].

The interaction between an antibody and an antigen is characterized by high affinity and high specificity [18] and by a reversible non-covalent interaction between the epitope and paratope, which includes forces like electrostatic forces, hydrogen bonds, van der Waals bonds and hydrophobic interactions [19]. Polar amino acids are often involved in the interaction between antibodies and antigens. The contacting surface areas of the antibody and antigen can vary between 600 and 900 A^2 according to the antigen size. A large proportion of CDR aromatic residues, especially tryptophane and tyrosine, are involved in the contact with the antigen. The affinity of the antibody to the antigen is expressed by the equilibrium constant between the antibody-antigen complex and free binding partners. The affinity constant K_A is in the range of 10^4 and 10^{11} L/mol. The interaction between an antibody and an antigen can be disturbed by detergents, by high salt concentrations, by extreme changes of pH.

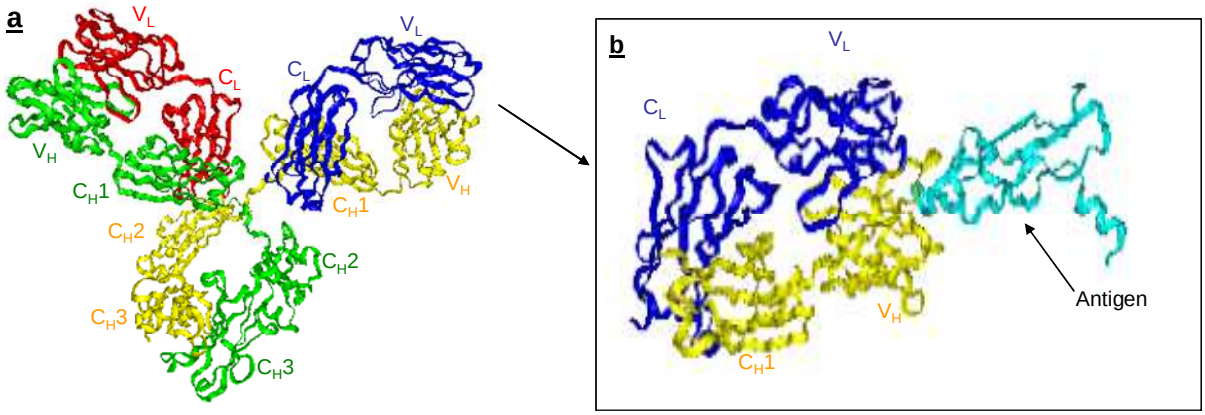

Figure 1: Schematic representation of X-Ray structure of: **a** mouse immunoglobulin G antibody (PDB: 1IGY). C_H1, C_H2 and C_H3 represent the constant regions of the heavy chain, C_L the constant half of light chain and V_H and V_L the variable regions of heavy, respectively light chain [20] and **b** Fab fragment from an anti-VEGF antibody in complex with its antigen (vascular endothelial growth factor (VEGF)) (PDB: 1CZ8) [21]. The light chain of the antibody is marked in blue and red and the heavy chain in green and yellow. The crystal structures are from Protein Data Bank and were created with BallView 1.3.2.

1.1.2 Analytical approaches for epitope identification

An important aspect for understanding the molecular recognition is the structure elucidation of the epitopes recognized by antibodies. The identification of the epitopes serves e.g. for the characterization of the active sites in enzymes [22] or for elucidation of protein conformations [23].

Several methods are used for the identification of epitopes, such as PepScan/epitope screening, sequence mutations, epitope mapping/affinity- mass spectrometry. All approaches are based on the analysis of the antibody-antigen interactions. PepScan or “epitope screening” method comprises synthesis and immunochemical assay of all possible overlapping peptides covalently bound to a solid support. The overlapped peptides are further tested for antigenicity by ELISA using a variety of antibodies. The method has initially been employed for linear epitopes, but it has been subjected to further optimization for discontinuous epitopes [24-26].

A variant of PepScan approach lies in chemical synthesis (alanine-scanning) or recombinant production (site-directed mutagenesis) of mutants to identify those amino acids which are involved in direct interaction with the antibody. Using alanine-scanning mutagenesis, each amino acid from the linear structure of the epitope is substituted with alanine and then the binding to the antibody is determined by ELISA [27-29].

For determination of epitope sequences, the X-ray structure analysis [21] and the multi-dimensional nuclear magnetic resonance spectroscopy [30] of immune complexes can be used.

Mass spectrometry is an approach used for the identification of the epitope peptides, which provides molecular structure information about the antigenic determinant. A general molecular approach for the identification of the epitopes from protein and peptide antigens using mass spectrometry was developed in our laboratory [31-33]. The method, called proteolytic epitope excision, is used for the identification of specific affinity-bound proteins and it is based on the fact that an antibody will protect the binding site(s) of a bound peptide or protein antigen from proteolytic cleavage. In

a first step, an antibody or a ligand is covalently immobilized on a stationary phase. The antigen is non-covalently bound to the antibody column resulting in the formation of the immune complex. The antibody-antigen complex presents a high association constant and the molecular structures involved in the immune complex (epitope and paratope) are shielded against proteolytic degradation. After proteolytic digestion of the antibody-antigen complex, the bound peptide-epitope will be dissociated under acidic conditions and analyzed by mass spectrometry (Figure 2). The digestion of affinity-bound antigen with various proteases allows the identification of the antibody-bound peptides, which will vary in length and sequence depending on the specificity and selectively of the individual protease for its cleaving site.

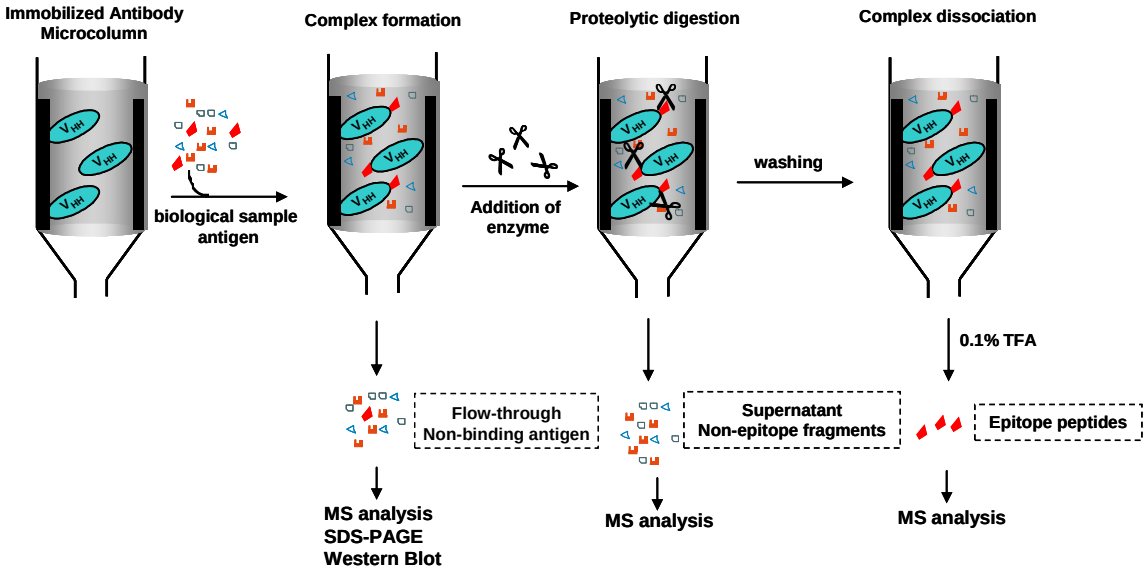

Figure 2: Schematic representation of the methodology of mass spectrometric epitope excision procedure. After preparation of the immobilized antibody microcolumn, the antigen is bound to the antibody and proteolytically degraded by different enzymes. The epitope is then dissociated by addition of 0.1 % TFA and analyzed by mass spectrometry.

In contrast with epitope excision in which the antigen is first bound to the antibody and subsequently digested, in epitope extraction, the antigen is first proteolytically digested in solution and the resulting peptide fragments are allowed to react with the immobilized antibody. Because of the high specificity of the antibody-antigen interactions, only the peptide fragments that contain the epitope will interact with the antibody. After acidic dissociation, the bound epitope peptide will be collected and analyzed by mass spectrometry (Figure 3).

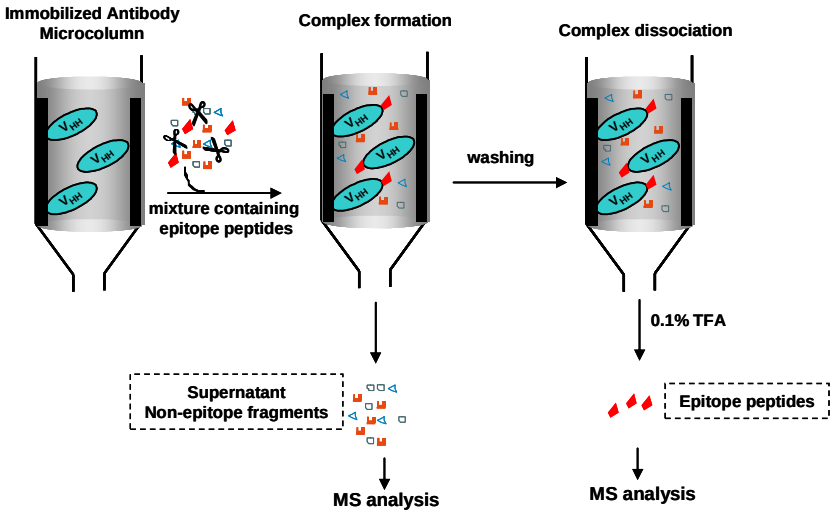

Figure 3: Schematic representation of the methodology of mass spectrometric epitope extraction. The antigen is digested in solution and then the peptide mixture is added to the antibody immobilized column. After separation of the unbound peptides, the epitope is dissociated by adding 0.1 % TFA and characterized by mass spectrometry.

One of the major goals of this thesis was to identify the β-amyloid peptide epitope recognized by a single chain llama anti-Aβ antibody, called Aβ-nanobody, and human Cystatin C (HCC), which may directly provide lead structures for vaccine development [34].

1.2 Analytical methods for protein characterization of structures and affinity binding interactions

1.2.1 Analytical strategies for protein structure analysis

As proteins are key molecules in living organisms, it is important to have knowledge about their structure. Protein structure analysis can provide important insights and applications in science, biotechnology, nutrition and medicine [35]. The knowledge of the primary structure is the basic for understanding the tertiary structure and function of proteins. The primary structure includes not only the amino acid sequence of a protein, but also the formation of disulphide bridges and post translational modifications, such as glycosylations and phosphorylations. One method is the sequence analysis of the encoding DNA and is based on the formation of the nucleotide sequence of encoding DNA followed by the transcription into the amino acid sequence [36, 37]. Another method consists in total hydrolysis of proteins followed by amino acid analysis, giving information about amino acid sequence. This

approach is used for the quantification of amino acids in proteins [38]. Other methods used for primary structure determination are Edman sequencing [39] and tandem mass spectrometry [40].

The secondary structure is giving the first information about the three-dimensional structure of proteins. Various spectroscopic methods are used for the determination of secondary structural elements, e.g. IR, RAMAN and CD spectroscopy [41]. Also, several secondary structure prediction programs have been developed [42]. Circular dichroism spectroscopy has been used to examine the secondary structure of proteins and polypeptides. In the far ultraviolet (far-UV), the spectra of these molecules are dominated by the $n \rightarrow \pi^*$ and $\pi \rightarrow \pi^*$ transitions of amide groups. The geometries of the polypeptide backbones influence their secondary structure [43, 44].

X-Ray crystallography and nuclear magnetic resonance (NMR) methods have been used to characterize the tertiary and quaternary structures. X-Ray crystallography is used for determining the three-dimensional structure of protein complexes. A critical step is however the crystallization of the sample to obtain a high purity crystal. The experiments require large amounts of sample with high purity and a wide range of conditions (temperature, pH, protein concentration) to find optimal experimental conditions [3, 45, 46]. Nuclear magnetic resonance (NMR) spectroscopy can provide information about protein structure, but also includes the investigation of dynamic features of molecular structures. A limitation of this method is the macromolecule size, sample amount, time-consuming data collection and resolution. Using NMR, the protein structures are determined in solution under physiological conditions or the solutions can be changed to quite extreme non-physiological conditions for studies of protein denaturation. NMR is also employed to determine the structure of antibody-antigen complexes. For this purpose, the antigen binding region (Fab) fragment or perhaps even the entire antibody molecule can be used [47-50].

1.2.2 Bioaffinity characterization of protein interactions

Since many years, molecular interactions have been investigated by Surface Plasmon Resonance (SPR). SPR has been established as a tool for the analysis of

biomolecular recognition processes at a biosensor surface and has been applied to the quantification of a diversity of biopolymer interactions [51, 52].

A recently explored alternative to SPR is the surface acoustic wave (SAW) technology, which uses piezoelectric materials to generate an acoustic wave [6–9], using the electro-mechanical coupling that is achieved by the piezoelectric effect (Figure 4). SAW is becoming increasingly important for the study of biomacromolecular interactions due to its high sensitive detection in liquid media (such as aqueous solutions) [53]. Advantages of SAW are the direct and rapid determination of association/dissociation constants using small sample amounts and without labelling approaches or recalibration for buffer changes [6]. The biosensors are sensitive to mass, viscosity and density. While providing sensitive and accurate determinations of binding/dissociation constants (K_i or K_D), a major limitation of all bioaffinity methods is the lack of direct identification of the affinity bound ligands.

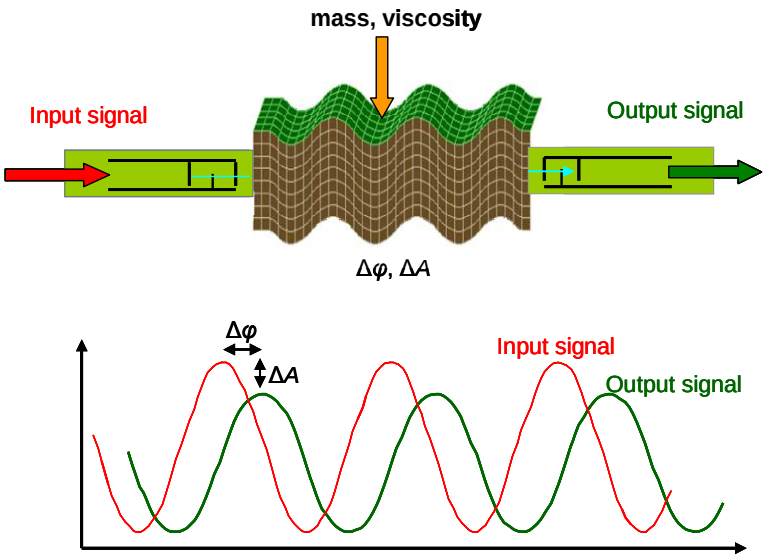

Figure 4: Principle of the surface acoustic wave (SAW) biosensor: an electric field is transformed in a mechanical wave through a piezoelectric effect. When the surface mass loading and liquid viscosity change, the wave will change its amplitude and phase and it is converted into electrical signal for processing. Δφ represents the phase shift and ΔA the amplitude difference.

1.3 Mass spectrometric methods for structural characterization of polypeptides

Mass spectrometry is a widely used analytical technique for the analysis of proteins, peptides, oligonucleotides and protein-ligand complex formation under physiological

conditions. Proteins can be analyzed by mass spectrometry to reveal e.g. the homogeneity of a mixture, to verify the amino acid substitutions, to confirm the complete or partial amino acid sequences and to detect post-translational modifications. Various mass spectrometric methods have been developed over the past two decades, such as Fast-Atom-Bombardment (FAB), Field Desorption (FD), ^{252}Cf-Plasmadesorption. Some advantages of mass spectrometry are e.g. high resolution, high mass accuracy and sensitivity, short analysis time and low sample consumption.

A mass spectrometer consists of an ion source, a mass analyser that measures the mass-to-charge ratio (m/z) of the ionized analytes and a detector that registers the number of ions at each m/z value. Introduction of new soft ionization techniques such as electrospray (ESI) (Nobel Prize for Chemistry in 2002 for John B. Fenn) [54] and matrix assisted laser desorption ionization (MALDI) (Nobel Prize for Chemistry in 2002 to Koichi Tanaka) [55] increases the importance of mass spectrometry.

MALDI mass spectrometry enables the analysis of very small amounts of proteins and peptides (< fmol) and it is used for the characterization of synthetic peptides, recombinant proteins, post-translational and chemical modifications. For MALDI mass spectrometric analysis, the sample is first co-crystallized with a matrix, usually an UV-absorbing weak organic compound. For peptides and proteins, the following matrices are used: α-cyano-4-hydroxycinnamic acid (HCCA), 3,5-dimethoxy-4-hydroxycinnamic acid (sinapinic acid) and 2,5-dihydroxybenzoic acid (DHB). HCCA is the most commonly used for peptides with lower mass (< 2500 Da) and sinapinic acid for higher mass peptides (> 2500 Da). Using an UV laser beam at the surface of the analyte-matrix complex, the matrix absorbs the laser energy and vaporizes the matrix with the analyte causing desorption and ionization of the sample. In Figure 5a a schematic representation of ion formation in MALDI process is shown [56-60].

In electrospray ionization sources, multiple charged ions ($[M+nH]^{n+}$ can be generated from large molecules in the gas phase. The analyte in aqueous acidic solution containing a mixture of organic substances (e.g. methanol, ethanol or acetonitrile) and organic acids (e.g. acetic acid, formic acid) is sprayed from a very small capillary with a weak flux after applying a strong electric field. The high electric field is

obtained by applying a potential difference of 3-6 kV between the capillary needle and counter-electrode and induces a charge accumulation at the liquid surface located at the end of the needle. As a result, a highly charged droplet is formed. At low voltages, the droplet is spherical, then starts to deform under the pressure of the accumulated charges at the needle tip in the high electric field. When the electric field increases, the surface tension is broken and the shape of the droplet changes to so called ´Taylor cone` and the spray will be formed. The spray formation is facilitated by a heated inert gas, most often nitrogen, which is injected coaxially (Figure 5b) [54, 61-63].

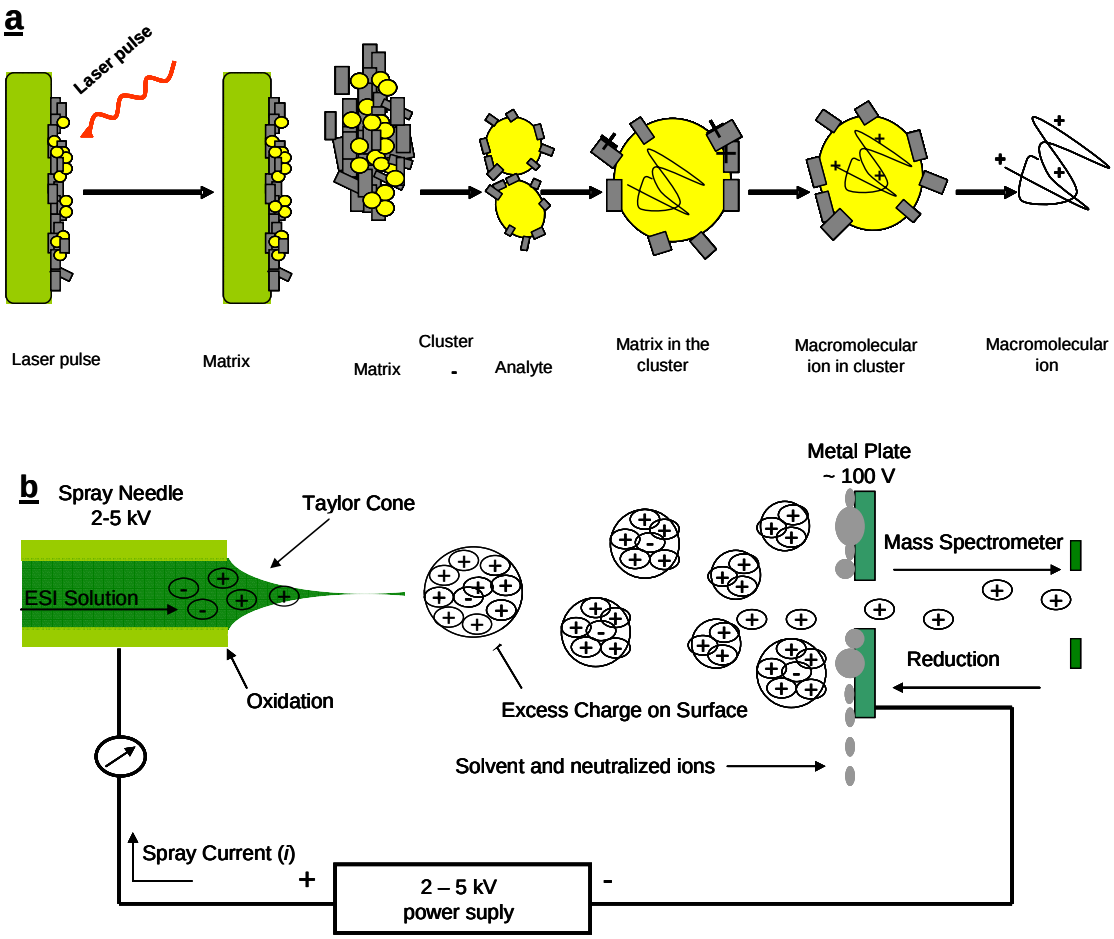

Figure 5: Schematic representation of the: **a** ion formation in MALDI mass spectrometry: the ionization is triggered by a laser beam. The used matrix absorbs the laser energy. **b** electrospray ionization process. From the left part: Taylor cone, droplet formation, Coulomb fission with droplet evaporation, gas phase ion formation in the transfer capillary [64].

Usually, MALDI is coupled with TOF (time of flight) analysers and used to identify proteins, known as peptide-mass fingerprint, whereas ESI is mostly been coupled to ion traps and triple quadrupole instruments and used to generate fragment ions spectra of selected precursor ions [62].

1.4 Key proteins involved in neurodegenerative diseases

Neurodegenerative diseases correspond to a large group of neurological disorders, characterized by structural transition of disordered proteins to highly ordered deposits called amyloids. Each disease is defined by a key protein, known as intrinsically disordered or unstructured protein (IDPs/IUPs), e.g. β-amyloid peptide and tau-protein in Alzheimer's disease (AD), α-synuclein in Parkinson's disease (PD), polyglutamine stretch of huntingtin in Huntington's disease or prion protein in prion disorders, such as Creutzfeldt-Jakob disease (CJD), Gerstmann-Straussler-Scheinker syndrom (GSS), Fatal Familial Insomnia (FFI). Recent advances in molecular biology, immunopathology and genetics showed that these diseases might share a common pathogenic mechanism, which consists in abnormal accumulation and processing of modified and damaged proteins. Neurodegenerative disorders are known as protein conformational or protein misfolding diseases. The obvious consequences of misfolding are protein aggregation and fibril formation, loss of function and gain of toxic function. Some proteins have an intrinsic propensity to adopt a pathologic conformation, which becomes evident with aging or at high concentrations [65].

1.4.1 Amyloid-β peptide and Alzheimer's disease

The most common form of dementia among elderly is Alzheimer's disease (AD), which is characterized by progressive loss of memory and general cognitive decline. AD was first described by the german physician Alois Alzheimer (1864 – 1915). In 1906, he examined a 51-year-old woman (Auguste D.) whose personality and mental abilities were obviously deteriorating: she forgot things, became paranoid and acted strangely. Upon her death, Alzheimer examined her brain at autopsy and noted dense deposits surrounding the nerve cells (neuritic plaques). Inside the nerve cells he observed twisted bands of fibres (neurofibrillary tangles). He also found that the cell body and nucleus of nerve cells disappeared [66].

AD is one of the major health problems worldwide affecting more than 36 million people. Recent statistics showed that the number of affected people will increase to 65.7 million by 2030 and 115.4 million by 2050 [67]. The greatest known risk factor

for AD is increasing age. The majority of people with Alzheimer's are 65 and older (Figure 6) [68]. Studying the pathology, genetics and biochemistry of AD is a way to settle disease's mystery; real advances are being made in understanding both genetic and biochemical mechanisms of pathogenesis and accurate disease diagnosis.

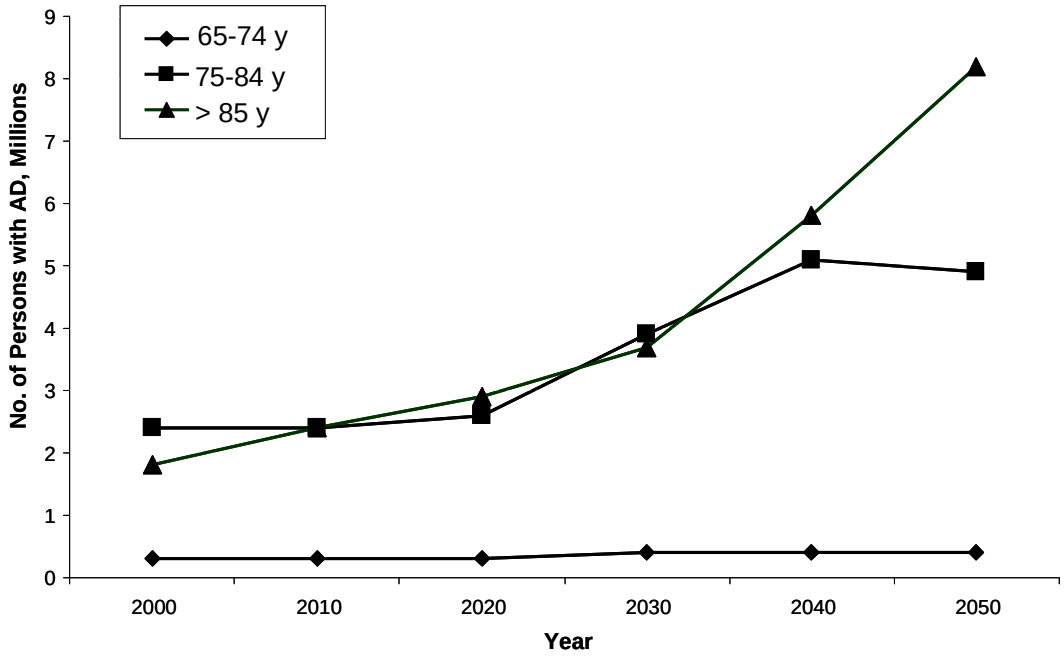

Figure 6: Projected number of persons in US population with AD by age groups, 65 to 74 years old, 75 to 84 years old and 85 years and older, using the 2000 US Census Bureau middle series of population growth [68].

The early clinical symptoms are minor memory loss, less energy and spontaneity, depression, while later symptoms include disorientation, confusion and behaviour changes. In advanced stages of AD, patients become more and more irresponsible and might exhibit tremor, movement disturbance and urinary incontinence. The macroscopic examination of the brain in AD patients shows pronounced cortical atrophy, with shrinkage of the gyri in the frontal, temporal and parietal region, enlarged ventricles and loss of parenchyma. In other words, shrinkage of the entire brain is observed (Figure 7 a and b).

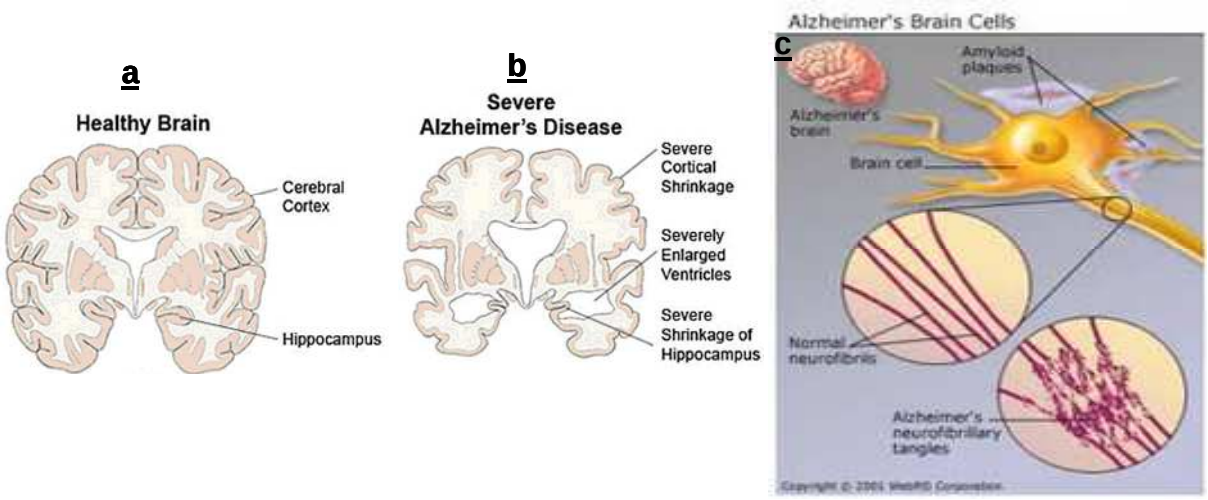

Figure 7: Brain cross section of: **a** healthy individual; **b** Alzheimer's disease patient: the brain presents a severe cortical shrinkage, the ventricles are enlarged and the hippocampus is severely shrinked (modified after http://www.freewebs.com/rbannerm/AD_2003.jpg). **c** Pathophysiological characteristics of Alzheimer's disease: amyloid plaques are extracellular deposits of Aβ surrounded by microglia, dystrophic neuritis and reactive astrocytes and neurofibrillary tangles are intracellular aggregates composed of a hyperphosphorylated form of the tau protein (from http://www.webmd.com/alzheimers/guide).

At the cellular level, neuronal dysfunction and degeneration leading to a reduction in synaptic density have as a result Alzheimer's disease. At the molecular level, the disease is defined by filamentous deposits, which occurs within axons, dendrites and terminals of neurons as neurofibrillary tangles (NFT), in the extracellular neurophil as amyloid plaques (APC) and around blood vessels as amyloid congophilic angiopathy (ACA). The amyloid deposits apparently appear in the terminal zones of neurons that develop NFT (Figure 7 c) [69]. A 4.5 kDa amyloid peptide has been shown to be the major constituent of both APC and ACA. The amyloid protein has been originally termed "beta-protein" or "amyloid A4". Beta protein (Aβ) is a 40 to 42 amino acid polypeptide proteolytically derived from a transmembrane protein named amyloid precursor protein (APP), which is encoded by a widely expressed gene on chromosome 21. The APP gene is spliced to produce several isoforms, ranging in length from 365 to 770 amino acids. Three of these isoforms, comprising 695, 751 and 770 amino acids, are associated with AD [70, 71]. This precursor protein is a type I transmembrane protein that can undergo two separate proteolytic pathways (Figure 8). In the amyloidogenic pathway, APP is cleaved by β-secretase at N-terminal of the Aβ-peptide, releasing $sAPP_{\beta}$ fragment and leaving 99 amino acid C-terminal fragment (CTF) attached to the membrane, termed C99. C99 is then cleaved by the γ-secretase, within its intramembrane region, releasing the Aβ peptide

(40 to 42 amino acids) and APP intracellular domain fragment (AICD) [72]. In the non-amyloidogenic pathway, α-secretase cleaves within the Aβ region at Lys-16, which results in the release of a soluble ~ 110 - 120 kDa sAPPα fragment and a C-terminal domain fragment, which has 83 amino acids, known as C83. C83 is retained in the membrane and is also cleaved by γ-secretase, releasing a non-toxic 3 kDa fragment known as p3 and APP intracellular domain. These two separate components (amyloidogenic and non-amyloidogenic) from the processing of APP may have important consequences in both diseased and normal physiology [73-75]. The pathogenic role of β-amyloid peptide was first described by Hardy in 1992 by the amyloid cascade hypothesis [76, 77]. The amyloid cascade hypothesis suggests that a lack of balance between the production and clearance of Aβ in the brain is the initiative event of the disease and has as a result the accumulation and aggregation of Aβ, and finally leads to neuronal degeneration and dementia. After the APP processing and the release of β-amyloid peptide, aggregation initially leads to soluble oligomers, which then form amyloid fibrils and amyloid plaques.

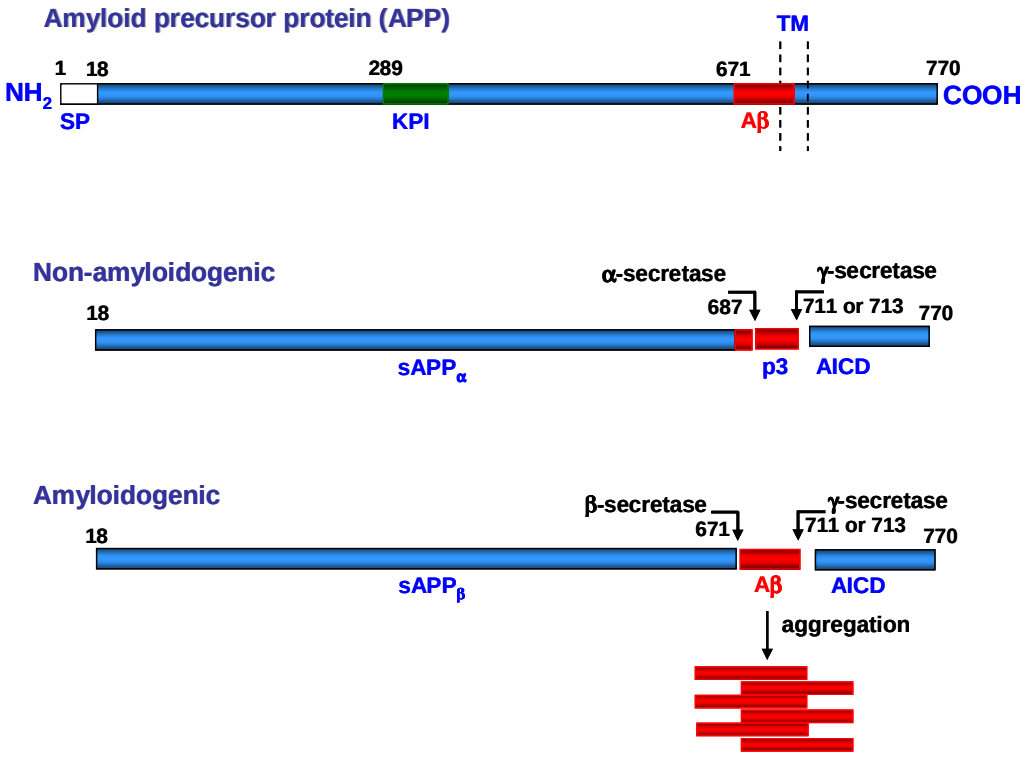

Figure 8: Amyloid precursor protein processing pathway. The non-amyloidogenic cleavage by α-secretase leads to the formation of a soluble N-terminal domain sAPPα and a short cytoplasmic C-terminal tail. The amyloidogenic cleavage by β- and γ- secretases leads to the formation of the N-terminal domain sAPPβ, a C-terminal domain and the releasing of β-amyloid peptid. SP: signal peptide; KPI: Kunitz-type proteinase inhibitor domain; AICD: APP intracellular domain fragment; TM: transmembrane; modified from [74]).

1.4.2 Formation of amyloid plaques

One hallmark of Alzheimer's disease (AD) is represented by the extracellular deposition of fibrous protein aggregates in the form of amyloid plaques. Understanding the mechanism of amyloid plaques formation within the brain could provide key answers to AD pathogenesis [78].

Aggregation of β-amyloid peptide (Aβ) leads to different types of Aβ aggregated forms, from dimers to the large mature insoluble Aβ fibrils found in the brain. The insoluble Aβ fibrils have long time been considered as the pathological hallmark of AD, rather than a cause. In the recent years, many data have suggested that the insoluble Aβ fibrils are not the disease causing agent. Instead, the soluble, pre-fibrillar Aβ oligomers are the proximate effectors of synapse loss and neuronal injury [79].

The elucidation of the Aβ aggregation pathway is a very complex work. The proposed model of Aβ fibrillization is a nucleation-dependent polymerization mechanism that needs seeding by an ordered nucleus, followed by the production of oligomers through addition of further Aβ molecules. In a nucleation-dependent polymerization the kinetic of polymer formation reveals a lag phase. The duration of the lag phase depends on the protein concentration, which is controlled by the values of association and dissociation rate constants, as well by the number of monomers in the nucleus. A critical concentration is necessary for the polymer formation. At equilibrium, a specific amount of the monomer will be in equilibrium with the polymer [80-82]. The minimum concentration required for the formation of Aβ fibrils is 10 - 40 µM for Aβ(1-40) and about five fold lower for Aβ(1-42). In cerebrospinal fluid, the physiological Aβ concentration in healthy individuals is in the lower nanomolar range (< 10 nM) and in AD patients brains is not significantly higher [83].

The aggregation pathways might differ for the same Aβ peptide at different initial Aβ concentrations. Moreover, it has been shown that the Aβ(1-40) and Aβ(1-42) aggregates use different pathways, but the common point of these models is the formation of an Aβ oligomer as a nucleus, the growth of the nuclei via protofibrils and fibrils that *in vivo* might associate to plaques [84-86]. The fibril formation is a reversible process, although the real equilibrium between Aβ monomers and fibrils is

permitted to exist only at the fibril end. For the soluble Aβ(1-40) monomer, an equilibrium concentration of 0.7 – 1 μM has been determined. The concentration is independent from the total concentration of Aβ(1-40) in aggregation experiments [86, 87].

1.4.3 Therapeutic strategies for Alzheimer's disease

Currently, two types of drugs are authorized for the treatment of AD. The first treatment is based on the inhibition of acetyl cholinesterase (AChE), because many symptoms of dementia are closely related to cholinergic dysfunction. Until now, four cholinesterase inhibitors have been approved for the treatment of mild AD: tacrine, donepezil, rivastigmine and galantamine. The treatment with these drugs produces modest symptomatic improvement in patients, but it does not slow the progression of the disease [88-90]. An alternative treatment is performed with memantine, a N-methyl-D-aspartate (NMDA) receptor antagonist, which appears to prevent the neuronal excitotoxic effect exerted by high levels of glutamate. Memantine has been approved for the treatment of moderate to severe Alzheimer dementia [91-93].

Several therapeutic strategies have been proposed based on the knowledge of Aβ formation and the effects of soluble Aβ oligomers on the synaptic function. Inhibition of β- and γ-secretase should decrease Aβ generation, but might cause unwanted side effects. Another therapeutic strategy would consist in lowering the level of soluble Aβ oligomers [79].

Aβ immunotherapy is a promising strategy for reducing the level of Aβ in the brain. Immunological approaches have been proposed as a strategy for diagnostics and treatment of neurodegenerative diseases. Two types of antibodies specific to Aβ have been identified and characterized to dissagregate and/or to inhibit amyloid fibril deposition: (i), Aβ-plaque specific antibodies resulting from active immunization with Aβ(1-42), that disaggregate Aβ-plaques; and (ii), physiological Aβ-autoantibodies that inhibit fibril formation. Aβ-plaque specific antibodies generated by active immunization with Aβ(1-42) and Aβ-derived aggregates have been shown to reduce the neurotoxicity and reverse the memory deficits in APP-transgenic mice, and are characterized by the recognition and binding of a specific N-terminal Aβ-epitope. This

epitope peptide contains the residues (4-10) (FRHDSGY), which are accessible in Aβ(1-42) as well as in oligomeric and protofibrillar Aβ. Although an early clinical trial of immunization of AD patients with Aβ(1-42) indicated initial good tolerability, the clinical evaluation was stopped after approximately 6% of the vaccinated patients developed severe meningo-encephalitic inflammations [94-97]. In contrast, physiological Aβ-autoantibodies isolated from serum of healthy individuals and AD patients were found to specifically recognize the C-terminal part of Aβ. The carboxy-terminal epitope comprises residues (21-37) of Aβ and thus the Aβ-aggregation domain. Aβ-autoantibodies lead to a shift of Aβ from the central Aβ pool into the periphery and interfere with the early steps of plaque development (i.e. they abolish oligomerization of Aβ) [98]. A potential therapeutic concept for AD is passive immunization with intravenous immunoglobulin (IVIg) containing naturally occurring Aβ-autoantibodies [99].

The differential recognition of the C-terminal Aβ-autoantibody epitope and the N-terminal plaque-specific epitope provided the basis for the main goals of the present dissertation.

Unpaired variable domains of single heavy chain antibody (V_{HH}) fragments (nanobodies) (Figure 9), have recently been considered to have high potential for various medical applications. Because of their capability to prevent the unfolding of amyloidogenic protein variants or even clear existing aggregates *in vitro*, nanobodies are expected to be a therapeutic alternative for treating amyloidosis disorders such as AD. V_{HH}, termed nanobody, represents the smallest antigen binding unit with a molecular size of ~15 kDa, in comparison to single-chain antibody fragments consisting of variable domains of heavy and light chains connected by a peptide linker (scFv, 30 kDa), to Fab fragments (60 kDa) and to the whole IgG antibodies (150 kDa) [100]. Nanobodies have favourable properties for biophysical studies, including small size, high solubility and stability [101-103]. The concept of single-domain antibody (dAb) was first introduced by Ward *et al.* [104]. The discovery of camelid heavy-chain antibodies naturally devoided of light chains opened up a new opportunity to develop dAb with improved properties [103]. Camelid V_{HHs} display similar functional characteristics with respect to specificity and affinity compared to classical antibodies [105, 106]. Dromedary subclasses were originally named IgG1,

IgG2 and IgG3 in order of decreasing molecular weight. The sera from camels (*Camelus bactrianus*) and llamas contained similar heavy–chain antibodies. Compared to dromedaries, a slightly lower percentage of heavy-chain antibodies are observed in llamas.

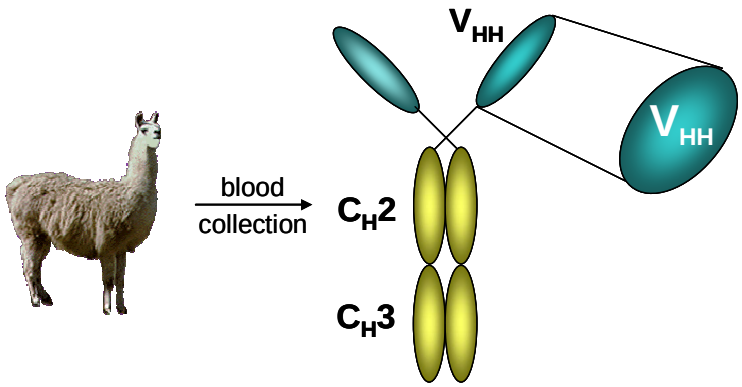

Figure 9: Heavy-chain antibody from *Llama Glama* obtained after immunization of the animal. V_{HH}, called nanobody, represents the smallest fragment of a single-chain antibody.

The present dissertation is focused on the characterization of Aβ-nanobodies and the elucidation of the β-amyloid epitope peptide recognized by the Aβ-nanobodies.

Human Cystatin C (HCC) (Figure 10) with a molecular weight of 13 kDa is the main cysteine protease inhibitor in mammalian body fluids [107] and has been found in high concentrations in cerebrospinal fluid (CSF). Immunohistological studies have shown that the protease inhibitor Cystatin C and other proteins such as apolipoprotein E, clusterin, transthyretin and gelsolin co-deposit with Aβ [108-110]. A wide spectrum of biological activities has been associated with HCC, such as modulation of neuropeptide activation and neurite proliferation [111, 112]. While wild type Cystatin C shows no aggregation tendency, the naturally occurring mutant L68Q presents a high tendency to form amyloid fibrils, causing hereditary cerebral hemorrhage of the amyloidosis-Icelandic type. The presence of HCC in Aβ-plaques has been suggested to result from its binding to APP. Alternatively, HCC may bind to Aβ prior to the secretion or following the deposition in brain. Sastre *et al.* found that the association of HCC with Aβ causes an inhibition of fibril formation and suggested an N-terminal Aβ-sequence to be responsible for the interaction, with formation of a stoichiometric HCC-Aβ complex [111]. Human Cystatin C has a protective role in Alzheimer's disease, by preventing the formation of the toxic forms of Aβ and by direct protection of neuronal cells from Aβ toxicity [113-115].

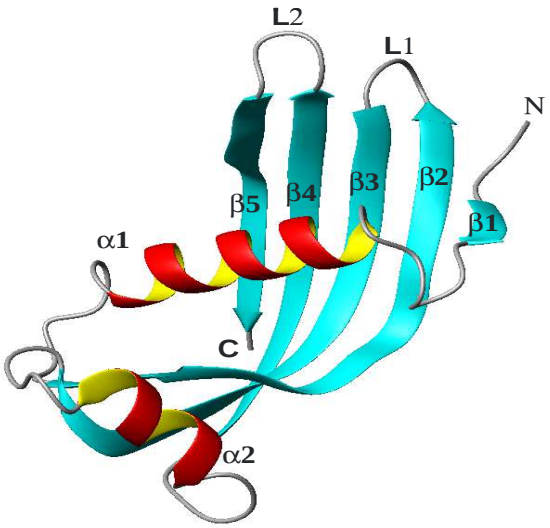

Figure 10: Ribbon representation of human Cystatin C (HCC) (pdb File 1 CEW). Secondary structure of HCC: L1: loop 1; L2: loop 2; α1: α - helix 1; α2 : α-helix 2; β1 – β5: β-sheet 1 – 5.

The identification and characterization of the binding epitope of HCC in the central domain of Aβ was studied in the present dissertation. The protease inhibitor has an important role in the aggregation process and amyloidogenesis. Blocking the hydrophobic core of the HCC, the Aβ oligomerization can be inhibited and the fibril formation can be regulated. Moreover, the identification of the binding site in HCC is important for the oligomerization studies of Cystatin C. New oligomerization inhibitors may be designed based on the HCC-epitope.

1.5 Scientific goals of the dissertation

Alzheimer's disease (AD), a major neurodegenerative disorder in the elderly, is characterized by behavioural changes and decline in cognitive functions. AD is being recognized as one of the most important medical problems in the elderly. A main characteristic of AD is the accumulation of Aβ-peptide aggregates in the brain. An early diagnosis and full recovery after treatment are not yet possible. Anti-Aβ antibodies are among other compounds capable to disrupt Aβ fibrils, protofibrils and oligomers or to prevent the aggregation of Aβ-peptides.

In order to develop potential therapeutically active vaccines, it is important to determine the epitope to be targeted and the efficient antibody-mediated mechanism of Aβ clearance in order to reach maximal efficacy. Accordingly, the elucidation and structural characterization of a fibril inhibiting Aβ-epitope was a main scientific goal of this dissertation.

The main scientific goals of the present dissertation are summarized as follows:

1) *Epitope identification of single chain llama anti-Aβ antibodies using mass spectrometry and immunoanalytical methods.*

   Mass spectrometry was successfully used for the characterization of single chain llama anti-Aβ antibodies, called Aβ-nanobodies. Using proteolytic excision/extraction methods, the epitope recognized by Aβ-nanobodies was identified. In order to identify the functional epitope, sequence mutagenesis studies together with ELISA analysis were carried out on a series of peptides encompassing mutated epitope sequence.

2) Characterization of binding affinities between Aβ-nanobodies and Aβ(1-40) and (17-28) peptides

   For interaction studies between Aβ-nanobodies and Aβ(1-40) and Aβ(17-28), two different approaches were employed. In the first approach, the binding between the antibodies and the peptides was studied using affinity-mass spectrometry, while in the second experimental set-up, the affinity was determined by surface acoustic wave biosensor.

3) Molecular aggregation of Aβ(1-40) in vitro

   First molecular studies of Aβ(1-40) aggregation were carried out by different analytical methods such as gel electrophoresis and DOT-BLOT immunoassay. The β-sheet conformation of the aggregates was characterized by thioflavin T assay.

4) *Epitope identification and structural characterization of the neuroprotective protease inhibitor Cystatin C with Alzheimer's Aβ-amyloid peptide.*

   The identification of Aβ-amyloid epitope peptide recognized by human Cystatin C and of binding fragment of human Cystatin C to immobilized Aβ(1-40) peptide was carried out by proteolytic excision and extraction in combination with mass spectrometry. The identification of the Aβ-epitope peptide was confirmed by alanine scanning mutagenesis and ELISA. The complex formation between human Cystatin C fragments and β-amyloid epitope peptide was investigated by mass spectrometry.

2 Results and discussion

2.1 Structural characterization of Aβ-specific antibodies

2.1.1 Structural comparison between conventional immunoglobulins and single-domain antibodies

The vertebrates have the amazing capacity to produce immunoglobulins against virtually any molecule. Because the immunoglobulins interact with their antigens with high specificity and affinity, they are extremely useful in a variety of applications, such as biotechnology, biochemistry, diagnosis and even human therapy. In clinical trials, conventional immunoglobulins represent at least 25 % of used proteins [116-118]. Conventional immunoglobulin is composed of two types of polypeptide chains, two identical heavy (50 kDa) and two identical light chains (25 kDa). Heavy and light chains are linked together by disulfide bridges and non-covalent interactions (Figure 11 a). Each light chain contains a variable region and a constant region. In comparison with the light chain, heavy chain has one variable region and three distinct constant regions. The variable region, comprising the N-terminal domain of each light and heavy chain, includes three connecting loops termed complementarity determining regions (CDRs). The CDRs constitute a single surface which interacts with the antigens.

Antibodies in *Camelidae* (camels and llamas) contain only heavy-chain homodimers; therefore, they are called heavy-chain antibodies (HcAb) (Figure 11 b). The light chain and the first domain of the constant region (C_H1) of the heavy chain are missing [103]. The antigen binding site of the HcAb consists of a single variable domain, referred to as V_{HH} to distinguish them from the classical V_H. The absence of the light chains leads to a reduction of antigen-binding sites with only three (instead of six) complementarity determining regions (CDRs) [119]. CDR1 and CDR2 from mouse or human VHs present a restricted number of possible conformations with different lengths and amino acids compositions. The V_{HH}s from camel or llamas differ significantly from mammalian V_Hs [10, 120, 121]. The CDR3 in camels or llamas is significantly larger than in mouse or human, resulting in an increased antigen binding

surface, which partially compensates the lack of the light chain [122]. The HcAbs represent a major fraction in the serum of camelids, up to ~ 50 % in dromedaries. After the dromedaries and llamas are immunized, it is possible to isolate the antibody fragments (V_{HH}s), which have only a single domain with 118 - 136 residues.

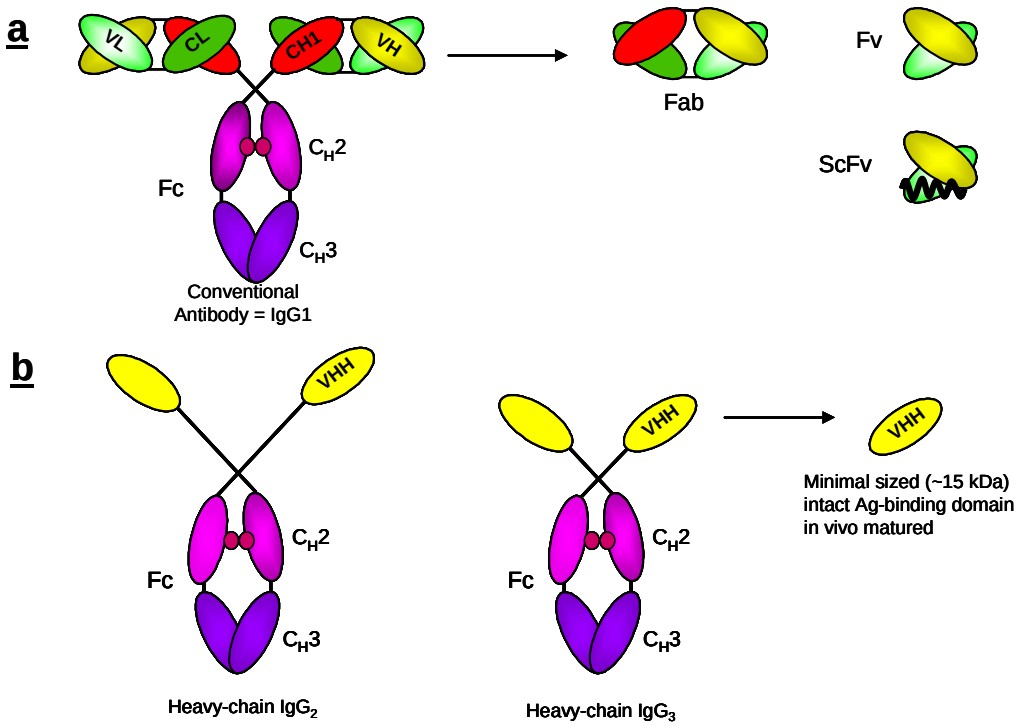

Figure 11: Schematic representation of: **a** conventional antibody (IgG 1) and the corresponding fragments, Fab, scFv and Fv and **b** "heavy-chain" camel antibodies (IgG2 and IgG3). Fab: Fragment antigen binding region; scFv: single chain fragment from variable region; Fv: variable region of the antibody.

On the V_{HH} surface, three hydrophobic residues are present at position 44, 45 and 47 (after Kabat numbering [123]). In the conventional immunoglobulins, these residues which interact with the variable region (V_L) are substituted by hydrophilic amino acids. Another difference between camel or llama V_{HH}s and conventional V_H is the additional disulfide bridge among CDR1 and CDR3 [124]. Different crystal structures of V_{HH}s alone or in complex with antigens were solved previously [125]. An example is the crystal structure of cAb - Lys3 camel antibody in complex with hen egg-white lysozyme. The CDR3 from the camel antibody is longer than any other CDR3 loop of the conventional V_H region [126-128].

2.1.2 Primary structure characterization of Aβ-specific single-chain antibodies

Specific nanobodies (Nb) to Aβ1-40 were obtained after immunization of llama (*Llama glama*). A llama received six injections of a mixture of Aβ(1-40) and Aβ(1-42) one time in a week. After forty-five days, 50 mL blood were collected. Using Hitrap Protein A and protein G columns, different plasma IgG subclasses were separated. mRNA was extracted from lymphocytes and a cDNA library of 2 x 10^7 transformants, containing the V_{HH} genes amplified from the peripheral blood lymphocytes, was constructed in the phagemid vector pHEN4. This library (library 92) was screened by panning against Aβ(1-40) and Aβ(1-42). The enrichment of Aβ(1-40) specific phages after each round of selection was assessed by a 'phage ELISA'. A significant enrichment could be observed for library 92 after three rounds of selection. After three rounds of *in vitro* selection, four V_{HH}s specific to Aβ(1-40) were isolated from the library (Nb_3, Nb_9, Nb_26 and Nb_27, termed Aβ- nanobodies). The library selection with phage display and with the bacterial two-hybrid system, expression and purification of nanobodies, SPR measurements, epitope mapping with BacterioMatch and data analysis were performed by Dr. Cecile Vincke, at Vrije University, Brüssel, Belgien.

In the present work, Nb_3 and Nb_9 recognizing Aβ(1-40) were initially characterized by SDS-PAGE. In order to assess the purity of the Aβ-nanoboies, 5 µg from each nanobody were run into the gel. The gel stained with Coomassie blue, indicated that nanobodies were free from other components and that the molecular masses were around 14 kDa (Figure 12 b).

Nb_3 and Nb_9 have each 130 amino acids. The location of the complementarity determining regions (CDRs) in the nanobodies was estimated using the Kabat rules. CDR1 contains 7 amino acids, CDR2 10 amino acids and CDR3 14 amino acids (Figure 12 a).

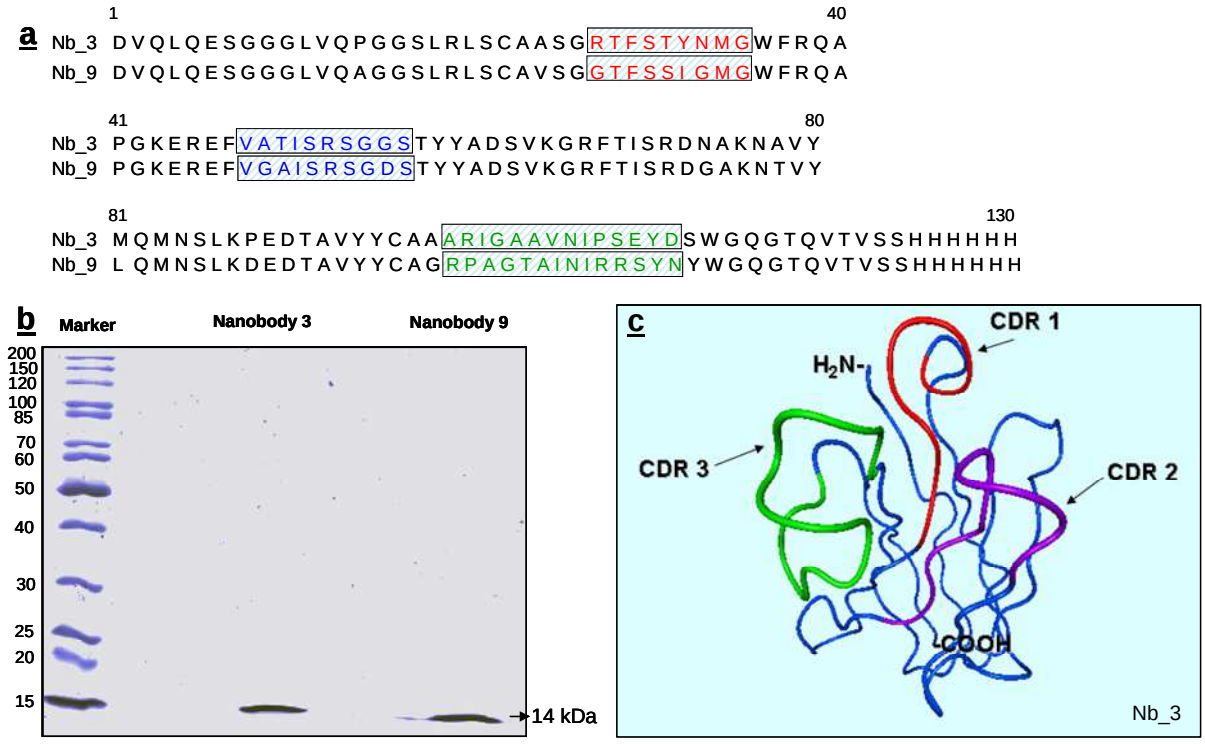

Figure 12: **a** Sequence alignment of Nb_3 and Nb_9 with marked CDRs: CDR1 in red, CDR2 in purple and CDR3 in green. **b** SDS-PAGE of Nb_3 and Nb_9. A band at ~ 14 kDa was observed, which corresponds to Nb_3 and Nb_9. **c** Ribbon representation of Nanobody 3 using Hyperchem 7. CDR: complementarity determining region.

The molecular masses of the intact Nb_3 and Nb_9 were determined by ESI- FTICR mass spectrometry (Figure 13). The measurements were performed at Bruker Daltonics in Bremen using an Apex Qe 9.4 T instrument equipped with an Apollo II electrospray source. For performing the experiments, each sample was diluted in 50 % methanol, 0.1 % formic acid (ESI-solvent) and the samples were introduced in the electrospray source at a flow rate of 120 µL / h. The mass spectra were externally calibrated with arginine cluster and deconvoluted with MaxEntropy method of the DataAnalysis 3.4. The monoisotopic molecular mass determined from the mass spectrum was 14122.79 for the Nb_3 and 14066.80 for the Nb_9, in agreement with amino acid sequences.

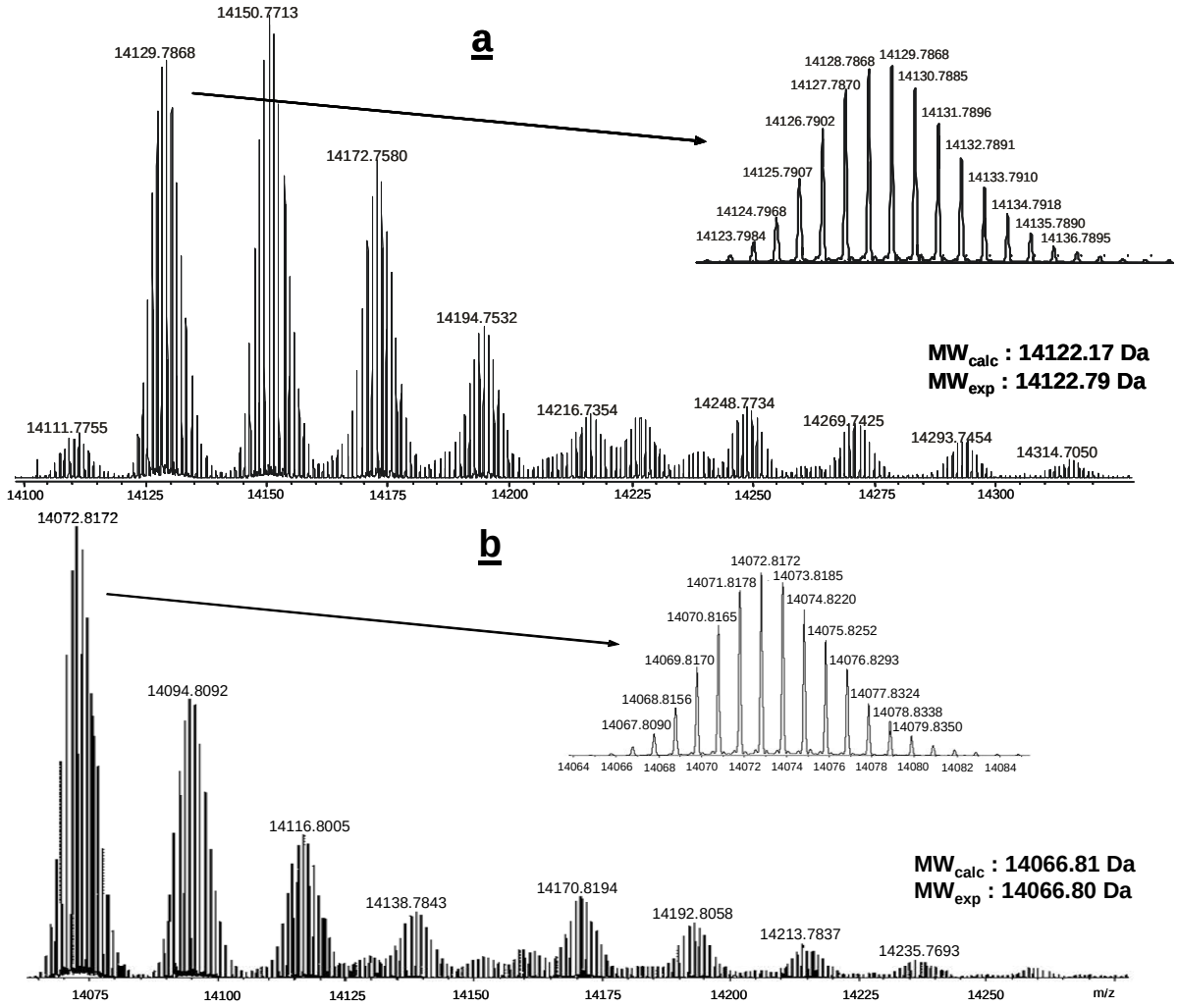

Figure 13: **a** ESI- FTICR mass spectrum of the Nb_3. **b** ESI- FTICR mass spectrum of the Nb_9.

2.1.3 Synthesis and characterization of a CDR3 peptide from an Aβ-specific single-chain antibody

To investigate whether Nb_3 contains a CDR region that might be suitable to function as a microantibody, the amino acid sequence was analyzed and the CDR-regions were determined according to the rules of Kabat [9]. After analysis of a theoretical molecular model of the nanobody, the CDR3- region was picked as a potential candidate. According to the computer simulation, the CDR3- domain exhibits a typical and very dominant loop-structure, which might be responsible for the main binding interaction, creating an extensive antigen-interaction surface. Additionally, the CDR3- region represents the longest complementarity determining region. The Kabat rules, which are based on amino acid sequence analysis of antibodies, depict

length, position and conserved amino acids before and after complementarity determining regions (CDR). Due to the fact that the substituted conserved amino acids in single chain antibodies occur mainly in the N-terminal region, the identification of the CDR3 regions was not hindered.

The CDR3-peptide was synthesized using standard Fmoc-SPPS and purified by RP-HPLC. Figure 14 shows the high resolution ESI-FTICR mass spectrometric characterization of the CDR3-peptide after purification. The $[M+2H]^{2+}$ ion, showing a m/z of 737.8738, is the most prominent in the mass spectra and was determined with high accuracy.

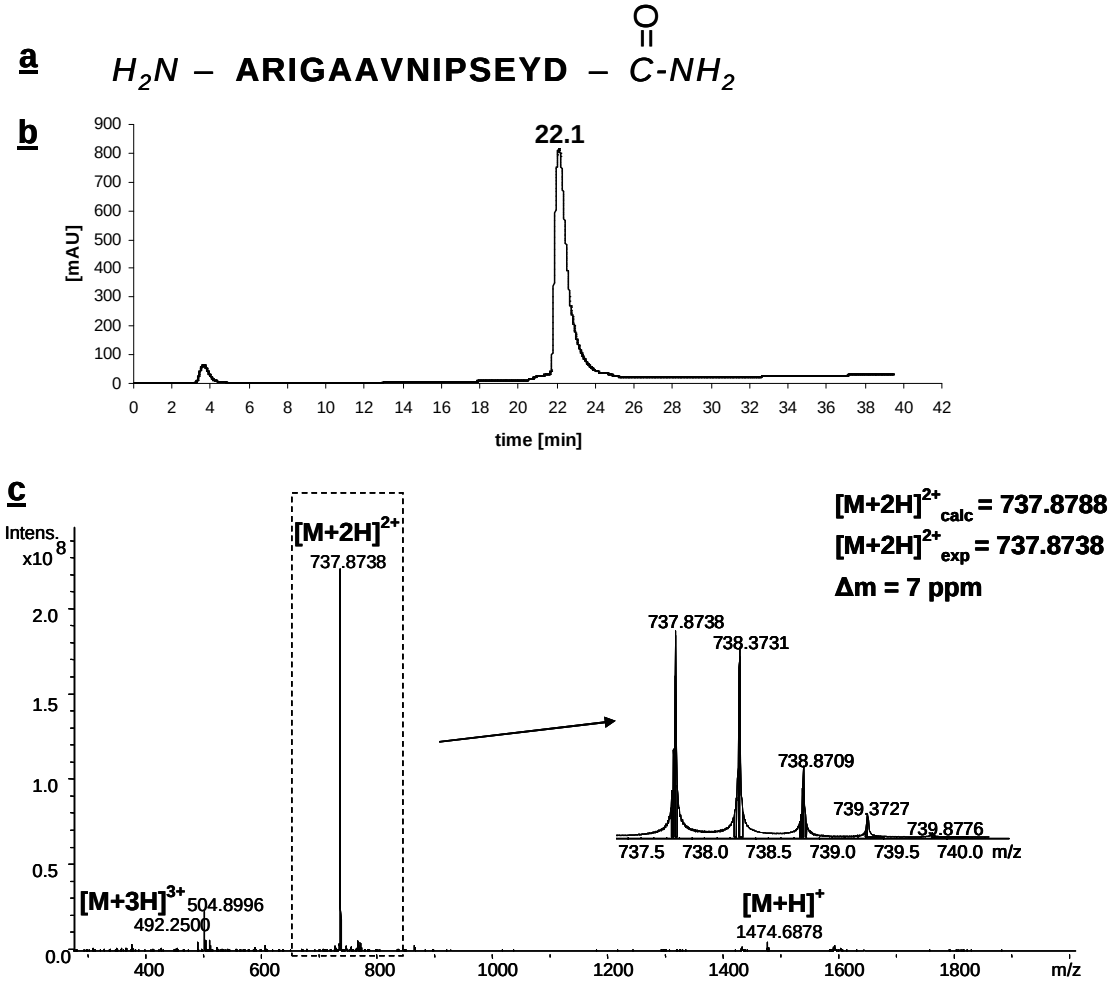

Figure 14: **a** Amino acid sequence of CDR3-peptide from Nb_3. **b** Analytical RP-HPLC profile of the synthetic CDR3-peptide **c** ESI-FT-ICR mass spectrum of purified CDR3-peptide. $[M+2H]^{2+}$ calculated/experimental: 737.8788 /737.8738 (Δm = 7 ppm).

The secondary structure of CDR3 synthetic peptide was further determined by circular dichroism spectroscopy in water and TFE. The addition of TFE is known to stabilize peptides and proteins in an ordered conformation. TFE has a significant

lower dielectric constant hence strengthening the interaction between charged groups. TFE strengthens intramolecular hydrogen bonds and is thought to interrupt hydrophobic interactions [10]. A first experiment was conducted to determine the optimal concentration of the peptide solution for CD measurements, which was found to be at 100 µM, showing the best high signal to noise (Figure 15 a). In aqueous environment, the CDR3-peptide adopted mostly a random coil structure. The term "random coil" structure is not implicating that the adopted structure in water is not well defined. The α-helical conformation is indicated by the formation of two minima at around 208 and 220 nm (Figure 15 b).

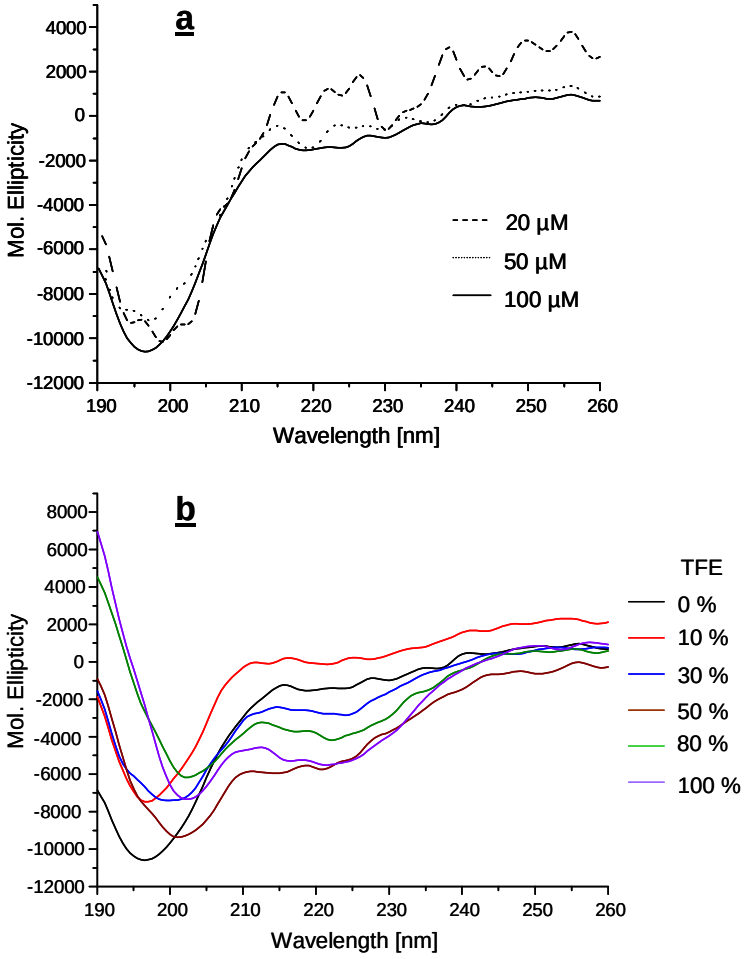

Figure 15: **a** CD spectra of CDR3-peptide at 20, 50 and 100 µM concentration. **b** CD spectra of the CDR3-peptide at different concentrations of TFE. The peptide mostly adopts random coil structure in water and it shows a slight tendency to adopt α-helical structures when TFE is present in high concentrations. The α-helical structure is characterized by two minima (~208 nm and ~220 nm).

2.2 Epitope elucidation of Aβ-specific single-chain antibodies

The identification and structural characterization of the Aβ epitope recognized by Aβ-nanobodies is one of the main goals of this dissertation. Epitope mapping is a key method for the identification of specific interaction structures. For the elucidation of the specific binding sites in peptides and proteins and for the identification of the epitopes, several analytical methods were developed [129-131]. In order to identify the Aβ-epitope peptide, proteolytic excision and extraction were carried out in combination with mass spectrometry.

2.2.1 Structure analysis of Aβ-peptides by proteolytic degradation and mass spectrometry

The proteolytic degradation of Aβ(1-40) peptide with different proteases was performed. Several proteases were used for the degradation of Aβ(1-40) peptide, e.g. trypsin, chymotrypsin, GluC-protease and LysC-protease.

Proteases, proteinases or proteolytic enzymes are enzymes that catalyze the cleavage of peptide bonds in proteins and are present in many cells, where they have different functions, such as being involved in important regulatory pathways, in cell growth and apoptosis or degrading misfolded proteins. One example of these enzymes is represented by serine proteases (trypsin, chymotrypsin) so called because in the active site an essential serine residue specific for the enzymatic activity is present. Both enzymes are endopeptidases, because the cleavage occurs in the internal peptide bond, but they have different specificities [132].

Chymotrypsin has a large hydrophobic binding pocket, cleaves peptide bonds selectively at the C-terminal side of the large hydrophobic amino acids such as phenylalanine (Phe), tryptophan (Trp), tyrosine (Tyr), methionine (Met) and other amide bonds in peptides at slower rates, such as leucine (Leu). Trypsin is a monomeric enzyme and the aspartate replaces serine at the bottom of the binding pocket. The enzyme is specific for cleaving peptide bonds towards the carboxyl terminus of the positively charged residues arginine and lysine [133]. All serine

proteases (e.g. trypsin, chymotrypsin) have the same catalytic mechanism. Chymotrypsin has the active site marked by serine (Ser) 195. The side-chain of Ser195 interacts with imidazole ring of histidine (His) 57, which further interacts to the carboxylate group of aspartate (Asp) 102. This arrangement of amino acids is called catalytic triad [134, 135]. In trypsin, an aspartate residue (position 189) is present in place of a serine residue in chymotrypsin and forms a salt bridge with the positively charged group at the end of the substrate lysine and arginine side chains [136].

Aβ(1-40) peptide was first digested with trypsin at an enzyme to substrate ratio of 1:20, for 4 h at 28 °C. The digestion was carried out in PBS buffer. The MALDI-TOF mass spectrum of the Aβ(1-40) after trypsin digestion is shown in Figure 16. The results are summarized in Appendix 4.

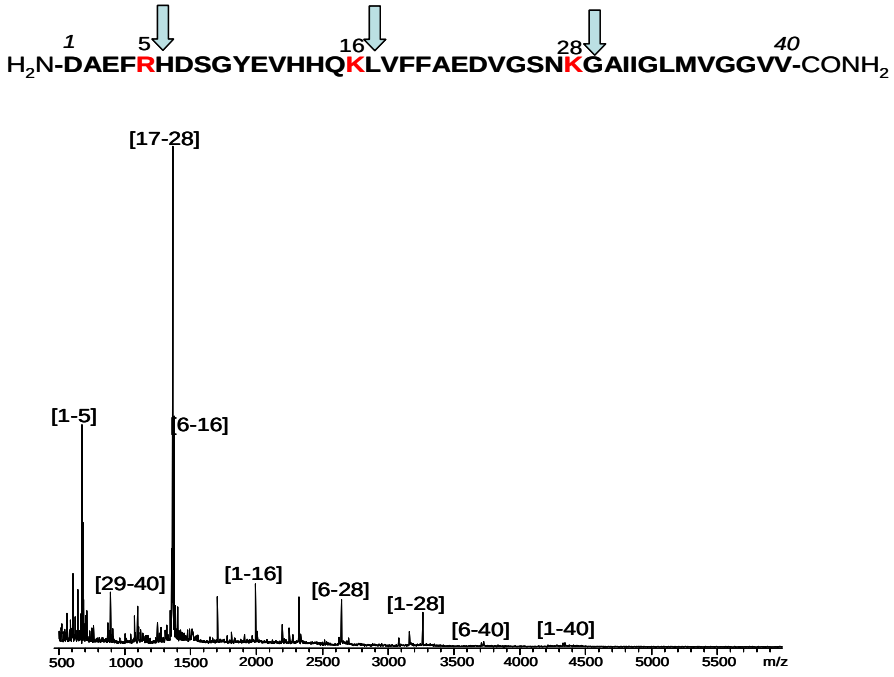

Figure 16: MALDI-TOF mass spectrum of Aβ(1-40) tryptic digestion in solution. All expected peptide fragments are present in the mass spectrum.

As a further proteolytic enzyme, chymotrypsin was used in order to analyse the cleavage pattern of Aβ peptide. The peptide was digested at an enzyme to substrate ratio of 1:50, for 3 h at 37 °C in PBS. The MALDI-TOF mass spectrum of the chymptryptic digestion showed in Figure 17 indicated that the released peptide fragments covered the entire sequence. The results from the chymotryptic digestion

of Aβ(1-40) peptide with experimental and calculated molecular masses of the resulted fragments are summarized in Appendix 5.

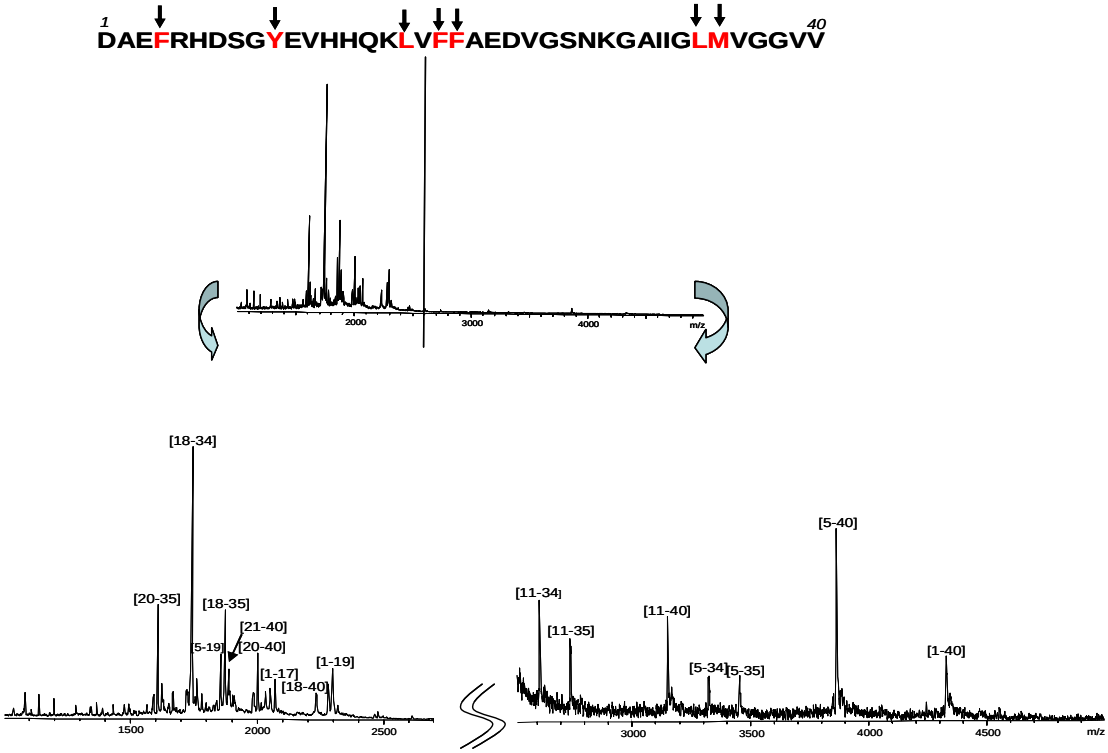

Figure 17: MALDI-TOF mass spectrum of Aβ(1-40) digested in solution with chymotrypsin.

The proteolytic enzyme GluC was further used. GluC is an endoprotease which cleaves the peptide bonds specifically at the C-terminal of the glutamic and aspartic acid residues. Aβ(1-40) peptide was digested at an enzyme to substrate ratio of 1:20 for 2 h at 37°C in PBS. The MALDI-TOF mass spectrum of Aβ(1-40) peptide after digestion with endoprotease GluC in solution showed almost all expected peptide fragments (Figure 18). In Appendix 6, the results from the GluC digestion of Aβ(1-40) peptide are summarized.

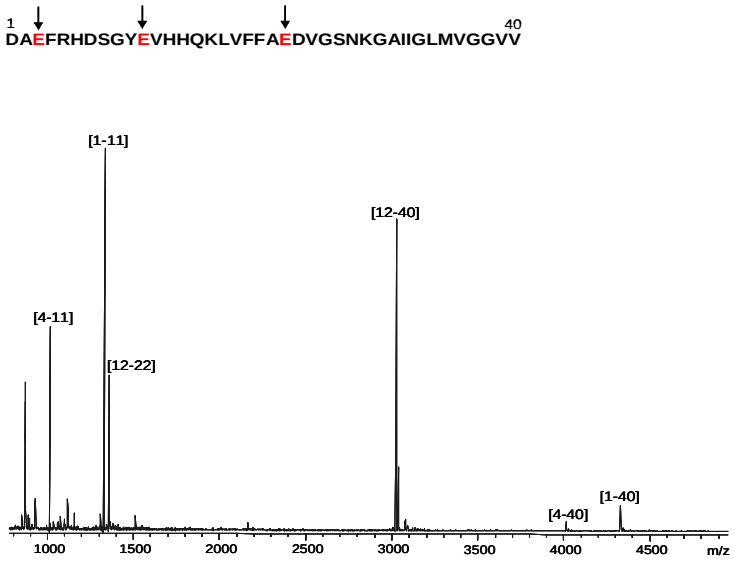

Figure 18: MALDI-TOF mass spectrum of Aβ(1-40) peptide using endoprotease GluC in solution digestion.

In conclusion, all results obtained after cleaving the Aβ(1-40) by different proteolytic enzymes covered the complete peptide sequence. According to these results, epitope elucidation studies presented in Chapter 2.2.2 indicate that the N- terminal and the middle part of the Aβ(1-40) are the most accessible for the antibody or protein binding, and lead to the identification of the Aβ- epitope peptide.

2.2.2 Affinity-mass spectrometric identification of an Aβ- epitope recognized by Aβ- nanobodies

Affinity- mass spectrometry method is based on the specific and reversible interaction between two molecules, for example an antibody and an antigen. The approach consists in the covalent immobilization of one of the two binding partners to an insoluble matrix and transfer of this matrix into a chromatographic column (Figure 19). By selective adsorption, only the complementary binding partner is bound reversibly to the affinity column, while other molecules are washed away from the column. Through a change of the solvent composition (adding acids such as 0.1 % trifluoroacetic acid), the complex is dissociated from the column and the binding partner is eluted.

The main application of affinity mass-spectrometry is to purify biological active substances such as antibodies, nucleic acids or enzymes. Furthermore, this

approach is used for the concentration of diluted protein solutions and to separate the denatured proteins from the biological active ones [137, 138]. There are several methods available for covalent immobilization of biomolecules, e.g. peptides or proteins, on the matrix. The immobilization of Aβ-nanobodies on N-hydroxysuccinimide (NHS)-activated Sepharose was used for identification of Aβ-epitope. This method has some advantages, such as chemical stability of the formed amide bond and the high coupling yield of immobilization. The binding of the biomolecules to the matrix material has been done via the amino group of the N-terminus and lysine side chains, which attack nucleophilic the carboxylic acid ester groups of the activated Sepharose. After the removal of succinimide group, a stable amide bond is formed by which the molecules are permanently immobilized to the matrix (Figure 19 b) [139].

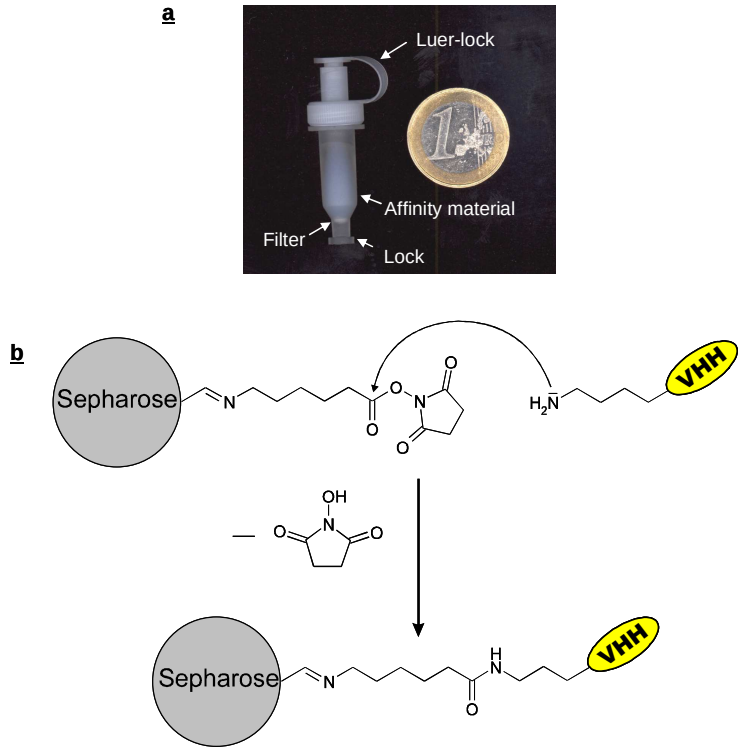

Figure 19: **a** Schematic representation of an affinity column: the microcolumn is filled with NHS-activated Sepharose. **b** Reaction of immobilizing the Aβ-nanobodies on the NHS-activated Sepharose. The reaction takes place at the free amino-terminus of the nanobody molecule with the elimination of NHS molecule. The new bond is chemically very stable.

For the immobilization on the NHS activated Sepharose, the nanobody was first dissolved in coupling solution and then added to the matrix. After 2 h incubation at 20 °C the matrix was washed sequentially with blocking buffer and washing buffer.

The blocking step was necessary for the removal of the excess of the reactive groups, since otherwise would exist a possibility that the peptides or proteins used in the next affinity step would covalently bind to the matrix. The microcolumn was then stored at 4 ^{o}C in PBS. Due to the covalent binding of the nanobody to the Sepharose matrix the affinity column could be used many times without considerable loss of affinity.

For the identification of the Aβ-epitope, both epitope excision- and extraction-mass spectrometry were performed. In the epitope excision approach, the antigen was first bound to the immobilized antibody and then a proteolytic enzyme added. The peptide fragments that contain the epitope remained bound to the antibody and dissociated from the antigen-antibody complex under acidic condition [31]. This characteristic stability of antigen-antibody complexes has been employed for the development of a general mass spectrometric approach for identifying protein epitopes, as initially shown by limited proteolytic cleavage of immune complexes using mass spectrometric peptide mapping [31]. Epitope excision has the advantage of being suitable for both linear and discontinuous epitopes (Figure 20) [32, 94, 130]. In contrast to epitope excision, in epitope extraction the antigen is proteolytically cleaved before reacting with the antibody, and the peptide fragments that contain the epitope are selectively bound to the antibody. The unbound peptides that remain in the supernatant are removed by washing. Epitope extraction is frequently best suited for the determination of linear epitopes [140, 141]. For mass spectrometric analysis of the epitope, the affinity-bound peptides are eluted from the antibody using 0.1 % TFA [94, 142], 4 M $MgCl_2$ [31] or 0.1 M glycine (pH 2.3) [129, 143].

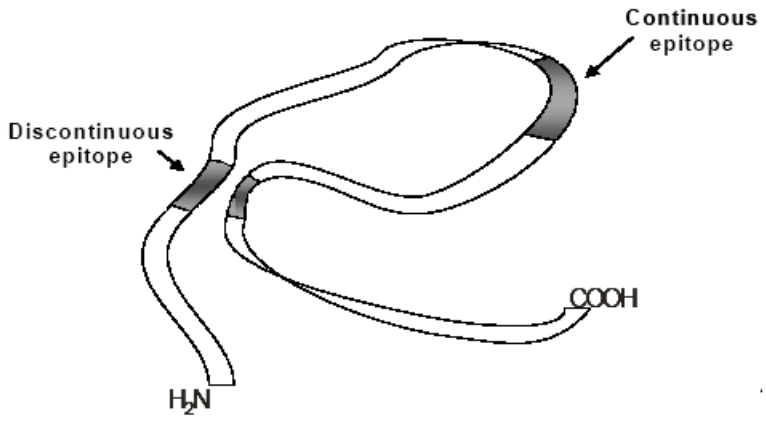

Figure 20: Schematic representation of different types of epitopes: a continuous (linear) epitope containing a contiguous series of amino acids and a discontinuous epitope consisting

of amino acid residues localized on different regions of the amino acid sequence of the antigen.

Both epitope excision- and extraction-mass spectrometry were employed to identify the Aβ- epitope of the Aβ- nanobodies. For epitope excision, Aβ(1-40) was added to the Nb_3 microcolumn, and the trypsin protease added to the immune complex. The trypsin cleaves areas from Aβ-peptide which is not involved in the complex with the antibody. The non-epitope peptides (supernatant) were removed by washing with PBS and the nanobody-bound peptide fragment mixture eluted by acidification with 0.1 % TFA. The mass spectrum of the elution fraction from the Nb_3 microcolumn revealed the presence of two epitope fragments corresponding to Aβ(17-28) and Aβ(1-28), respectively.

In the epitope extraction experiment, Aβ(1-40) was first digested in solution by trypsin and the proteolytic fragments characterized by MALDI-TOF-MS, which showed all expected cleavage products. The tryptic mixture was then added to the Nb_3 column. The supernatant fraction contained several fragments corresponding to Aβ(17-28), Aβ(1-16), Aβ(17-40), Aβ(6-40) and Aβ(1-40), and subsequent washing was performed until no background ions were detected. In the MALDI-TOF mass spectrum of the elution fraction a single major peak was found at m/z 1326.5, which corresponded to Aβ(17-28) (Figure 21).

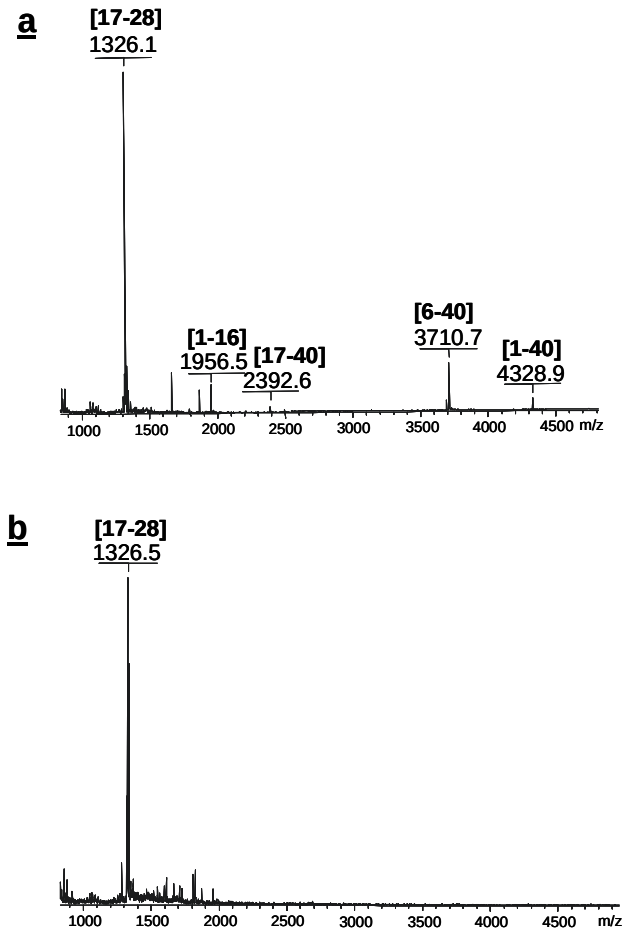

Figure 21: MALDI-TOF mass spectrum of **a** the supernatant fraction obtained after digestion of Aβ(1-40) with trypsin protease and addition of the fragment mixture to the Nb_3 affinity microcolumn. **b** the elution fraction after proteolytic extraction of Aβ(1-40) with trypsin.

In order to ascertain the minimal epitope recognized by the Nb_3, Aβ(1-40) was digested with additional endoproteases. After treatment of the Nb_3-Aβ(1-40) complex with endoproteinase GluC, in the elution fraction only a single fragment at m/z 3022 (Aβ(12-40)) remained bound to the affinity matrix; consistent with the results provided by epitope excision, the fragment Aβ(12-40) was identified upon epitope extraction. Proteolytic cleavage of Glu-22 was not observed confirming that this residue is shielded in the immune complex.

The Aβ(12-40) peptide identified by proteolytic excision with GluC-protease was synthesized by SPPS and used for epitope excision and epitope extraction using endoproteinase LysC. After epitope excision using Lys C- protease, the fragments Aβ(12-28), Aβ(17-28) and Aβ(12-40) were identified in the elution fraction (Figure 22 a). Using epitope extraction, Aβ(12-40) was digested with LysC in solution and the resulting peptide fragment mixture subjected to the Sepharose-immobilized

nanobody. The mass spectrum of the elution fraction contained an ion at m/z 1326.06 corresponding to Aβ(17-28), together with Aβ(12-40) at m/z 3022.06 (Figure 22 b).

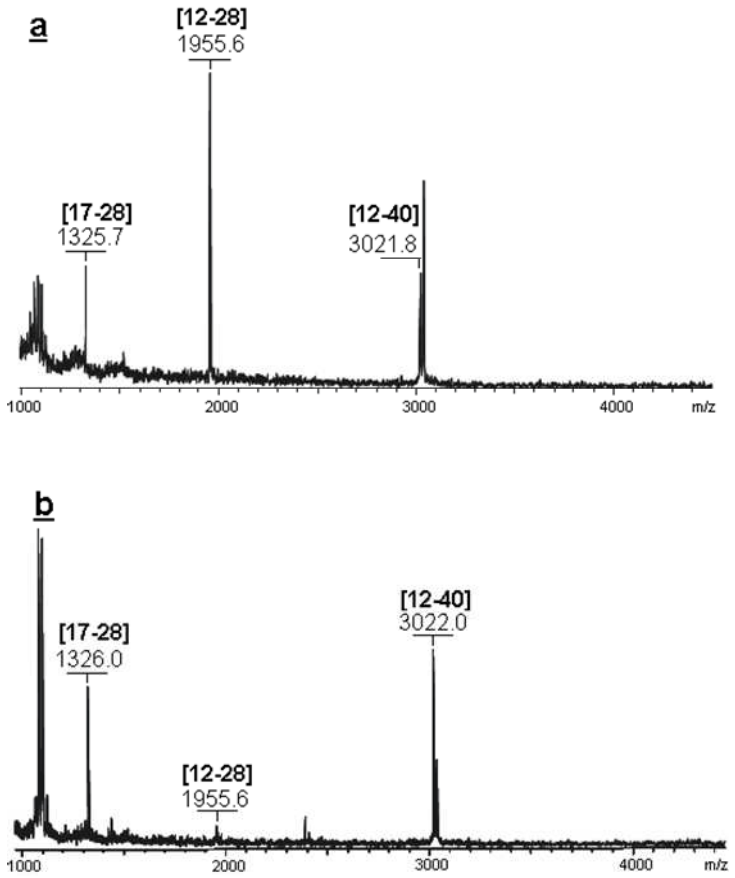

Figure 22: MALDI-TOF mass spectrum of **a** the elution fraction after proteolytic excision of Aβ(12-40) with immobilized Nb_9 on the affinity microcloumn using LysC -protease. Three fragments can be observed in the spectrum, the smallest fragment which remained bound to the nanobody column was Aβ(17-28). **b** the elution fraction after proteolytic extraction of Aβ(12-40) with Nb_9 using LysC digestion. The spectrum showed three fragments, the smallest one which remained bound to the Aβ-nanobody column was Aβ(17-28).

Further epitope excision and extraction- MS experiments were carried out with Aβ(1-40) using α-chymotrypsin. MALDI-TOF mass spectrometric analysis of the elution fractions after epitope excision and extraction experiments showed several fragments covering the sequence Aβ(17-28), which confirmed the binding epitope to the nanobodies .

The results of proteolytic excision and extraction of Aβ(1-40) with Nb_3 immobilized nanobody are summarized in Table 1.

Table 1: a) Peptide fragments obtained after epitope excision and epitope extraction of Aβ(1-40) with Nb_3 using different enzymes. b) Summary of the epitope excision and extraction of Aβ(12-40) with Nb_3.

a)

Enzyme	$[M+H]^+_{exp/calc}$	Aβ fragment	Sequence
Trypsin	2644.3 / 2644.8	[6-28]	HDSGYEVHHQKLVFFAEDVGSNK
	1326.5 / 1326.4	[17-28]	LVFFAEDVGSNK
Chymotrypsin	1886.1 / 1886.2	[21-40]	AEDVGSNKGAIIGLMVGGVV
	2033.6 / 2033.3	[20-40]	FAEDVGSNKGAIIGLMVGGVV
	2280.1 / 2279.7	[18-40]	VFFAEDVGSNKGAIIGLMVGGVV
	3152.1 / 3151.7	[11-40]	EVHHQKLVFFAEDVGSNKGAIIGLMVGGVV
	3456.6 / 3455.9	[5-35]	RHDSGYEVHHQKLVFFAEDVGSNKGAIIGLM
	3325.5 / 3325.7	[5-34]	RHDSGYEVHHQKLVFFAEDVGSNKGAIIGL
	3866.9 / 3867.4	[5-40]	RHDSGYEVHHQKLVFFAEDVGSNKGAIIGLMVGGVV
GluC	3022.3 / 3021.5	[12-40]	VHHQKLVFFAEDVGSNKGAIIGLMVGGVV
	4329.4 / 4329.8	[1-40]	DAEFRHDSGYEVHHQKLVFFAEDVGSNKGAIIGLMVGGVV

b)

Enzyme	$[M+H]^+_{exp/calc}$	Aβ fragment	Sequence
Lys C	1326.2 / 1326.4	[17-28]	LVFFAEDVGSNK
	1956.5 / 1956.2	[12-28]	VHHQKLVFFAEDVGSNK

Identical epitope excision and extraction experiments were performed with the Nb_9. Epitope excision using trypsin provided the fragments Aβ(6-40) and Aβ(17-28), while after epitope extraction, the elution fraction revealed the major epitope peptide Aβ(17-28) together with minor abundances of Aβ(6-28) and Aβ(1-28). Using GluC-protease, in the elution fraction upon epitope extraction with immobilized Nb_9, the fragments Aβ(12-40), Aβ(4-40) and Aβ(1-40) were identified. The elution fraction after epitope excision revealed the Aβ(12-40) fragment, confirming that the epitope is not contained in the *N*-terminal sequence and indicating that the nanobody recognizes the middle domain of Aβ. The results for epitope excision and extraction for immobilized Nb_9 are summarized in Table 2.

Table 2: a) Peptide fragments obtained after epitope excision and epitope extraction of Aβ(1-40) with Aβ-nanobody (Nb_9) using different enzymes. b) Summary of the epitope excision and extraction of Aβ(12-40) with Aβ-nanobody (Nb_9).

a)

Enzyme	$[M+H]^+_{exp/calc}$	Aβ fragment	Sequence
Trypsin	1325.9 / 1326.4	[17-28]	LVFFAEDVGSNK
GluC	3711.7 / 3711.2	[6-40]	HDSGYEVHHQKLVFFAEDVGSNKGAIIGLMVGGVV
	4013.8 / 4013.5	[4-40]	FRHDSGYEVHHQKLVFFAEDVGSNKGAIIGLMVGGVV
	3022.3 / 3021.5	[12-40]	VHHQKLVFFAEDVGSNKGAIIGLMVGGVV
	4329.4 / 4329.8	[1-40]	DAEFRHDSGYEVHHQKLVFFAEDVGSNKGAIIGLMVGGVV

b)

Enzyme	$[M+H]^+_{exp/calc}$	Aβ fragment	Sequence
Lys C	1325.7 / 1326.4	[17-28]	LVFFAEDVGSNK
	1955.6 / 1956.2	[12-28]	VHHQKLVFFAEDVGSNK

Overall, using different proteolytic enzymes, it was possible to obtain detailed information about the sequences recognized by the Nb_3 and Nb_9. The minimal sequence (17-28) was determined by epitope excision- and extraction- mass spectrometry using trypsin and LysC for the Nb_3, and trypsin and LysC for Nb_9. The information provided by the specific enzymes (trypsin, α-chymotrypsin and GluC) significantly contributes to the unequivocal identification of the epitope. After tryptic digestion, the *N*-terminal part of the Aβ-peptide was cleaved. Proteolytic cleavage of Glu-22 was not observed confirming that this residue is shielded in the immune complex. Noteworthy, the Phe-20 residue is cleaved at very low rate indicating that the activity of α-chymotrypsin at this site might be sterically hindered. The mass spectrometric approach for the elucidation of the epitope recognized by the Nb_3 and Nb_9 leads to the identification of the middle sequence Aβ(17-28) (LVFFAEDVGSNK).

2.2.3 Mass spectrometric characterization of Aβ-peptides

In order to perform the affinity mass spectrometry experiments and to characterize the identified epitope, several Aβ peptides were synthesized by solid phase peptide synthesis (SPPS) using Fmoc/t-Butyl chemistry.

Aβ(1-40) peptide was first synthesized by SPPS using Fmoc chemistry on a semi-automatic peptide synthesizer EPS-221 (Intavis, Germany) on Rink Amide MBHA resin. The C-terminal amino acid of the peptide is attached to the Rink Amide MBHA resin. The resin is insoluble in the solvents used for the peptide synthesis (e.g. DMF), but has the tendency to swell in volume in these solvents. The amino acids used in SPPS are most often Fmoc based temporary α-amino protected. If the amino acid side chain contains a functional group, a “permanent protected group” such as t-butyl (trityl, 4-methyloxytrityl) is used. The permanent protecting group is usually stable during SPPS and is cleaved together with the peptide from the resin in the last step.

The first step in the SPPS was the removal of the N-terminal Fmoc protecting group from the resin using a mixture of 2 % DBU (1,8-diaza-bicyclo[5.4.0]undec-7-ene), 2 % piperidine in DMF (dimethylformamide). The next step was the activation of the carboxyl group of the N-terminal-Fmoc protected amino acid by benzotriazol-1-yl-N-oxy-tris-pyrrolidinophosphonium-hexafluorophosphate (PyBop/NMM) in order to attach the first amino acid to the resin. The resin was washed with DMF after every synthesis cycle to remove all reagents or by-products which were in excess. The deprotection and coupling steps were repeated until the desired peptide was obtained. After the completion of synthesis, the peptides were cleaved from the resin. The yield of Aβ(1-40) after solid phase peptide synthesis and purification was around 30 - 40%.

Due to the high hydrophobicity of the C-terminal domain resulting in a high propensity to aggregate in solution as well as on-resin during the elongation of the peptide, Aβ(1-40) was further synthesized on a Tenta Gel RRam resin (Rapp polymers). The resin is employed for difficult sequences. Furthermore, Aβ(1-40), Aβ(12-40) and Aβ(17-28) were synthesized manually by Fmoc/t-butyl strategy on Tentagel RRam resin (Table 3). The Fmoc- deprotection was performed using a mixture of 2 % DBU,

2 % piperidine in DMF. The coupling of the C-terminal of the N-α-Fmoc protected amino acid was carried out in a solution containg a mixture of PyBoP and NMM (N-methyl-morpholine) in DMF. The activated amino acid was then added to the resin. The efficacy of each coupling step was established by different colorimetric tests, such as Kaiser test, Bromophenol blue and chloranil test. The Kaiser test is based on the reaction of ninhydrin with primary amines, the bromophenol blue test can detect all types of amines and the chloranil test is for the detection of secondary amino groups.

Table 3: Aβ peptides synthesized by SPPS using Fmoc/t-butyl strategy.

Peptide	**Sequence**	**$[M+H]^+_{calc}$ / $[M+H]^+_{exp}$**	**Δm (ppm)**
Aβ(1-40)	DAEFRHDSGYEVHHQKLVFFAEDV GSNKGAIIGLMVGGVV	4329.9 / 4329.0	207
Aβ(12-40)	VHHQKLVFFAEDVGSNKGAIIGLMV GGVV	3022.5 / 3022.7	66.1
Aβ(17-28)	LVFFAEDVGSNK	1324.6 / 1324.9	227

After the cleavage from the resin, the synthesised peptides were precipitated with t-butylmethyl-ether, washed with diethyl ether and dissolved in 5 % acetic acid prior to freeze-drying.

The molecular weight of crude peptides was determined by mass spectrometry. Crude peptides were then purified by reverse phase-high performance chromatography (RP-HPLC) on a Vydac C4 column (250×10 mm I.D; Grace Davison). The column is usually employed for the separation of hydrophobic peptides and proteins. A linear gradient elution (0 min 0 % B; 5 min 0 % B; 50 min 90 % B) with solvent A (0.1 % TFA in water) and solvent B (80 % acetonitrile in 0.1 % TFA) has been applied.

For purified peptides, analytical RP-HPLC using a Vydac C4 column (250×4.6 mm I.D.) with 5 µm silica (300 Å pore size) (Hesperia CA) was carried out and the major peak was analyzed by mass spectrometry. The analytical HPLC of Aβ(1-40) indicated a major peak at 31.9 retention time. The fraction was collected, lyophilized

and analyzed by MALDI mass spectrometry. The MALDI-TOF mass spectrum of the Aβ(1-40) showed a molecular $[M+H]^+$ ion at 4329.0 and the $[M+2H]^{2+}$ ion at 2165.1 (Figure 23).

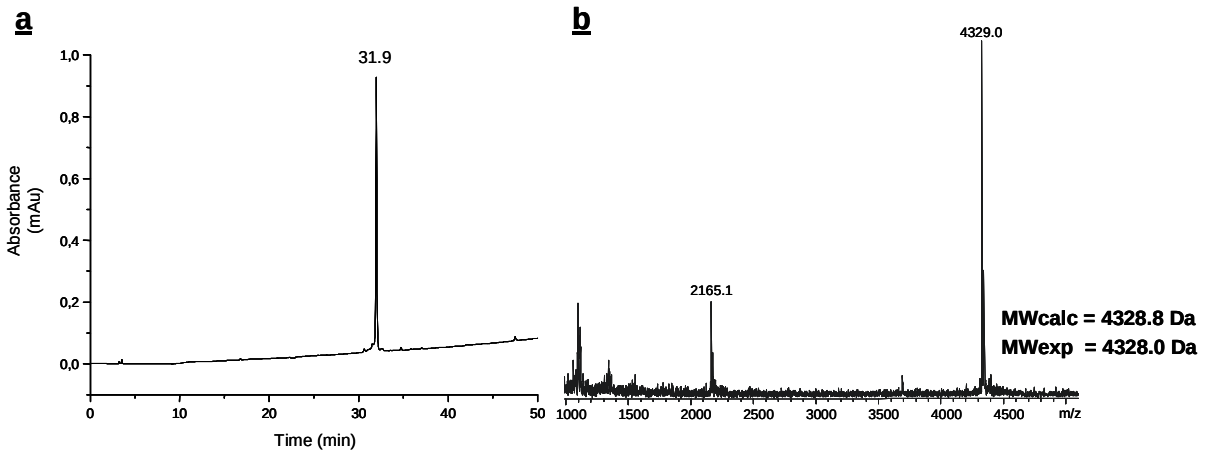

Figure 23: a. RP-HPLC and b. the corresponding mass spectrum of Aβ(1-40).

Aβ(17-28) epitope peptide was synthesized by SPPS. The purified Aβ(17-28) peptide was analyzed by analytical HPLC and mass spectrometry. In the MALDI-TOF mass spectrum of the purified Aβ(17-28) a signal at m/z 1324.9, corresponding to $[M+H]^+$ ion could be identified (Figure 24).

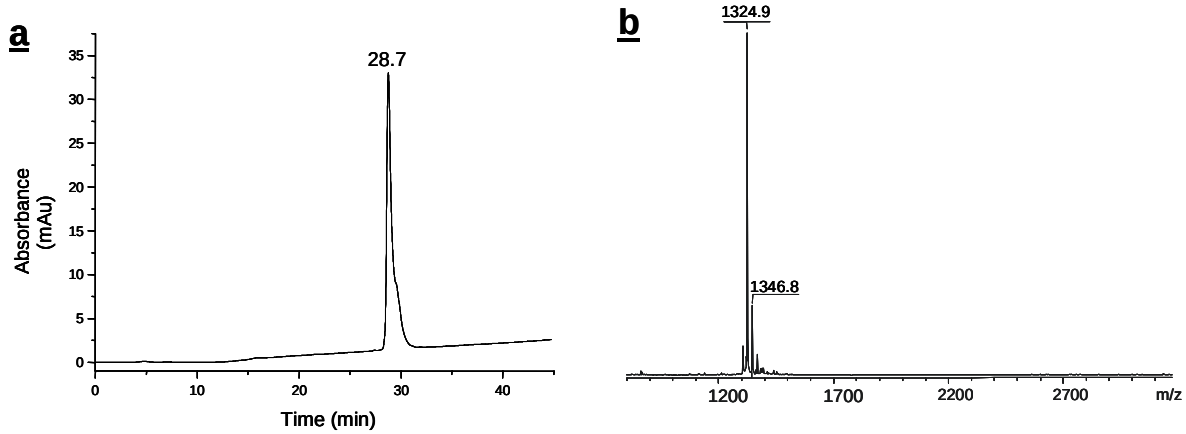

Figure 24: Analytical RP-HPLC profile and MALDI-TOF mass spectrum of Aβ(17-28).

After epitope identification (Chapter 2.2.2), the following biotinylated amyloid peptides encompassing the identified epitope were synthesized using Fmoc/t-butyl chemistry: Biotin-G_5-Aβ(1-40), Biotin-G_5-Aβ(12-40), Biotin-G_5-Aβ(1-16) and Biotin-G_5-Aβ(17-28), Biotin-G_5-Aβ(20-30), Biotin-G_5-Aβ(20-37). Alanine mutated Biotin-G_5-Aβ(17-28) peptides were also prepared in order to identify the functional epitope. The syntheses

were carried out on a Rink amide MBHA resin using a semi-automated peptide synthesiser. The activation of the carboxyl groups was performed with PyBop/NMM in DMF. At the N-terminal part five glycines were added. After completion of the synthesis, the N-terminus was biotinylated on the resin using 5 equiv of D-(+) Biotin. After cleavage of the crude peptide from the resin, the products were purified by semi-preparative RP-HPLC. The pure peptides were characterized by analytical RP-HPLC and mass spectrometry (Figure 25).

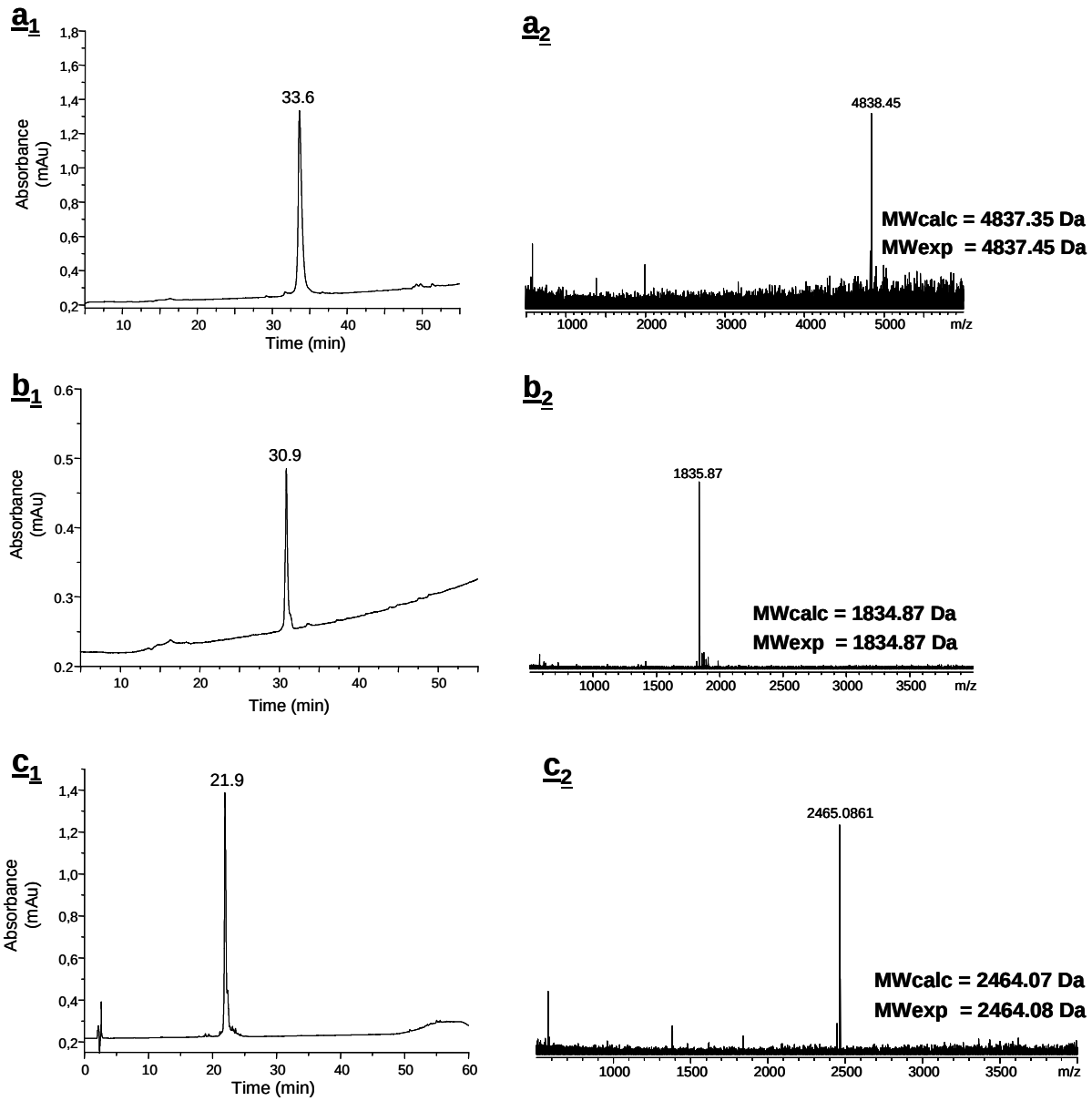

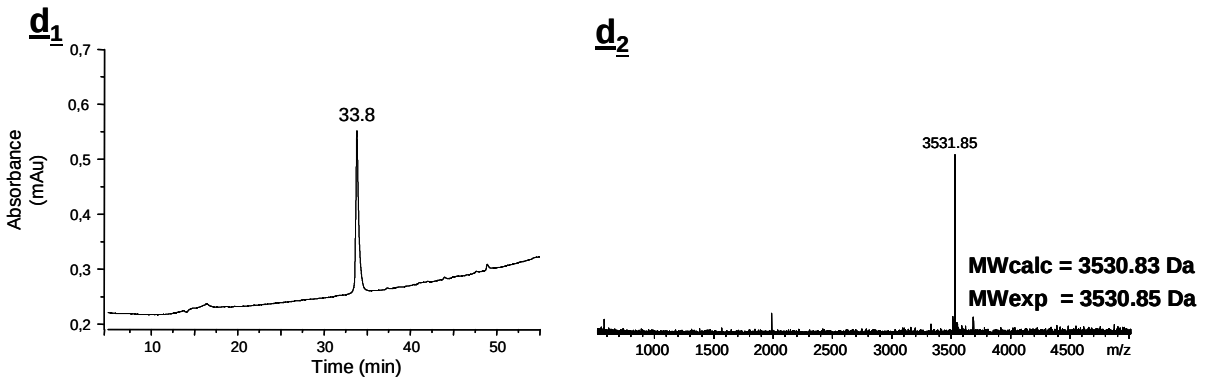

Figure 25: **a**$_1$, **a**$_2$: RP-HPLC and MALDI-FTICR - mass spectrum of biotin-G_5 Aβ(1-40); **b**$_1$, **b**$_2$: RP-HPLC and MALDI-FTICR mass spectrum of biotin G_5 Aβ(17-28); **c**$_1$, **c**$_2$: RP-HPLC and mass spectrum of biotin-G_5 Aβ(1-16); **d**$_1$, **d**$_2$: RP-HPLC and MALDI-FTICR mass spectrum of biotin-G_5 Aβ(12-40).

2.2.4 Secondary structure determination of the Aβ(17-28) epitope peptide

Conformational analysis of the Aβ(17-28) epitope was performed by circular dichroism (CD) spectroscopy. The method has been used for monitoring the conformational changes and determination of secondary structure of peptides and proteins. All spectra were recorded at 25°C in quartz cells of 0.1 cm path-length, within a wavelength range between 190 - 260 nm. The results were expressed as molar ellipticities. CD spectra recorded in water showed a negative band at 198 nm and a small shoulder around 225 nm (Figure 26 a). This result suggested the presence of a mixture of conformers, with predominance of an unordered structure. Changes of conformation were detected in the presence of TFE. TFE is known to preferentially stabilize proteins and peptides in ordered conformation [144, 145]. A helical conformation was observed in 30 % TFE/water up to 100 % TFE (v/v). The spectra recorded in 10 % TFE/water (v/v) showed a negative band at 200 nm, characteristic of a random coil conformation. An isodichroic point was observed at 202 nm (Figure 26 b) when the spectra acquired at different concentrations of TFE were superimposed, suggesting a random coil - α-helix transition [146, 147].

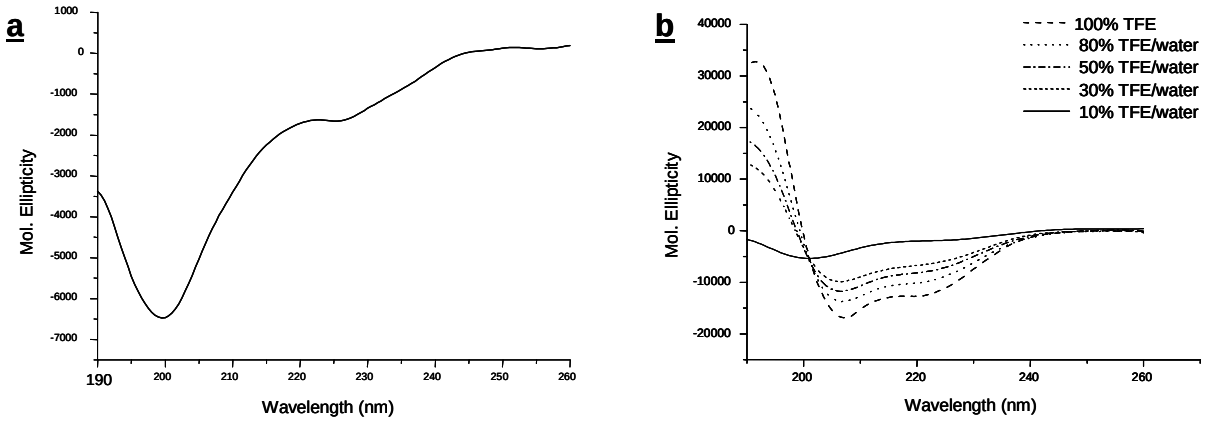

Figure 26: CD spectra of Aβ(17-28) in: a) water b) 10%, 30%, 50%, 80% and 100 % TFE.

In order to further characterize the changes in the structure of Aβ(17-28) epitope, model studies were performed using the molecular modelling programs Hyperchem and BallView 1.3.2. The three-dimensional solution structure of Aβ(1-40) has been determined using NMR spectroscopy at pH 5.1, in aqueous sodium dodecyl sulfate (SDS) micelles and was published in the Protein Data Bank under the entry 1 BA4 (pdb file) [148]. The corresponding pdb file was opened with BallView 1.3.2. The amino acids 17 to 28 were selected and then copied in Hyperchem. Structural model is shown in Figure 27 in stick representation. The backbone of the peptide is shown as ribbon figure. Aβ(17-28) epitope peptide showed a structured part represented by an α-helix.

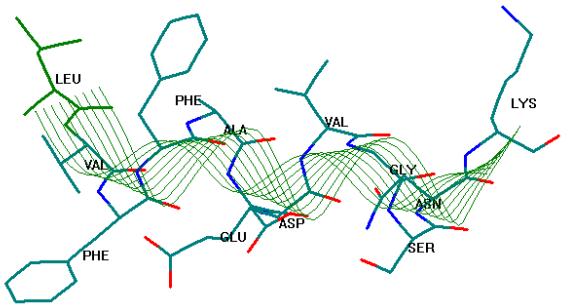

Figure 27: Molecular modelling of the Aβ(17-28) peptide. The structure was determined using two modelling programs BallView 1.3.2 and Hyperchem 5.0.

2.2.5 Binding studies of single-domain antibodies to Aβ-peptides

Epitope excision and extraction in combination with mass spectrometry were employed for the identification of the epitope recognized by Aβ- nanobodies and led to the identification of the Aβ(17-28). Considering these results, a further goal of the dissertation was to compare the specificity and affinity of the Aβ(17-28) epitope by indirect ELISA, using synthetic peptides with and without Aβ(17-28) sequence. The peptides Aβ(1-40), Aβ(12-40), Aβ(17-28), Aβ(20-30), Aβ(21-37), Aβ(1-16), each elongated by a pentaglycine spacer and biotinylated at the *N*-terminus, were prepared by SPPS as presented in the Experimental part. For ELISA binding studies, the Aβ- nanobodies were first coated on microtiter plates at a fixed concentration (2.5 ng/µL) and the biotinylated Aβ-peptides added after blocking the unspecific binding sites (Figure 28). The bound biotinylated peptides were detected by an HRP-conjugated antibody. After adding OPD/H_2O_2 substrate, the absorbance was measured using a Wallac 1420 Victor^2 ELISA Plate Counter at 450 nm. In order to provide accurate background subtraction, duplicate wells of each biotinylated peptide dilution without Aβ-nanobodies were used.

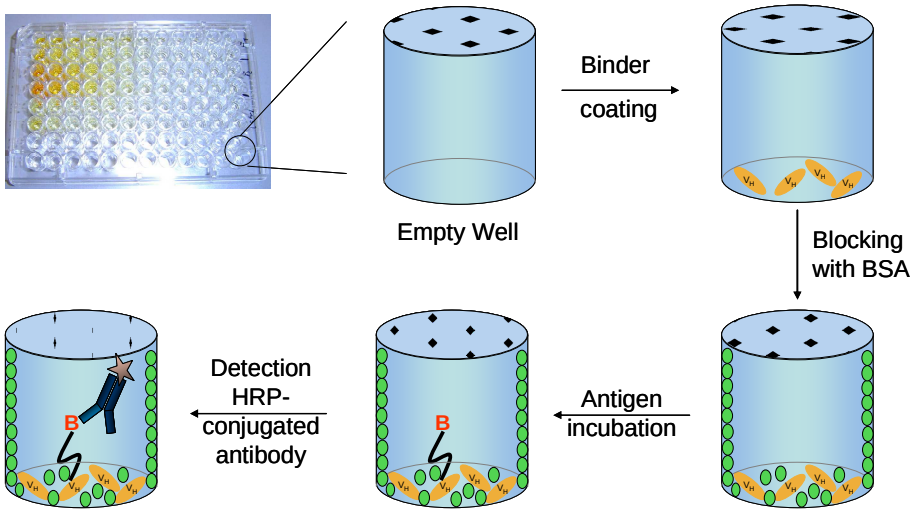

Figure 28: Schematic representation of the ELISA experiments. The Aβ-nanobody is bound on the ELISA plate. After blocking the unspecific binding sites, the antigen is added in 12 serial two fold dilutions. The antigen is detected by horse radish peroxidise (HRP)-conjugated antibody.

In order to comparatively determine the binding of the Aβ(1-40) on the Aβ-nanobodies 3 and 9, an ELISA experiment has been performed using antigen

dilutions and a fixed concentration of Aβ-nanobody as previously described. After ploting the OD_{450} (optical density at 450 nm) vs concentration (Figure 29), the concentration needed for obtaining an OD_{450} 1 was calculated in order to determine quantitatively the binding of the Aβ(1-40) to Nb_3 and Nb_9. The lowest amount of Aβ(1-40) which gave an OD_{450} = 1 in ELISA was 0.0427 µmol/L for Nb_3 and 0.0774 µmol/L for Nb_9. Biotin-G_5-Aβ(1-40) react with both Nb_3 and Nb_9.

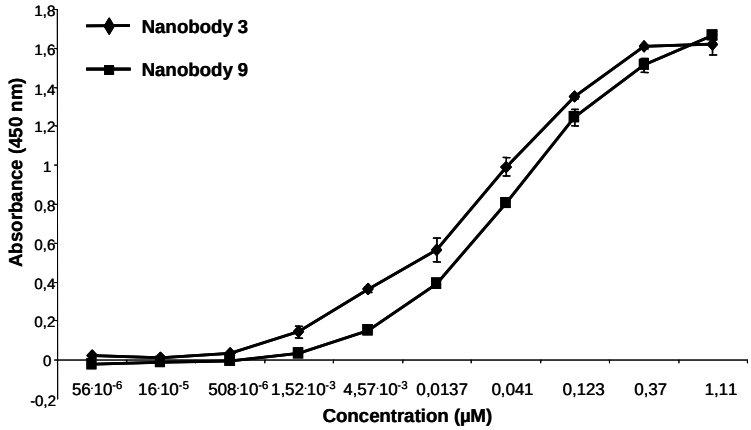

Figure 29: ELISA binding studies of nanobody 3 and 9 to β-amyloid peptide(1-40).

The comparison of the binding affinities of five peptides towards the Nb_3 is shown in Figure 30. The ELISA experiment shows that both N-terminal [1-16] and middle part [20-30] of the Aβ- peptide have no binding affinity to Nb_3. The lowest amount of Aβ(12-40) and of Aβ(17-28) respectively, which gave an OD_{450} = 1 in ELISA was 0.0799 µmol/L and 2,10 µmol/L respectively for Nb_3. These results indicate that Aβ(17-28) has a higher affinity for Nb_3 than Aβ(12-40).

Taken together, all Aβ-peptides comprising the Aβ(17-28) epitope bound to the Aβ-nanobodies, in agreement with the proteolytic- MS data.

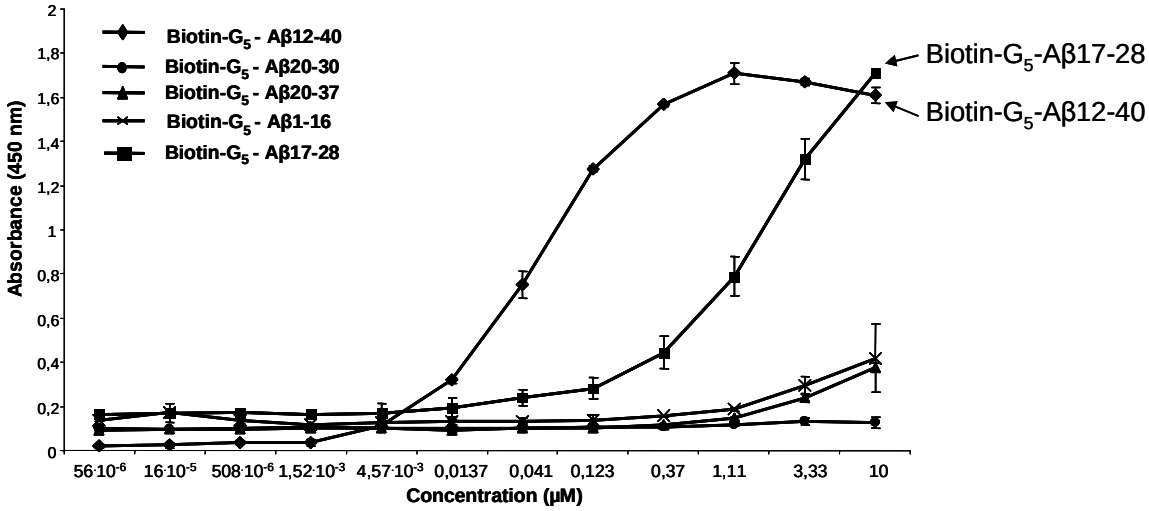

Figure 30: Binding of Nb_3 to amyloid peptides spanning different domains of Aβ(1-40): (■) Aβ(17-28), (♦) Aβ(12-40), (●) Aβ(20-30), (x) Aβ(1-16), (▲) Aβ(20-37). Background signals from wells without antigen have been subtracted.

2.2.6 Characterization of Aβ(17-28) epitope by alanine scanning mutagenesis

In order to characterize the functional Aβ(17-28) epitope peptide, the reactivities of the Aβ-nanobodies towards synthetic peptides containing alanine-single-site mutations (Figure 31 b) were investigated by ELISA. For the alanine scanning mutagenesis experiments all Aβ peptides were synthesized with a pentaglycine spacer and biotin at the N-terminus, in order to ensure free accessibility of the epitope.

The Nb_3 was immobilized on microtiter plates at a fixed concentration (2.5 µg/µL). After blocking, the alanine mutated peptides were added in twofold dilutions using a stock solution of 1 µg/µL. As detection antibody, HRP-goat anti-biotin antibody was used. In order to provide accurate background subtraction, duplicate wells of each peptide dilution without nanobody were used.

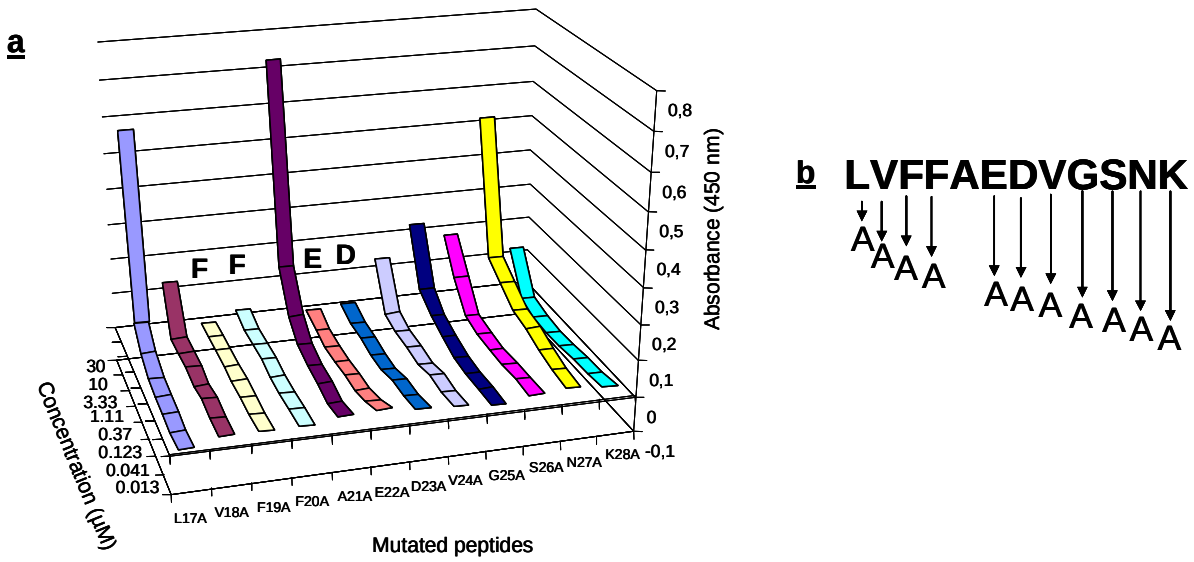

Figure 31: **a** Affinity binding studies showing the recognition of alanine-mutated peptides by the Nb_3, as measured by indirect ELISA. The peptides which contain alanine instead of L17, N27 show no binding. **b** Schematic representation of the alanine mutated epitope peptides that were used in ELISA experiments.

The results (Figure 31 a) indicate significant differences between the affinities of the alanine-mutated epitope peptides. Some amino acids are very important for the binding to the nanobody. The peptides Aβ(17-28)V18A, V24A, S26A, K28A had an intermediate affinity to the nanobody. The residues F19, F20, A21, E22 and D23 were found essential for the binding to the nanobody. The peptides with mutation F19A, F20A, E22A and D23A did not give any response in ELISA, while the wild-type A21 showed binding to the nanobody. The mutated peptides L17A and N27A indicated almost an identical binding to the nanobody, which was slightly decreased compared to the wild type peptide.

In summary, alanine scanning mutagenesis was found to be a good method for characterizing the functional epitopes.

2.3 Identification and quantification of interactions between Aβ-specific single-domain antibodies and Aβ-peptides by affinity-mass spectrometry

2.3.1 Affinity-mass spectrometric characterization of Aβ(1-40) and Aβ(17-28)

Affinity-mass spectrometry was used for the investigation of specific interaction between Aβ(1-40) and Aβ-nanobodies (Figure 32). For this purpose, Nb_3 and Nb_9 were separately immobilized on the matrix material (NHS-activated Sepharose). The coupling reaction took place via the ε-amino group of Lys residues or N-terminal α-amino groups.

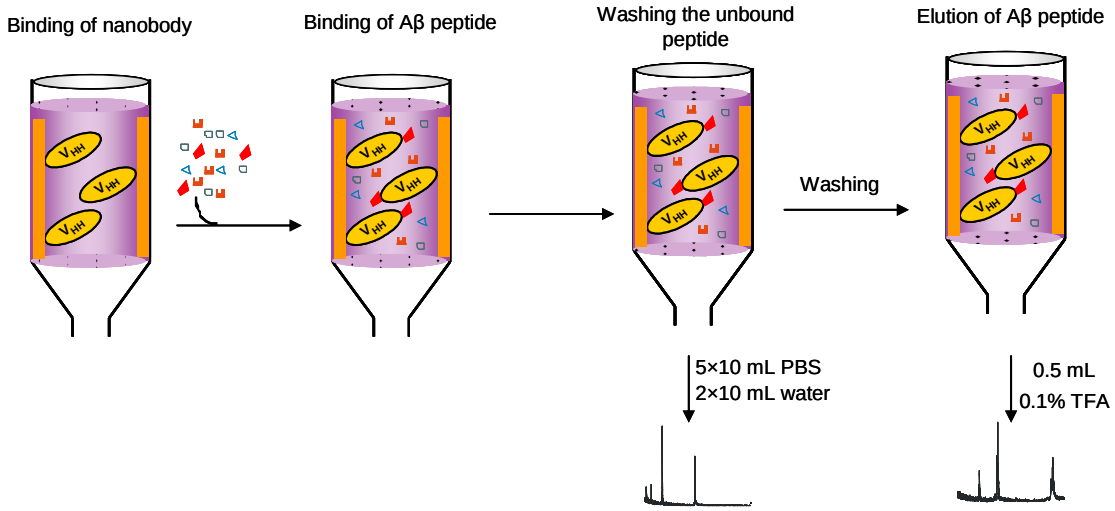

Figure 32: Schematic representation of the affinity- mass spectrometry method: nanobody immobilization, binding of the Aβ peptide, washing the unbound peptide and elution by changing the pH using 0.1 % TFA.

The peptide was dissolved in PBS buffer and exposed to the immobilized nanobody column. After 2 h incubation, the unbound peptide was removed, the column was washed several times and the antigen-nanobody complex was dissociated with 0.1 % TFA. The supernatant containing the unbound peptide, the washing and elution fractions were collected and analyzed by mass spectrometry (Figure 33). Mass spectrometric data showed the specific binding of Aβ(1-40) to Nb_3. No Aβ(1-40) peptide was detected in the washing fraction, but in the mass spectrum of the elution fraction signals at m/z 4329.8 and 2165.3, corresponding to $[M+H]^+$, respectively $[M+2H]^{2+}$ ions could be identified. Due to the covalent binding of the nanobody to the Sepharose matrix, the affinity column was used several times without considerable loss of affinity.

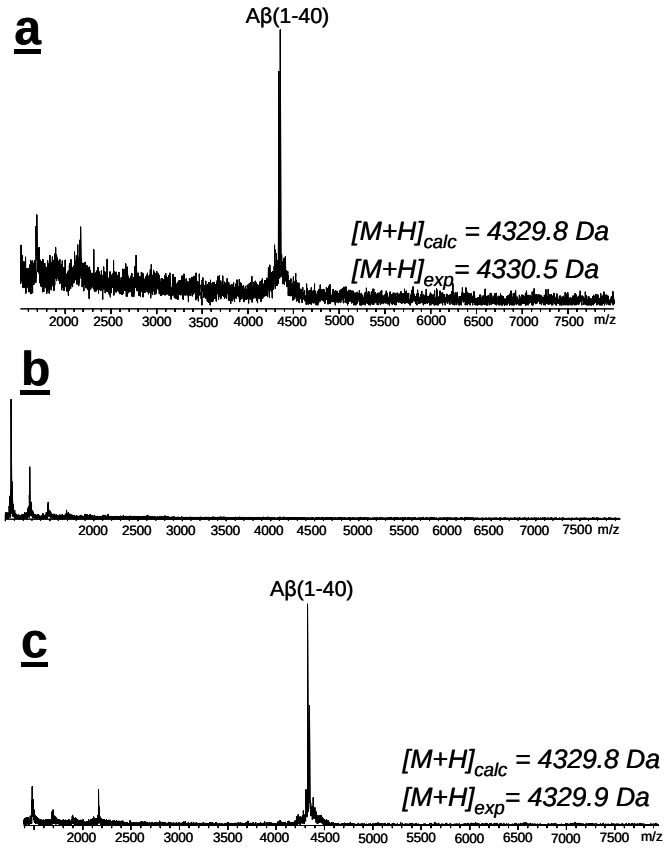

Figure 33: Affinity- mass spectrometry of Aβ(1-40) with Nb_3. In the supernatant (**a**), due to an excess of the peptide, the unbound Aβ(1-40) was present and in the wash fraction (**b**) no peptide. The elution fraction (**c**) showed the bound Aβ(1-40) to Nb_3.

An affinity- mass spectrometry experiment was performed in order to confirm that the Aβ(17-28) peptide is the antigenic determinant for Nb_3 and Nb_9. As an example, the Nb_9 was immobilized on NHS-activated Sepharose. The Aβ(17-28) epitope peptide was dissolved in PBS buffer and added to the immobilized nanobody. The supernatant was collected and the column washed until no mass spectrometric signal could be observed. The complex was dissociated under acidic conditions and analyzed by mass spectrometry. Mass spectrometric data showed the specific binding of Aβ(17-28) to the Nb_9. No Aβ(17-28) peptide was detected in the washing fraction, but in the mass spectrum of the elution fraction could be identified a signal at m/z 1324.6 ($[M+H]^+$) (Figure 34).

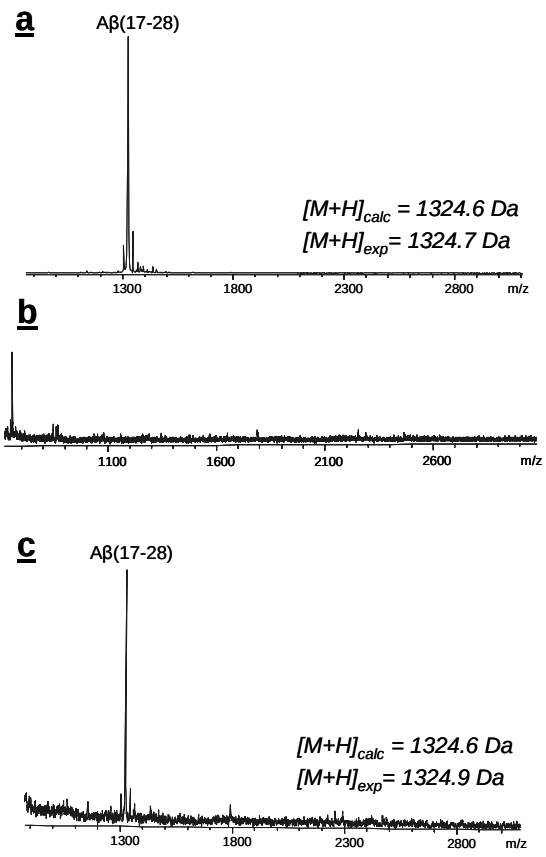

Figure 34: Binding of Aβ(17-28) to Nb_9 studied by affinity- mass spectrometry. MALDI-TOF mass spectrum of the supernatant (**a**) shows the unbound peptide, in the washing fraction (**b**) no fragment is present and in the elution fraction (**c**) the presence of the epitope peptide has been determined.

2.3.2 Binding of Aβ-nanobodies to Aβ-peptides using SAW-biosensor

During the past years, different methods such as immunoaffinity analysis by ELISA and Western Blot, isothermal calorimetry and surface plasmon resonance (SPR) were used for the characterization of protein-ligand interaction [149]. In particular, SPR has been long established as a “gold standard” for analysis of biomolecular recognition processes at a biosensor surface and for quantification of different biopolymer interactions [150, 151]. Biosensors have several applications not only in basic research fields, but also in medical diagnostics, food quality control, detection of explosives and drugs, genetic screening and environmental monitoring [152].

The surface acoustic wave (SAW) technology was employed for bioaffinity detection. The SAW technology, as an alternative to SPR, has recently gained increasing importance owing to its high detection sensitivity [149, 153]. SAW biosensors (e.g.

the S-sens K5 SAW sensor), on the basis of piezoelectric crystals are highly sensitive towards surface effects and are proved to be capable to detect and quantify mass and viscosity changes due to biomolecular interactions [154]. The S-sens K5 SAW biosensor (SAW instruments) consists of a read-out system into which the gold-coated quartz sensor is placed and the signals from the five sensor elements are recorded independently in real-time. The biosensor is operated in Love-wave geometry and is working at two fixed frequencies with a difference of about 0.3 MHz [153, 155]. Using two fixed frequencies, with φ(f1) – φ(f2) = 180° at a frequency range between 130 and 170 MHz, the influence of physical parameters, such as temperature, salts and viscosity on the sensor signal is significantly reduced. Different surface materials are used for SAW biosensor, mostly involving gold surfaces. Other examples of surfaces are the ones coated with alkanethiols, carboxymethylated dextrans in combination with biotin/streptavidin interactions [156], ZnO surfaces [157], or SiO_2 surfaces [158]. In the present work a gold-coated sensor chip was used. On the gold surface, a self assembled monolayer (SAM) was formed and used as a linker for the covalent immobilization of different molecules. For the formation of SAM, the gold-coated sensor chip was incubated overnight in a solution of mercaptohexanoic acid, thereby allowing for later coupling of proteins to the carboxylic groups on the chip. After activation of the carboxylic groups with a mixture of EDC/NHS, an increasing of the signal was observed. This can be explained by conversion of carboxyl groups of the SAM, present on the chip surface, into active N-hydroxysuccinimide ester. The next step was the covalent immobilization of ligand1 (e.g. peptide dissolved in phosphate buffer) on the sensor chip. Unreacted active ester groups were afterwards deactivated by ethanolamine. In order to ensure the near physiological conditions, the solvent was changed from water to phosphate buffer, causing a signal shift. The affinity binding of the analyte to the ligand was characterized by signal increase. The injection of HCl 0.1 M abolished the affinity and the signal decreased. The analyte was then eluted from the gold-chip (Figure 35).

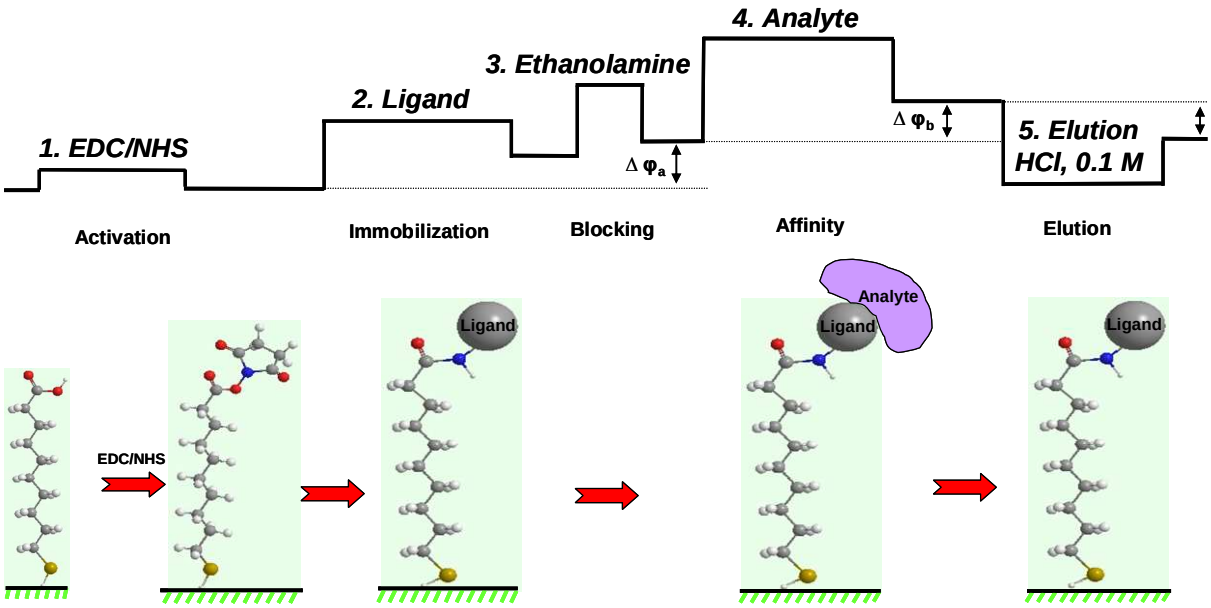

Figure 35: Schematic representation of phase shift of a single sensor element: activation of SAM using EDC and NHS (1), covalent immobilization of the ligand (2), blocking with ethanolamine (3), affinity binding of analyte (with a phase shift $\Delta\varphi_a$) (4), elution of the analyte using HCl, pH 2 ($\Delta\varphi_b$) (5) (SAM – self assembled monolayer; NHS – N-hydroxysuccinimide; EDC - N-(3-dimethylaminopropyl)-N-ethylcarbodiimide).

A specific binding between Aβ(1-40) and Aβ(17-28) to Nb_3 and Nb_9 was analyzed as a function of time with SAW biosensor. On the gold-chip surface, a self assembled monolayer (SAM) of 16-mercaptohexadecanoic acid was formed. The SAM was activated using N–hydroxysuccinimide (NHS) and N-(3-dimethylaminopropyl)-N-ethylcarbodiimide (EDC). In the first experiment, Aβ(1-40) was immobilized on the activated SAM and the free ester groups were blocked with ethanolamine. The affinity binding of 200 nM Nb_3 to Aβ(1-40) was analyzed at 25 °C in phosphate buffer. Using the sensitivity of the Love-wave sensor (515 ° cm^2 μg^{-1}), the bound mass has been calculated.

Further experiments were carried out for monitoring the affinity binding of 200 nM Aβ-nanobodies to 10 µM Aβ peptides. The affinity binding studies using SAW biosensor indicate that Nb_3 and Nb_9 bound specifically to the immobilized Aβ(1-40) and Aβ(17-28). Determination of dissociation constants was performed by increasing the concentration of Aβ-nanobodies (5 – 2000 nM) to the Aβ(1-40) and Aβ(17-28) peptides immobilized on the biosensor surface. After each injection, the unbound nanobody and the biosensor surface were regenerated with HCl 0.1 M. For further evaluation, the sensogram was exported into OriginPro 7.5 program and the

integrated FitMaster was applied. Figure 36 shows the resulting overlay plot and the individual fitting assuming a simple mono-molecular growth model of kinetic analysis of the binding events. Using FitMaster, the pseudo-first order kinetic constants k_{obs} were determined and plotted versus Aβ-nanobodies (Nb_3 and Nb_9). By applying the equation $k_{obs} = k_{off} + k_{on} * C$, a linear best fit was obtained and the dissociation constant (K_D) was established from $K_D = k_{off}/k_{on}$. The K_D values were found in nanomolar range.

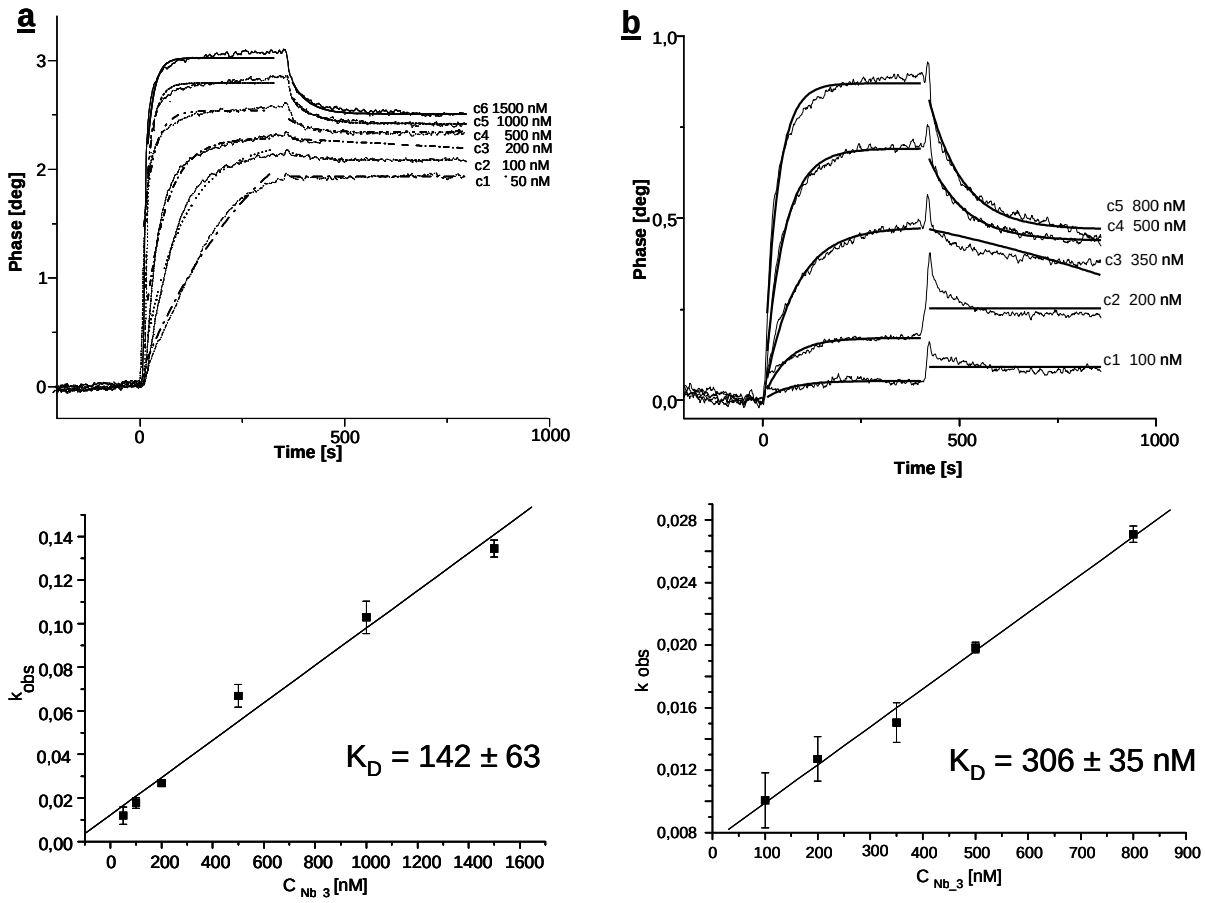

Figure 36: K_D determination of Nb_3 on **a** Aβ(1-40) and **b** Aβ(17-28) using SAW biosensor.

Affinity constants (K_D) of the Nb_3 and Nb_9 for the Aβ(1-40) and Aβ(17-28) using SAW biosensor are summarized in Table 4. Nb_3 showed a slightly higher affinity for Aβ(1-40) (K_D, 142 nM) in comparison with Aβ(17-28) (K_D, 306 nM) (Figure 36). The dissociation constants of Nb_9 showed a slightly higher affinity to Aβ(1-40) (K_D, 207 nM) as for Aβ(17-28) (K_D,745 nM) (Figure 37).

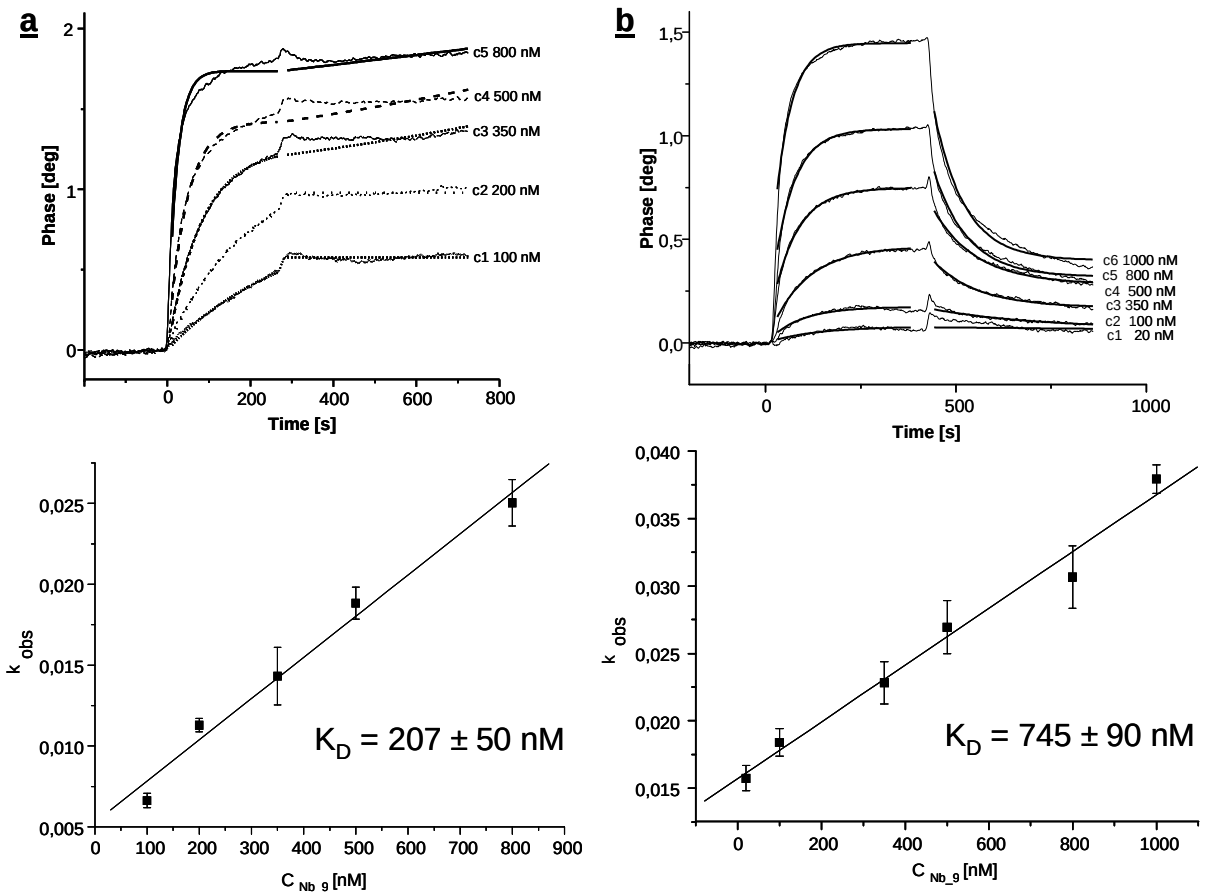

Figure 37: K_D determination of Nb_9 nanobody to immobilized **a** Aβ(1-40) and **b** Aβ(17-28).

Table 4: Kinetic rate and equilibrium dissociation constants of the Nb_3 and Nb_9 to the Aβ(1-40) and Aβ(17-28).

No.	Ligand	Antibody	k_{on} (nM^{-1} sec^{-1})	k_{off} (sec^{-1})	K_D (nM)
1	Aβ(1-40)	Nb_3	$8.583\ 10^{-5}$	0.0122	142 ± 63
		Nb_9	$2.547\ 10^{-5}$	0.00528	207 ± 50
2	Aβ(17-28)	Nb_3	$2.433\ 10^{-5}$	0.00747	306 ± 35
		Nb_9	$2.105\ 10^{-5}$	0.01569	745 ± 90

The SAW biosensor was shown to be a highly efficient tool for sensitive kinetic determination of interactions and precise evaluation of kinetic constants.

2.3.3 Affinity- mass spectrometric analysis of a CDR3-peptide to Aβ(1-40)

An affinity- mass spectrometry experiment was carried out to proof the affinity of the synthetic CDR3- peptide towards the Aβ(1-40). Cys-Aβ40 was therefore covalently linked to an Ultralink Iodoacetyl matrix (see Chapter 2.4.2) and the synthetic peptide was added to the affinity column. Subsequent mass spectrometric analysis of the supernatant, washing and elution fraction gave information about the affinity based on the reversible interaction of these two molecules. As indicated by the base peak chromatograms and the LC-ESI- ion trap mass spectrum of the supernatant fraction, the unbound CDR3-peptide could be detected, due to an excess of the peptide. The signal of the $[M+H]^+$ ion (m/z of 1474.63) showed the presence of the peptide in the supernatant fraction (Figure 38). After extensive washing steps, the washing fraction was free of CDR3-peptide.

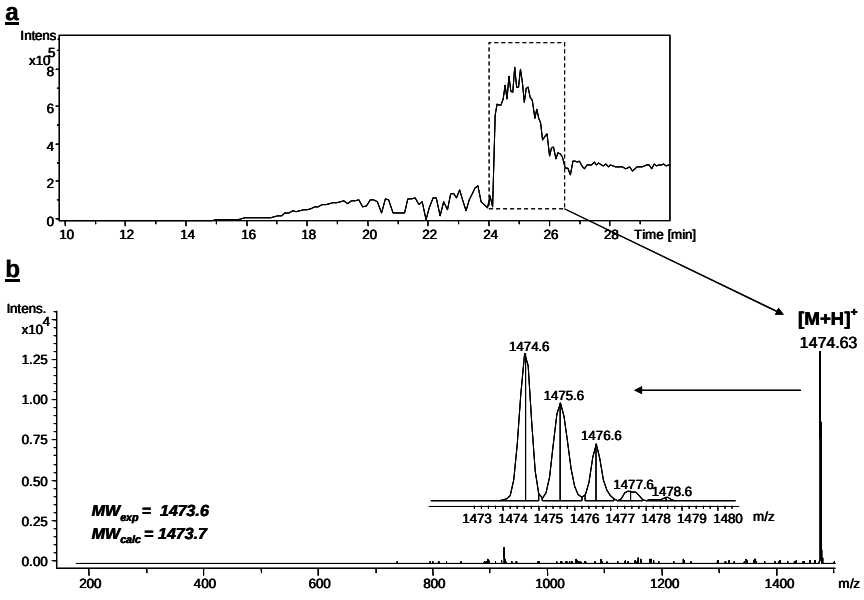

Figure 38: **a** Base peak chromatogram (LC-MS separation) showing a peak with the retention time ~25 minutes, representing the unbound CDR3-peptide. **b** LC-ESI-ion trap mass spectrum of the supernatant fraction.

When slightly acidic elution buffer was added onto the column, the dissociation of the CDR3-peptide from the cys-Aβ40 column could be detected, prooving the affinity of the small CDR3-peptide to Aβ. In the mass spectrum of the elution fraction of the CDR3-peptide, $[M+2H]^{2+}$ ion with a m/z of 737.8 was present (Figure 39).

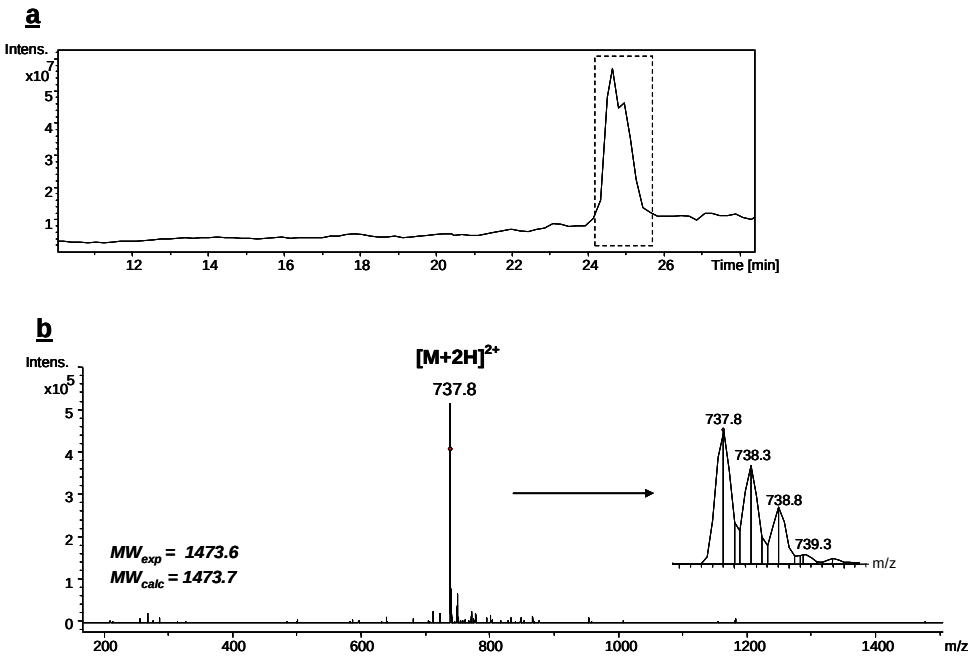

Figure 39: **a** Base peak chromatogram (LC-MS separation) showing a peak with the retention time ~25 minutes, representing the dissociated CDR3-peptide. **b** LC-ESI-ion trap mass spectrum of the elution fraction confirmed the identity of the synthetic peptide.

The sequence information of CDR3–peptide was determined from the MS/MS fragmentation spectrum of the doubly charged precursor ion with m/z 737.8 (Figure 40). From these data, the amino acid sequence of the peptide was determined as ARIGAAVNIPSEYD based on the complete b and y series observed in the spectrum.

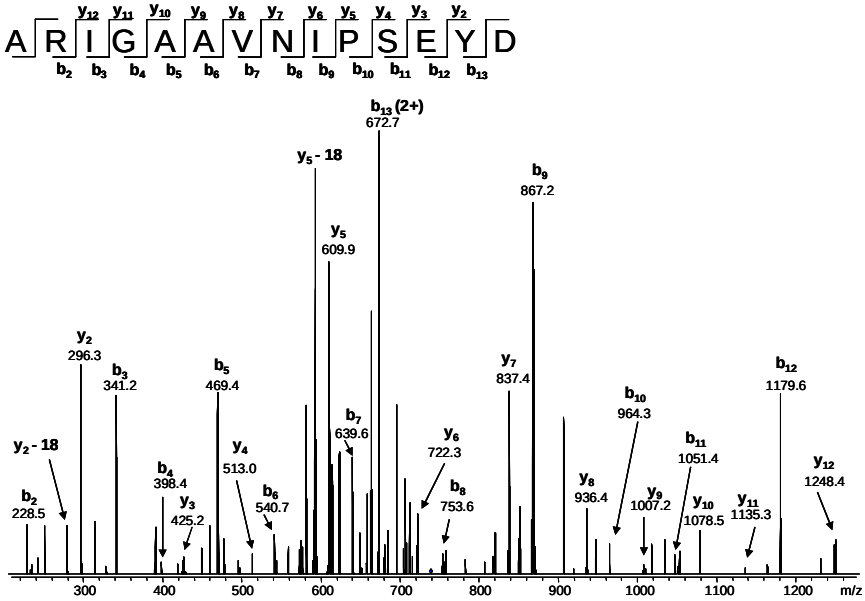

Figure 40: LC/ESI-ion trap-MS/MS mass spectrum of the elution fraction of affinity mass spectrometry experiment. MS/MS fragmentation mass spectrum of ion 737.8 (2+) led to the identification of CDR3-peptide.

Affinity- mass spectrometric analysis showed that the CDR3-peptide had affinity to Aβ(1-40) and the sequence was confirmed by MS/MS fragmentation.

2.4 Epitope structure identification and interaction of Aβ-peptides with the neuroprotective protein Cystatin C

2.4.1 Primary structure characterization of human Cystatin C

The Cystatin "superfamily" includes proteins that contain multiple cystatin-like sequences. Cystatins are generally the classical inhibitors of C1 cysteine proteinases. Several years ago new proteins were discovered, which contain cystatin domains, but have no inhibitory activities. The cystatin superfamily contains all these proteins together with family 1, 2 and 3 [159, 160]. Family 1 contains the stefins A and B (known as Cystatin A and B and no disulphide loops are present), family 2 are known as cystatins (molecular masses between 13-14 kDa). Some members of the family 2 are glycosylated and are represented by Cystatin C, D, SA, SN and S. The family 3 cystatins are called kininogens and have molecular masses in the range of 88-114 kDa. The major characteristics of cystatin superfamily are presented in the Table 5.

Table 5: Major characteristics of cystatin superfamily.

Characteristics	Family 1	Family 2	Family 3
Molecular mass (kDa)	Ca. 11	13-14	Low: 50-68 High: 88-114
Disulphide bonds	0	2	6
Glycosylated	No	No	Yes
Located	Mainly intracellularly	Mainly extracellularly	Intravascularly
Cystatins	Human: Stefin A and Stefin B Rat: cystatin α and β	Human: C,D,S,S1,S2,SN,SA, D Rat: C,S Mouse: C Chicken egg white, bovine colostrums	Human, rat, bovine: L-kininogen, H-kininogen Rat: T-kininogen Ox: kininogen

In the present dissertation, the interaction between human Cystatin C and Aβ(1-40) was investigated. Several amyloidogenic proteins such as Cystatin C, apolipoprotein E, clusterin, witronectin, transtitetin, and gelsolin have been found to be co-localized with Aβ(1-40) peptides in the brain as elements of amyloid plaques and to co-immunoprecipitate with amyloid-beta precursor protein [114, 161, 162].

Human Cystatin C is known as Cystatin-3 (gene symbol CST3), Gamma-Trace or post-Gamma-Globulin from early literature [163]. This protein is a non-glycosylated, low molecular weight inhibitor of cysteine proteases and is involved in various biological and pathological processes. Cystatin C is composed of 120 amino acid residues (Figure 41) and has a molecular weight of 13 kDa. In 1961, Cystatin C was described as a constituent of normal cerebrospinal fluid and of urine from patients with renal failure [164, 165]. A few years later it was found to be present in serum and in different body fluids, such as saliva, colostrum, seminal fluid and ascites [166-168].

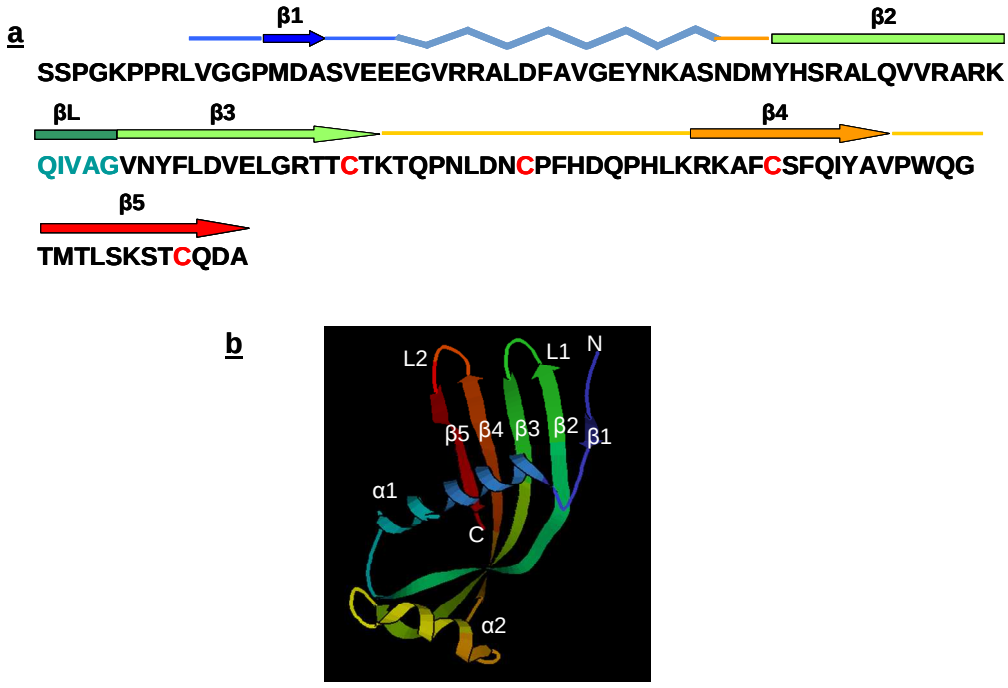

Figure 41: a. Amino acid sequence of human Cystatin C. L1, L2 – loop 1 and 2; β1-β5 – β-strand; α1, α2 – helix 1 and helix 2. b. Ribon representation of human Cystatin C (1CEW pdb).

Human Cystatin C (HCC) was first characterized by SDS-PAGE gel electrophoresis, Western blot (Figure 42) and mass spectrometry in order to confirm its purity. A small

amount of HCC was loaded on the SDS gel. After Coomassie staining one band was observed, with a molecular weight of around 13 kDa.

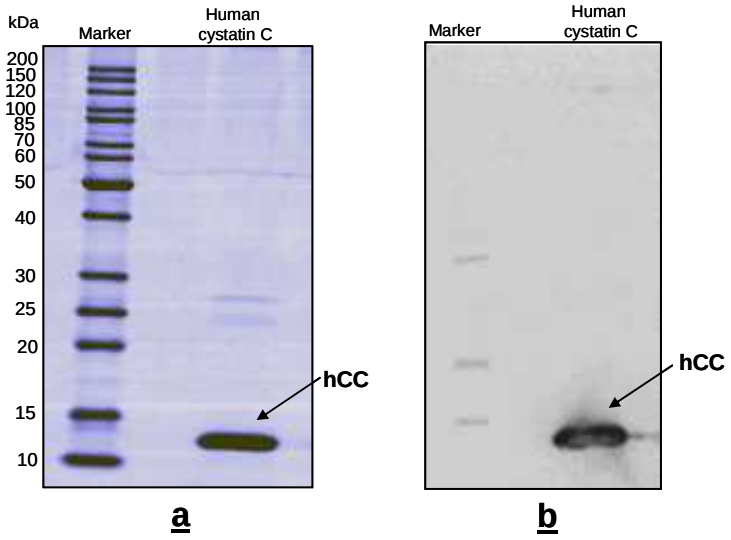

Figure 42: a. SDS-PAGE of human Cystatin C. b. Western Blot of human Cystatin C using as a detection antibody - anti-Cystatin (clone cyst 13) antibody.

The molecular mass of HCC was determined by ESI-FTICR mass spectrometry (Figure 43). The measurements were performed by using an Apex II mass spectrometer (Bruker Daltonics) equipped with a 7T superconducting magnet, an Apollo source and an API1600 ESI control unit. The monoisotopic molecular mass determined from the mass spectrum was 13338.69 Da.

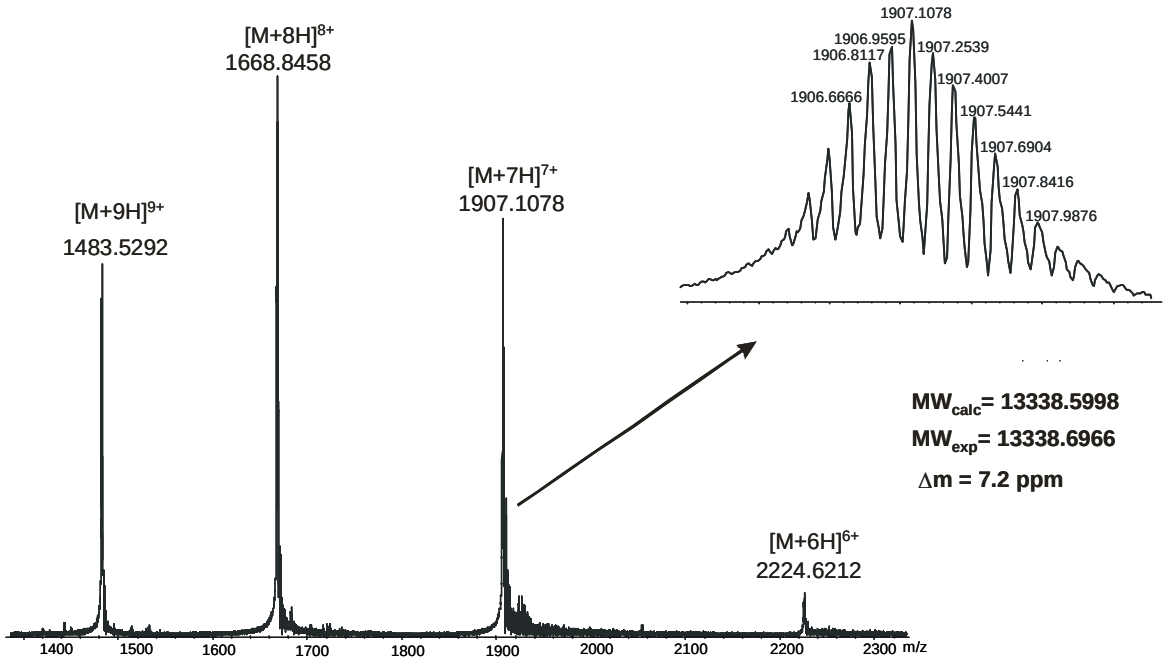

Figure 43: ESI-FTICR mass spectrum of human Cystatin C.

2.4.2 Identification of the of Aβ(1-40) epitope to human Cystatin C using different proteases

Proteolytic excision and extraction in combination with mass spectrometry, as previously used for antibody-antigen interaction studies, was employed for the identification of the protein-peptide complex binding sites. The identification of the epitope recognized by the β-amyloid peptide was performed using an affinity column containing 100 µg of immobilized HCC on Sepharose (the column was prepared according to the procedure described in Experimental part) (Figure 44).

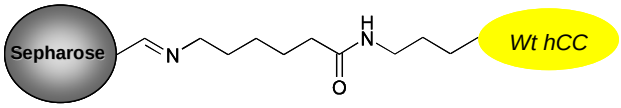

Figure 44: Schematic representation of binding of human Cystatin C to NHS-Sepharose.

In a first experiment, 50 µg of Aβ(1-40) were dissolved in PBS and were allowed to react with the HCC for 2 h. The first washing step was performed for the removal of the excess of peptide: the column was washed with 70 mL of PBS and 20 mL water. The last mL of the washing buffer was collected and subjected to mass spectrometric analysis in order to see whether excess of peptide was still present. The affinity bound peptides were then dissociated under acidic conditions with 0.1% TFA. In Figure 45, the MALDI- mass spectra of the supernatant, washing and elution fractions are shown. The corresponding Aβ(1-40) ($[M+H]^+_{calc}$ of 4328.8) molecular mass was identified in the supernatant and elution fractions. This result confirmed the binding between the immobilized HCC protein and Aβ(1-40) and also the complete removal of the non-specifically bound peptide fragments.

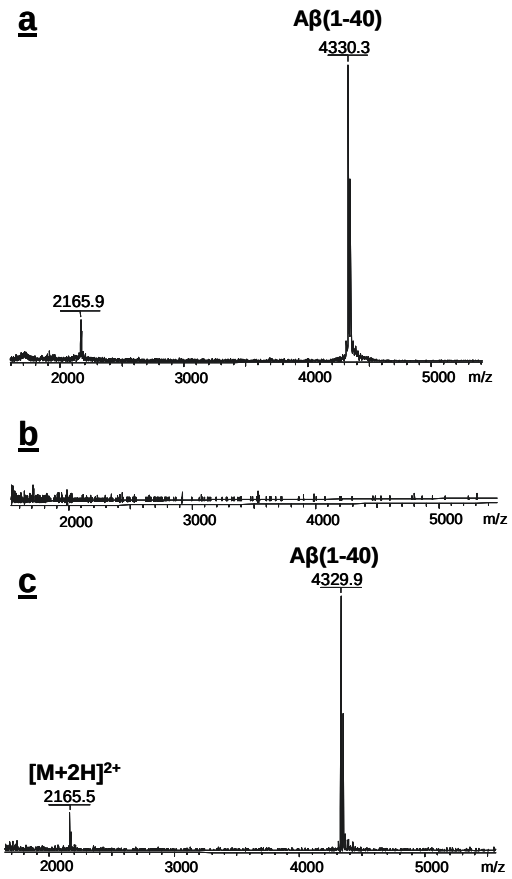

Figure 45: Affinity- mass spectrometric analysis of synthetic Aβ(1-40) with the immobilized human Cystatin C; MALDI-TOF mass spectra of the **a** Supernatant, **b** Last wash, **c** Elution fractions.

For the mass spectrometric identification of the Aβ- epitope, proteolytic excision- and extraction techniques with proteolytic enzymes, such as trypsin, LysC- protease, GluC- protease, carboxypeptidase and pronase were performed.

In a first attempt, trypsin was employed. Aβ(1-40) has 3 possible cleavage sites for trypsin: Arg-5, Lys-16 and Lys-28. The peptide was digested in solution for 2, 4, 6 h in order to optimize the cleavage conditions. Further, the Aβ(1-40) in complex with the wt HCC was digested by trypsin and the mass spectrum of the elution fraction contained an ion at m/z 3710.9, corresponding to Aβ(6-40) fragment ($[M+H]^+_{calc.}$= 3711.2) and an ion at m/z 4329.0 corresponding to the Aβ(1-40) (Figure 46 a). The ions m/z 1325.5, 1955.0 and 3708.6 were identified as singly charged ions of the [17-28], [17-40] and [6-40] fragments in the supernatant fraction.

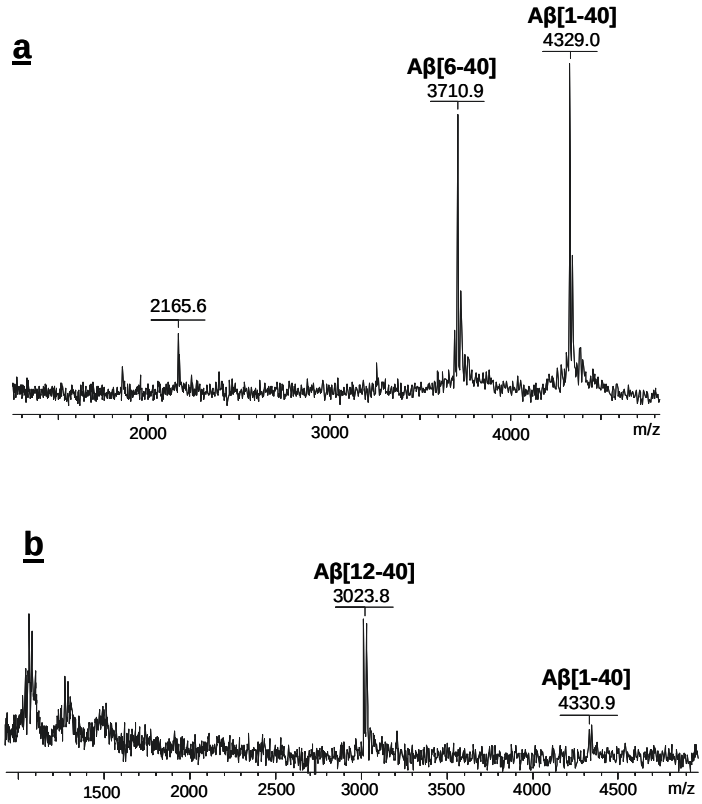

Figure 46: **a** MALDI-TOF mass spectrum of the elution fraction after epitope excision using trypsin showing the Aβ(6-40) and Aβ(1-40) peptides. **b** MALDI-TOF mass spectra of the elution fraction after epitope extraction using GluC showing the Aβ(12-40) and Aβ(1-40) peptides.

A second enzyme used for proteolytic extraction was endoproteinase GluC from *Staphylococus aureus* strain V8. The enzyme has the capability to cleave peptide bonds at the carboxyl side of glutamyl residues if the reaction is carried out in ammonium bicarbonate. If the reaction is carried out in phosphate buffer, the enzyme provides cleavage at the carboxyl side of both glutamyl and aspartyl residues. Because in Aβ(1-40) sequence 3 aspartyl residues and 3 glutamyl residues are present, the proteolytic cleavage was performed in phosphate buffer. The digestion of Aβ(1-40) with GluC- protease for 2 h resulted in cleavage at Glu-11 residue. The Aβ(1-40) was cleaved in solution by GluC- protease and the proteolytic mixture was added on the immobilized HCC column and allowed to react. The analysis of the unbound peptide fragments by MALDI-TOF mass spectrometry revealed the presence of the fragments [4-11], [12-22], [4-22] and [12-40], whereas the mass spectrum of the elution fraction contained an abundant ion at m/z 3023.8 that corresponded to the amino acid sequence [12-40] (Figure 46 b).

Considering the sequence Aβ(12-40) which was identified by proteolytic cleavage with endoproteinase GluC, further experiments were designed. Using endoproteinase Lys-C, additional information for the epitope identification was obtained. For the next experiments, Aβ(12-40) was synthesized by Fmoc-SPPS and purified by RP-HPLC. Endoproteinase Lys-C isolated from the bacterium *Lysobacter enzymogenes* is a serine endoprotease. The enzyme hydrolyzes peptide bonds at the carboxyl side of lysyl residues and also the Lys-Pro and Lys-Glu are cleaved [169]. The mass spectrum acquired for the peptide mixture resulting from the digestion of Aβ(12-40) by endoproteinase Lys-C revealed 3 ions: [29-40], [17-28] and [17-40]. The mass spectrometric analysis of the elution fraction led to the identification of [17-28] fragment, while the supernatant contained the fragments [17-28] and [12-28] (Figure 47 b and c).

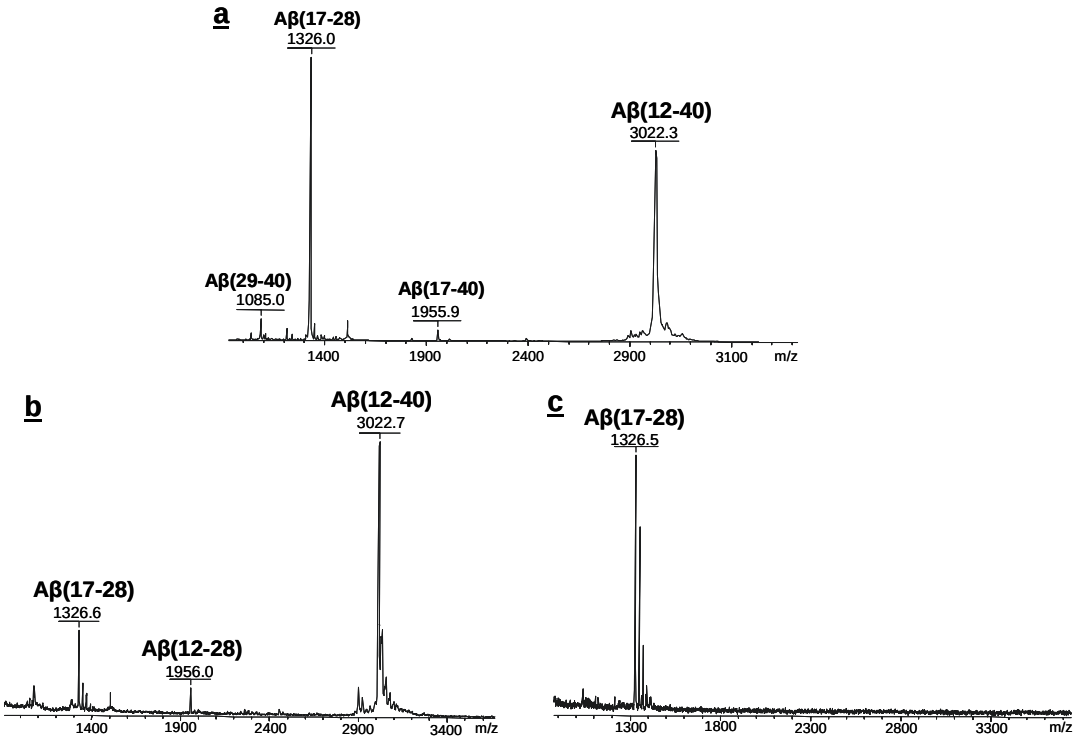

Figure 47: MALDI-TOF mass spectra of **a** the peptide mixture produced by proteolytic digestion Aβ(12-40) with Lys C in solution **b** the supernatant of the epitope extraction **c** the elution fraction after epitope extraction.

To examine whether the amino acid sequence of the epitope can be further reduced, epitope excision experiments using carboxypeptidase Y and pronase were performed. Carboxypeptidase Y, originally termed *yeast* proteinases C, is a serine exopeptidase with broad amino acid specificity. It is able to release every amino acid from the carboxyl-terminus of peptides, but the most prominent feature of the enzyme

is its ability to release proline from peptides and proteins [170, 171]. The mass spectrum of the elution fraction showed the amino acid fragment [12-29], corresponding to the m/z 2012.5 ($[M+H]_{calc.}$= 2012.3). Pronase is a non-specific protease, which is essentially breaking down proteins into the single amino acids, as shown for Aβ(1-40) which was completely digested in 2 h. Epitope excision-MS using pronase provided a single Aβ-peptide fragment as the minimal epitope eluted from the HCC column, which was identified as Aβ(17-24), LVFFAEDV (Figure 48).

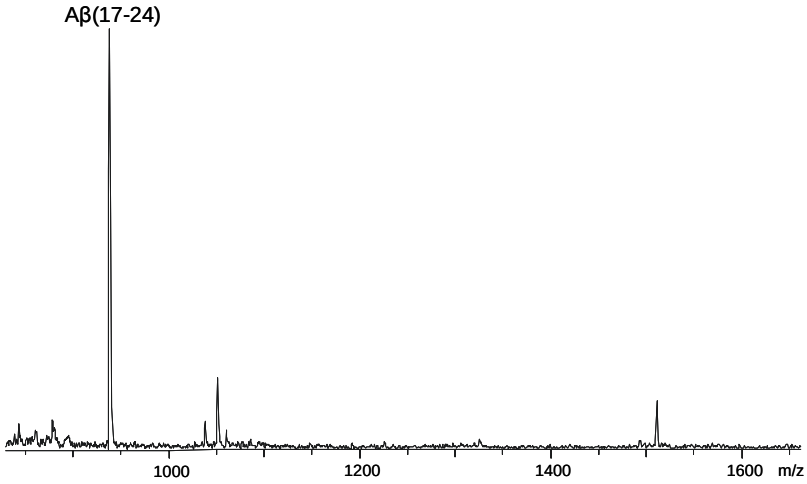

Figure 48: MALDI-TOF mass spectrum of the elution fraction after epitope excision of Aβ(1-40) using pronase showed the presence of Aβ(17-24) fragment.

Different proteolytic enzymes provided detailed information about the Aβ sequence recognized by the human Cystatin C and are summarized in Table 6. The minimal sequence [17-24] was found by epitope excision using pronase. However, other specific enzymes, such as trypsin, GluC and Lys-C provided significant results for the epitope identification. Proteolytic cleavages of Glu-22 and Asp-23 by GluC were not observed, which confirmed that these residues were shielded in the immune complex. The results ascertained that the human Cystatin C recognized the epitope located in the middle part of the Aβ(1-40), within the amino acids [17-24].

Table 6: Summary of mass spectrometric epitope excision and extraction data for Aβ(1-40) antigenic determinant recognized by wt HCC.

Enzyme	Peptide	Sequence	$[M+H]_{calc}$ m/z	$[M+H]_{exp.}$ m/z
Trypsin	**Aβ(6-40)**	HDSGYEVHHQKLVFFAEDVGSNKGAIIGLMVGGVV	**3708.9**	**3709.5**
Glu-C	**Aβ(12-40)**	VHHQKLVFFAEDVGSNKGAIIGLMVGGVV	**3021.6**	**3021.1**
Lys-C	**Aβ(17-28)**	LVFFAEDVGSNK	**1325.5**	**1326.2**
Carboxypeptidase	**Aβ(12-29)**	VHHQKLVFFAEDVGSNKG	**2012.3**	**2012.5**
Pronase	**Aβ(17-24)**	LVFFAEDV	**938.4**	**938.6**

While the synthetic Aβ(17-24) showed only minimal binding affinity, high affinity was found for Aβ(17-28), suggesting some conformational requirement for the Aβ-epitope binding to wt HCC. According to these results, Aβ(17-28) was used as a model peptide for further affinity studies.

2.4.3 Identification of the epitope of human Cystatin C to Aβ(1-40)

A similar methodology was employed for the identification of the binding epitope peptide from wt HCC by immobilization of the Aβ(1-40) peptide on an affinity microcolumn. Since previous studies in our laboratory had shown that NHS-activated sepharose is not suitable for the immobilization of short peptides, an UltraLink- Iodoacetyl gel was used for the immobilization and in order to enhance the stability of the Aβ-affinity column. In this system, the linker is attached to the peptide via a thioether bond. Immobilization of Cys-Aβ(1-40) peptide on UltraLink iodoacetyl-sepharose (Figure 49) is presented in detail in Experimental section.

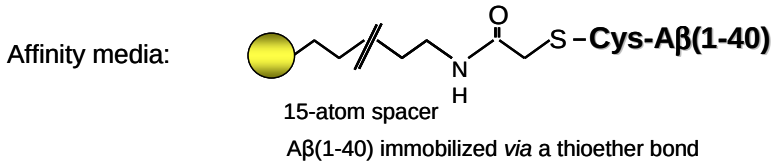

Figure 49: Schematic representation of Cys-Aβ(1-40) bound to UltraLink iodoacetyl-sepharose.

For immobilization on the UltraLink iodoacetyl sepharose, the Aβ(1-40) peptide was prepared with an additional N-terminal Cys residue. Cys-Aβ(1-40) was synthesized by SPPS according to the Fmoc/t-Butyl strategy and the crude peptide was purified

by RP-HPLC. The mass spectrum of Cys-Aβ(1-40) indicated a m/z 4432.07 ($[M+H]^+_{calc}$ = 4432.05) (Figure 50).

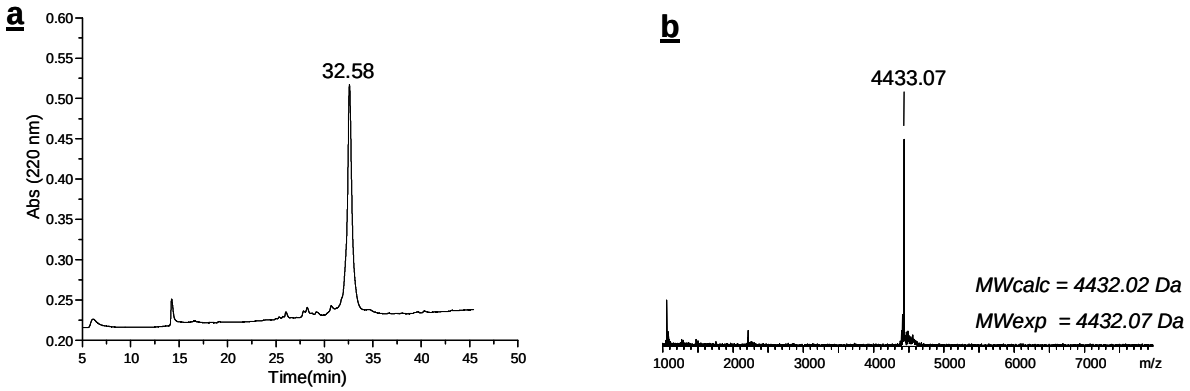

Figure 50: RP-HPLC profile and mass spectrometric characterization of Cys-Aβ(1-40).

2.4.3.1 Identification of human Cystatin C binding regions by mass spectrometric epitope excision and extraction

In order to identify the HCC epitope peptide recognized by β-amyloid peptide (1-40), epitope excision mass spectrometric experiments were performed. In the first experiment, wt HCC was digested in solution for 14 h at 37°C at an enzyme to substrate ratio of 1:20 by trypsin and analyzed by MALDI-TOF MS. The mass spectrum provided peptides fragments of nearly the complete sequence ([1-24], [26-36], [37-45], [9-24], [54-93], [76-92], [71-92] fragments), except the C-terminal fragments (Figure 51).

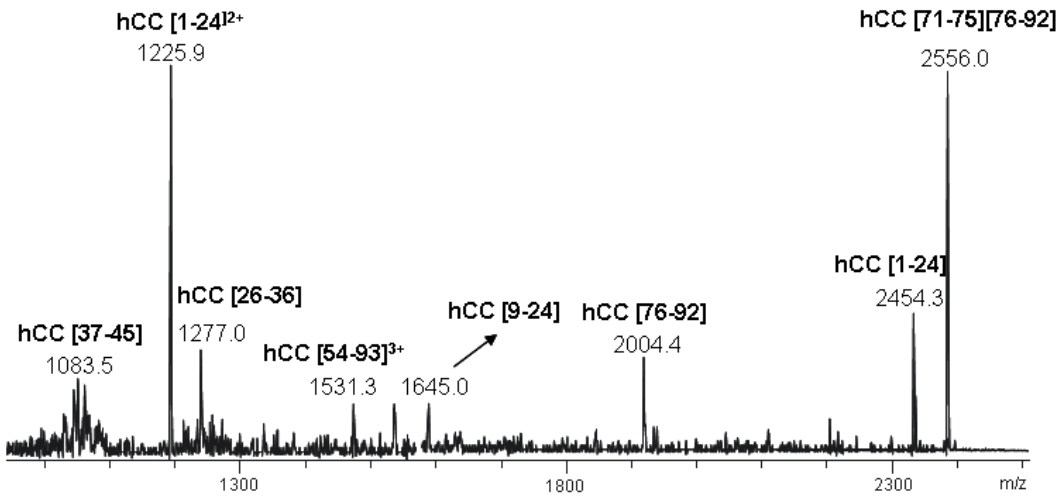

Figure 51: MALDI-TOF mass spectrum of in solution digestion of wt HCC with trypsin after 14 h incubation time at 37°C.

Epitope excision- and extraction- MS experiments were performed with trypsin using identical conditions to those applied for the Aβ-epitope identification (see Chapter 2.4.2). The mass spectrum of the supernatant upon epitope excision with trypsin showed that the N-terminal part of HCC did not interact with Aβ, because this domain is exchanged during 3D domain swapping and involved in dimer formation [172]. The elution fraction of the affinity-bound peptides provided two C-terminal epitope peptides, HCC(93-120) and HCC(94-120), corresponding to m/z 3167.4 and 3011.2 (Figure 52). The Lys-114 residue was not cleaved in the complex, meaning that this residue was shielded from the digestion, indicating that the Aβ-binding site was located at the C-terminal domain of HCC. The presence of the Aβ fragments in the elution fraction indicated that the Cys-Aβ column was not very stable for several experiments.

a NH_2-SSPGKPPRLVGGPMDASVEEEGVRRALDFAVGEYNKASNDMYHSRALQVVRA RKQIVAGVNYFLDVELGRTTCTKTQPNLDNCPFHDQPHLKRKAFCSFQIYAVPWQGT MTLSKSTCQDA^{120}-COOH

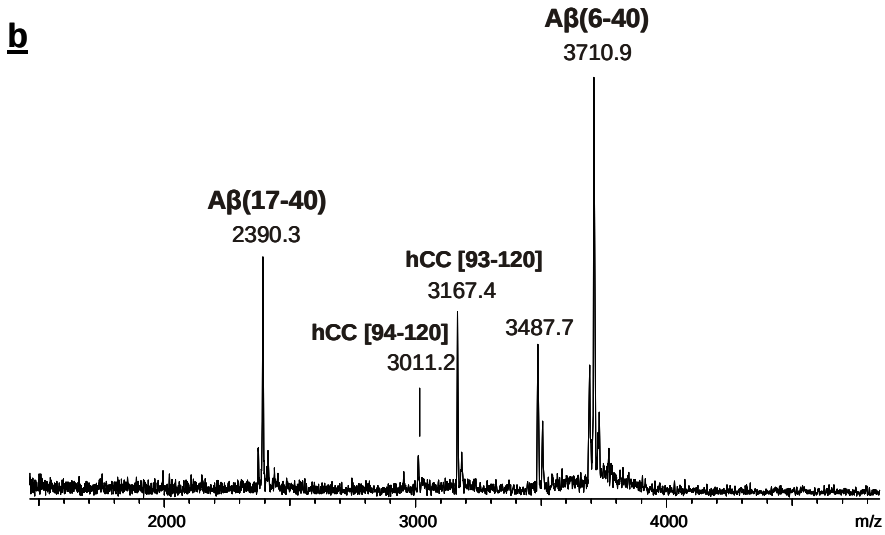

Figure 52: **a** Amino acid sequence of the wt HCC. The fragment [93-120] is highlighted in red. **b** Mass spectrometric identification of the HCC binding epitope to Aβ(1-40). Tryptic HCC fragments eluted after epitope excision from the Aβ(1-40)-HCC complex showed two peptide fragments, HCC (93-120) and HCC (94-120).

In order to identify the minimal HCC epitope, an epitope excision experiment using pronase was carried out. The mass spectrum of the elution fraction provided the shortest proteolytic fragment eluted from the wt HCC-Aβ complex, as being the fragment HCC(101-117) at m/z 1885.3 ($[M+H]^+_{calc}$ = 1885.2) (Figure 53).

a H_2N-SSPGKPPRLVGGPMDASVEEEGVRRALDFAVGEYNKASNDMYHSRALQVVRA RKQIVAGVNYFLDVELGRTTCTKTQPNLDNCPFHDQPHLKRKAFCSFQIYAVPWQGT MTLSKSTCQDA^{120}-COOH

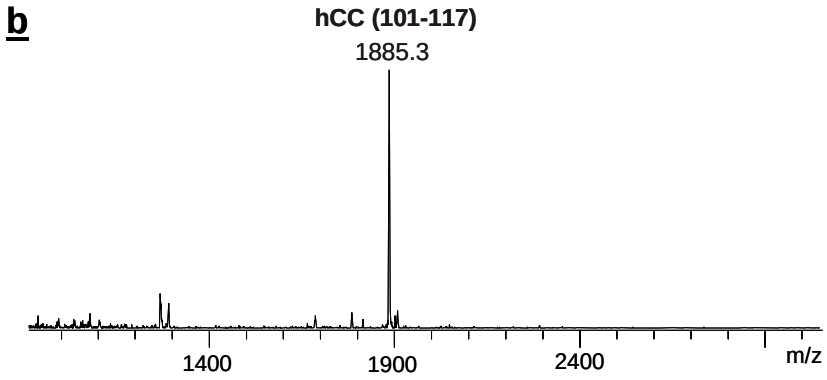

Figure 53: **a** Amino acid sequence of the wt HCC. The peptide fragment eluted after epitope excision experiment is highlighted in red. **b** MALDI-TOF mass spectrum of the wt HCC protein fragment eluted after epitope excision using pronase.

The Aβ- binding site identified in wt HCC is located in the C-terminal part within the L2 loop and β5 strand of HCC, which comprises the external part of the protein and are exposed to the environment. The C-terminal binding epitope enables interaction of the Aβ peptide with the L2-β5 part without any restriction.

2.4.3.2 Affinity-mass spectrometric characterization of human Cystatin C epitopes

After identification of wt HCC epitope peptides by mass spectrometry, a further aim of the study was the investigation of the binding of the HCC(93-120) and HCC(101-117) to Aβ(1-40).

For the affinity mass spectrometric studies, HCC(93-120) and HCC(101-117) were prepared manually on TentaGel Ram resin by SPPS according to the Fmoc/t-Butyl strategy as described in the Experimental part. The crude peptides were purified by RP-HPLC and characterized by mass spectrometry, as shown in Figure 54.

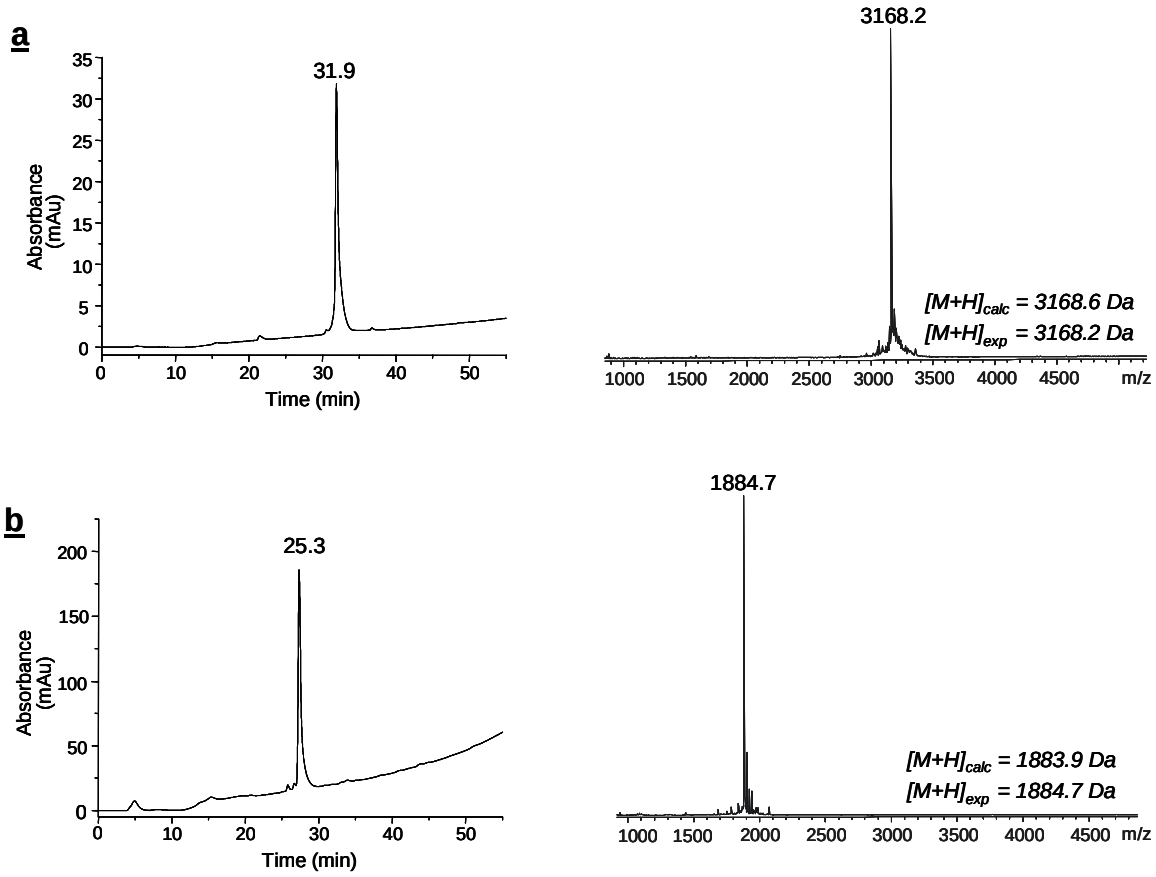

Figure 54: RP-HPLC profile of the **a** HCC(93-120) fragment and the corresponding mass spectrum with a m/z 3168.2 and **b** HCC(101-117) fragment and the corresponding mass spectrum with a m/z 1884.7.

The interaction between HCC(93-120) and HCC(101-117) was studied by affinity-mass spectrometry. In a first step the peptides were dissolved in PBS buffer and exposed to Aβ(1-40) column. After 1 h of incubation at 20 °C the column was washed with 80 mL buffer and the unbound peptide was removed. The complex was dissociated with 0.1% TFA. The supernatant containing the unbound peptide, the washing and elution fractions were collected and analyzed by mass spectrometry. Mass spectrometric data showed the specific binding of HCC(93-120) and HCC(101-117) to the Aβ(1-40). No peptide fragment was detected in the washing fraction. MALDI-TOF mass spectrum of the elution fraction provided the identification of ions corresponding to both peptides HCC(93-120) at m/z 3165.9 and HCC(101-117) at m/z 1884.2 as shown in Figure 55.

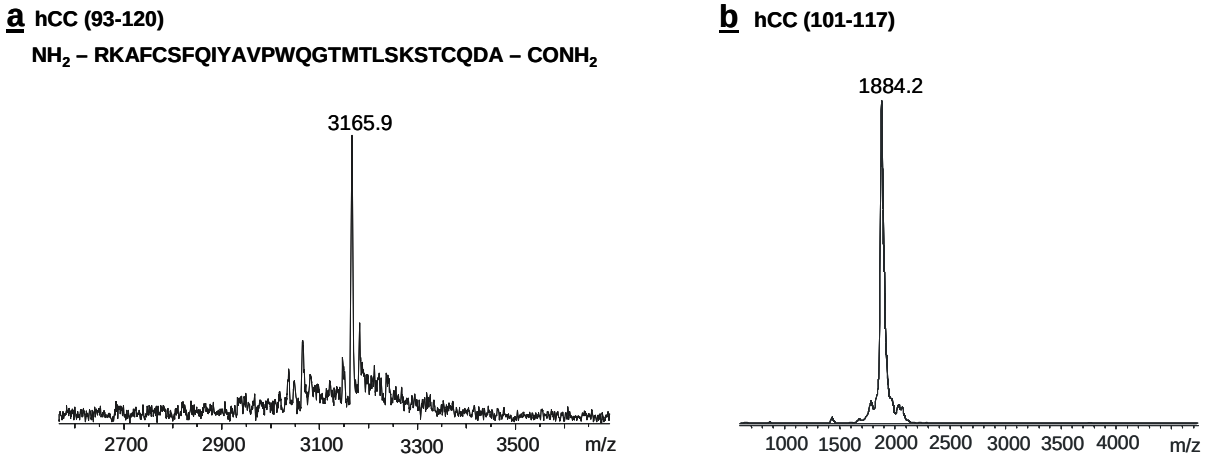

Figure 55: MALDI-TOF mass spectra of the elution fractions of the synthetic peptides HCC(93-120) (**a**) and HCC(101-117) (**b**).

2.4.4 Secondary structure determination of human Cystatin C epitopes

For monitoring the conformational changes and for determination of the secondary structural content in peptides and proteins, circular dichroism spectroscopy can be employed. The conformation of the synthetic peptides is also very important for their biological activity. The measurements were performed in different buffers, at 25°C in quartz cells of 0.1 cm path-length. The spectra were averages of six scans between 190 and 260 nm and the results were expressed in molar ellipticities. The CD spectra of HCC(93-120) peptide were recorded in water, PBS and different concentrations of TFE/water (Figure 56). The concentration of the peptide was 30 µM. Under these conditions, the peptide was completely dissolved. In water and PBS, the CD spectra showed a minimum at 198 nm (π-π* transitions), which indicated a random coil

conformation. The CD spectra of the peptide recorded in 100 % TFE showed that the peptide adopted a helical conformation, with a π-π* band at approximately 208 nm and the n-π* band at 223 nm. With the increasing percentage of water (90%), the conformation changed to a random coil conformation, with a negative band at 200 nm.

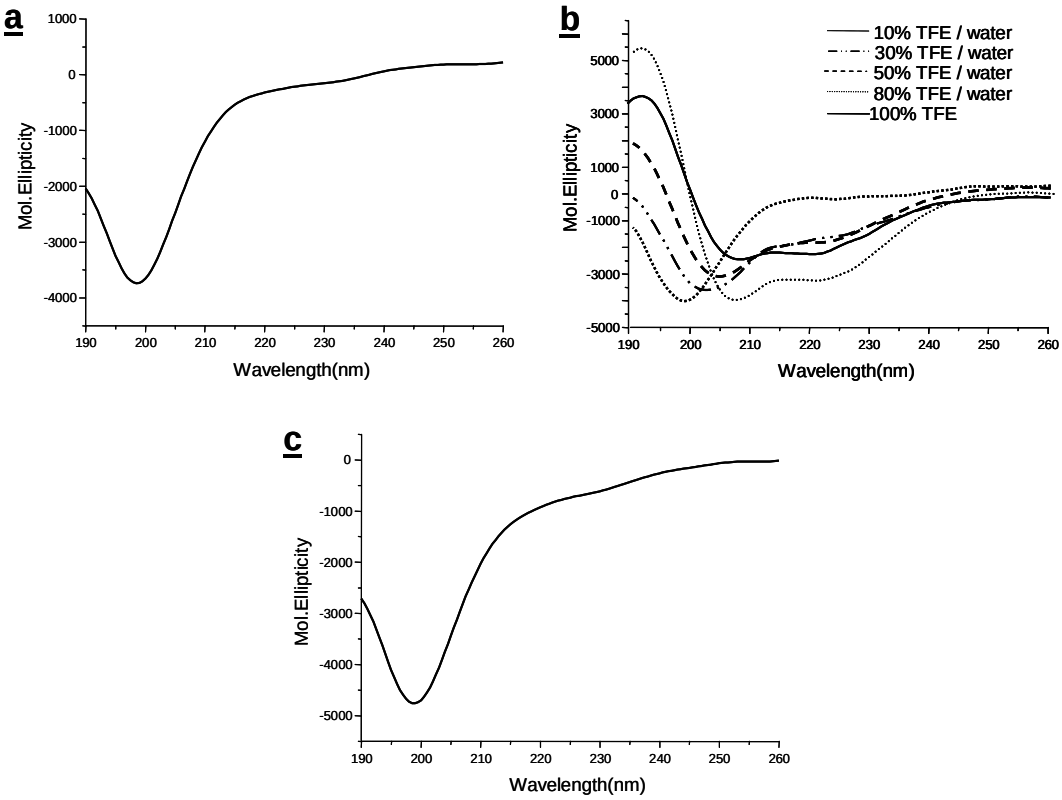

Figure 56: Secondary structure determination of HCC(93-120) in water (**a**), different concentration of TFE (from 10% to 100%) (**b**) and PBS buffer (**c**).

The CD spectra of HCC(101-117) peptide recorded under different conditions are shown in Figure 57. The spectrum recorded in water showed a negative band at 198 nm (π-π* transitions) and a negative shoulder at 225 nm, indicating the presence of a mixture of conformers, with the predominance of an unordered structure. In 80% TFE up to 30% TFE/water (v/v) the peptide adopted helical conformation (the π-π* band at 208 nm and the n- π* band at 223 nm). The spectra recorded in 10% TFE/water (v/v) had a negative band at 200 nm, characteristic to a random coil conformation. The changes of conformation were detected in the presence of TFE.

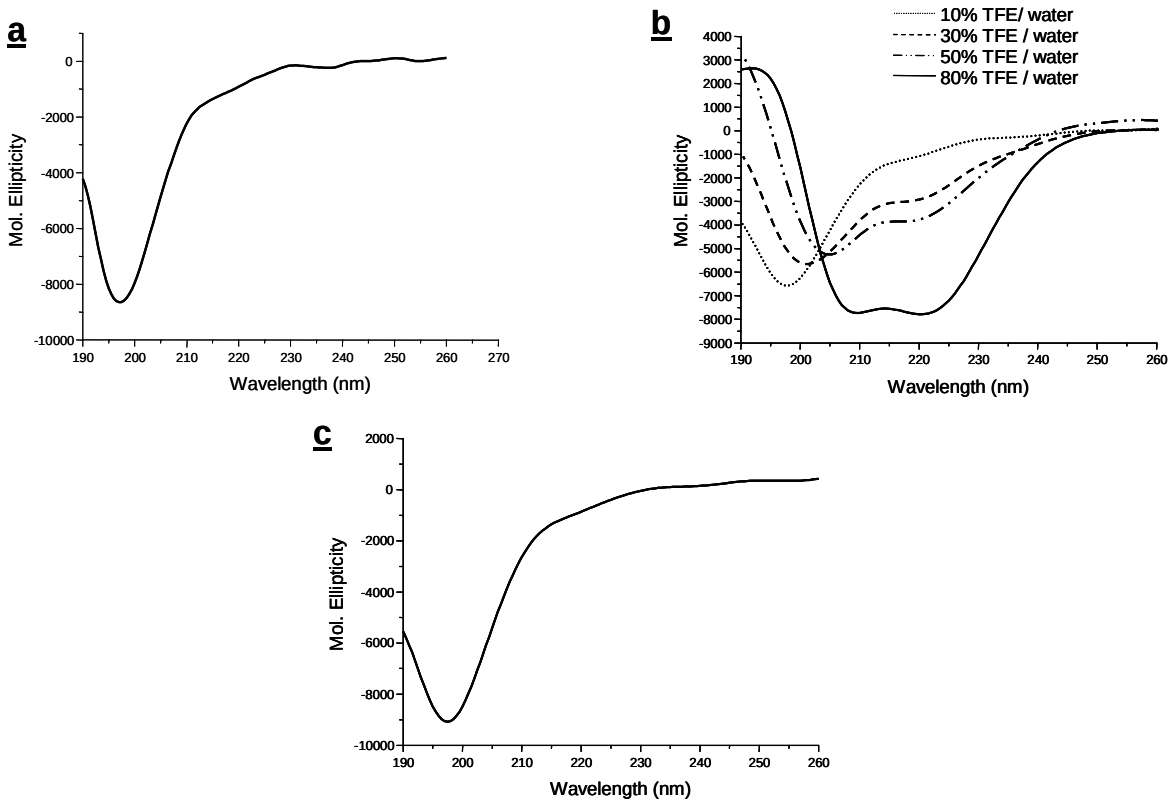

Figure 57: Secondary structure determination of HCC(101-117) in water (**a**), 10% to 80 % TFE/water (**b**) and PBS buffer (**c**).

Additional information about the HCC(93-120) and HCC(101-117) peptides were obtained by molecular dynamic simulation. For the analysis, BallView, a molecular modelling program, was used in order to assign the structure of the peptides as shown in Figure 58.

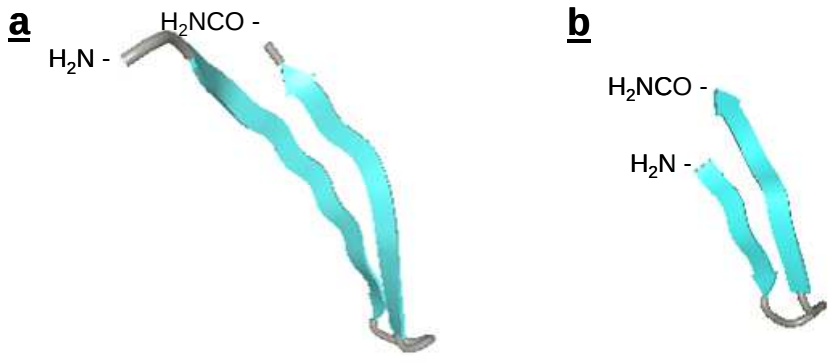

Figure 58: Molecular modelling of the three dimensional structure of **a** HCC(93-120) and **b** HCC(101-117). The structures were obtained using the BallView program.

In order to characterize the complex between HCC and Aβ peptide, molecular dynamics calculations were performed by Dr. Sylwia Rodziewicz-Motowidlo at the

University of Gdansk. For molecular dynamics calculations, an initial complex HCC-Aβ-peptide ligand was built from the HCC monomer [109] and the full length Aβ(1-40). Starting conformations employed for Aβ were either helical (PDP code 1Z0Q), or β-hairpin (PDB code 2BGE). Approximately 30000 HCC-Aβ starting complexes were built using ClusPro [173] and GRAMM-X [174] programs, 16 of which were selected for subsequent molecular dynamics calculations. Simulations were carried out using the AMBER 8.0 program (University of California, San Francisco) and the all-atom parm94 force field. The crude complexes were initially minimized *in vacuo* to remove closed *van der Waals* contacts. Before surrounding the HCC-ligand complex with water molecules, Na^+ and Cl^- charge-balancing counterions were added in positions with favourable ionic interactions to neutralize charges on the HCC-ligand surface, and all structures were optimised by energy minimization in water. After minimization, the molecular dynamics for all complexes were calculated (Figure 59). Simulations of complexes in solution were performed under periodic boundary conditions in a closed, isothermal and isobaric (NTP) ensemble. Throughout the simulation solute and solvent were coupled to a constant-temperature (300 ^oK) heat bath and a constant-pressure (P = 1 atm) bath. All hydrogen-containing bonds were constrained using the SHAKE algorithm allowing a time step of 0.001 ps. An Ewald summation was used for non-bonded interactions, and coordinates were saved every 1000 steps. The time during all molecular dynamics simulations was 3000 ps. The time period of molecular dynamics (MD) was about 3000 ps without constrains, and when the complexes started to dissociate, MD calculations were interrupted. Refinement analyses were carried out using the AMBER package and MolMol graphical programs. Molecular dynamics calculations were performed for sixteen HCC-Aβ complexes. In all these complexes, the initial structure of Aβ peptide (α-helix or β-strand) was changed during the molecular dynamics calculations, whereas the HCC protein structure was stable. In almost all complexes calculated, hydrophobic and electrostatic interactions between HCC and Aβ were formed.

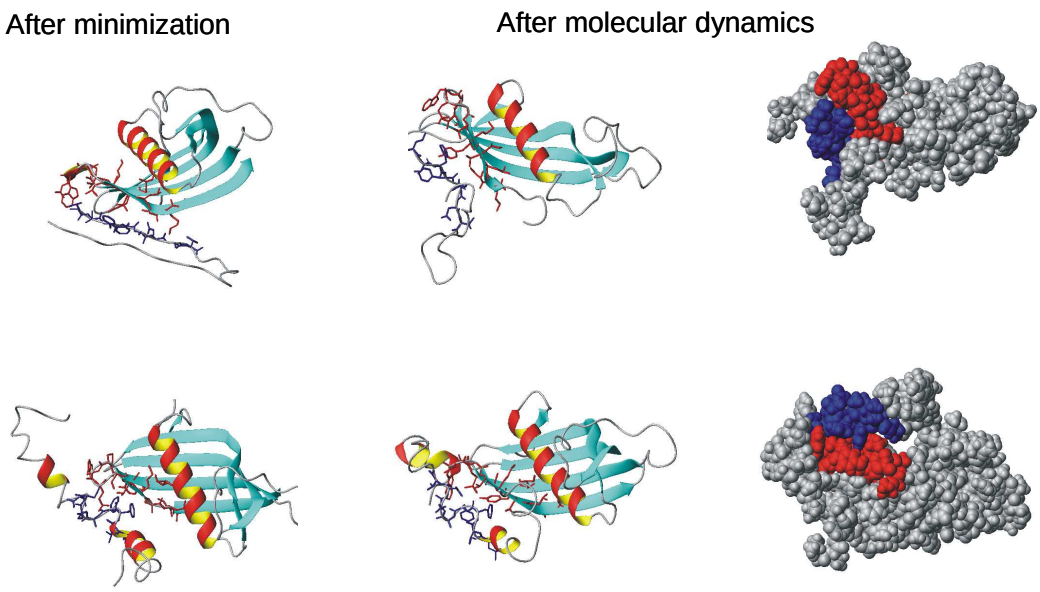

Figure 59: Molecular dynamics studies for wt HCC-Aβ(1-40) complexes.

In Figure 60, the stable HCC-Aβ complex is shown. The figure shows hydrophobic interactions between Tyr-102, Val-104 and Trp-106 residues of HCC (colored in blue) and Phe-19, Phe-20 and Val-24 residues of Aβ (colored in red) forming a hydrophobic cluster. In addition, the carbonyl groups of Phe-19 and Asp-23 (βCO) of Aβ form stable hydrogen bonds with the Gln-107 (γNH) and Thr-109 (OH) residues of HCC, in full agreement with the mass spectrometric epitope identifications. It may be suggested that the hydrophobic domains of Aβ and the L2-loop of HCC-protein “glue” together to form a stable complex. In addition, the L2 loop of HCC protein is covered by Aβ peptide and is not available for the external factors. The N- and C-terminal sequences of Aβ are not binding to HCC and therefore are cleaved by proteolytic enzymes.

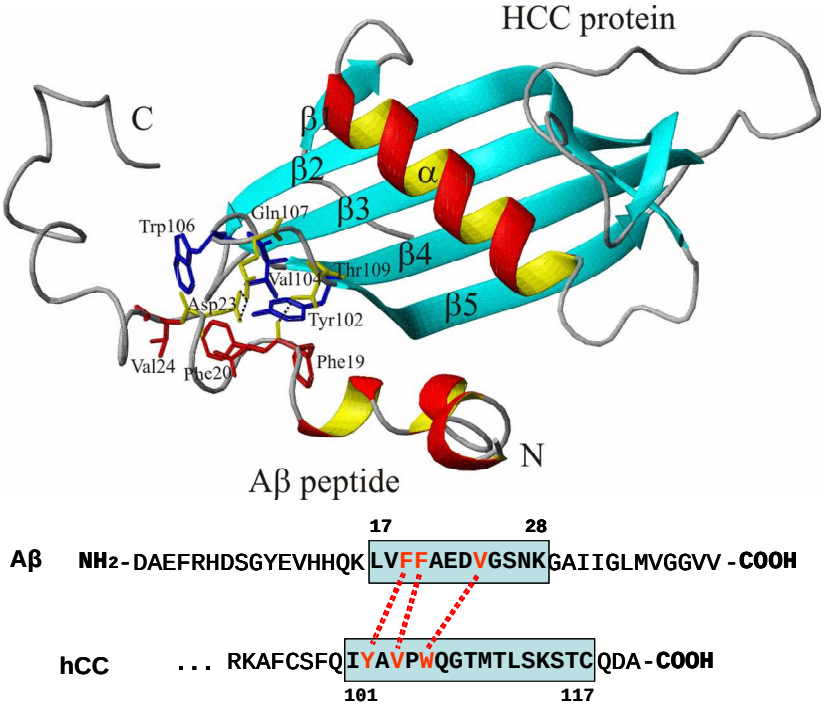

Figure 60: Interaction structure of the wt HCC-Aβ(1-40) complex revealed by molecular dynamics simulation. Hydrophobic interactions between HCC and Aβ, Tyr-102, Val-104 and Trp-106 residues of HCC are colored in blue, Phe-19, Phe-20, Val-24 residues of Aβ are colored in red. Hydrogen bonds between Gln-107 and Thr-109 residues of HCC and Asp-23 and Phe-19 of Aβ are indicated by black dashed lines, respectively; amino acids and carbonyl groups (Phe-19) forming hydrogen bonds are colored in yellow.

2.4.5 Binding studies of human Cystatin C to Aβ peptides

Epitope excision and extraction experiments in combination with mass spectrometric analysis employed for the identification of the antigenic determinant recognized by human Cystatin C led to the identification of the Aβ(17-28) fragment. Considering these results, a further aim of the dissertation was to compare the antigenic binding properties of Aβ(1-40) to wt HCC and of Aβ(17-28) to different HCC fragments using indirect ELISA.

For this purpose, a suitable ELISA approach for the analysis of Aβ-HCC complex was developed. In a first experiment, wt HCC was adsorbed on the 96-microtiter plate and the binding to the Aβ(1-40), Aβ(12-40), Aβ([1-16] and Aβ(17-28) peptides was probed. In order to make suitable the accessibility of the detection antibody to the system, a pentaglycine spacer and biotin were attached to the N-terminal part to the Aβ sequences. As a detection antibody, a HRP goat anti-biotin antibody was used. No anti-HCC or anti-Aβ antibodies were used in order to exclude a possible

interference of the antibody epitope with the binding sites of the HCC-Aβ complex. The plot of the absorbance vs. peptide concentration is shown in Figure 61. The highest binding was found for Aβ(17-28) as well as for the carboxy-terminal peptides Aβ(12-40) and the complete Aβ-sequence, while the *N*-terminal peptide Aβ(1-16) did not show any binding. These results are consistent with the mass spectrometric data obtained in the epitope determination.

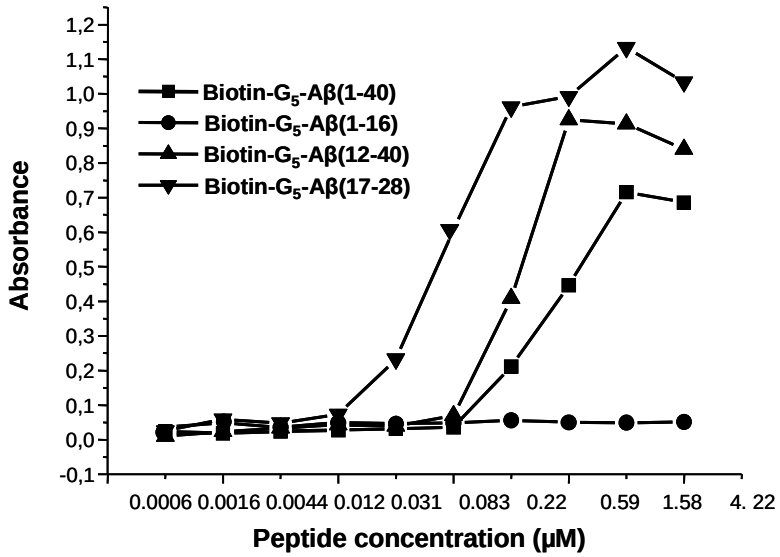

Figure 61: Binding properties of wt HCC to amyloid peptides spanning different domains of Aβ(1-40): (●) Aβ(1-16), (■) Aβ(1-40), (▲) Aβ(12-40) and (◀) Aβ(17-28). Background signals from wells without wt HCC have been subtracted.

Further comparative ELISA with the Aβ(17-28) epitope were performed using the C-terminal HCC peptides identified by epitope excision-mass spectrometry. For this experiment, the plate was coated with wt HCC, HCC(93-120), HCC(101-117) and HCC(101-114) fragments, and eight serial dilutions of the Aβ(17-28) were added (Figure 62). As a detection antibody, a HRP- goat anti-biotin antibody was employed, and the absorbance was measured at 450 nm. The results confirmed the *C*-terminal HCC epitope, with the carboxy-terminal sequence being essential for binding affinity to Aβ.

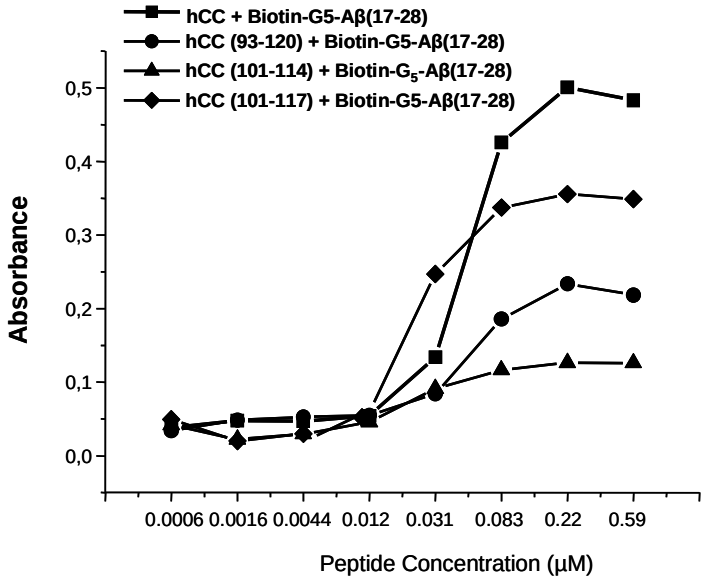

Figure 62: Binding of Aβ(17-28) to (■) wt HCC, (●) HCC(93-120), [▲] HCC(101-114) and (♦) HCC(101-117).

2.4.6 Characterization of the Aβ- epitope peptide by alanine scanning mutagenesis

The mass spectrometric experiments for the determination of the epitope recognized by wt HCC protein led to the identification of the middle sequence of the β-amyloid peptide, Aβ(17-28) (LVFFAEDVGSNK). In order to characterize the functional β-amyloid (17-28) epitope, the reactivities of the wt HCC towards synthetic peptides containing alanine-single-site mutations were investigated by ELISA. For the alanine scanning mutagenesis experiments all Aβ peptides were synthesized with a pentaglycine spacer and biotinylated at N-terminus, in order to ensure free accessibility of the epitope after binding.

The wt HCC was immobilized on the plates at a fixed concentration. After blocking, the alanine mutated peptides were added in 12 serial three fold dilutions using a stock solution of 1 µg/µL in PBS buffer. As detection antibody, HRP- goat anti-biotin antibody was used. In order to provide accurate background substraction, duplicate wells of each alanine mutations biotinylated peptides dilution without wt HCC were used.

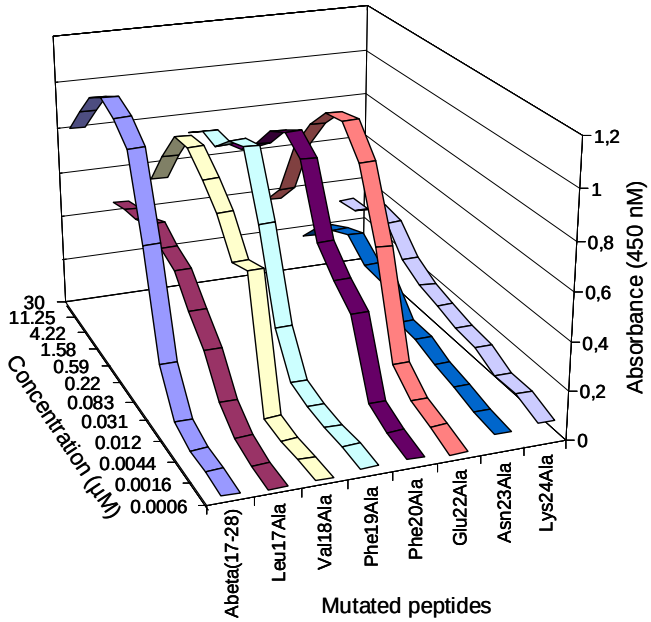

Figure 63: ELISA-detected reactivity of alanine mutants to the wt HCC. The relative immunoreactivities of the wild type Aβ(17-28) and mutant peptides to the wild type human Cystatin C were assested by indirect ELISA as described in the Experimental section.

The results (Figure 63) showed significant differences between the affinities of the alanine-mutated epitope peptides. Some amino acids are important for the binding to wt HCC. The peptides Aβ(17-28) V18A, F19A, F20A, E22A had an intermediate affinity to the wt HCC. The residues L17, D23, V24 were found to be essential for the binding to the wt HCC. The wild-type A21 gave a positive response to wt HCC.

In summary, alanine scanning mutagenesis proved to be a suitable method for characterizing the functional epitopes.

2.4.7 Binding affinity analysis of human Cystatin C epitopes to Aβ(1-40) and Aβ(17-28) peptides by SAW- biosensor

The dissociation constant determination of β-amyloid polypeptides to human Cystatin C fragments (93-120) and (101-117) was performed by SAW biosensor.

In a first set of experiments, the SAM of the gold-chip was activated with a mixture of EDC/NHC (see Experimental Part) and the HCC(93-120) was immobilized on the biosensor surface. The unreacted activated carboxyl groups were blocked with ethanolamine and the solvent was changed from water to phosphate buffer to ensure

the near physiological conditions. A series of injections using increasing concentrations of peptide (from 1.22 to 19 nM) were applied. For the determination of the association kinetics of the Aβ(1-40) to the immobilized HCC(93-120), the data were extracted from the sensor signals for all concentrations using the monomolecular growth model. For determining the corresponding dissociation kinetics, the exponential decay model was employed. Using the OriginPro 7.5 software, the changes of the sensor phase signals were fitted (Figure 64).

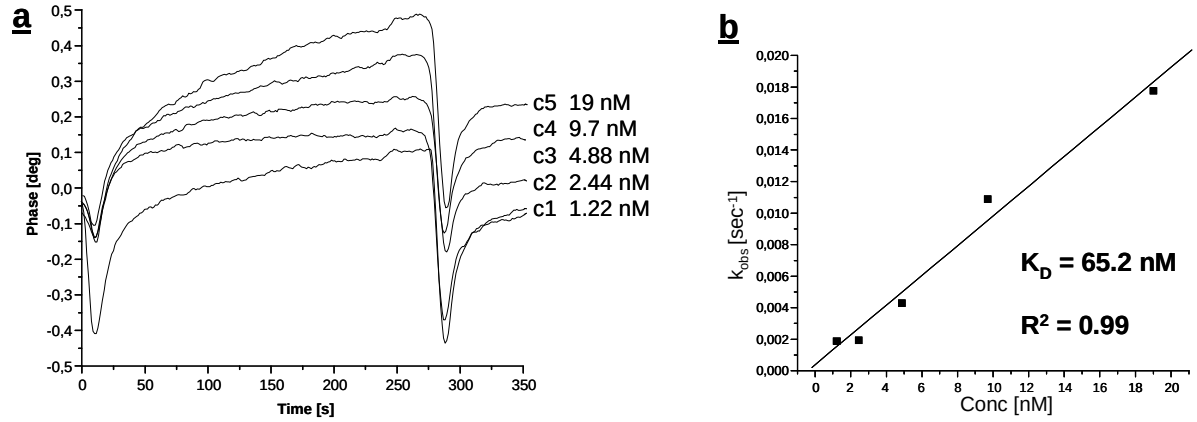

Figure 64: K_D determination of Aβ(1-40) on HCC(93-120) fragment using SAW biosensor. **a** The fitted curves of the increased binding; **b** Pseudo-first kinetic constant plotted versus concentration. The linear regression was applied for K_D of 65.2 ± 5.75.

In the second set of experiments, the interaction between HCC(93-120) and Aβ(12-40) and Aβ(17-28) respectively was studied. After activating the gold-chip with EDC/NHS, the HCC(93-120) fragment was immobilized at a concentration of 10 μM on the sensor chip, followed by blocking with ethanolamine. The running buffer was then changed to PBS and the experiment was continued with a series of injections at increasing peptide concentrations. After each injection, the bound peptide was dissociated in order to reach the baseline and the surface was regenerated with a pulse of HCl 0.1 M.To evaluate the results, the curves were exported into OriginPro and the integrated FitMaster was applied. A K_D value of 2.04 μM was obtained for Aβ(12-40) and 1.77 μM for Aβ(17-28).

Further experiments were performed in order to monitor the binding between HCC(101-117) and β-amyloid peptides (1-40), (17-28) and (12-40). HCC(101-117) was immobilized at a concentration of 10 μM on the gold-chip coated with 16-mercaptohexadecanoic acid. In order to study the binding between the

HCC(101-117) and β-amyloid polypeptides, the running buffer was changed to PBS and a series of injections of increasing peptide concentrations (1.95 nM to 1.25 µM) were applied. After each injection, the gold-chip surface was regenerated with a pulse of HCl 0.1 M and the resulting curves were then exported into OriginPro 7.5 for evaluation. The integrated FitMaster was applied. K_D values of 345.1 nM for Aβ(1-40) (Figure 65), 1.72 µM for Aβ(12-40) and 1.28 µM for Aβ(17-28) were obtained.

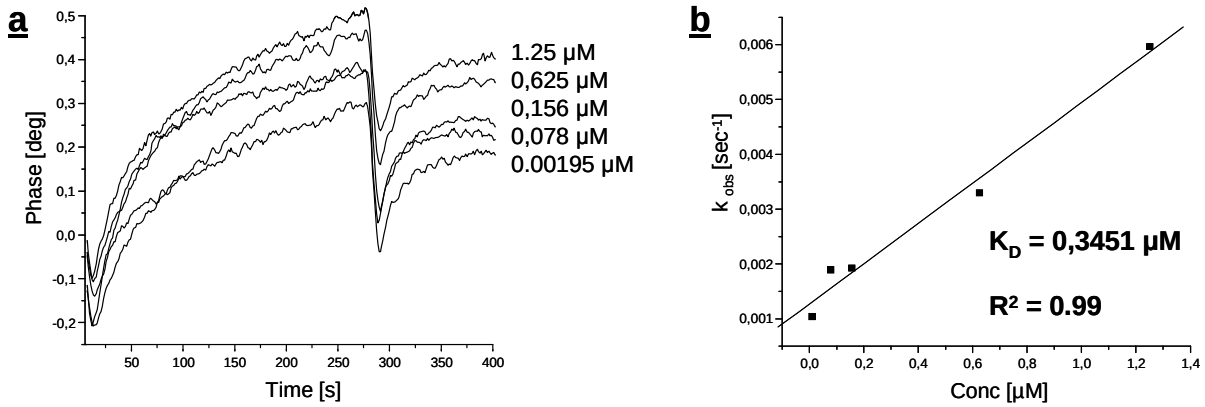

Figure 65: Dissociation constant determination of Aβ(1-40) on immobilized HCC(101-117) fragment using SAW biosensor. **a** The fitted curves of the increased binding; **b** Pseudo-first kinetic constant plotted versus concentration. The linear regression was applied for K_D of 345.1 ± 76.47 nM.

Dissociation constant determinations of the human Cystatin C fragments [93-120] and [101-117] for the β-amyloid peptides (1-40), (12-40) and (17-28) obtained from SAW biosensor are summarized in Table 7. Aβ(1-40) exhibited a higher affinity for HCC(93-120) with K_D value of 65.2 nM, than for HCC(101-117) with a K_D value of ~ 345 nm. Aβ(12-40) exhibited a lower affinity to HCC(93-120) (K_D = 2040 nM). The affinity of Aβ(12-40) to HCC(101-117) was higher (K_D = 1729.9 nM). Aβ(17-28) peptide had the lowest affinity for HCC(93-120) with a K_D of 1770 nM.

Table 7: Kinetic rate and equilibrium dissociation constants of human Cystatin C fragments [93-120] and [101-117] for the Aβ(1-40, (12-40) and (17-28).

No.	Ligand	Analyte	k_{on} (nM^{-1} sec^{-1})	k_{off} (sec^{-1})	K_D (nM)
1	hCC(93-120)	Aβ(1-40)	0.94418	0.06164	65.2 ± 5.75
		Aβ(12-40)	0.00514	0.0105	2040 ± 163.22
		Aβ(17-28)	0.0057	0.01013	1770 ± 304.47
2	hCC(101-117)	Aβ(1-40)	0.00127	0.00368	345.1 ± 76.47
		Aβ(12-40)	0.00237	0.00137	1729.9 ± 147.64
		Aβ(17-28)	0.0024	0.00309	1287.5 ± 199.73

2.4.8 Characterization of human Cystatin C epitopes and Aβ(17-28) epitope complexes by mass spectrometry

Using affinity- mass spectrometry, Aβ(17-28), HCC(93-120) and HCC(101-117) fragments showed a specific interaction with each other. However, this evidence is due to the methodology only of indirect nature. In order to characterize and prove the complex formation between Aβ(17-28) and human Cystatin C fragments, nano ESI-FTICR experiments were performed. The electrospray ionization, known as a “soft” ionization method, represents an established method for the identification of biopolymer complexes. A possibility of efficient detection of specific non-covalent complexes is the combination of high resolution and mass accuracy of FTICR-mass spectrometry [175, 176]. By changing certain device parameters in the electrospray mass spectrometer, as for example the desolvation potential, the covalent complexes can be specifically distinguished from non-covalent complexes, which is crucial for the structural characterization of complexes.

In order to investigate how the composition of the solvent has an impact on the charge distribution of human Cystatin C fragments in complex with Aβ(17-28), different spectra at different pH values were recorded. In 5 mM ammonium acetate buffer, with and without methanol at pH 6, no complex formation could be observed. By increasing the pH-value, the protonation of molecules was difficult, leading to less ion signals with lower charge numbers. Under these solvent conditions, it is therefore necessary to scan at higher mass range to capture all relevant signals. In general, the pH-value and the concentration of the buffer should be optimized, so that the ion signals fall in the m/z range of the mass spectrometer. The stability of non-covalent complexes in solution is highly dependent on the solvent conditions.

The complex formation has been observed in 0.5 mM ammonium acetate, pH 6 and a molar ratio of 1:1 between human Cystatin C fragments and β-amyloid peptides (1-40) and (17-28). The pH-value was adjusted with diluted acetic acid. The complex formation occurs at 20 °C after 1 h shaking and the mixture was analyzed by nano-ESI-FTICR mass spectrometer.

The complex between HCC(93-120) and Aβ(17-28) epitope yielded molecular ions $[M+3H]^{3+}$ (m/z 1497,6012) and $[M+4H]^{4+}$ (m/z 1123,4403) (Δm 6.5 ppm) (Figure 66). Thus, the ESI- mass spectrometric analysis of the peptide complex ascertained the specific interaction of the C-terminal human Cystatin C with the Aβ epitope located in the middle- of β-amyloid peptide (1-40).

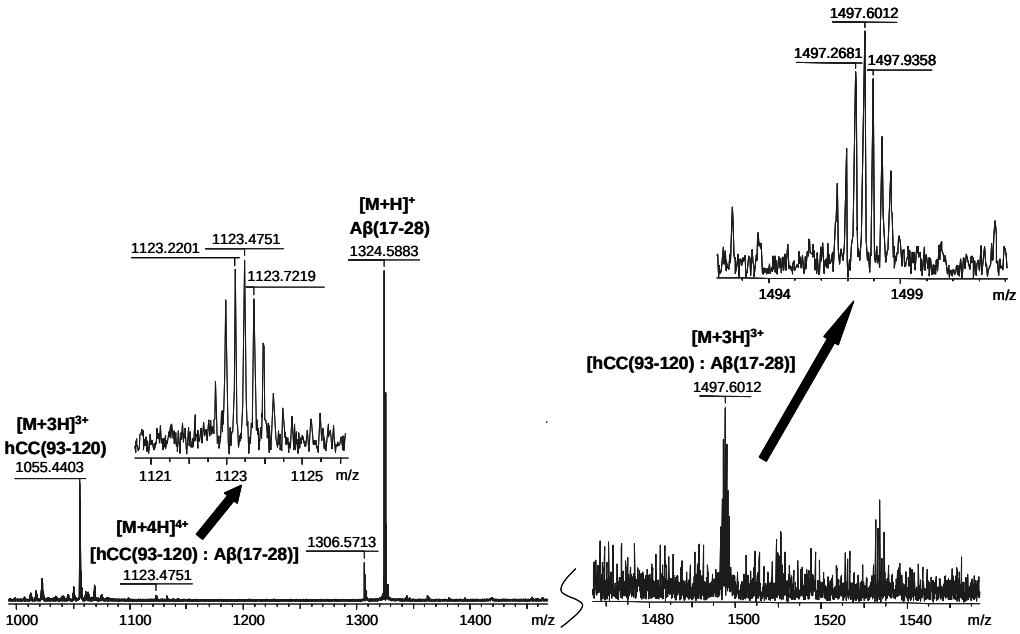

Figure 66: Nano-ESI-FTICR mass spectrum of HCC(93-120) in complex with β-amyloid (17-28) epitope peptide.

The nano-ESI-FTICR mass spectrum of the peptide complex between the HCC(101-117) fragment and the Aβ(17-28) epitope peptide is shown in Figure 67. The specific formation of a stoichiometric complex between the two minimal epitope peptides was ascertained by the triply charged molecular ion $[M+3H]^{3+}$ (m/z 1070,1408) of the complex, which were determined with a relative mass accuracy of approximately 5 ppm.

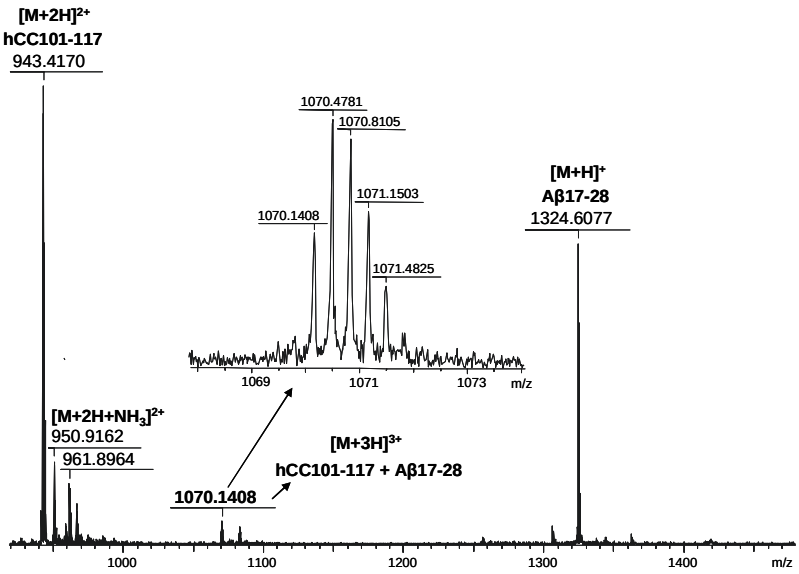

Figure 67: Nano-ESI-FTICR mass spectrum of HCC(101-117) in complex with β-amyloid (17-28) epitope.

2.5 Formation of Aβ- oligomers and inhibition of oligomerization with neuroprotective Cystatin C-epitope peptides

2.5.1 Pathways of Aβ(1-40) aggregation

Alzheimer's disease (AD) is the most common cause of late-life dementia that occurs in aged population [177]. Accumulation and fibrillar association in senile plaques of β-amyloid peptide (Aβ) is considered to be one of the causes of cognitive decline and neurodegeneration in AD [178, 179]. This is considered to be also the primary cause of toxicity in AD [180]. Aβ is considered to be a key in the pathogenesis of AD, because is the main constituent of amyloid plaques. Aβ peptide is a self-aggregating peptide of 39-43 amino acids derived from proteolytic processing of amyloid precursor protein (APP), a transmembrane glycoprotein that is expressed during normal cellular metabolism [181, 182]. In normal aging process, APP is processed by α-secretase, which cleaves within Aβ domain and produces a large soluble sAPPα domain and the C-terminal fragment containing p3 (C83). The C-terminal fragment can be further cleaved by γ-secretase. In AD, APP is cleaved by β-secretase at the N-terminus of Aβ region and at the C-terminus by γ-secretase. The β-secretase yields sAPPβ fragment and c99. A second cleavage occurs at the C-terminus of Aβ peptide by γ-secretase that release Aβ from c99. γ-secretase can cleave the C-

terminus of APP to produce shorter Aβ peptide (1-40) or the longer Aβ peptide (1-42) (Figure 68). In the cerebrospinal fluid, Aβ(1-40) was found to be the predominant form of Aβ [183].

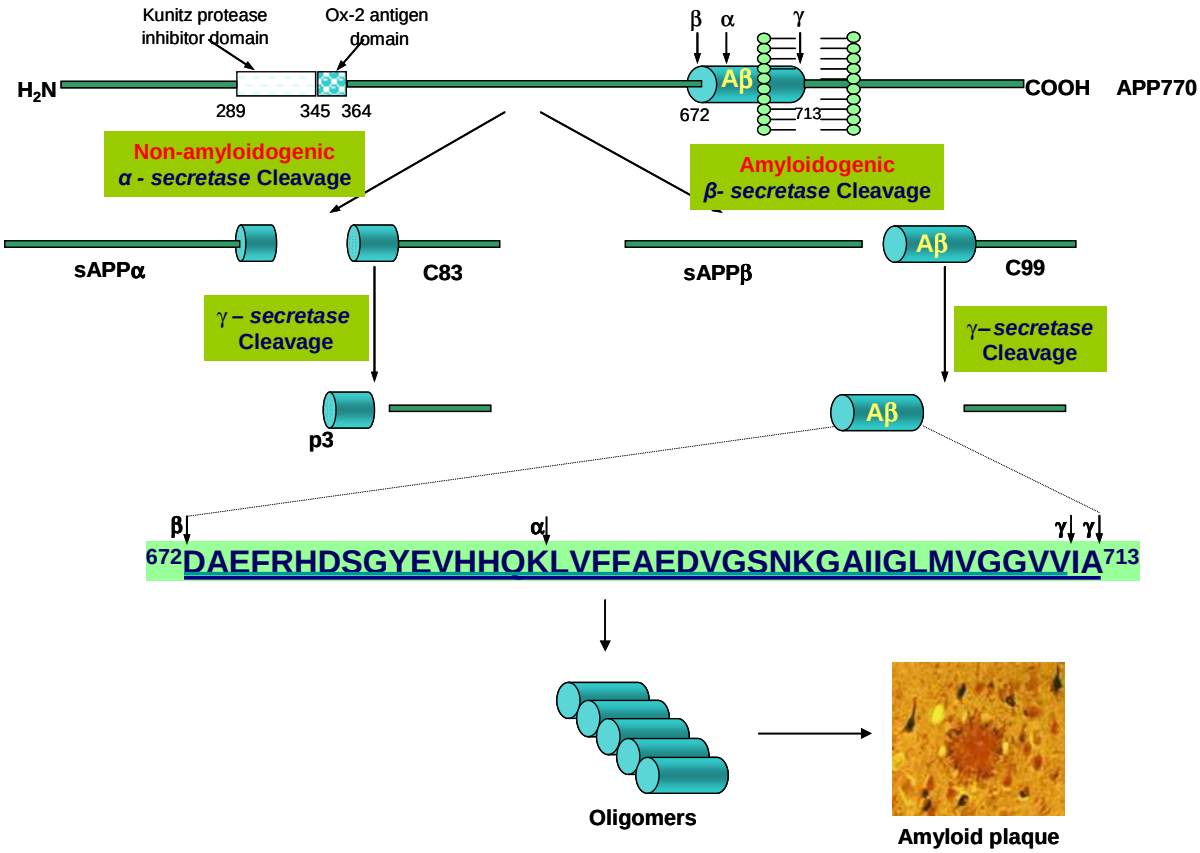

Figure 68: Schematic representation of the proteolytic processing pathway of the amyloid precursor protein: In the amyloidogenic pathway, β-secretase cleaves APP at one end of the β-amyloid peptide: sAPPβ is released into the space outside the neuron. γ-secretase cleaves APP at the other end of the β-amyloid peptide and β-amyloid peptides clump into soluble oligomers. Some oligomers clump together with other cellular material, forming increasingly insoluble fibrils. This clumping process leads to the insoluble plaques that are found in abundance in AD. In the non-amyloidogenic pathway, α-secretase cleaves the APP within the part that would form Aβ peptide. sAPPα is released outside the neuron and γ-secretase cleaves the remaining fragment (modified after [184-186])

The mechanism of aggregation is extremely complex and the two major peptides follow different pathways. The analysis of the assembly pathway of Aβ *in vitro* and biochemical characterization of Aβ deposits isolated from AD brain indicate that Aβ(1-40) exists as monomers, dimers, trimers, tetramers in rapid equilibrium, while Aβ(1-42) forms pentamer and hexamer units that assemble further to form early protofibrils and amyloid fibrils. From all these species, the most toxic appear to be the small oligomers, because are the proximate effectors of synapse loss and neuronal injury [79]. The formation of the amyloid fibrils is accepted as a form of nucleated

polymerization. This reaction is characterized by a slow nucleation step, known as “lag phase”, where little or no change in fibril concentration can be detected. The “lag phase” is followed by a rapid fibril elongation step, where a large mass percentage of the starting protein material is changed into fibrils, as shown in Figure 69 [187].

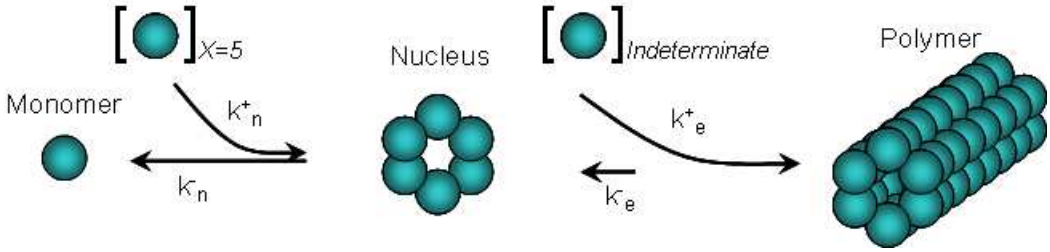

Figure 69: Nucleation dependent polymerization reaction showing an unfavourable self-association of a specific number of monomers (in this case 6) to form a fibril nucleus and the favourable addition of an unspecified number of monomers to the nucleus during fibril formation.

In order to continue the elucidation of the polymerization process, a complexity appears in the numbers, types of assembly paths (“on-pathway” and “off-pathway” for fibril formation) and the resulting structures. Figure 70 shows “on-pathway” of fibril assembly. Aβ peptide is considered to be a “natively unstructured” monomer. The “unstructured“ monomer associates into a partially structured monomer, which self-associates to a paranucleus. A paranucleus, suggested to be a pentamer or a hexamer, is the basic unit of the protofibrils. By a favourable kinetic, the protofibrils associate into the amyloid-type fibrils [188].

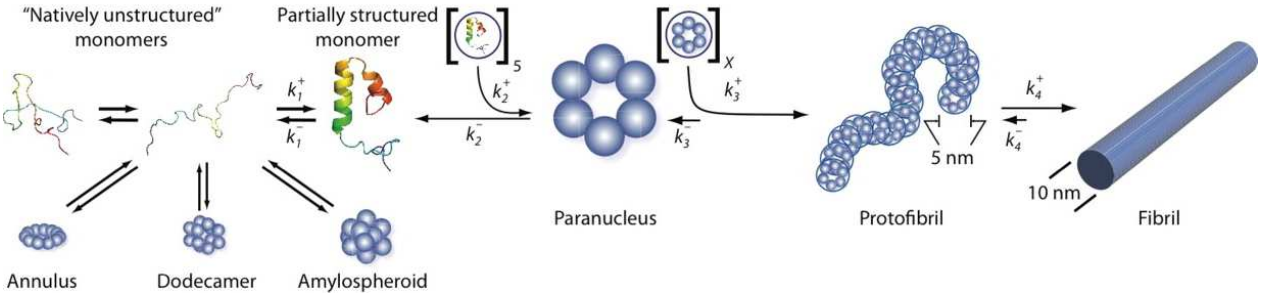

Figure 70: “On- pathway” of fibril assembly: A natively unstructured monomer (Aβ) forms a partially structured monomer that self-associates to form a paranucleus (a nucleus for fibril elongation). Paranuclei self-associate to form protofibrils. Protofibrils are relatively narrow (~ 5 nm), short flexible structures. The maturation of protofibrils yields classical amyloid fibrils, with ~10 nm diameter [188].

Another model for the fibril formation pathway is based on the proof that an α-helix-containing intermediate may be involved into the fibrillization process. At the level of

oligomers with α-helical structure occurs the transition to a β-sheet conformation. Only high-ordered and insoluble oligomers show β-sheet structure [189, 190]. In this case, fibril growth indicates that the reaction is a cooperative process with a constant elongation rate and that the aggregation mechanism is considered to be as “assembly via oligomeric intermediates”. This mechanism is known to be an isodesmic polymerization, where there is no separate nucleation and elongation phase.

2.5.2 Characterization of Aβ-oligomers *in vitro*

2.5.2.1 Preparation and characterization of Aβ-oligomers

In order to understand the pathogenesis of AD and to find new effective strategies for prevention or treatment of AD, it is important to elucidate the Aβ aggregation. Aβ possesses a high propensity to aggregate and represents a model for intrinsically unstructured proteins (IUPs). The aggregates can be divided into several morphologically different types, from oligomers, amorphous aggregates to amyloid-like fibrils. Until now, the molecular structure of Aβ oligomers is still unknown. Different experimental designs have been used to prepare oligomeric and protofibrillar Aβ species from synthetic or recombinant Aβ peptides. *In vitro* formation of aggregates and amyloid fibrils from synthetic and recombinant form of Aβ peptides has been shown to be indistinguishable from aggregates and fibrils isolated from AD brain [191, 192]. This suggests that *in vitro* studies are relevant for elucidating the molecular mechanism(s) of amyloid formation *in vivo*. In the present work, the lyophilized Aβ was treated with NaOH, TFE or hexafluoroisopropanol (HFIP), followed by incubation at 37 ° C with shaking for different period of times. NaOH was used to disrupt preformed aggregates and increase the solubility [193, 194]. HFIP and TFE break up hydrophobic interactions in aggregated amyloid preparations and have a role in stabilizing the α-helical structure. These properties lead to disturbing of pre-existent β-sheet structure [144, 195]. The incubation conditions and the code for each sample are summarized in Table 8.

Table 8: *In vitro* incubation conditions for the formation of Aβ(1-40) aggregation products.

	Code	Buffer	Concentration (µM)	Temperature (°C)
synthetic Aβ(1-40)	A1	TFE/ 20 mM PBS	100; 50; 25	37
	A2	HFIP /20 mM PBS	50	37
	A3	NaOH / 20 mM PBS	50	37
recombinant Aβ(1-40)	A4	HFIP / 20 mM PBS	50	37
	A5	NaOH / 20 mM PBS	50	37

In order to ascertain which concentration was suitable for oligomers formation, the synthetic Aβ(1-40) (A1) was first dissolved in TFE and dried under vacuum. The pellet was re-dissolved in 20 mM PBS with a final concentration of 100 µM, 50 µM and 25 µM and incubated for 4 and 7 days (Figure 71). The oligomers formation was monitored by Tris-Tricine-PAGE and the gels were stained with Coomassie blue. In all samples, the monomers and tetramers were present after 4 days of incubation. After 7 days of incubation, four bands corresponding to monomer, trimer, tetramer and protofibrils were present in the sample with 50 µM Aβ(1-40). Therefore, 50 µM of sample was used for further experiments.

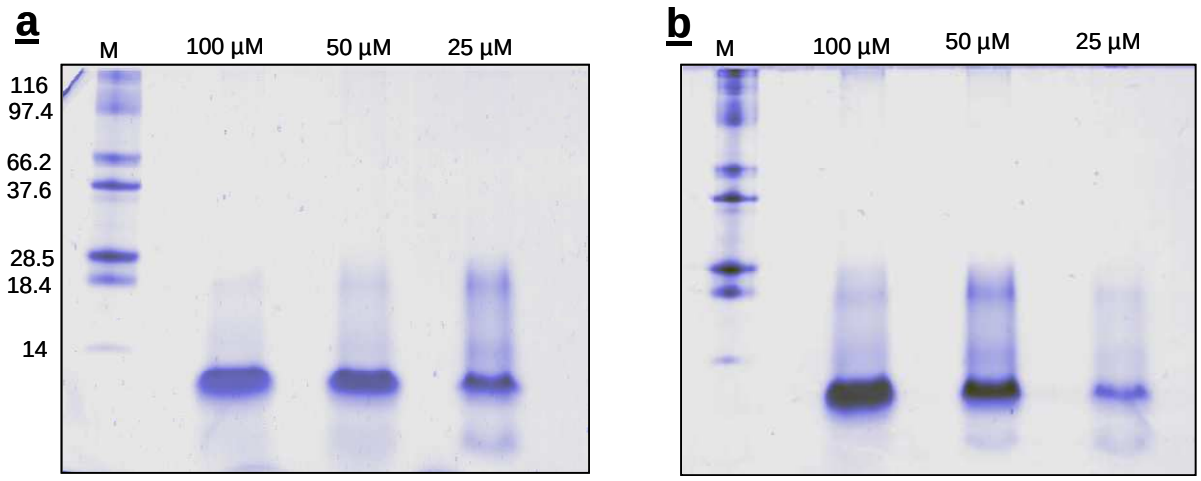

Figure 71: 10 % Tris-Tricine gel electrophoresis of synthetic (A1) Aβ(1-40) using different concentration of the peptide. Aβ(1-40) was dissolved in TFE and then incubated in 20 mM PBS buffer for **a** 4 **b** 7 days. The gels were stained with Coomassie blue.

In the first experiment, Aβ(1-40) (A1) was dissolved in TFE, which was then removed under vacuum. The peptide was re-dissolved in 20 mM PBS buffer and incubated for

0 h, 1 h, 2 h, 3 h, 4 h and 2, 4, 7 days at 37 °C under shaking. Thereafter, the samples were loaded onto a 10 % Tris-Tricine PAGE for separation of the aggregation products. After staining the gel with silver nitrate, four bands corresponding to the monomer, trimer, tetramer and protofibrils products were detected (Figure 72).

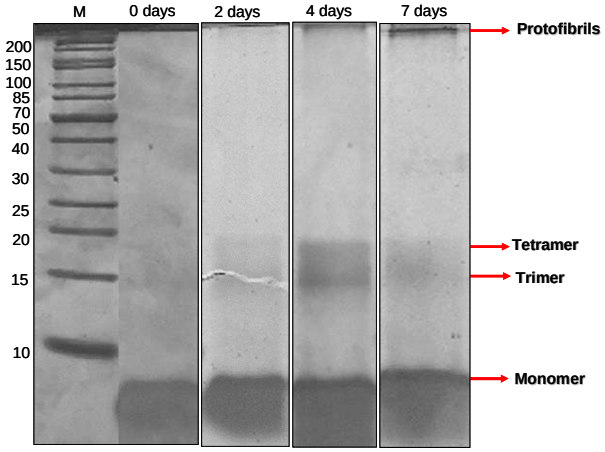

Figure 72: Characterization of Aβ(1-40) aggregation process by gel electrophoresis. The oligomers (A1) were separated by 10 % Tris-Tricine-PAGE and stained with silver nitrate. The bands corresponding to monomer, trimer, tetramer and protofibrils were detected after four and seven days.

Aβ protofibrils were obtained by dissolving the synthetic (A3) and recombinant (A5) peptides at a concentration of 1 mM in 1 mM NaOH and by adding 10 mM NaOH in order to change rapidly the highly acidic TFA salt peptide through its isoelectric point to a pH of ~7.0 – 7.5 [196]. The treatment of Aβ peptides with alkali prior dissolving it in PBS buffer was effective in decreasing the number of pre-existent aggregates [197]. The peptides were incubated for 0, 2, 4 and 7 days at a final concentration of 500 µM in PBS buffer (see Experimental part). The monitoring of the protofibrils formation was made by 10 % 1D-Tris-tricine polyacrylamide gel electrophoresis. After 2, 4 and 7 days, bands corresponding to a mixture of monomer and protofibrils were detected (Figure 73 a and b).

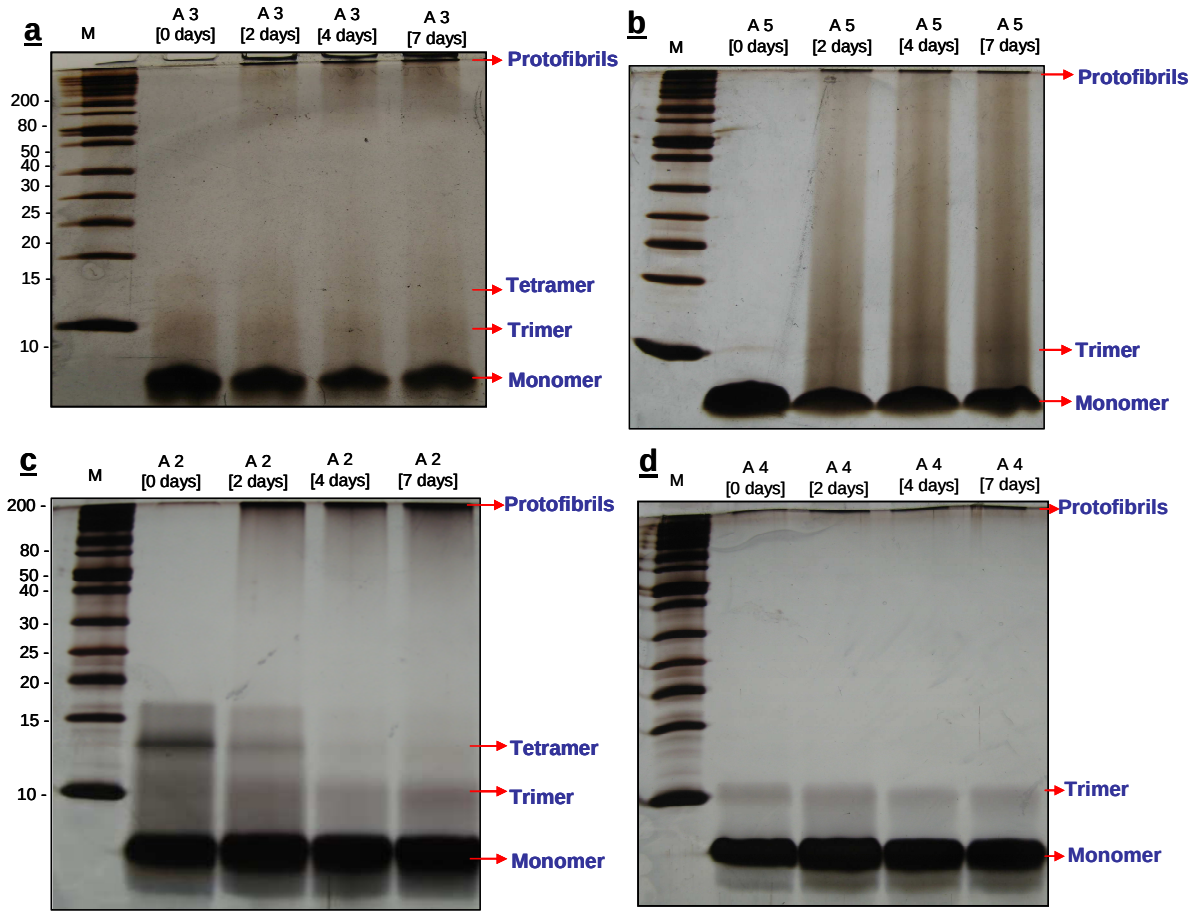

Figure 73: Tris-tricine gel separation of **a** synthetic (A3) and **b** recombinant Aβ(1-40) (A5) oligomerization products obtained by dissolving the peptide in 10 mM NaOH and incubated in PBS buffer, pH 7.4 at 37°C for 0, 2, 4 and 7 days; **c** synthetic and **d** recombinant Aβ(1-40) oligomerization products obtained by dissolving the peptides in HFIP and incubated in PBS buffer at 37 °C for 0, 2, 4 and 7 days with shaking. The gels were stained with silver nitrate.

Furthermore, structural characterization of synthetic (A2) and recombinant (A4) Aβ(1-40) peptides was performed by dissolving the lyophilized peptides in HFIP. HFIP was then removed under vacuum. The peptide film was re-dissolved in 20 mM PBS and incubated for 0, 2, 4 and 7 days at 37 °C [198]. The aliquots were frozen, lyophilized and the oligomerization process was monitored by 10 % Tris-tricine gel electrophoresis (Figure 73 c and d). In the gels it could be observed the transition from monomer, trimer and tetramer to high quantity of protofibrils after 7 days.

Aβ-aggregation products were assessed for their binding affinity to different antibodies by Dot blot analysis. Different concentrations of Aβ(1-40), 100 µM (1), 50 µM (2), 25 µM (3), 12.5 µM (4), 6.25 µM (5), 3.125 µM (6), 1.56 µM (7) incubated for 2 days were spotted on nitrocellulose membranes and unspecific binding sites were

blocked. After washing, the membranes were incubated with anti-Aβ antibodies (Appendix 7: anti-Aβ(1-16) (6E10) (**a**); anti-Aβ(17-28) (4G8) (**b**); anti-APP antibody (**c**)) for 2 h at 25 °C. After further washing and addition of the detection antibody, membranes were developed and exposed on a film, and the exposed films developed by using an automated Canon camera. Anti-Aβ(1-16) and anti-APP antibodies gave an intensive response at concentrations 1, 2 and 3 of Aβ(1-40). Anti-Aβ(17-28) gave intensive responses for all Aβ(1-40) concentrations. These antibodies should recognize only the monomeric Aβ(1-40) and not the oligomers. An explanation for the results is the existence of equilibrium between monomers and oligomers.

2.5.2.2 Aggregation analysis using Thioflavin-T assay

Thioflavin T (ThT), first introduced in 1959 by Vassar and Culling, is a cationic benzothiazol dye that binds to amyloid fibrils and is used to stain, diagnose and analyse the kinetic and structural properties of amyloid fibrils both *in vitro* and *in vivo* [199]. Upon binding to fibrils, ThT exhibits a dramatic shift of the excitation maximum from 385 nm to 450 nm and the emission maximum from 445 nm to 482 nm [200]. ThT fluorescence originates only from the dye bound to amyloid fibrils. In comparison with other amyloid dyes (e.g. Congo red or methyl violet), ThT has been recommended to be used in many experimental systems due to its high solubility in water and moderate affinity to fibrils [201-203] . It has been demonstrated that ThT binds equally to fibrils prepared from synthetic and recombinant peptides or proteins [204].

In order to investigate the effect of ThT concentration on its intrinsic fluorescence properties, an experiment using different concentrations of ThT (from 0 µM to 100 µM) and 2 concentrations of Aβ(1-40) (10 µM and 50 µM) was perfomed. The intensity of the excitation at 450 nm and emission at 486 nm of aqueous ThT solutions from 0 to 100 µM are shown in Figure 74. Upon 5 µM concentration of ThT, an increase of the intensity was observed, which is closely related to the concentrations at which micelle formation occurs. A high signal was present in the sample with 50 µM Aβ(1-40), which corresponds to the presence of more fibrils in solution.

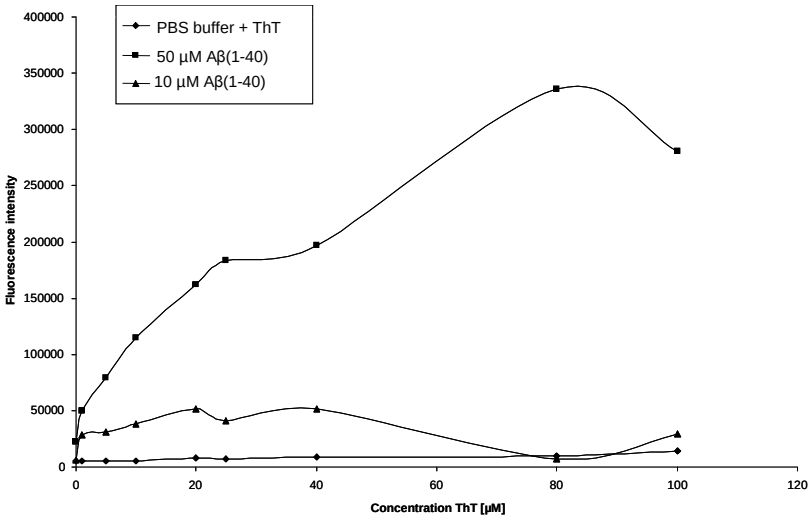

Figure 74: ThT binding titrations measuring ThT emmission 486 nm. Protein concentrations were 0 µM, 10 µM and 50 µM.

In vitro oligomerization products of Aβ(1-40) were prepared by dissolving the synthetic and recombinant Aβ(1-40) peptides in NaOH and HFIP. The solvents were removed under vaccum and the pellet was re-dissolved in 20 mM PBS. The samples were incubated at 37 °C with agitation in a microcentrifuge tube for 0, 2, 4 and 7 days. As a control, a blank was provided with 20 µM ThT in PBS. Determinations were carried out in 96-well plates (black; black bottom) using a fluorescence plate reader (Perkin Elmer Victor^2). Fluorescence was measured at an excitation of 450 nm and emission of 486 nm. The results showed that in both experiments, with previous dissolving the samples in NaOH and HFIP, the aggregation rates increase in the order synthetic Aβ(1-40) (labelled A2 and A3) < recombinant (labelled A4 and A5) Aβ (1-40) (Figure 75).

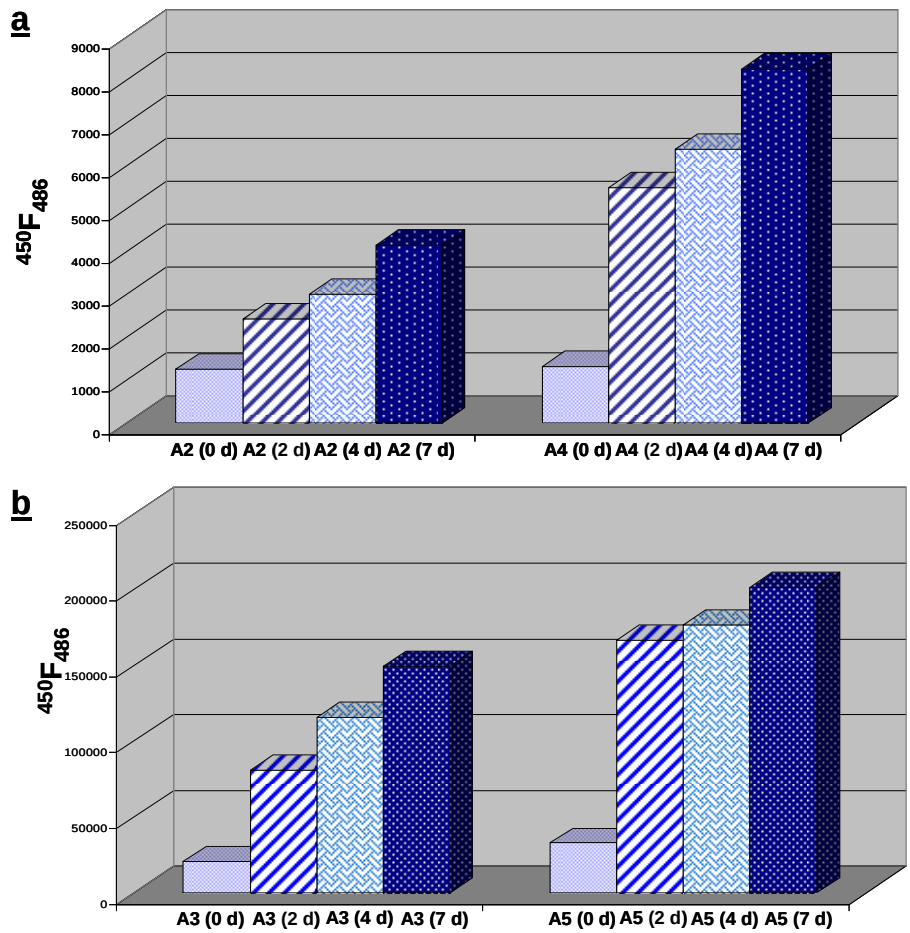

Figure 75: ThT assay of **a** synthetic (A2) and recombinant (A4) Aβ(1-40) peptides dissolved in HFIP. After evaporation, the pellet was re-dissolved in 20 mM PBS and the samples were incubated for 0, 2, 4 and 7 days. **b** synthetic (A3) and recombinant (A5) Aβ(1-40) peptides dissolved in NaOH and incubated in 20 mM PBS 0, 2, 4, and 7 days. The aggregation rate increases in the following order synthetic Aβ (A2, A3) < recombinant Aβ (A4, A5).

Figure 75 compares the fibrillization patterns of synthetic and recombinant Aβ(1-40) peptides, both dissolved in HFIP (A2, A4) and NaOH (A3, A5) monitored by the increase in ThT fluorescence. The recombinant Aβ(1-40) showed in both cases the fastest rate of fibril formation, whereas synthetic Aβ(1-40) formed fibrils at a slower rate.

2.5.3 Inhibition studies of Aβ aggregation by human Cystatin C peptides

The presence of human Cystatin C (HCC) in amyloid deposits has been intriguing. The function of HCC in the brain is unclear at present, but a wide spectrum of activities have been assumed in conjunction with other protease inhibitors in the central nervous system, such as modulation of neuropeptide activation and

degradation, neurite proliferation and neuronal protection. It has recently been reported that HCC is overexpressed in the neurons particularly susceptible to AD degenerative processes, including the entorhinal cortex, hippocampus and temporal cortex, and it has been proposed that Cystatin C may play a role in AD pathogenesis.

The results of proteolytic excision- mass spectrometry showed that the Aβ binding site is located at the C-terminal region of HCC within residues (101-117). The epitope recognized by HCC is important for the Aβ aggregation. The Aβ-epitope identified comprises a part of the hydrophobic core at residues (17-22) (LVFFA) and the β-turn for fibril formation located within residues (25-28). The HCC binding results confirm that HCC efficiently binds to this region, and by blocking the residues (17-28) it can influence the Aβ oligomerization, decreasing neurotoxicity and plaque formation. The HCC binding site in Aβ identified here is different from that proposed by Sastre et al., as our results ascertain binding at the central domain of Aβ, not at an N-terminal sequence as previously suggested. The observed blocking of HCC binding to Aβ by an anti-Aβ(1-17) antibody may be well explained by steric hindrance of HCC access to the binding site starting at Leu-17. Selenica et al. showed that HCC reduced the *in vitro* formation of soluble oligomers and protofibrils of Aβ(1-42); however, HCC did not dissagregate preformed Aβ- oligomers.

In the first inhibition experiment, HCC(93-120) and Aβ(1-40) (50 µM) were dissolved in TFE and then incubated at 37 °C with different molar equivalents (1:0.5, 1:1, 1:2, 1:3) of HCC(93-120) in 20 mM PBS for 18 h to 7 days (Figure 76). The sample which contains no HCC served as a control. In the presence of HCC(93-120), Aβ(1-40) shows a significant decrease in aggregation rate after 4 days in a molar ratio of 1:2. At a molar ratio of 1:3, ThT fluorescence increase (no inhibition was present), due to a higher concentration of HCC(93-120). It has been shown that at a higher concentration, HCC(93-120) forms aggregates.

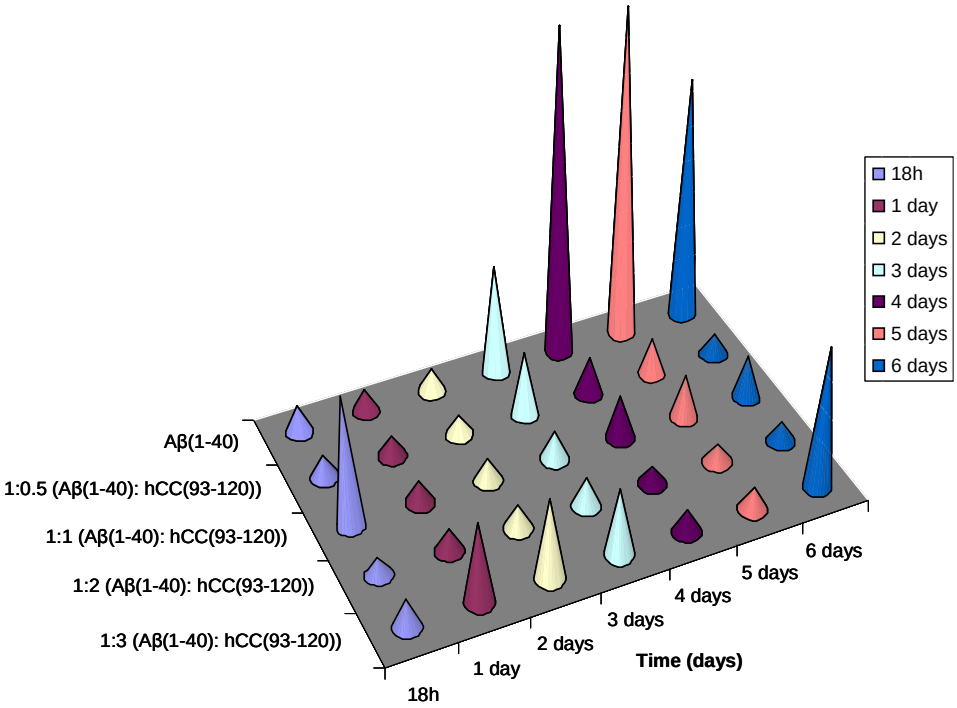

Figure 76: Inhibition studies of Aβ40 and HCC(93-120). The molar ratio between Aβ(1-40) and HCC(93-120) was as follow: 1:0.5, 1:1, 1:2, 1:3.

A further experiment was carried out using HCC(101-117) as inhibitor. First, Aβ(1-40) was dissolved in TFE and after solvent evaporation, the pellet was re-dissolved in 20 mM PBS and incubated with HCC(101-117) for 0 to 7 days. The molar ratio between Aβ(1-40) and HCC(101-117) was as follow: 1:0.25, 1:0.5, 1:1, 1:2, 1:3 (Figure 77). The samples were incubated at 37 °C under shaking. The fluorescence was measured in 96-well plates using a plate reader (Perkin Elmer, Victor^2). An excitation of 450 nm and emission of 486 nm have been used for the measurements. At ratios of 1:0.25 and 1:0.5, a decrease in the fluorescence intensity could be observed, due to a less amount of fibrils in solution. At ratios 1:1, 1:2 and 1:3, the presence of more fibrils could be detected in the sample mixtures.

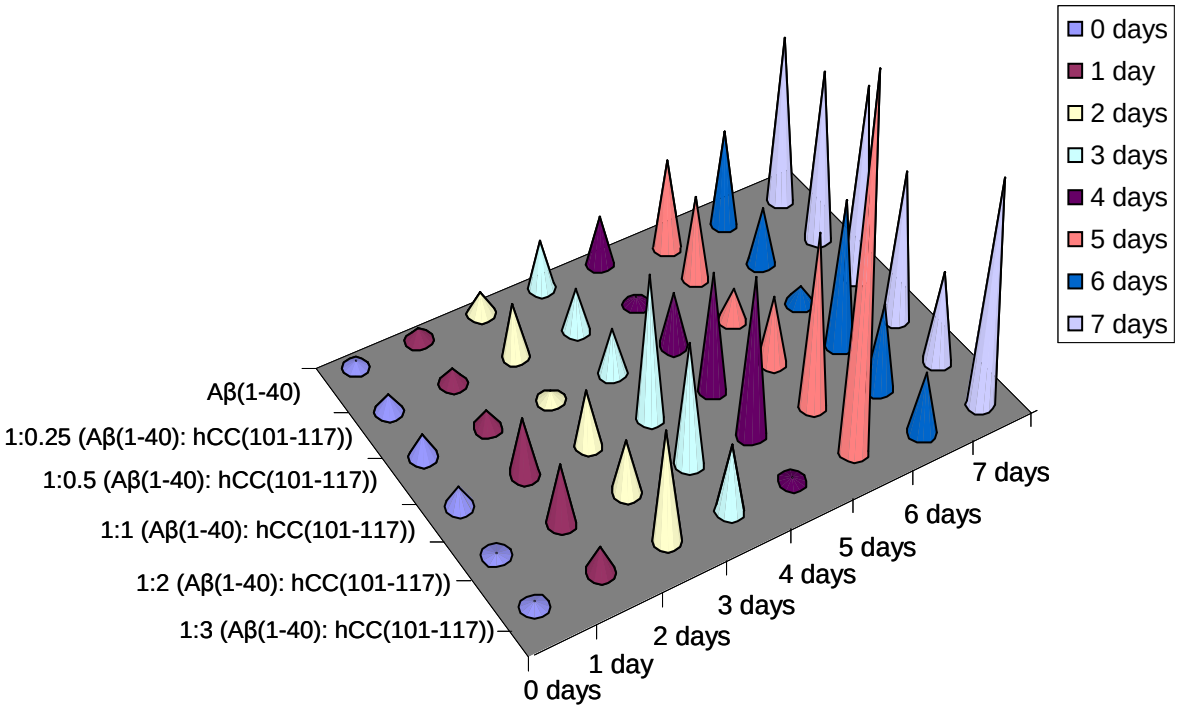

Figure 77: Inhibition studies of Aβ(1-40) and HCC (101-117) at a molar ratio of 1: 0.25, 1:0.5, 1:1, 1:2 and 1:3.

Furthermore, Aβ-aggregation and inhibition of aggregates by HCC(101-117) and HCC(93-120) were carried out by Dot blot analysis. The samples were first spotted on nitrocellulose membranes and unspecific binding sites were blocked. After washing, the membranes were incubated with anti-Aβ oligomers antibody (A11; from Chemicon und Invitrogen) for 2 h at 25 °C. After further washing and addition of the detection antibody, membranes were developed and exposed on a film (exposure time 10-30 sec), and the exposed films developed by using an automated Canon camera. The Dot blot responses of anti-Aβ oligomers antibodies are shown in Figure 90. Both antibodies gave a positive response for the Aβ(1-40) incubated 4 days (labelled with 1 and 3 in Figure 90 a and c) and 6 days (labelled 1 and 3 in Figure 90 b and d). When the synthetic Aβ(1-40) was incubated *in vitro* with HCC(93-120) for 4 days (labelled 3 in Figure 90 a and c) and 6 days (labelled 3 in Figure 90 b and d) and with HCC(101-117) for 4 days (labelled 4, Figure 90 a and c) and 6 days (labelled 4 b and d), the presence of oligomers was reduced.

Our results suggest that the presence of HCC in Aβ solution can decrease oligomerization and slow down the aggregation process.

In the *in vivo* experiments (performed by Stephan Käser at the University Hospital in Tübingen at Hertie Institute for Clinical Brain Research) on the APPPS1-Mice the HCC(101-117) has been infused using osmotic pumps in the right ventricles of the mice brains. After 4 weeks, the animals were sacrified, the brain removed and immunostained. Later was observed that the pump was not placed correctly into the cerebrospinal fluid, but into the parenchyma. The preliminary results from *in vivo* experiments showed that the Aβ-deposits throughout the brain were significantly reduced due to the infusion of HCC(101-117) into the parenchyma and further studies will be performed.

3 Experimental Part

3.1 Proteins, Enzymes and Antibodies

Human angiotensin II, human bradykinin, human angiotensin I, human neurotensin,human adrenocorticotropic hormone (ACTH), bovine insulin β-chain oxidized, bovine insulin, bovine serum albumin: **Sigma.**
Sequence grade TPCK-modified trypsin, Porcine: **Promega**. Pronase, Streptomyces griseus: **Calbiochem**, α-Chymotrypsin TLCK-treated, Endoproteinase Glu-C from *Staphylococcus aureus*, strain V8: **Sigma,** Endoproteinase Lys-C, sequencing grade from *Lysobacter enzymogene*: **Roche.**

Table 9: Antibodies

Type	Company
Mouse anti-amyloid-β 1-16, monoclonal, clone AB10	Chemicon
Mouse anti-amyloid–β 17-24, monoclonal, clone 4G8	Chemicon
Rabbit anti-amyloid oligomers, polyclonal antibody, clone A11	Chemicon
Rabbit anti-oligomer antibody unconjugated, polyclonal, clone A11	Invitrogen
Horseradish peroxidase (HRP) goat-anti mouse	Jackson Immuno Research
Horseradish peroxidase (HRP) goat-anti biotin	Jackson Immuno Research
Horseradish peroxidase (HRP) goat-anti rabbit	Jackson Immuno Research
Horseradish peroxidase (HRP) goat-anti human	Jackson Immuno Research

Aβ-nanobodies were kindly obtained from the cooperation with Professor Serge Muyldermans, Department of Cellular and Molecular Interactions, Laboratory of Cellular Immunology, Vlaams Interuniversitair Institut voor Biotechnologie, Vrije Universiteit Brussel, Belgium and human Cystatin C protein was obtain from Dr. Paulina Czaplewska, Department of organic chemistry, University of Gdansk, Poland**.**

3.2 Materials and reagents

The reagents and solvents used were of analytical grade, or highest available purity. The following commercially available reagents were used in this work: activated CH-Sepharose 4B, polyoxyethylensorbitanmonolaureat (Tween20), 2,2,2-trifluoroethanol (TFE), α-cyano-4-hydroxycinnamic acid (HCCA), diethanolamine, dimethylsulfoxide (DMSO), trichloroacetic acid (TCA), Coomassie Brilliant Blue G250: **Sigma**; N-α-Fmoc protected amino acids, NovaSyn TGR resin: **NovaBiochem** or **Reanal;** D-(+)-Biotin: **Calbiochem**; t-buthylmethylether,N-methylmorpholine (NMM), piperidine, 1,8-diazabicyclo-[5.4.0]undec-7-ene (DBU), trifluoroacetic acid (TFA), triethylsilane, triisopropylsilane, iodoacetamide, agarose, bromophenol Blue, TEMED: **Fluka**; N,Ndimethylformamide (DMF): **Acros Organics**; Hydrochloric acid, sodium hydroxide, urea, thiourea: **Merck**; deionized water: **Millipore**; disodium hydrogen phosphate-2-hydrate (Na2HPO4): **Riedel-de Haen**; acetic acid, sodium chloride, silver nitrate, 2-Amino-2-hydroxymethyl-propane-1,3-diol (Tris), ethanol, acetonitrile (MeCN), tris-(hydroxymethyl)-aminomethane (Tris): **Roth**; dichloromethane (DCM): **VWR;**

3.3 Solid Phase Peptide Synthesis (SPPS)

The peptide sequences described in this work were synthesized by SPPS according to Fmoc/tBu strategy either manually or using a semiautomated peptide synthesizer EPS 221 (Abimed, Germany). The semiautomated peptide synthesizer is based on a pipetting robot operated from a keypad controller with a disc drive. Separate software allows the modification of the program on a standard PC according to the scale of the synthesis and the sequence-related difficulties of the peptide to be synthesized.

For the peptides which were synthesized using a semi-automatic peptide synthesizer, the following protocol was used:

(a) washing the resin with DMF (3 X 1 min);

(b) deprotection with 2 % DBU, 2 % piperidine in DMF (15 min);

(c) DMF washing (3 X 1 min);

(d) coupling of 5 equiv of Fmoc amino acid derivative using PyBop:NMM in DMF for activation of the amino acid (45 min);

(e) DMF washing (3 X 1 min).

The protocol for the manual solid phase peptide synthesis was as follows:

(a) DMF washing (5 x 0.5 min);

(b) deprotection with 2 % DBU, 2 % piperidine in DMF (2+2+5+10 min);

(c) DMF washing (10 x 0.5 min);

(d) coupling of 5 equiv of Fmoc amino acid derivative: PyBop : NMM in DMF (45 min);

(e) DMF washing (10 x 0.5 min);

(f) DCM washing (3 x 0.5 min);

(g) Monitor the coupling steps by bromophenol blue assay, ninhydrin assay or cloranil assay to assess the presence of free amines.

NovaSyn®TGR-resin (Novabiochem) was generally used (Figure 78), and the peptides were synthesized in amidated form at the C-terminal. For the difficult sequences, TentaGel RRAM-resin (Rapp) was used (Figure 79).

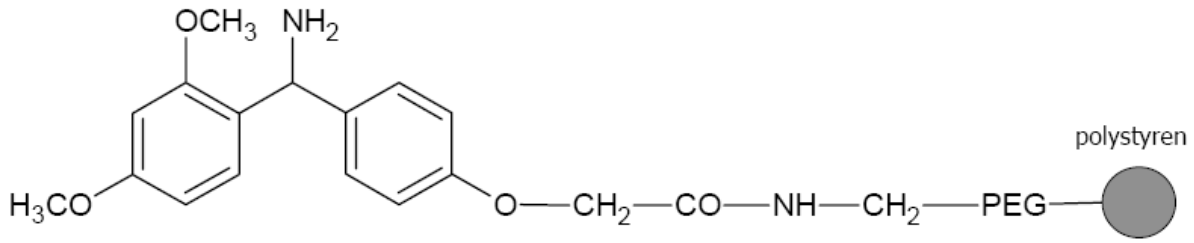

Figure 78: Schematic representation of NovaSyn®TGR-resin.

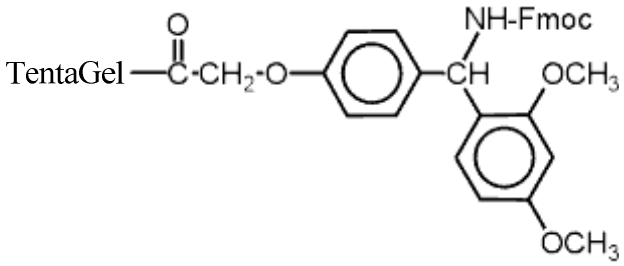

Figure 79: Schematic representation of TentaGel RRAM resin.

The amino acids used were N(α)-fluorenylmethyloxycarbonyl (Fmoc) protected (see Appendix 1).

The general scheme of Fmoc-SPPS employed is shown in Figure 80.

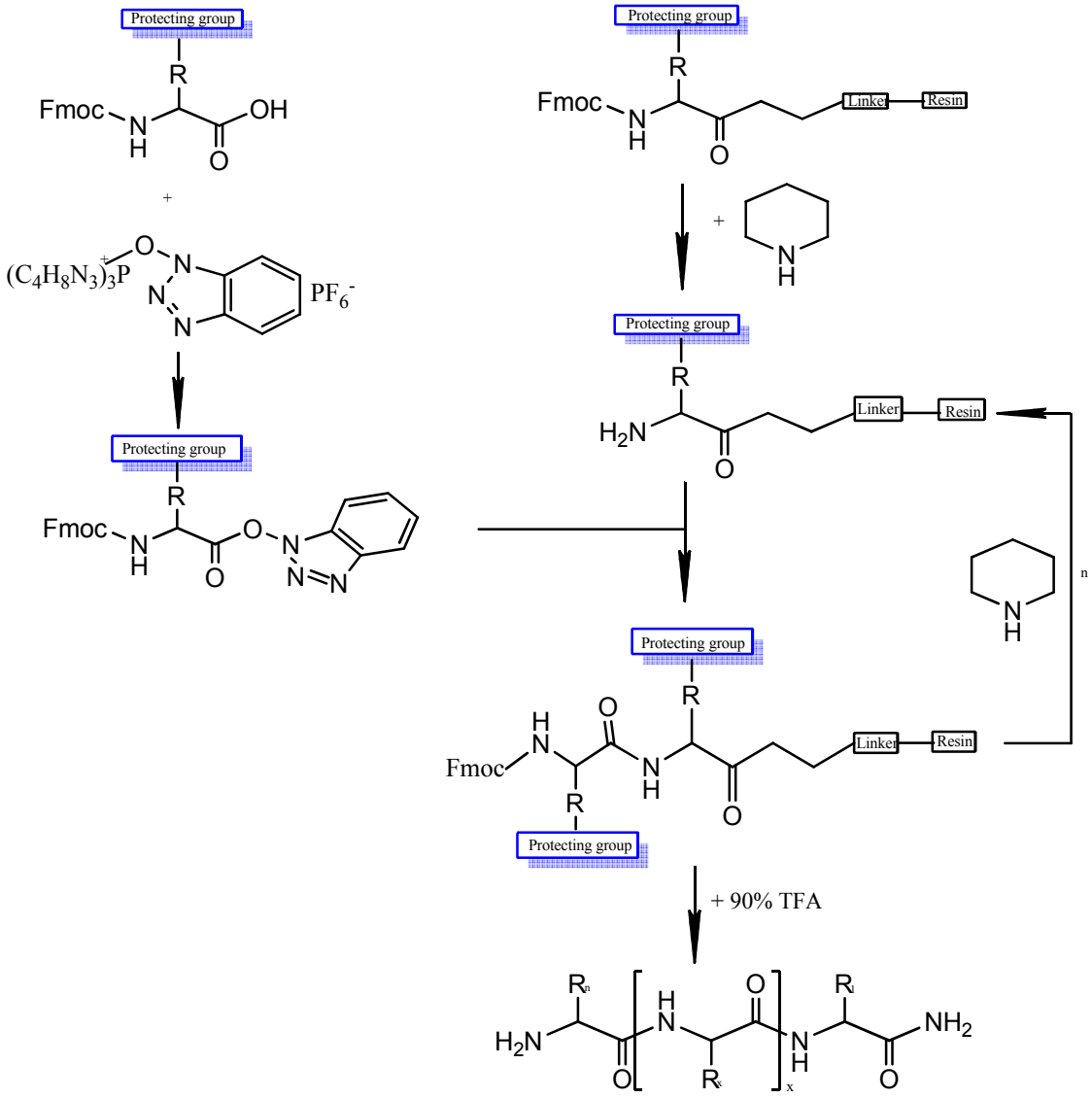

Figure 80: Schematic representation of the solid phase peptide synthesis.

Monitoring the coupling:

Bromophenol blue Test

Bromophenol blue test can detect all types of amines (Figure 81) [205]. The DIPEA or collidine traces have to be removed carefully before the test will be performed. The presence of traces of acid can lead to a false negative result. The beads may be inspected under a microscope.

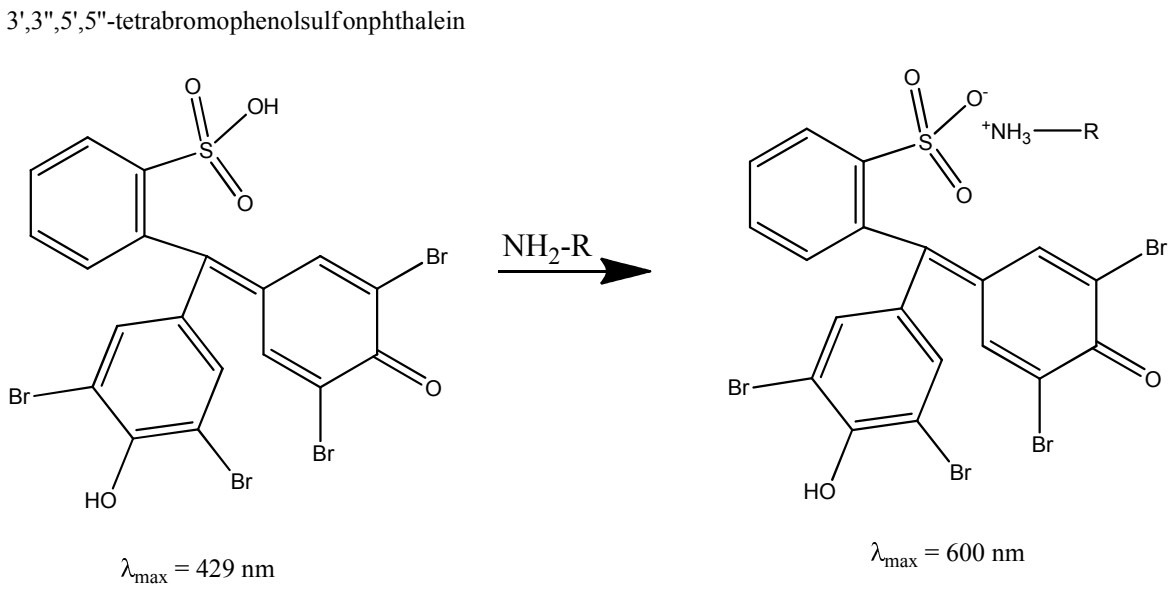

Figure 81: Schematic representation of bromophenol blue test.

Test solutions: 0.05 % bromophenol blue in DMA.

A few resin beads are placed in a small eppendorf and 10-15 drops of solution are added. The beads are immediately inspected.
Results: Blue beads: positive,
Colorless beads: negative.

Kaiser Test

The Kaiser test [206] is based on the reaction of ninhydrin with amines. It is a very sensitive test for primary amines, visualized by an intense blue color, and somewhat less suitable for secondary amines, being detected by development of a brownish red color. Usually the color is developed mainly in the beads and partly in the

supernatant. The intensity of color depends on the nature of the amino terminus to be detected; rather unspecific shades are obtained with N-terminal (side-chain protected) Asp, Asn, Cys, Ser, and Thr. Brownish red beads result with N-terminal Pro (Figure 82). However, prolonged heating as well as overheating should be avoided as it may cause Lys(Boc) cleavage or Fmoc removal (by pyridine).

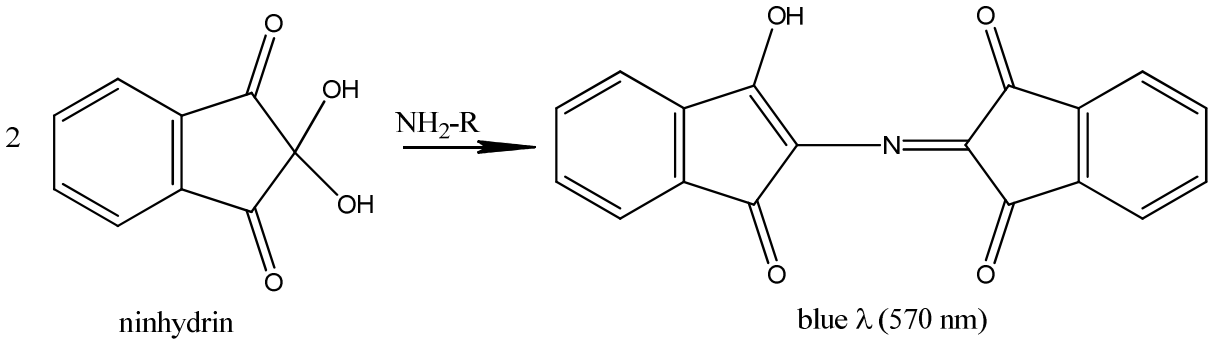

Figure 82: Schematic representation of ninhydrin test**.**

Test solutions:

A. 2.5 g ninhidrin in 100 mL ethanol

B. 40 g phenol in 10 mL ethanol

C. 65 mg KCN in 100 mL d.i. water (2 mL 0.001 M aqueous KCN in 98 mL pyridine).

A few resin beads were placed in a small test tube and 2-3 drops of each solution are added. The tube was placed in an oven and the reaction left to develop for 5 min at 100 °C.

Results: Resin and solution blue (variable intensity - from light to dark blue): positive,
Resin and solution colourless to light yellow: negative.

The Acetaldehyde/Chloranil Test

This sensitive test has been developed for reliable detection of secondary amino groups [207], but it also detects primary amines. Only the beads will be colored in case of a positive test.

Test solutions:

A. 2 % acetaldehyde in DMF

B. 2 % chloranil in DMF.

A few beads of resin are placed in a small test tube and 2-3 drops of each solution are added. After a short mixing, the mixture was left at 25 °C for 5 min and the beads were inspected.

Results: Dark blue to green beads: positive.

Colorless to yellowish beads: negative.

Biotinylation of peptides on-resin appears to be an attractive method for preparing peptides with biotinyl moiety at the amino-terminus. The reaction took place between N-terminal free amino group and the carboxy group of D-(+)-biotin, using a 5 folds molar excess of biotin to the amount of resin. The biotin was activated as a benzotriazolyl ester with PyBOP in the presence of NMM. After coupling and final deprotection of the Fmoc group, the peptide-resin was washed with DMF. Biotinylated peptides were then cleaved from the resin.

Cleavage of the peptides from the resin

The following cleavage mixture was used to cleave the peptides synthesized by Fmoc chemistry from the resin:

- 95 % TFA, 2.5 % triisopropylsilane, 2.5 % water.

After cleavage, the mixture of resin and free peptide was filtered and the resin rinsed with TFA. The filtrate was precipitated using cold *tert*-buthyl-methyl-ether (10 mL ether/mL cleavage mixture). The precipitate was filtered off and then washed several times with diethylether up to the elimination of TFA and scavengers. The solid material was solubilized in 5 % acetic acid (aqueous solution) prior to freeze-drying.

3.4 Reverse Phase High Performance Liquid Chromatography (HPLC)

High performance liquid chromatography is one of the most powerful tools in biochemistry and analytical chemistry. It is a chromatographic technique which has the ability to separate, identify, quantify and purify the compounds that are present in any sample that can be dissolved in a liquid. Molecules that possess some degree of hydrophobic character, such as proteins and peptides, can be separated by RP-HPLC with excellent recovery and resolution. The separation mechanism depends on the different physicochemical and chemical interactions between the solute molecule

in the mobile phase and the immobilized hydrophobic ligand, e.g. the stationary phase.

The sample to be analysed is introduced via a manual injector directly into the stream of mobile phase and is retarded by specific interactions with the stationary phase as it transverses the length of the column. The reversed-phase packings are based on silica, with bonded hydrocarbon chains (C_4, C_8, C_{18}) referred to as alkylsilane groups. Polypeptides are eluted from the reverse phase column with aqueous solvents containing an ionic modifier to adjust the pH and an organic modifier to displace and elute the peptide. Reverse phase chromatography generally uses gradient elution. The gradient separates the mixtures as a function of the affinity of the analyte for the current mobile phase composition relative to the stationary phase.

An increasing gradient in the organic modifier is applied by using a two-phase mobile system:
- Solvent A: 0.1 % (v/v) TFA in water
- Solvent B: 80 % (v/v) acetonitrile, 0.1 % (v/v) TFA in water.

Analytical RP-HPLC was performed on a UltiMate 3000 system (Dionex, Germering, Germany), equipped with LPG-3400A pumps, using different column depending on the hydrophobicity of the sample to be analyzed: Vydac C4 column (250×4.6 mm I.D.) with 5 µm silica (300 Å pore size) (Hesperia CA), analytical Nucleosil 300-7 C18 column (250 x 4 mm I.D.) with 7 µm silica and 300 Å pore size (Macherey-Nagel, Düren, Germany). The chromatograms were recorded by UV detection at 220 nm, employing the VWD-3400 variable wavelength detector of the UltiMate system, with a flow cell of PEEK, 0.4 mm long and an internal volume of 0.7 µl. The fractions were collected manually.

Semipreparative RP-HPLC was carried out on a Thermo scientific SpectraSystem (Thermo scientific, Germany) using semipreparative Vydac C4 column, 250 x 10 mm I.D. with 10 µm silica 300 Å pore size (Grace Davison). Chromatograms were recorded by UV detection at 220 nm and the fractions were collected manually.

3.5 Enzymatic digestion

3.5.1 In-solution proteolytic digestion using trypsin

Peptides and proteins to be proteolytically digested were solubilised in 10 mM NH_4HCO_3, pH 8 at concentrations of 0.5-1 µg/µL. Alternatively enzymatic digestion was carried out in phosphate buffer saline containing 5 mM Na_2HPO_4, 150 mM NaCl, pH 7.5. Stock solutions of the sequence grade TPCK-modified porcine trypsin 1 µg/µL in 50 mM acetic acid were stored at - 20 °C. Trypsin was added to the sample at an enzyme to substrate ratio of 1:20 (w/w) and 1:50 (w/w) and the digestion was performed at 37 °C. The reaction was monitored in time by removal of sample aliquots, quenching by freezing in liquid nitrogen or by adding 5 µL 0.1 % TFA and subsequent mass spectrometrical analysis of the proteolytical peptides [208].

3.5.2 In-solution proteolytic digestion using endoproteinase GluC

The lyophilized endoproteinase GluC was reconstituted in water to a final concentration of 1 µg/µL. The stock solution was stored at - 20 °C. Digestion of peptides was performed in PBS containing 5 mM Na_2HPO_4, 150 mM NaCl, pH 7.8. An enzyme to substrate ratio of 1:20 was employed. The incubation time was between 4 and 20 h at 37 °C.

3.5.3 In-solution proteolytic digestion using endoproteinase LysC

Endoproteinase Lys-C was reconstituted in 50 µl water. This results in a solution containing 0.1 µg/µL enzyme, 50 mM HEPES, pH 8.0, 10 mM EDTA and 5 µg/µL raffinose. The digestion was carried out at 37 °C, in 25 mM Tris HCl, pH 8.5, containing 1 mM EDTA for 5 h. The amount of enzyme was 1:20 of the protein by weight.

3.5.4 In-solution proteolytic digestion using alpha-chymotrypsin

Stock solutions of alpha-chymotrypsin 1 µg/µL were prepared in 1 mM HCl containing 2 mM $CaCl_2$. The solution was stored at - 20 °C as frozen aliquots for 1 week. For peptide digestion a ratio of 1:20 (w/w) or 1:50 (w/w) chymotrypsin: peptide was used.

The digestion was performed for 2, 4, 6, 8, 24 h, at 37 ºC in PBS containing 5 mM Na_2HPO_4, 150 mM NaCl, pH 7.5.

3.5.5 In-solution proteolytic digestion using pronase

The enzyme is supplied as lyophilized powder. Stock solutions of 10 µg/µL were prepared in water and stored at 4 °C for maximum one week. Pronase digestions were performed at 40 ºC in PBS containing 5 mM Na_2HPO_4, 150 mM NaCl, pH 7.5. An enzyme to substrate ratio of 1:1 (w/w) and concentrations of 0.1 µg/µL for the peptides and 0.5 µg/µL for pronase were used.

3.6 Immunoanalytical experiments

3.6.1 Preparation of antibodies column

The antibody (100 µg) immobilization on the affinity material was performed using the dry N-hydroxysuccinimidyl (NHS)-activated 6-aminohexanoic acid-coupled Sepharose 4B (Sigma, St. Louis, USA). The antibody was first dissolved in 200 µL coupling buffer (0.2 M $NaHCO_3$, 0.5 M NaCl, pH 8.3). The antibody or the protein solution was added to the dry and transferred into a microcolumn (MoBiTec, Goettingen, Germany). The coupling reaction was performed for 1 h at 25 °C. The matrix was washed sequentially with blocking buffer (0.1 M amino ethanol, 0.5 M NaCl, pH 8.3) and washing buffer (0.1 M CH_3COONa, 0.5 M NaCl, pH 4). Each solvent was used with a total volume of 56 mL (seven times 8 mL). The microcolumn was stored at 4 ^{o}C in PBS (5 mM $Na_2HPO_4 \cdot 2H_2O$, 150 mM NaCl, pH 7.5).

3.6.2 Antigen-antibody binding by affinity mass spectrometry

The antigen dissolved in PBS was applied to the antibody or protein column. After 2 h incubation at 25 °C, the supernatant was removed by blowing out the column using a syringe. The matrix was subsequently washed with 50 mL PBS, pH 7.5. After removal of the unbound peptide, the antigen-antibody complex was dissociated from the affinity matrix by the addition of 500 µL 0.1 % TFA (pH 2). The column was shaken gently for 15 min and the released peptide was collected in a microreaction cup. The samples were then lyophilized and desalted by the ZIP-TIP^{TM} procedure

(Millipore, USA) before mass spectrometric analysis. The column was regenerated by washing first with 10 mL 0.1 % TFA pH 2, followed by 20 mL PBS, pH 7.5.

3.6.3 Preparation of antigen column

3 mg of synthetic Cys-Aβ1-40 peptide were dissolved in 10 mL coupling buffer containing 50 mM Tris-HCl, 5 mM EDTA (pH 8.5) to a final concentration of 3 mg/mL. This solution was added to 1 mL of UltraLink Iodoacetyl gel dried of liquid and the coupling reaction was allowed to take place for one our at 25 °C under gentle mixing, followed by 30 minutes without shaking. The matrix-coupling product was loaded onto a 2.5 mL column allowing the solution to drain. The column was washed with 3 mL of coupling buffer and the non-specific binding sites on gel were blocked 2 times for 45 min with 1 mL of 50 mM L-Cysteine•HCl in coupling buffer. This procedure was repeated twice. At the end, the column was washed with 5 mL of 1 M NaCl and 5 mL of 0.1 M phosphate, 0.15 M NaCl (pH 7.2) and stored at 4 °C.

3.6.4 Protein-antigen interaction by affinity mass spectrometry

The wild type human Cystatin C (HCC) dissolved in PBS (pH 7.5) was applied to the Aβ(1-40) column. After 2 h incubation at 25 °C, the supernatant was removed by blowing out the column using a syringe. The matrix was subsequently washed with 50 mL PBS, pH 7.5. After removal of the unbound peptide, the protein-antigen complex was dissociated from the affinity matrix by the addition of 500 µL 0.1 % TFA (pH 2). The column was shaken gently for 15 min and the released peptide was collected in a microreaction cup. The column was regenerated by washing first with 10 mL 0.1 % TFA pH 2, followed by 20 mL PBS, pH 7.5.

3.6.5 Epitope excision and extraction

Epitope excision experiment was performed by adding the antigen (5 - 50 µg) to the antibody microcolumn (MoBiTec, Goettingen) followed by gentle shaking for 2 h at 20 °C to allow complete binding of antigen. After removing the unbound peptide by washing with 50 - 100 mL PBS, pH 7.5, the remaining affinity bound peptide was digested for 2 h by addition of protease (Trypsin, Chymotrypsin, GluC- protease,

LysC-protease or Pronase) applied in an enzyme to substrate ratio of 1:20. Proteolytic non-epitope fragments were collected in a microreaction cup and the matrix was washed with 50 mL PBS (0.1 M Phosphate; 0.15 M NaCl; pH 7.5). The immune complex was dissociated from the affinity matrix by incubation with 500 µL 0.1 % TFA, pH 2 for 15 min. The released epitope and non-epitope peptides were lyophilized and stored until mass spectrometric analysis.

For the epitope extraction experiment, the proteolytic digestion of 5 - 50 µg peptide or protein took place in a microreaction cup for at least 2 h using different proteases. The proteolytic digest mixture was then applied to the microcolumn and incubated for 2 h at 20 °C. The washing and elution steps were the same as described above.

3.6.6 Enzyme-Linked Immunosorbent Assay (ELISA)

3.6.6.1 Binding of Aβ peptides to single domain antibodies

Binding of synthetic Aβ peptides: BG_5-Aβ(1-40), BG_5-Aβ(12-40), BG_5-Aβ(20-30), BG_5-Aβ(20-37) and BG_5-Aβ(1-16) to Aβ-nanobodies (Nb_3 or Nb_9) was determined by ELISA. 96-well ELISA plates (BioRad, Hercules, CA) were coated overnight, at 20 °C with 100 µL/well of 2,5 µg/mL antibody in PBS. After washing the wells with PBS-T 0.05 % Tween- 20 v/v in PBS-phosphate buffer saline (5 mM Na_2HPO_4, 150 mM NaCl, pH 7.5), non-specific absorption sites were blocked with 5 % BSA in PBS. After washing four times with PBS-Tween (200 µL/well), 100 µl/well of biotinylated peptides (12 three fold serial dilutions prepared in 5 % BSA (Sigma Aldrich, Steinheim, Germany) were added and incubated for 2 h at 20 °C. The plates were washed four times with 200 µL/well PBS-Tween. Anti-Biotin horseradish-peroxidase-conjugated antibody (Jackson Immuno Reseach, West Grove, PA) was incubated for 1 h at 20 °C. Wells were washed three times with PBS– Tween and once with 50 mM sodium phosphate-citrate buffer, pH 5. 100 µL/well of 0.1 % o-phenylenediamine dihydrochloride (OPD) (Merck, Darmstadt, Germany) in phosphate-citrate buffer containing 0.006 % of H_2O_2 (Merck Darmstadt, Germany) were added to the plates. The absorbance was measured at λ = 450 nm on a Wallac 1420 Victor^2 ELISA Plate Counter (Perkin Elmer, Boston, MA).

3.6.6.2 Binding of human Cystatin C to Aβ peptides

Direct ELISA was performed as follow: 96-well ELISA plates were coated overnight, at 20 °C with 100 µL/well of 2.5 µg/mL human Cystatin C in PBS. After washing the wells with PBS-T (0.05% Tween- 20 v/v in PBS, pH 7.5), non-specific absorption sites were blocked with 5 % BSA in PBS. Then, the plates were washed four times with PBS-T (200 µL/well) and 100 µL/well of biotinylated peptides (12 three fold serial dilutions prepared in 5% BSA) were added and incubated for 2 h at 20 °C. The plates were washed four times with 200 µL/well PBS-Tween. Anti-Biotin horseradish-peroxidase-conjugated antibody was incubated for 1 h at 20 °C. Wells were washed three times with PBS - Tween and once with 50 mM sodium phosphate-citrate buffer, pH 5. 100 µL/well of 0.1 % OPD in phosphate-citrate buffer containing 0.006 % of H_2O_2 were added to the plates. The absorbance was measured at λ = 450 nm on a Wallac 1420 Victor ELISA Plate Counter (Perkin Elmer).

3.6.6.3 Alanine scanning mutagenesis

All assays were performed in 96-well plates coated overnight at 20 °C with 100 µL/well of 2.5 µg/mL antibody in PBS. Wells were washed four times with PBS-T (0.05 % v / v Tween in PBS, pH 7.5). For background subtraction, triplicate wells containing PBS have been incubated in the first step. The wells were blocked with BSA 5 % w/v in PBS for 2 h and washed with PBS-T. Peptide samples were prepared and diluted in PBS. 100 µL/well of biotinylated peptides (12 three fold serial dilutions prepared in 5 % BSA) were added and incubated for 2 h at 20 °C. After washing steps, 100 µL of horseradish peroxidase-conjugated goat anti-biotin antibody (1 µg / mL in BSA 5 % w / v in PBS) was added and incubated for 2 h at 20 °C. The wells were washed three times with PBS-T, and twice with citrate phosphate buffer, pH 5.0. Wells were finally incubated at 20 °C with OPD [209-211] dissolved in citrate phosphate buffer, pH 5.0, and the enzyme reaction was monitored as a function of time at 450 nm using an ELISA plate reader (Victor2, Perkin Elmer Life/Analytical Sciences, Boston, MA, USA).

3.7 Surface acoustic wave biosensor measurements

The K5-SSens Biosensor used (SAW-Instruments, Bonn, Germany) is a chip-based bioaffinity system for marker free detection of affinity interactions and is based on the conversion of a high-frequency signal into a surface acoustic wave (SAW) due to the inverse piezoelectric effect. The velocity of the SAW is sensitive to changes in mass loading and viscosity, causing shifts in the signal's amplitude and/or phase that enable high-sensitivity detection, unlike most other biosensors, which are equipped with a readout unit containing a microfluidic cell [153, 212]. Thus, interactions on the gold-coated chip surface can be observed at near-physiologic conditions. The formation of the self assembled monolayer (SAM) occurs through chemical adsorption from a solution containing compounds with thiol groups. 10 µM of 16-mercaptohexadecanoic acid was prepared by dissolving 5.77 mg acid in 2 mL chloroform. The gold chip was immersed over night at 20 °C in the prepared solution. Thereafter, the chip was washed with chloroform and ethanol, and then dried. All reactions involved in the immobilization of the first partner of the affinity system were conducted in the micro-fluidic cell of the biosensors. The gold chip with a fresh SAM build on its surface was inserted in the instrument and a flow of water was allowed to wash the chip. The used flow rates were 20 to 30 µL / minute. The reactants were added as solutions that were injected using the autosampler. To immobilize a compound (antibody, protein or peptide) three steps are necessarily. First step: the carboxyl groups were activated with 200 nm EDC (1-ethyl-3-(3-dimethylaminopropyl) carbodiimide) and 50 mM NHS (N-hydroxysuccinimide) solutions, in a volumetric ratio of 1:1, forming carboxyl amides. In the autosampler was introduced a sample glass with 200 µL mixture of the both solutions and for the injection were used 150 µL. The reaction's mechanism of the activation is displayed in Figure 83.

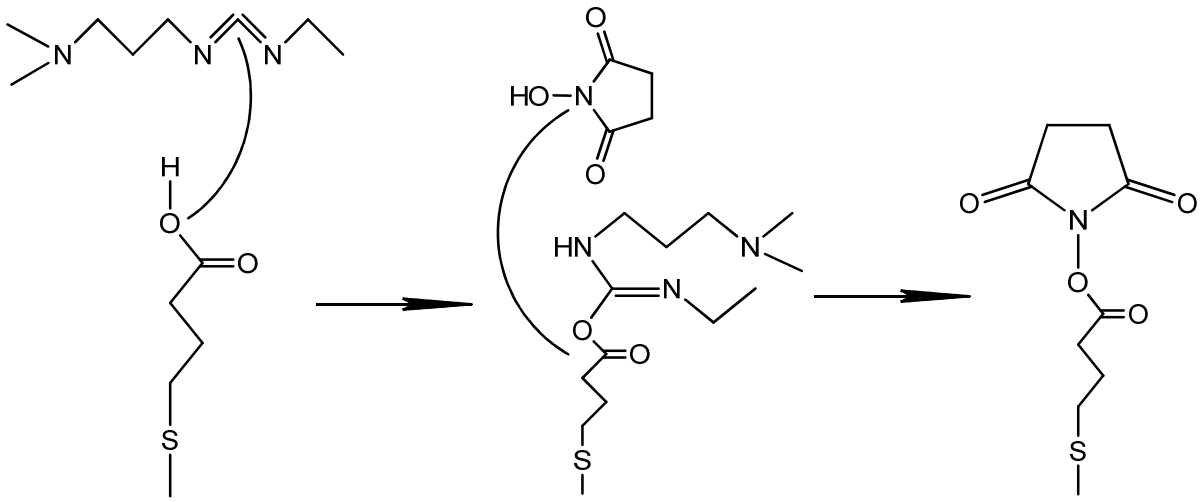

Figure 83: Mechanism of reaction in the EDC/ NHS activation of carboxyl group.

In the second step, the compound (antibody, protein or peptide) was immobilized. For the immobilization of peptides and proteins were used 10 µM final concentration and for the antibody 200 nM in order to achieve a maximum quantity of compound on the chip. The third step had the function of capping all the activated carboxyl groups that did not reacted with the compound to be immobilized. It consisted of a 1 M solution of ethanolamine, brought to pH 8.5. After the immobilization of a first compound, its affinity partner was also injected. This was done when the signal of the biosensor was equilibrated back after the change of the buffer from water (used during the immobilization) to PBS. For the study of the affinity interactions, PBS was used as running buffer. For the injection of the affinity partner were used different concentrations and volumes, according to the purpose of the experiment. In order to dissociate the complex, acidic conditions were used, injecting for example 50 mM glycine (pH 2) or 1 % acetic acid (pH 1.8). However, for dissociation of the antigen/antibody complexes, 0.1 M HCl (pH 1.8) was found to be best suited. Active surface of a channel is 0.072 cm^2. The quantity of bound compound to the chip can be evaluated from the measured phase shift (recorded with the K15 software) using the following sensitivity calibration factor:

$$515 = \frac{\varphi(^\circ)}{m(\mu g) * A(cm^2)}.$$

3.8 Circular Dichroism Spectroscopy

Circular dichroism is a form of light absorption spectroscopy that measures the differences in the absorption of left-handed polarized versus right-handed polarized light which arise due to structural asymmetry. This method is remarkably sensitive to the secondary structure of proteins and peptides. Secondary structure can be determined in the “far-UV”, between 190 and 260 nm. The chromophore is the peptide bond and the signal arises when it is located in a folded environment. The spectral features of each secondary structural shape are summarized below:

Far UV-CD of random coil: - negative band below 200 nm, positive band at 212 nm

Far UV-CD of β-sheet: - negative band at 217 nm, positive band at 195 nm

Far UV-CD of α-helix: - negative band at 208 nm and 222 nm, positive band at 190 nm. Alpha-helix, beta-sheet and random coil conformations are illustrated in Figure 84.

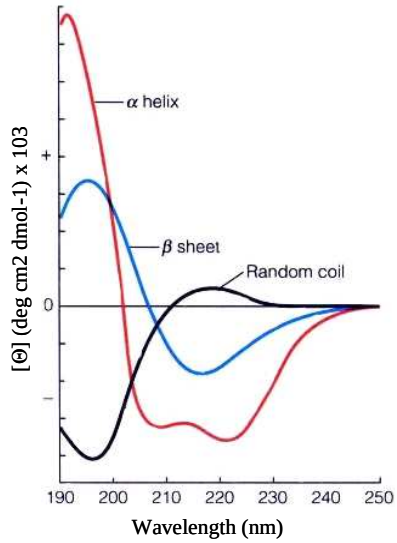

Figure 84: Circular dichroism spectra of poly-L-lysine in various conformations [213].

For the calculation of molar ellipticity [Θ] in deg cm^2 $dmol^{-1}$, the difference between the absorption between left and right of circular polarized light (AL-AR) was measured according to the Lambert-Beer law:

Θ= 33(AL-AR)

where Δε is the molar extinction coefficient;

where (AL-AR)=Δε*c*d, c is the molar concentration;

and Θ= Θ/ (10*c*d) [dmol-1 cm2],

d is the diameter of the cuvette

where Θ is measured in mdeg;
c is the concentration in mol/l.

Circular dichroism (CD) spectra were recorded on a Jasco spectropolarimeter; model J-715, equipped with a Xe lamp. The measurements were carried out at 20 °C in quartz cells of 0.05 cm path-length, under constant nitrogen flush. The instrument was calibrated with 0.06 % (w/v) ammonium-d-camphor-10-sulfonate in water. In order to improve the signal to noise ratio, the spectra were averages of six scans in a wavelength range between 270 and 180-190 nm. Results were expressed in terms of ellipticity, molar ellipticity or mean residue ellipticity (deg cm^2 $dmol^{-1}$) after subtraction of the solvent (PBS, Tris, water or TFE) baseline. Molar ellipticities were calculated with Jasco-700 Software.

3.9 Aggregation and inhibition assays

3.9.1 Sample preparation

Synthetic and recombinant Aβ(1-40) peptide was first dissolved in 100 % TFE or HFIP to ensure re-formation of monomers, and then lyophilized. The peptide was re-dissolved in 20 mM Na_2HPO_4 pH 7.4 and incubated for 0, 2, 4 and 7 days at 37 °C under shaking. The incubated samples were then stored at – 20 °C.

Aβ protofibrils were obtained by dissolving the synthetic and recombinant Aβ(1-40) peptides at a concentration of 1 mM in 1 mM NaOH and by adding 10 mM NaOH [196]. The peptides were incubated for 0, 2, 4 and 7 days at a final concentration of 500 µM in PBS buffer (70 mM NaCl, 1.35 mM KCl and 5 mM Na_2HPO_4/Na_2HPO_4, pH 7.4) and then stored at – 20 °C.

For the inhibition studies, different mixtures of Aβ(1-40) and HCC(93-120) and HCC(101-117) peptides (dissolved in 100 %TFE, lyophilized and re-dissolved in ice-cold 20 mM phosphate buffer, pH 7.4) were incubated at 37 °C for up to 7 days. Samples were removed from reactions at set time-points and analyzed by Tris-Tricine PAGE and Thioflavin T (ThT) assay.

3.9.2 Thioflavin assay

Binding of thioflavin T (ThT) to a β-sheet structure is one of the characteristics of amyloid–like proteins [214]. A stock solution of ThT (15.7 mM) was prepared in water, aliquoted into small samples and stored long term at - 20 °C in the dark. The aliquots were thawed only once and the remainder was discarding. Purified Aβ(1-40) was dissolved in 20 mM PBS and incubated at 37 °C with agitation in a microcentrifuge tube. As a control, a blank was provided with 20 µM ThT in water. The measurements were carried out in 96-well plate (black; black bottom) by using fluorescence plate reader (Wallac Victor 2 Multilabel Counter; Perkin Elmer). ThT assay was performed with CW-lamp (F450), emission filter (T486), measurement time of 1.0 s and a CW-lamp energy of 12385.

3.10 Electrophoresis methods

Gel electrophoresis is a technique in which charged molecules are separated according to physical properties as they are focused through a gel by an electrical field.

3.10.1 SDS-PAGE

SDS-PAGE was performed according to Laemmli 201 using the Mini-Protean II or Mini- Protean 3 gel electrophoresis system (BioRad, München, Germany). The dimension of the gel was 90 x 60 x 1 mm. SDS-polyacrylamide gels were cast between two glass plates using a Bio-Rad mini-gel casting system. To obtain optimal resolution of proteins, a stacking gel was poured over the top of the separating gel. The stacking gel has a lower concentration of acrylamide (larger pore size), lower pH and a different ionic content. This allows the proteins in a lane to be concentrated into a tight band before entering the separating gel and produces a gel with tighter or better separated protein bands. The size of the pores created in the gel is inversely related to the amount of acrylamide used. Gels with a low percentage of acrylamide are typically used to resolve large proteins and high percentage gels are used to resolve small proteins. Table 10 provides recipes for preparing gels with different acrylamide concentrations.

Table 10: Composition of SDS-polyacrylamide gels according to Laemmly.

Monomer concentration (%T, 2.6% C)	**Stacking gel**	**Separating gel**		
	5 %	10 %	12 %	15 %
4 x Stacking gel buffer [a]	2.5 mL	-	-	-
4 x Separating gel buffer [b]	-	6 mL	6 mL	6 mL
Water	5.8 mL	10mL	8.4 mL	6 mL
Acrylamide/bis solution [c] (30.8 % T, 2.6 % C)	1.7 mL	8 mL	9.6 mL	12 mL
APS [d]	85 µL	125 µL	125 µL	125 µL
TEMED [e]	20 µL	20 µL	20 µL	20 µL

[a] 0.5 M Tris-HCl, 0.4 % SDS (w/v), pH 6.8

[b] 1.5 M Tris-HCl, 0.4 % SDS (w/v), pH 8.8

[c] 30 % (w/v) Acrylamide, 0.8 % (w/v) N, N'- Methylenebisacrylamide

[d] 10 % (w/v) Ammonium persulfate

[e] N, N, N', N'- tetramethylethylenediamine

The pore size of the polyacrylamide gel can be changed by adjusting either the total monomer concentration (% T) or by adjusting the crosslinking monomer concentration (% C), where:

% T = [(g Acrylamide + g Bis-Acrylamide)/Total Volume] x 100

% C = [g Bis-Acrylamide/(g Acrylamide + g Bis-Acrylamide)] x 100

The most common method of changing the pore size is to adjust the total monomer concentration (% T). In diluting a stock solution, the crosslinking monomer concentration (% C) is independent of the final total monomer concentration (% T).

The sample was solubilized and denatured using the following sample buffer: 50 mM Tris-HCl, 4 % (w/v) SDS, 12 % (w/v) glycerol, 0.02 % (w/v) bromophenol blue, 6 M urea pH 6.8. If the sample contains a mixture of unknown proteins 100 mM DTT is added. The electrode (running) buffer was composed of 25 mM Tris, 192 mM Glycin

and 0.1 % SDS. Gel electrophoresis was carried out using a Power/PAC 1000 power supply (Bio-Rad, München, Germany) at a constant voltage of 60 V for ca. 30 min, until the tracking dye entered the separating gel, and at 120 V for ca. 2 h, until the tracking dye reached the anodic end of the separating gel. After separation in SDS-PAGE gels, proteins were visualised by silver staining or sensitive colloidal Coomassie as described below. The molecular weights of unknown proteins were estimated by running standard proteins of known molecular weights in a separate lane of the same gel.

3.10.2 Tris-Tricine PAGE gels

The polyacrylamide gel electrophoresis approach described by Schägger and Jagow [215] was employed for increased resolving power of proteins with molecular mass below 10 kDa. The stock solutions prepared for gel electrophoresis are given below:
Anode buffer: 0.2 M Tris, pH 8.9
Cathode buffer: 0.1 M Tris, 0.1 M Tricine, 0.1 % SDS
Gel buffer: 3 M Tris, 0.3 % SDS, pH 8.45

Table 11: Separation and stacking gel for 1 mm- thick gel.

Monomer concentration	Stacking gel	Separating gel	
(% T, 3 % C)	4 %	10 %	15 %
Gel buffer	3.1 mL	10 mL	10 mL
Glycerin	-	3.16 mL	3.16 mL
30 % Acrylamide	1.94 mL	9.8 mL	15 mL
Water	7.71 mL	7 mL	1.8 mL
APS	75 µL	150 µL	150 µL
TEMED	20 µL	20 µL	20 µL

Gel electrophoresis was carried out using a Power/PAC 1000 power supply (Bio-Rad, München, Germany) at a constant voltage of 60 V for ca. 30 min, until the tracking dye entered the separating gel, and at 120 V for ca. 2 h, until the tracking dye reached the bottom of the separating gel.

3.10.3 Coomassie Brilliant Blue staining

Coomassie blue staining is based on the binding of the dye Coomassie Brilliant Blue G250, which binds non-specifically to virtually all proteins in acid solution. Solutions employed in the staining procedure are presented in Table 12.

Table 12: Solutions employed in coomassie blue staining.

Name	Composition
Fixing	12 % (w/v) trichloroacetic acid
A	10 % (w/v) ammonium sulphate, 2 % phosphoric acid
B	5 % (w/v) Coomassie Brilliant Blue G-250
Washing solution	25 % methanol

The gel is incubated for 1 h in 100 mL fixing solution and for 12 h in staining solution. The staining solution is prepared prior to use, by mixing for 30 min 80 mL of the stock solution A with 2 mL stock solution B. 20 mL of methanol p.a. are added and the solution is mixed for 30 min. After staining, the gel is washed for 5 and 30 min with 25 % methanol [216] .

3.10.4 Silver staining after Heukeshoven and Dernick

Silver staining was performed according to Heukeshoven and Dernick (1985) [217]. Silver staining is one of the most sensitive methods for permanent visible staining of proteins in polyacrylamide gels. The gel was impregnated with soluble silver ions and development by treatment with formaldehyde, which reduces silver ions to form an insoluble brown precipitate of metallic silver. Solutions employed in the staining procedure are presented in Table 13.

Table 13: Solutions employed in silver staining procedure.

Name	Composition
Fixing solution	30 % (v/v) Ethanol, 10 % (v/v) acetic acid
Incubation solution	7,5 % Ethanol, 6,8 % Sodiumacetate, 0,125 % Glutardialdehyde, 0,2 % Sodium

	Thiosulfatpentahydrate
Silver solution	0,2 % Silvernitrate solution
Formaldehyde solution	37 % Formaldehyde in water
Developing solution	2,5 % Sodiumcarbonate in water
Stop solution	1 % Gylcine in water

3.11 Immunoanalytical assays

3.11.1 DOT-BLOT

2 µL peptides solution (1 µg/µL) in PBS (pH= 7.4) were spotted on nitrocellulose (NC) membrane. After the samples were dry for 5 min at 25 °C, the NC membranes were blocked for 2 h by using Roti®-Block solution in water. Membranes were then probed 1 h with mouse monoclonal antibody against different Aβ fragments (1:2500) in PBS-Tween buffer. The membranes were then washed three times in PBS-Tween buffer and probed again with a goat anti-mouse HRP-conjugate (1:5000, Sigma) in PBS-Tween for 1 h. After washing the membrane five times in wash buffer the immuno-positive spot were visualised by using ECL- Plus system (Amersham Pharmacia). The ECL- kit consists of two detection reagents, a luminol solution and an oxidizing solution which are added to react with the labelled secondary antibody. Detection reagent 1 decays to hydrogen peroxide, the substrate for peroxidase. Reduction of hydrogen peroxide by the enzyme is coupled to the light producing reaction by detection reagent 2, which contains luminol [218]. HRP-catalyzed oxidation of luminol by hydroperoxide ion in aprotic media generates an excited state product, 3-aminophtharate, which emits blue luminescent lights of 425-510 nm as it decays to +2 H_2O_2 the ground state (Figure 85). The antigen bound with HRP-labeled antibody shows a corresponding band on the X-ray film.

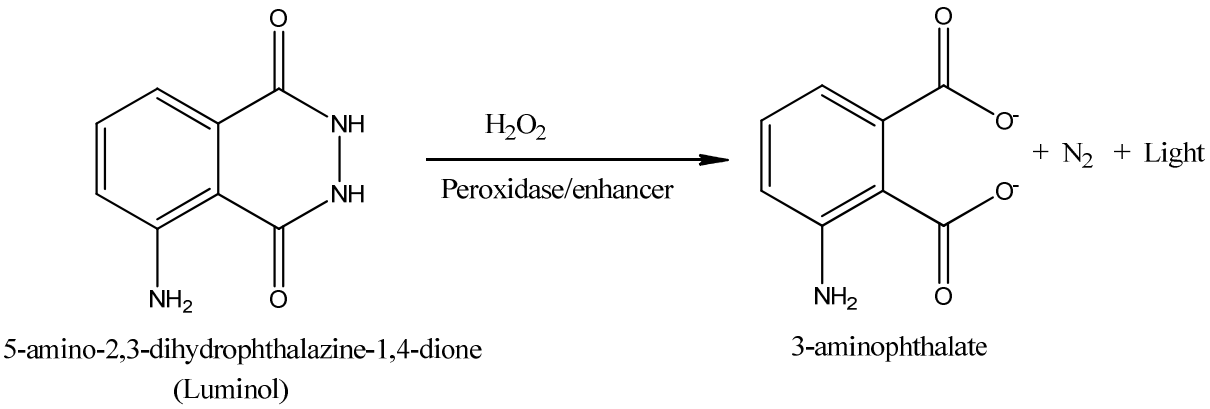

5-amino-2,3-dihydrophthalazine-1,4-dione
(Luminol)

3-aminophthalate

Figure 85: Reaction scheme of Luminol detection in Dot-Blot- or Western-Blot-experiments.

3.11.2 Western-BLOT

The term “blotting” refers to the transfer of biological samples from a gel to a membrane and their subsequent detection on the surface of the membrane. Western blotting (also called immunoblotting because antibodies are used to specifically detect its antigen) was introduced by Towbin, *et al*. in 1979 [219].

For the Western-Blot analysis the proteins were first separated by SDS-PAGE electrophoresis and then transferred onto a nitrocellulose membrane by a semidry blot procedure (Figure 86).

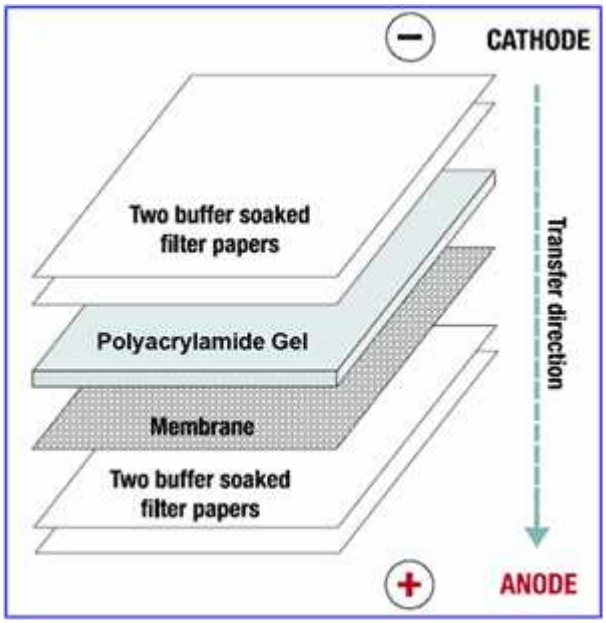

Figure 86: Schematic representation of protein blotting with a semi-dry transfer unit.

5 filter paper having the dimensions of blotted gels have been introduced into Towbin-buffer and than were introduced into the blotting instrument. Between filter papers was introduced a nitrocellulose membrane having the same dimensions of the blotted gels and also swollen into blotting buffer (25 mM Tris, 192 mM Glycine, 20 % Methanol, pH 8,3). Then the gel was introduced also for short time in blotting buffer and than on top of it were placed another 5 filter papers also swollen in blotting buffer. Special care was taken for removing all air bubbles between the filter papers. The blotting was performed using a constant current for 2 h.

After the sample was dry the membrane was immersed into PBS-0.5 % Tween buffer and than treated as in the Dot-Blot. The Western-Blots experiments were done as follows: the membrane containing the sample was first incubated for 1 h in block buffer. Then the solution of the first antibody (anti-Cystatin antibody) was applied and the membrane was incubated between 2 h. The dilutions of the antibodies were 1:5000. After washing the membrane 4 times (5-15 min) the secondary antibody was applied (goat anti-mouse HRP antibody) and incubated for 2 h. The dilutions were between 1:5000 to 1:10000. Then the membrane was again washed for 3 times (15-60 min). For the development was used a solution of Luminol (ECL-Western-Blotting-Reagents, Amersham) mixed and applied directly on the membrane. The exposure was done into a dark room by using a Film (Fuji Medical X-Ray Film). The exposure time was between 30 sec and 2 min. The exposed films were scaned by using Quantity1 programm. The following solutions were used: 1 mM NaH2PO4, 2.7 mM KCl, 133.6 mM NaCl, pH 7.3, 0.5 % (v/v) Tween-20 (PBS-T) and 10 % Rotti block in water (Block buffer).

Ponceau S-Test

To see if the proteins were absorbed onto the nitrocellulose membrane (in Western or Dot Blot experiments) the Ponceau S-Test was carried out. For this the membrane was immersed for 2 min into a Ponceau S-solution (0.1 % Ponceau S in 5 % acetic acid). Then the membrane was washed with water until the paper surface was clean and the protein spots were slightly red. In the buffer solution, the red color disappeared in a couple of minutes.

3.12 ZipTip clean up procedure

The ZipTip cleanup procedure was performed using ZipTip^{TM} C18 pipette tips from Millipore. A ZipTip pipette tip is a microcolumn with the resin prepacked into the narrow end of a 10 µl pipette tip. ZipTip pipette tips contain C_{18} or C_4 reversed-phase media for desalting and purifying peptide and protein samples. ZipTip C_{18} pipette tips are most applicable for peptides and low molecular weight proteins, while ZipTip C_4 pipette tips are most suitable for low to intermediate molecular weight proteins. The ZipTip method is described on Millipore website [220] consists mainly in five steps: wetting and equilibration of the ZipTip pipette tip, binding of the peptides and/or proteins to ZipTip pipette tip, washing and elution. Table 14 outlines the solutions required for use with ZipTip pipette tips containing C_{18} media.

Table 14: Solutions required for use with ZipTip pipette tips containing C18 media.

Solution	ZipTip C_{18} Pipette Tips
Wetting solution	50 % acetonitrile (MeCN) in water
Sample preparation	0.1 % trifluoroacetic acid (TFA) in water; final sample solution pH<4
Equilibration solution	0.1 % TFA in water
Washing	0.1 % TFA in water
Elution solution	0.1 % TFA/ 50 % MeCN

3.13 Mass spectrometric methods

The structural characterization of the single chain llama antibodies, synthetic Aβ peptides, epitope elucidation studies and different interactions between peptides were carried out using different mass spectrometric methods.

3.13.1 MALDI-TOF- mass spectrometry

For MALDI-TOF mass spectrometric analysis of proteins and peptides, samples are co-crystallized with an excess of organic matrix that absorbs at a specific wavelength (usually 337 nm). Typically, sinapinic acid (SA) is the matrix of choice for large

proteins, whereas α-cyano-4-hydroxy-cinnamic acid (HCCA) is the preferred matrix for peptide mapping. MALDI matrix is a nonvolatile solid material that absorbs the laser radiation resulting in the vaporization of the matrix and sample embedded in the matrix. The matrix also serves to minimize sample damage from the laser radiation by absorbing most of the incident energy and the matrix is believed to facilitate the ionization process.

α−cyano-4-hydroxycinnamic acid (HCCA) is recommended for peptides and proteins under 10 kDa of mass. Best results are obtained in the 500-5000 Da range and therefore HCCA is the matrix of choice for peptide mass fingerprinting, being usually used for MALDI-TOF mass spectrometry.

A good matrix should fulfil the following requirements:
Absorption at the wavelength of the laser radiation (λ= 337 nm) to provide sufficient energy deposition in the sample; and to be soluble in the same solvent as the analyte. They have to crystallize upon sample preparation;
The matrix prevents aggregation of the analyte molecules and is also believed to play an active role in the ionization process itself [221-223].

MALDI-TOF MS analysis was carried out with a Bruker Biflex linear TOF mass spectrometer (Bruker Daltonik, Bremen, Germany) equipped with a nitrogen UV laser (λmax=337 nm) and a delayed extraction system, a dual channel plate detector, a 26-sample SCOUT source, a video system and a XMASS data system for spectra acquisition and instrument control (Figure 87).

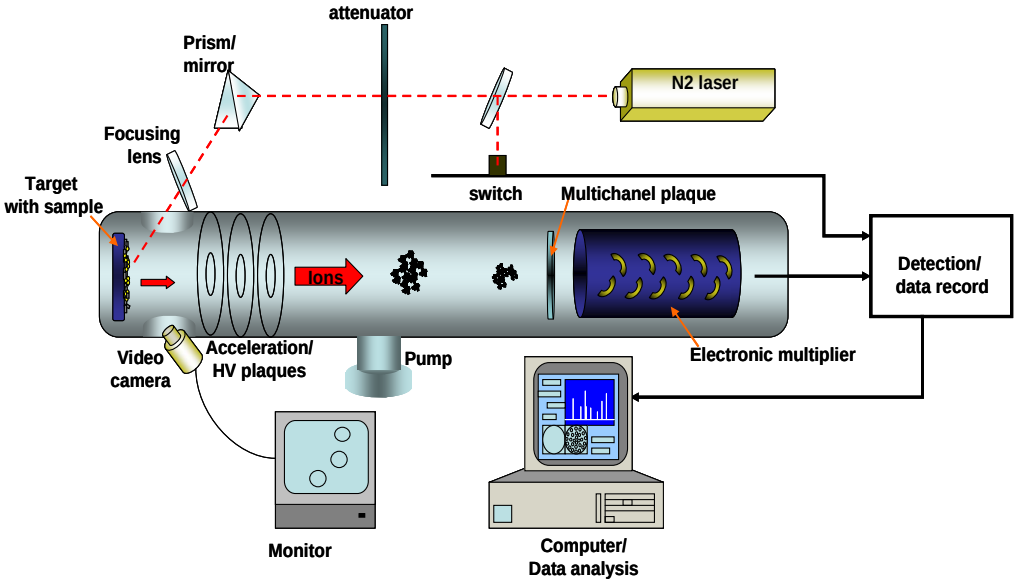

Figure 87: Schematic representation of a linear time-of-flight matrix-assisted laser desorption mass spectrometer.

For measurement 1 µL of a freshly prepared saturated solution of α-cyano- 4-hydroxy-cinnamic acid (HCCA) in acetonitrile / 0.1 % TFA (2:1) was applied onto the dry stainless steel MALDI target and 1µl of the sample solution was added. Desalting and concentration of the samples was achieved by using ZipTip C_{18}™ pipette tips (Millipore) as described before. Acquisition of spectra was carried out at an acceleration voltage (Vacc) of 20 kV and a detector voltage of 1.5 kV. 50 to 200 single shots were accumulated into a final spectrum. External calibration was carried out using the average masses of singly protonated ion signals of bovine insulin (5734.5 Da), bovine insulin β-chain, oxidized (3496.9), human neurotensin (1673.9 Da), human angiotensin I (1297.5 Da), human bradykinin (1061.2 Da) and human angiotensin II (1047.2 Da).

3.13.2 ESI-FTICR – mass spectrometry

ESI FT ICR mass spectrometric measurements were performed by using an Apex II mass spectrometer (Bruker Daltonics) equipped with a 7 T superconducting magnet (Magnex, Oxford, UK), a cylindrical infinity ICR analyzer cell, an Appolo source, and an API1600 ESI control unit. The sample solution was introduced through a PEEK capillary to the spraying needle using a syringe pump with a flow rate of 2 µL/min. Either dry gas, heat, or both are applied to the droplets before they enter the vacuum

of the mass spectrometer, thus causing the solvent to evaporate from the surface. As the droplet decreases in size, the electric field density on its surface increases. For the Apollo ESI source the current has been set to 3.5 kV on the end plate, 2.0 kV on the cylinder and 4.2 kV on the capillary transfer tip. The measurements have been performed using a capillary voltage of 70-150 V. The drying gas (nitrogen) was heated at 150° C. After a predefined accumulation time in the hexapole (0.1-2 sec) the voltage of the extraction plate was reversed and the ions were extracted for transmission to the ICR cell. The calibration was done with a solution of Angiotensin I. The fragmentation of the Angiotensin I have been done by using a capillary voltage of 120 V. The data processing was done using the XMass (Bruker, Bremen) program installed on the acquisition PC of the mass spectrometer.

A 10 µL aliquot of a freshly prepared Aβ(17-28) solution 100 µM (M_r 1323.68) in deionised water was added into 10 µL of an equimolar HCC(93-120) solution (M_r 3163.5) in 1 mM ammonium acetate, pH 6. The prepared solution was directly infused after incubation at 25 °C after 3 h. The stability of Aβ and HCC fragment under the experimental conditions was also checked. In Table 15 are summarized the conditions used for complex formation between HCC fragments and Aβ(1-40) and Aβ(17-28)

Table 15: The conditions used for complex formation between human Cystatin C fragments (93-120) and (101-117) and β-amyloid peptides (1-40) and (17-28).

Sample	Buffer	Buffer Concentration	pH	Concentration hCC : Aβ (µM)	Complex formation
hCC93-120 : Aβ(1 - 40)	CH_3COONH_4	5 mM	7.4	25 : 50	No
hCC93-120 : Aβ(1 - 40)	CH_3COONH_4 / MeOH	5 mM / 20 %	7.4	25 : 50	No
hCC93-120 : Aβ(1 - 40)	CH_3COONH_4	5 mM	6	25 : 50	No
hCC93-120 : Aβ(1 - 40)	CH_3COONH_4 / MeOH	5 mM / 20 %	6	25 : 50	No
hCC93-120 : Aβ(1 - 40)	CH_3COONH_4	2 mM	7.4	25 : 50	No
hCC93-120 : Aβ(1 - 40)	CH_3COONH_4	2 mM	6	25 : 50	No
hCC93-120 : Aβ(1 - 40)	CH_3COONH_4	0.5 mM	7.4	25 : 50	No
hCC93-120 : Aβ(1 - 40)	CH_3COONH_4	0.5 mM	6	25 : 50	No
hCC93-120 : Aβ(1 - 40)	CH_3COONH_4	0.5 mM	7.4	25 : 25	No
hCC93-120 : Aβ(1 - 40)	CH_3COONH_4	0.5 mM	6	25 : 25	Yes
hCC93-120 : Aβ(1 - 40)	CH_3COONH_4	0.5 mM	7.4	25 : 12.5	No
hCC93-120 : Aβ(1 - 40)	CH_3COONH_4	0.5 mM	6	25 : 12.5	No
hCC93-120 : Aβ(17-28)	CH_3COONH_4	0.5 mM	6	50 : 50	Yes
hCC93-120 : Aβ(17-28)	CH_3COONH_4	0.5 mM	6	25 : 25	Yes
hCC93-120 : Aβ(17-28)	CH_3COONH_4	0.5 mM	6	50 : 25	No
hCC93-120 : Aβ(17-28)	CH_3COONH_4	0.5 mM	6	25 : 50	No
hCC101-117 : Aβ(17-28)	CH_3COONH_4	0.5 mM	6	50 : 50	Yes

3.13.3 Liquid chromatographic/Ion trap mass spectrometric investigation

For LC/MS investigations, an Agilent Technologies (Waldbronn, Germany) HP1100 liquid chromatograph for binary gradient elution (pump model G1312A), including autosampler (G1313A) and a DAD (G1315 B), coupled to an Esquire 3000 ion trap mass spectrometer from Bruker Daltonics (Bremen, Germany) was used. For the LC separation, a binary gradient system consisting of solvent A (0.1 % formic acid in water) and solvent B (80 % acetonitrile, 0.1 % formic acid in water) was employed. The sample was dissolved in the solvent A. The injection volume was 5 µL. A 150 mm x 4.6mm x 3µm Discovery RP-18 column was used for the separation of the peptides. All LC/MS results were obtained using atmospheric pressure chemical ionization (APCI) in the positive ion mode. Mass spectra were recorded in the full scan mode, scanning from m/z 200 to 1500. Ion source parameters were 20 psi nebulizer gas and 10.0 L/min of drying gas with a temperature of 300 °C.

3.14 Computer Programms

3.14.1 GPMAW

General Protein/Mass Analysis for Windows (GPMAW) version 7.0 (Lighthouse Data, Denmark) [224] was employed in this work for the analysis of intact and proteolytically digested proteins with known sequence. The program enables manually editing of peptide sequences as well as the import of a sequence from a number of different formats with direct database search. The most common formats are Fasta format, Swiss-Prot and Genbank. Sequences can be saved in local files for future reference. Using this program the protein can be cleaved by automatic pre-defined methods or manually. Cross-links and chemical modifications can be entered in GPMAW and saved with the sequence. The peptides are displayed with a number of parameters including monoisotopic and average mass of single and multiply charged ions with 2 and 4 decimals, HPLC index, pI. A list containing the molecular masses of all MS/MS fragment ions can be invoked for the desired sequence. GPMAW may predict the secondary structure, the hydrophobicity and the antigenic sequences of a given protein or peptide.

3.14.2 BALLView 1.1.1

BALLView is an open source software [225, 226], employed in this work for the visualization and modeling of molecular structures. The program is able to import structures from the most common molecular structure formats (PDB, MOL, MOL2 and SD). Structures can be visualized with all standard graphical models and coloring methods. Different parts of a molecule can be freely visualized and selected for special tasks.

3.14.3 HyperChem 6.0

HyperChem 6.0 software was used for the molecular dynamic simulation of polypeptides. AMBER96 parameters were applied for the geometry optimization and the calculations were performed taking into account the presence of water molecules.

3.14.4 Amber 8.0

All simulations were carried out using the AMBER 8.0 program, and the all-atom AMBER force field. The crude systems were initially minimized *in vacuum* to remove close *van der Waals* contacts. This (and next minimization) consisted of 10 000 steps. Before surrounding the complex (HCC-ligand) with water molecules, Na^+ and Cl^- charge-balancing counterions were added in positions with favourable ion-residue interactions to neutralize charges on the protein-ligand surface. Next, all structures were optimised by energy minimization in water box. The typical box size was about 90×90×90 Å. The systems were diluted in TIP3P water. After minimization, the molecular dynamics for all systems were calculated. Simulations of complexes in solution were performed under periodic boundary conditions in a closed, isothermal, isobaric (NTP) ensemble. Throughout the simulation the solute and solvent were coupled to a constant-temperature (T = 300 and 500 K) heat bath and a constant-pressure (P = 1 atm) bath. All hydrogen-containing bonds were constrained using SHAKE algorithm allowing a time step of 0.0005 ps. A Ewald summation [227] was used for non-bonded interactions. Coordinates were saved every 1000 steps. The time length during all molecular dynamics was about 1500 ps. The time length of MD was about 3000 ps without constrains. When the complexes (protein-ligand) started

to dissociate, the MD calculations were interrupted. The precise analyse of obtained results was made by using AMBER package programs and programs like RasMol (v2.6) and MolMol [228].

4 Summary

One of the main characteristics of Alzheimer's Disease (AD) is the accumulation of extracellular plaques containing aggregates of neurotoxic β-amyloid (Aβ) peptides, derived from amyloid precursor protein (APP). A major goal of this thesis was the identification of the Aβ- epitope structure recognized by (a) single chain antibodies isolated from *Llama Glama* after immunization with Aβ(1-40); (b) human Cystatin C protein. Mass spectrometry has been developed in the last years as a powerful technique for the analysis of protein structures and biomolecular interactions. High mass accuracy and sensitivity, short analysis time and low sample consumption are important features of the mass spectrometric protein analysis. To obtain information on protein mixtures and to identify the structure of the molecular recognition domains, several affinity- based methods have been employed in combination with mass spectrometry. These approaches include chromatographic and electrophoretic separations, proteolytic degradation and mutations of specific amino acids. For the identification of molecular antigen recognition structures, highly efficient methods of mass spectrometry coupled with proteolytic epitope excision and extraction were developed in our laboratory. Using this methodology, the Aβ-plaque-specific epitope was identified in a previous study as the N-terminal sequence Aβ(4-10), which is also accessible in Aβ oligomers. Recently, the epitope recognized by Aβ-autoantibodies from human serum was identified as Aβ(21-37) and was shown to inhibit fibril formation.

In the first part of the thesis, single chain llama anti-Aβ antibodies were characterized by SDS-PAGE and mass spectrometry. Antibodies in *Camelidae* (camels and llamas) are called "heavy-chain" antibodies, because the light chain and the first domain of the constant region (C_H1) of the heavy chain are missing. Camelid V_{HHs} display similar functional characteristics with respect to specificity and affinity, comparable to classical antibodies, and have favourable properties for biophysical studies, e.g. small size and high solubility and stability. To investigate whether a single chain llama antibody may function as a microantibody, the amino acid sequence was analyzed and the CDR- regions were determined according to Kabat rules. Consequently, CDR3 was selected as a potential candidate. The CDR3 peptide was

synthesized by solid phase peptide synthesis, purified by HPLC and analyzed by mass spectrometry.

In the second part of the thesis, the Aβ-epitope recognized by single chain llama anti-Aβ antibodies was identified. Mass spectrometric analysis was combined with proteolytic excision and extraction approaches previously developed in our laboratory. For the epitope excision and extraction experiments, affinity columns were prepared by immobilizing the antibodies on NHS-activated Sepharose. For protein digestion trypsin, chymotrypsin, LysC and GluC-proteases were employed and the proteolytic mixtures subjected to MALDI-TOF-MS. The epitope excision and extraction, followed by mass spectrometric analysis, provided direct information on the epitope recognized by single chain llama anti-Aβ antibodies. The results revealed an epitope located in the mid-to-C-terminal part of Aβ(1-40), Aβ(17-28). The secondary structure of the identified Aβ(17-28) epitope was determined by CD spectroscopy. Comparative binding studies of single chain llama anti-Aβ antibodies with the epitope were performed by ELISA. To determine the functional epitope (amino acids within Aβ(17-28), which are essential for binding the single chain llama anti-Aβ antibodies), site-directed alanine mutated Aβ(17-28) peptides were synthesized. Selective identification of the affinity preserving mutant peptides was achieved by comparative ELISA studies.

In the third part of the dissertation, affinity- mass spectrometric methods were applied for the investigation of the specific interactions between Aβ-peptides and single chain llama anti-Aβ antibodies. Furthermore, the interaction between CDR3 peptide of a single chain llama anti-Aβ antibody and Aβ(1-40) was assessed by affinity- mass spectrometry. For the affinity studies, the single chain antibodies were immobilized on NHS-activated Sepharose. Aβ(1-40) and Aβ(17-28) were dissolved in PBS and exposed to the single chain llama antibody columns, while CDR3 peptide was added on Cys-Aβ(1-40) column. The unbound peptides were removed, the columns were washed several times and then the antigen-antibody complex was dissociated under acidic conditions. The supernatant, washing and elution fractions were collected and analyzed by mass spectrometry. Affinity binding studies were also performed using surface acoustic wave (SAW) biosensor, which is sensitive to mass loadings and viscosity changes. The method was applied to different antigen-antibodies systems.

The antigens were covalently immobilized on the surface of the biosensor chip. The dissociation constants of the interactions between the single chain antibodies, Aβ(1-40) and Aβ(17-28) (K_D) were found to be in the nanomolar range.

A fourth part of the dissertation was focused on the identification and characterization of the interaction structures between Aβ(1-40) and human Cystatin C (HCC) using an affinity- mass spectrometric approach, CD spectroscopy, ELISA and SAW biosensor. The results of the proteolytic excision and extraction in combination with mass spectrometry showed that the HCC biding site was located in the central region of Aβ(1-40), within residues (17-28), while the Aβ-binding site was located in the C-terminal part within L2 loop and β5 strand of wt HCC, within residues (101-117). The C-terminal binding epitope enables the interaction between L2-β5 part of wt HCC with Aβ peptide with the without any restriction. The binding specificities and affinities of the epitopes were analyzed by ELISA. Thus, comparative ELISA studies were performed with the Aβ(17-28) epitope and wt HCC, as well as with the C-terminal HCC peptides (HCC(93-120), HCC(101-117), HCC(101-114) fragments), which were identified by epitope excision mass spectrometry. The specific interaction between HCC(93-120) or HCC(101-117) fragments and Aβ*(*17-28*)* epitopes was shown by direct high resolution ESI- mass spectrometry.

In the last part of the thesis, *in vitro* characterization of Aβ(1-40) aggregation products employing gel electrophoresis, Dot blot and Thioflavin assay was performed. Furthermore, the inhibition of Aβ(1-40) oligomer formation by HCC fragments was investigated using the Thioflavin assay. *In vitro* aggregation of synthetic and recombinant Aβ(1-40) was carried out by dissolving the sample in trifluoroethanol (TFE), hexafluoroisopropanol (HFIP) and NaOH and followed by incubation at 37 °C in PBS for 0, 2, 4 and 7 days. The formation of oligomers and protofibrils was monitored by 1D-Tris-Tricine polyacrylamide gel electrophoresis, which indicated the presence of trimers, tetramers and protofibrils. The Thioflavin assay showed that in both experiments with previous solubilisation of the samples in NaOH or HFIP the aggregation rate was higher for recombinant Aβ(1-40) than for synthetic Aβ(1-40). The inhibition of Aβ(1-40) aggregation was carried out using different ratios between Aβ and HCC(93-120) or HCC(101-117) and analyzed by Thioflavin T assay. Using a two fold molar excess of HCC(93-120), Aβ(1-40) showed

a significant decrease of aggregation rate after 4 days. Using a 1:0.5 Aβ(1-40) : HCC(101-117) molar ratio, a decrease in the fluorescence intensity was observed, due to a partial inhibition of Aβ- aggregation.

The results obtained in the present work showed that single chain antibodies and human Cystatin C protein recognize the middle domain of Aβ-peptide, which can be applied to design new epitope conjugates. The interaction of HCC with Aβ may be an important neuroprotective mechanism in brain and may attenuate the oligomerisation of Aβ and play a regulating role in Aβ amyloidogenesis. Furthermore, the identification of the binding site in HCC should be of importance for aggregation studies of Aβ peptide and new oligomerisation inhibitors may be designed based on the HCC-epitope. *In vivo* preliminary studies showed that HCC(101-117) does in fact react with Aβ species and might have therefore a therapeutical utility in humans. It seems somehow a paradox that the interaction of two potentially amyloidogenic molecules might provide a lead to control or inhibit neuropathological changes in amyloidogenic diseases.

5 Zusammenfassung

Die Akkumulierung von extrazellularen Plaques mit dem neurotoxischen β-amyloid (Aβ) Peptid des Alzheimer-Amyloid-Vorläuferproteins APP als Hauptbestandteil ist ein Charakteristikum der Alzheimerschen Krankheit (AD). Ein Hauptziel dieser Arbeit war die Identifizierung der Aβ-Epitop-Strukturen von (a) single chain Antikörpern aus *Llama-Glama* nach Immunisierung mit Aβ(1-40); (b) des humanen Aβ-Inhibitoren Cystatin C Proteins. Die Massenspektrometrie hat sich in den letzten Jahren als leistungsfähige analytische Methode zur Analyse von Proteinstrukturen und biomolekularen Wechselwirkungen entwickelt. Hohe Massengenauigkeit und Empfindlichkeit, kurze Analysenzeiten und geringer Substanzenbedarf sind Hauptmerkmale der massenspektrometrischen Proteinanalytik. Eine Reihe von Methoden in Kombination mit der Massenspektrometrie wurde zur Analyse komplexer Proteingemische und Strukturaufklärung molekularer Erkennungsdomänen entwickelt. Hierzu gehören chromatographische und elektrophoretische Trennmethoden, proteolytischer Abbau und spezifische chemische Modifizierung. Für die Identifizierung von molekularen Strukturen der Antigen-Erkennung wurden proteolytische Excisions- und Extraktions-Methoden in Kombination mit Massenspektrometrie entwickelt. In einer früheren Arbeit konnte mit dieser Methode das Aβ-Plaque-spezifische Epitop als N-terminale Sequenz Aβ(4-10) identifiziert werden. Vor kurzem wurde das Epitop Aβ(21-37), das durch den Aβ-Autoantikörper aus menschlichem Serum erkannt wird, identifiziert und es konnte eine Hemmung der Fibrillenbildung gezeigt werden.

Im ersten Teil der Arbeit wurden Llama-anti-Aβ-Antikörper mittels SDS-PAGE und Massenspektrometrie charakterisiert. Antikörper in Camelidae (Kamele und Lamas) werden auch "heavy-chain" Antikörper genannt, weil die leichte Kette und die erste Domäne der konstanten Region (C_H1) der schweren Kette fehlen. Camelid VHHs zeigen bezüglich ihre Spezifität und Affinität ähnliche funktionelle Eigenschaften wie klassische Antikörper. Ferner eignen sie sich aufgrund z. B. ihrer geringen Größe, sowie guten Löslichkeit und Stabilität hervorragend für biophysykalische Untersuchungen. Um festzustellen, ob ein Llama-Antikörper auch als Mikroantikörper einsetzbar ist, wurde die Aminosäure-Sequenz analysiert, und die CDR-Regionen wurden entsprechend den Kabat-Regeln bestimmt. Dadurch wurde CDR3 als

potenzieller Kandidat ausgewählt. Das CDR3-Peptid wurde mittels Festphasen-Peptidsynthese synthetisiert, durch HPLC gereinigt und mittels Massenspektrometrie charakterisiert.

Im zweiten Teil der Arbeit wurden der Aβ-spezifischen Epitop des Lama Anti-Aβ Antikörpern unter Anwendung der in unserer Arbeitsgruppe entwickelten proteolytischen Excisions- und Extraktions-Methoden in Kombination mit Massenspektrometrie identifiziert. Durch Epitop-Excision und –Extraktion durch Verwendung verschiedener Proteasen (Trypsin, α-Chymotrypsin, LysC und GluC proteases) und MALDI-TOF-MS konnte die Epitop-Feinstruktur Aβ(17-28) identifiziert werden. Affinitätsuntersuchungen (ELISA) mit synthetischen, biotinylierten Aβ-Peptiden bestätigen die Bindungsspezifität des Epitops. Zur Charakterisierung der funktionellen Bedeutung der einzelnen Aminosäuren wurden spezifische Mutagenesen (Alanin scan) des synthetischen Aβ(17-28)-Peptids durchgeführt. Die Affinitätsbestimmung der Aβ-Peptidmutanten erfolgte durch vergleichende ELISA-Bindungsstudien.

Im dritten Teil der Dissertation wurden Affinitäts-massenspektrometrische Methoden für Untersuchung der spezifischen Wechselwirkungen zwischen Aβ-Peptide und Lama-anti-Aβ-Antikörpern angewendet. Darüber hinaus wurde die Wechselwirkung zwischen CDR3-Peptid aus Lama Anti-Aβ-Antikörper und Aβ (1-40) durch Affinitäts-Massenspektrometrie bestimmt. Für die Affinitätsstudien wurden die Lama-Antikörper auf NHS-aktivierter Sepharose immobilisiert. Aβ(1-40) und Aβ(17-28) wurden in PBS gelöst, auf die Lama-Antikörpern Säulen aufgetragen und inkubiert. Für das CDR3 Peptid wurde analog eine Cys-Aβ(1-40) Säule verwendet. Die ungebundenen Peptide wurden durch mehrfache Waschschritte entfernt, und anschließend wurde der Antikörper-Antigen-Komplex unter sauren Bedingungen dissoziiert und eluiert. Die jeweiligen Wasch- und Elution-Fraktionen wurden gesammelt und mittels Massenspektrometrie analysiert. Affinität- Bindungsstudien wurden auch mit einem SAW-Biosensor durchgeführt. Die SAW- Methode wurde auf verschiedene Antigen-Antikörper-Systeme angewendet. Die Antigene wurden auf der Oberfläche des Biosensorchips immobilisiert. Die bestimmten Dissoziation-Konstanten KD zwischen Lama-Antikörper und Aβ(1-40) und Aβ(17-28) befinden sich im nanomolaren Bereich.

Im vierten Teil der Dissertation wurden die Wechselwirkungsstrukturen zwischen Aβ(1-40) und humanem Cystatin C (HCC) mittels Affinitäts-Massenspektrometrie, ELISA, CD-Spektroskopie und SAW Biosensor identifiziert und charakterisiert. Die Ergebnisse der proteolytischen Exzision und Extraktion in Kombination mit Massenspektrometrie zeigten, dass die HCC Bindungsstelle im mittleren Bereich von Aβ(1-40) innerhalb der Aminosäuresequenz (17-28) angeordnet ist, während sich die Aβ-Bindungsstelle im C-terminalen Teil HCC(101-117) befindet. Die Bindungsspezifitäten und Affinitäten der Epitope wurden mittels ELISA analysiert. So wurden vergleichende ELISA-Studien mit dem Aβ(17-28)-Epitop und wt HCC, sowie mit den C-terminalen Peptiden HCC (HCC(93-120), HCC(101-117) und HCC(101-114) durchgeführt, die durch Epitop-Exzision Massenspektrometrie identifiziert wurden. Die spezifische Wechselwirkung zwischen HCC(93-120) und HCC(101-117), mit dem Aβ(17-28) Epitop wurde durch direkte hochauflösende ESI-Massenspektrometrie gezeigt.

Im letzten Teil der Arbeit wurden Aggregationsprodukte von Aβ(1-40) *in vitro* mittels Gelelektrophorese, Dot-Blot und Thioflavin T-Assay charakterisiert. Auβerdem wurde die Hemmung der Aβ(1-40) Oligomerenbildung durch HCC Fragmente mit der Thioflavin-T Methode untersucht. Die *in vitro* Aggregation von synthetischem und rekombinantem Aβ(1-40) wurde durch lösen in TFE, HFIP und NaOH und anschlieβender Inkubation bei 37 °C in Phosphat- Puffer über 7 Tage verfolgt. Die Bildung von Oligomeren und Protofibrillen wurde durch 1D-Gelelektrophorese kontrolliert, die die Anwesenheit von Trimeren, Tetrameren und Protofibrillen zeigte. Der Thioflavin-T Assay zeigte, dass in beiden Versuchen mit Solubilisierung der Proben in NaOH oder HFIP die Aggregationsrate für rekombinantes Aβ(1-40) im Gegensatz zu synthetischem Aβ(1-40) erhöht war. Die Hemmung der Aβ(1-40) Aggregation wurde unter Verwendung verschiedener Konzentrationen von Aβ und HCC(93-120) sowie HCC(101-117) mittels Thioflavin-T Assay analysiert. Mit einem zweifachen Überschuss von HCC(93-120) zeigte Aβ(1-40) eine signifikante Verringerung der Aggregationsrate.

Die Ergebnisse in der vorliegenden Arbeit zeigten, dass Lama-Antikörper und humanes Cystatin C-Protein eine mittlere Domäne des Aβ-Peptids erkennen. Dieses Erbgebniss bietet eine gute Grundlage, um neue Epitop-Konjugate zu entwickeln.

Die Interaktion von HCC und Aβ könnte ein wichtiger neuroprotektiver Mechanismus sein und die Bildung von Aβ-Oligomeren verringern, und eine wichtige regulierende Rolle in der Aβ-Amyloidogenese spielen. Basierend auf dem HCC-Epitop könnten weitere Aggregationsuntersuchungen von Aβ-Peptid sowie Entwicklungen von neuen Inhibitoren gegen die Oligomerenbildung von groβer Bedeutung sein. Erste Studien *in vivo* zeigen, dass HCC(101-117) tatsächlich mit Aβ-Spezies reagiert und daher von therapeutischem Nutzen sein konnte.

6 Bibliography

1. Bissantz, C., Kuhn, B., and Stahl, M. (2010) A medicinal chemist's guide to molecular interactions. *J Med Chem.* p. 5061-84.
2. Rebek, J., Jr. (2009) Molecular recognition and self-assembly special feature: Introduction to the molecular recognition and self-assembly special feature. *Proc Natl Acad Sci U S A*, **106**(26): p. 10423-4.
3. Bernado, P., Mylonas, E., Petoukhov, M.V., Blackledge, M., and Svergun, D.I. (2007) Structural characterization of flexible proteins using small-angle X-ray scattering. *J Am Chem Soc*, **129**(17): p. 5656-64.
4. Jones, S. and Thornton, J.M. (1996) Principles of protein-protein interactions. *Proc Natl Acad Sci U S A*, **93**(1): p. 13-20.
5. Levin, K.B., Dym, O., Albeck, S., Magdassi, S., Keeble, A.H., Kleanthous, C., and Tawfik, D.S. (2009) Following evolutionary paths to protein-protein interactions with high affinity and selectivity. *Nat Struct Mol Biol*, **16**(10): p. 1049-55.
6. Dalton, J.A. and Jackson, R.M. (2010) Homology-modelling protein-ligand interactions: allowing for ligand-induced conformational change. *J Mol Biol*, **399**(4): p. 645-61.
7. Olsson, T.S., Williams, M.A., Pitt, W.R., and Ladbury, J.E. (2008) The thermodynamics of protein-ligand interaction and solvation: insights for ligand design. *J Mol Biol*, **384**(4): p. 1002-17.
8. Torres, F.E., Kuhn, P., De Bruyker, D., Bell, A.G., Wolkin, M.V., Peeters, E., Williamson, J.R., Anderson, G.B., Schmitz, G.P., Recht, M.I., Schweizer, S., Scott, L.G., Ho, J.H., Elrod, S.A., Schultz, P.G., Lerner, R.A., and Bruce, R.H. (2004) Enthalpy arrays. *Proc Natl Acad Sci U S A*, **101**(26): p. 9517-22.
9. MacCallum, R.M., Martin, A.C., and Thornton, J.M. (1996) Antibody-antigen interactions: contact analysis and binding site topography. *J Mol Biol*, **262**(5): p. 732-45.
10. Al-Lazikani, B., Lesk, A.M., and Chothia, C. (1997) Standard conformations for the canonical structures of immunoglobulins. *J Mol Biol*, **273**(4): p. 927-48.
11. Padlan, E.A. (1994) Anatomy of the antibody molecule. *Mol Immunol*, **31**(3): p. 169-217.

12. Murphy, K., Travers, P., Walport, M. (2007) Janeway's Immunobiology: Garland Science. 928.
13. Laver, W.G., Air, G.M., Webster, R.G., and Smith-Gill, S.J. (1990) Epitopes on protein antigens: misconceptions and realities. *Cell*, **61**(4): p. 553-6.
14. Van Regenmortel, M.H.V. (1996) Mapping Epitope Structure and Activity: From One-Dimensional Prediction to Four-Dimensional Description of Antigenic Specificity. *Methods*, **9**(3): p. 465-72.
15. Cerutti, M.L., Ferreiro, D.U., Sanguineti, S., Goldbaum, F.A., and de Prat-Gay, G. (2006) Antibody recognition of a flexible epitope at the DNA binding site of the human papillomavirus transcriptional regulator E2. *Biochemistry*, **45**(51): p. 15520-8.
16. Zhu, C., Liu, X., Feng, J., Zhang, W., Shen, B., Ou'yang, W., Cao, Y., and Jin, B. (2006) Characterization of the neutralizing activity of three anti-human TNF monoclonal antibodies and prediction of their TNF epitopes by molecular modeling and mutant protein approach. *Immunol Lett*, **102**(2): p. 177-83.
17. Braden, B.C. and Poljak, R.J. (1995) Structural features of the reactions between antibodies and protein antigens. *FASEB J*, **9**(1): p. 9-16.
18. Fisher, R.D., Ultsch, M., Lingel, A., Schaefer, G., Shao, L., Birtalan, S., Sidhu, S.S., and Eigenbrot, C. (2010) Structure of the complex between HER2 and an antibody paratope formed by side chains from tryptophan and serine. *J Mol Biol*, **402**(1): p. 217-29.
19. Goldsby, R.A., Kindt, J. T., Osborne, A. B., Kuby J., ed. *Immunology*. 5th ed. 2003, W.H. Freeman and Comany: New York.
20. Harris, L.J., Skaletsky, E., and McPherson, A. (1998) Crystallographic structure of an intact IgG1 monoclonal antibody. *J Mol Biol*, **275**(5): p. 861-72.
21. Chen, Y., Wiesmann, C., Fuh, G., Li, B., Christinger, H.W., McKay, P., de Vos, A.M., and Lowman, H.B. (1999) Selection and analysis of an optimized anti-VEGF antibody: crystal structure of an affinity-matured Fab in complex with antigen. *J Mol Biol*, **293**(4): p. 865-81.
22. Gerlofs-Nijland, M.E., Assmann, K.J., van Son, J.P., Dijkman, H.B., te Loeke, N.A., van der Zee, R., Wetzels, J.F., and Groenen, P.J. (2003) Epitope mapping of monoclonal antibodies directed to aminopeptidase A and their relevance for albuminuria in mice. *Nephron Exp Nephrol*, **94**(1): p. e25-34.

23. Owens, J., Lewis, R.M., Cantor, A., Furie, B.C., and Furie, B. (1984) Monoclonal antibodies against human abnormal (des-gamma-carboxy)prothrombin specific for the calcium-free conformer of prothrombin. *J Biol Chem*, **259**(22): p. 13800-5.
24. Carter, J.M. (1994) Epitope mapping of a protein using the Geysen (PEPSCAN) procedure. *Methods Mol Biol*, **36**: p. 207-23.
25. Geysen, H.M., Meloen, R.H., and Barteling, S.J. (1984) Use of peptide synthesis to probe viral antigens for epitopes to a resolution of a single amino acid. *Proc Natl Acad Sci U S A*, **81**(13): p. 3998-4002.
26. Barderas, R., Desmet, J., Timmerman, P., Meloen, R., and Casal, J.I. (2008) Affinity maturation of antibodies assisted by in silico modeling. *Proc Natl Acad Sci U S A*, **105**(26): p. 9029-34.
27. Kristensen, C., Kjeldsen, T., Wiberg, F.C., Schäffer, L., Hach, M., Havelund, S., Bass, J., Steiner, D.F., and Andersen, A.S. (1997) Alanine Scanning Mutagenesis of Insulin. *Journal of Biological Chemistry*, **272**(20): p. 12978-12983.
28. Colf, L.A., Bankovich, A.J., Hanick, N.A., Bowerman, N.A., Jones, L.L., Kranz, David M., and Garcia, K.C. (2007) How a Single T Cell Receptor Recognizes Both Self and Foreign MHC. *Cell*, **129**(1): p. 135-146.
29. Teplyakov, A., Obmolova, G., Wu, S.-J., Luo, J., Kang, J., O'Neil, K., and Gilliland, G.L. (2009) Epitope Mapping of Anti-Interleukin-13 Neutralizing Antibody CNTO607. *Journal of Molecular Biology*, **389**(1): p. 115-123.
30. Paterson, Y., Englander, S.W., and Roder, H. (1990) An antibody binding site on cytochrome c defined by hydrogen exchange and two-dimensional NMR. *Science*, **249**(4970): p. 755-9.
31. Suckau, D., Kohl, J., Karwath, G., Schneider, K., Casaretto, M., Bitter-Suermann, D., and Przybylski, M. (1990) Molecular epitope identification by limited proteolysis of an immobilized antigen-antibody complex and mass spectrometric peptide mapping. *Proc Natl Acad Sci U S A*, **87**(24): p. 9848-52.
32. Macht, M., Fiedler, W., Kurzinger, K., and Przybylski, M. (1996) Mass spectrometric mapping of protein epitope structures of myocardial infarct markers myoglobin and troponin T. *Biochemistry*, **35**(49): p. 15633-9.
33. Fiedler, W., Borchers, C., Macht, M., Deininger, S.O., and Przybylski, M. (1998) Molecular characterization of a conformational epitope of hen egg

white lysozyme by differential chemical modification of immune complexes and mass spectrometric peptide mapping. *Bioconjug Chem*, **9**(2): p. 236-41.

34. Juszczyk, P., Paraschiv, G., Szymanska, A., Kolodziejczyk, A.S., Rodziewicz-Motowidlo, S., Grzonka, Z., and Przybylski, M. (2009) Binding epitopes and interaction structure of the neuroprotective protease inhibitor cystatin C with beta-amyloid revealed by proteolytic excision mass spectrometry and molecular docking simulation. *J Med Chem*, **52**(8): p. 2420-8.
35. Strancar, J., Kavalenka, A., Urbancic, I., Ljubetic, A., and Hemminga, M.A. (2010) SDSL-ESR-based protein structure characterization. *Eur Biophys J*, **39**(4): p. 499-511.
36. Maxam, A.M. and Gilbert, W. (1992) A new method for sequencing DNA. 1977. *Biotechnology*, **24**: p. 99-103.
37. Sanger, F., Nicklen, S., and Coulson, A.R. (1992) DNA sequencing with chain-terminating inhibitors. 1977. *Biotechnology*, **24**: p. 104-8.
38. Hawke, D.H., Lahm, H.W., Shively, J.E., and Todd, C.W. (1987) Microsequence analysis of peptides and proteins: trimethylsilylisothiocyanate as a reagent for COOH-terminal sequence analysis. *Anal Biochem*, **166**(2): p. 298-307.
39. Edman, P. and Begg, G. (1967) A protein sequenator. *Eur J Biochem*, **1**(1): p. 80-91.
40. Hunt, D.F., Yates, J.R., 3rd, Shabanowitz, J., Winston, S., and Hauer, C.R. (1986) Protein sequencing by tandem mass spectrometry. *Proc Natl Acad Sci U S A*, **83**(17): p. 6233-7.
41. Pelton, J.T. and McLean, L.R. (2000) Spectroscopic methods for analysis of protein secondary structure. *Anal Biochem*, **277**(2): p. 167-76.
42. Barton, G.J. (1995) Protein secondary structure prediction. *Curr Opin Struct Biol*, **5**(3): p. 372-6.
43. Whitmore, L. and Wallace, B.A. (2008) Protein secondary structure analyses from circular dichroism spectroscopy: methods and reference databases. *Biopolymers*, **89**(5): p. 392-400.
44. Sreerama, N. and Woody, R.W. (2000) Estimation of protein secondary structure from circular dichroism spectra: comparison of CONTIN, SELCON, and CDSSTR methods with an expanded reference set. *Anal Biochem*, **287**(2): p. 252-60.

45. Szymczyna, B.R., Taurog, R.E., Young, M.J., Snyder, J.C., Johnson, J.E., and Williamson, J.R. (2009) Synergy of NMR, computation, and X-ray crystallography for structural biology. *Structure*, **17**(4): p. 499-507.
46. Pusey, M.L., Liu, Z.J., Tempel, W., Praissman, J., Lin, D., Wang, B.C., Gavira, J.A., and Ng, J.D. (2005) Life in the fast lane for protein crystallization and X-ray crystallography. *Prog Biophys Mol Biol*, **88**(3): p. 359-86.
47. Larsson, A.M., Stahlberg, J., and Jones, T.A. (2002) Preparation and crystallization of selenomethionyl dextranase from Penicillium minioluteum expressed in Pichia pastoris. *Acta Crystallogr D Biol Crystallogr*, **58**(Pt 2): p. 346-8.
48. Wuthrich, K. (1990) Protein structure determination in solution by NMR spectroscopy. *J Biol Chem*, **265**(36): p. 22059-62.
49. Wishart, D. (2005) NMR spectroscopy and protein structure determination: applications to drug discovery and development. *Curr Pharm Biotechnol*, **6**(2): p. 105-20.
50. Rosen, O. and Anglister, J. (2009) Epitope mapping of antibody-antigen complexes by nuclear magnetic resonance spectroscopy. *Methods Mol Biol*, **524**: p. 37-57.
51. Homola, J. (2008) Surface plasmon resonance sensors for detection of chemical and biological species. *Chem Rev*, **108**(2): p. 462-93.
52. Ayela, C., Roquet, F., Valera, L., Granier, C., Nicu, L., and Pugniere, M. (2007) Antibody-antigenic peptide interactions monitored by SPR and QCM-D. A model for SPR detection of IA-2 autoantibodies in human serum. *Biosens Bioelectron*, **22**(12): p. 3113-9.
53. Lange, K., Rapp, B.E., and Rapp, M. (2008) Surface acoustic wave biosensors: a review. *Anal Bioanal Chem*, **391**(5): p. 1509-19.
54. Fenn, J.B., Mann, M., Meng, C.K., Wong, S.F., and Whitehouse, C.M. (1989) Electrospray ionization for mass spectrometry of large biomolecules. *Science*, **246**(4926): p. 64-71.
55. Tanaka, K., Waki, H., Ido, Y., Akita, S., Yoshida, Y., Yoshida, T., and Matsuo, T. (1988) Protein and polymer analyses up to m/z 100 000 by laser ionization time-of-flight mass spectrometry. *Rapid Communications in Mass Spectrometry*, **2**(8): p. 151-153.

56. Karasawa, A., Nakaho, K., Kakutani, T., Minobe, Y., and Ehara, Y. (1991) Nucleotide sequence of RNA 3 of peanut stunt cucumovirus. *Virology*, **185**(1): p. 464-7.
57. Zenobi, R. and Knochenmuss, R. (1998) Ion formation in MALDI mass spectrometry. *Mass Spectrometry Reviews*, **17**(5): p. 337-366.
58. Knochenmuss, R. (2006) Ion formation mechanisms in UV-MALDI. *Analyst*, **131**(9): p. 966-86.
59. Beavis, R.C., Chaudhary, T., and Chait, B.T. (1992) α-Cyano-4-hydroxycinnamic acid as a matrix for matrixassisted laser desorption mass spectromtry. *Organic Mass Spectrometry*, **27**(2): p. 156-158.
60. Fitzgerald, M.C., Parr, G.R., and Smith, L.M. (1993) Basic matrices for the matrix-assisted laser desorption/ionization mass spectrometry of proteins and oligonucleotides. *Anal Chem*, **65**(22): p. 3204-11.
61. Wilm, M.S. and Mann, M. (1994) Electrospray and Taylor-Cone theory, Dole's beam of macromolecules at last? *International Journal of Mass Spectrometry and Ion Processes*, **136**(2-3): p. 167-180.
62. Aebersold, R. and Mann, M. (2003) Mass spectrometry-based proteomics. *Nature*, **422**(6928): p. 198-207.
63. De Hoffmann, E., Stroobant, V., ed. *Mass Spectrometry: Principle and Applications*. 3rd ed. 2007, John Wiley & Sons Ltd,: Chichester.
64. Cech, N.B. and Enke, C.G. (2001) Practical implications of some recent studies in electrospray ionization fundamentals. *Mass Spectrom Rev*, **20**(6): p. 362-87.
65. Uversky, V.N. (2009) Intrinsic disorder in proteins associated with neurodegenerative diseases. *Front Biosci*, **14**: p. 5188-238.
66. Alzheimer, A. (1907) Eine eigenartige Erkrankung der Hirnrinde, in Allgemeine Zeitschrift für Psychiatrie und Psychisch-Gerichtliche Medizin. p. 146-148.
67. http://www.ahaf.org/alzheimers/about/.
68. Hebert, L.E., Scherr, P.A., Bienias, J.L., Bennett, D.A., and Evans, D.A. (2003) Alzheimer disease in the US population: prevalence estimates using the 2000 census. *Arch Neurol*, **60**(8): p. 1119-22.
69. Beyreuther, K., Bush, A.I., Dyrks, T., Hilbich, C., Konig, G., Monning, U., Multhaup, G., Prior, R., Rumble, B., Schubert, W., and et al. (1991)

Mechanisms of amyloid deposition in Alzheimer's disease, in Ann N Y Acad Sci. p. 129-39.

70. Tamayev, R., Zhou, D., and D'Adamio, L. (2009) The interactome of the amyloid beta precursor protein family members is shaped by phosphorylation of their intracellular domains. *Mol Neurodegener*, **4**: p. 28.
71. Gralle, M. and Ferreira, S.T. (2007) Structure and functions of the human amyloid precursor protein: the whole is more than the sum of its parts. *Prog Neurobiol*, **82**(1): p. 11-32.
72. Selkoe, D.J. and Podlisny, M.B. (2002) Deciphering the genetic basis of Alzheimer's disease. *Annu Rev Genomics Hum Genet*, **3**: p. 67-99.
73. Turner, P.R., O'Connor, K., Tate, W.P., and Abraham, W.C. (2003) Roles of amyloid precursor protein and its fragments in regulating neural activity, plasticity and memory. *Prog Neurobiol*, **70**(1): p. 1-32.
74. Cam, J.A. and Bu, G. (2006) Modulation of beta-amyloid precursor protein trafficking and processing by the low density lipoprotein receptor family. *Mol Neurodegener*, **1**: p. 8.
75. Allinson, T.M., Parkin, E.T., Turner, A.J., and Hooper, N.M. (2003) ADAMs family members as amyloid precursor protein alpha-secretases, in J Neurosci Res. p. 342-52.
76. Hardy, J. and Selkoe, D.J. (2002) The amyloid hypothesis of Alzheimer's disease: progress and problems on the road to therapeutics. *Science*, **297**(5580): p. 353-6.
77. Hardy, J.A. and Higgins, G.A. (1992) Alzheimer's disease: the amyloid cascade hypothesis. *Science*, **256**(5054): p. 184-5.
78. Fraser, P.E., Levesque, L., and McLachlan, D.R. (1993) Biochemistry of Alzheimer's disease amyloid plaques. *Clin Biochem*, **26**(5): p. 339-49.
79. Haass, C. and Selkoe, D.J. (2007) Soluble protein oligomers in neurodegeneration: lessons from the Alzheimer's amyloid beta-peptide. *Nat Rev Mol Cell Biol*, **8**(2): p. 101-12.
80. Bishop, M.F. and Ferrone, F.A. (1984) Kinetics of nucleation-controlled polymerization. A perturbation treatment for use with a secondary pathway, in Biophys J. p. 631-44.
81. Ferrone, F. (1999) Analysis of protein aggregation kinetics. *Methods Enzymol*, **309**: p. 256-74.

82. Kodaka, M. (2004) Interpretation of concentration-dependence in aggregation kinetics. *Biophys Chem*, **109**(2): p. 325-32.
83. Finder, V.H. and Glockshuber, R. (2007) Amyloid-beta aggregation. *Neurodegener Dis*, **4**(1): p. 13-27.
84. Arimon, M., Diez-Perez, I., Kogan, M.J., Durany, N., Giralt, E., Sanz, F., and Fernandez-Busquets, X. (2005) Fine structure study of Abeta1-42 fibrillogenesis with atomic force microscopy. *FASEB J*, **19**(10): p. 1344-6.
85. Lomakin, A., Chung, D.S., Benedek, G.B., Kirschner, D.A., and Teplow, D.B. (1996) On the nucleation and growth of amyloid beta-protein fibrils: detection of nuclei and quantitation of rate constants. *Proc Natl Acad Sci U S A*, **93**(3): p. 1125-9.
86. O'Nuallain, B., Shivaprasad, S., Kheterpal, I., and Wetzel, R. (2005) Thermodynamics of A beta(1-40) amyloid fibril elongation. *Biochemistry*, **44**(38): p. 12709-18.
87. Williams, A.D., Sega, M., Chen, M., Kheterpal, I., Geva, M., Berthelier, V., Kaleta, D.T., Cook, K.D., and Wetzel, R. (2005) Structural properties of Abeta protofibrils stabilized by a small molecule. *Proc Natl Acad Sci U S A*, **102**(20): p. 7115-20.
88. Giacobini, E. (2000) Cholinesterase inhibitors stabilize Alzheimer's disease. *Ann N Y Acad Sci*, **920**: p. 321-7.
89. Francis, P.T., Palmer, A.M., Snape, M., and Wilcock, G.K. (1999) The cholinergic hypothesis of Alzheimer's disease: a review of progress. *J Neurol Neurosurg Psychiatry*, **66**(2): p. 137-47.
90. Cummings, J.L. (2003) Use of cholinesterase inhibitors in clinical practice: evidence-based recommendations. *Am J Geriatr Psychiatry*, **11**(2): p. 131-45.
91. Lipton, S.A. (2005) The molecular basis of memantine action in Alzheimer's disease and other neurologic disorders: low-affinity, uncompetitive antagonism. *Curr Alzheimer Res*, **2**(2): p. 155-65.
92. Ferris, S.H. (2003) Evaluation of memantine for the treatment of Alzheimer's disease. *Expert Opin Pharmacother*, **4**(12): p. 2305-13.
93. Klafki, H.W., Staufenbiel, M., Kornhuber, J., and Wiltfang, J. (2006) Therapeutic approaches to Alzheimer's disease. *Brain*, **129**(Pt 11): p. 2840-55.
94. McLaurin, J., Cecal, R., Kierstead, M.E., Tian, X., Phinney, A.L., Manea, M., French, J.E., Lambermon, M.H., Darabie, A.A., Brown, M.E., Janus, C.,

Chishti, M.A., Horne, P., Westaway, D., Fraser, P.E., Mount, H.T., Przybylski, M., and St George-Hyslop, P. (2002) Therapeutically effective antibodies against amyloid-beta peptide target amyloid-beta residues 4-10 and inhibit cytotoxicity and fibrillogenesis. *Nat Med*, **8**(11): p. 1263-9.

95. Check, E. (2002) Nerve inflammation halts trial for Alzheimer's drug. *Nature*, **415**(6871): p. 462.
96. Nicoll, J.A., Wilkinson, D., Holmes, C., Steart, P., Markham, H., and Weller, R.O. (2003) Neuropathology of human Alzheimer disease after immunization with amyloid-beta peptide: a case report. *Nat Med*, **9**(4): p. 448-52.
97. Orgogozo, J.M., Gilman, S., Dartigues, J.F., Laurent, B., Puel, M., Kirby, L.C., Jouanny, P., Dubois, B., Eisner, L., Flitman, S., Michel, B.F., Boada, M., Frank, A., and Hock, C. (2003) Subacute meningoencephalitis in a subset of patients with AD after Abeta42 immunization. *Neurology*, **61**(1): p. 46-54.
98. Stefanescu, R., Iacob, R.E., Damoc, E.N., Marquardt, A., Amstalden, E., Manea, M., Perdivara, I., Maftei, M., Paraschiv, G., and Przybylski, M. (2007) Mass spectrometric approaches for elucidation of antigenantibody recognition structures in molecular immunology. *Eur J Mass Spectrom (Chichester, Eng)*, **13**(1): p. 69-75.
99. Dodel, R.C., Du, Y., Depboylu, C., Hampel, H., Frolich, L., Haag, A., Hemmeter, U., Paulsen, S., Teipel, S.J., Brettschneider, S., Spottke, A., Nolker, C., Moller, H.J., Wei, X., Farlow, M., Sommer, N., and Oertel, W.H. (2004) Intravenous immunoglobulins containing antibodies against beta-amyloid for the treatment of Alzheimer's disease. *J Neurol Neurosurg Psychiatry*, **75**(10): p. 1472-4.
100. Ewert, S., Cambillau, C., Conrath, K., and Pluckthun, A. (2002) Biophysical properties of camelid V(HH) domains compared to those of human V(H)3 domains. *Biochemistry*, **41**(11): p. 3628-36.
101. Dumoulin, M., Conrath, K., Van Meirhaeghe, A., Meersman, F., Heremans, K., Frenken, L.G., Muyldermans, S., Wyns, L., and Matagne, A. (2002) Single-domain antibody fragments with high conformational stability. *Protein Sci*, **11**(3): p. 500-15.
102. Muyldermans, S. (2001) Single domain camel antibodies: current status. *J Biotechnol*, **74**(4): p. 277-302.

103. Hamers-Casterman, C., Atarhouch, T., Muyldermans, S., Robinson, G., Hamers, C., Songa, E.B., Bendahman, N., and Hamers, R. (1993) Naturally occurring antibodies devoid of light chains. *Nature*, **363**(6428): p. 446-8.

104. Ward, E.S., Gussow, D., Griffiths, A.D., Jones, P.T., and Winter, G. (1989) Binding activities of a repertoire of single immunoglobulin variable domains secreted from Escherichia coli. *Nature*, **341**(6242): p. 544-6.

105. van der Linden, R.H., Frenken, L.G., de Geus, B., Harmsen, M.M., Ruuls, R.C., Stok, W., de Ron, L., Wilson, S., Davis, P., and Verrips, C.T. (1999) Comparison of physical chemical properties of llama VHH antibody fragments and mouse monoclonal antibodies. *Biochim Biophys Acta*, **1431**(1): p. 37-46.

106. Muyldermans, S., Cambillau, C., and Wyns, L. (2001) Recognition of antigens by single-domain antibody fragments: the superfluous luxury of paired domains. *Trends Biochem Sci*, **26**(4): p. 230-5.

107. Janowski, R., Kozak, M., Jankowska, E., Grzonka, Z., Grubb, A., Abrahamson, M., and Jaskolski, M. (2001) Human cystatin C, an amyloidogenic protein, dimerizes through three-dimensional domain swapping. *Nat Struct Biol*, **8**(4): p. 316-20.

108. Levy, E., Sastre, M., Kumar, A., Gallo, G., Piccardo, P., Ghetti, B., and Tagliavini, F. (2001) Codeposition of cystatin C with amyloid-beta protein in the brain of Alzheimer disease patients. *J Neuropathol Exp Neurol*, **60**(1): p. 94-104.

109. Rodziewicz-Motowidlo, S., Wahlbom, M., Wang, X., Lagiewka, J., Janowski, R., Jaskolski, M., Grubb, A., and Grzonka, Z. (2006) Checking the conformational stability of cystatin C and its L68Q variant by molecular dynamics studies: why is the L68Q variant amyloidogenic? *J Struct Biol*, **154**(1): p. 68-78.

110. Calero, M., Pawlik, M., Soto, C., Castano, E.M., Sigurdsson, E.M., Kumar, A., Gallo, G., Frangione, B., and Levy, E. (2001) Distinct properties of wild-type and the amyloidogenic human cystatin C variant of hereditary cerebral hemorrhage with amyloidosis, Icelandic type. *J Neurochem*, **77**(2): p. 628-37.

111. Sastre, M., Calero, M., Pawlik, M., Mathews, P.M., Kumar, A., Danilov, V., Schmidt, S.D., Nixon, R.A., Frangione, B., and Levy, E. (2004) Binding of cystatin C to Alzheimer's amyloid beta inhibits in vitro amyloid fibril formation. *Neurobiol Aging*, **25**(8): p. 1033-43.

112. Carrette, O., Demalte, I., Scherl, A., Yalkinoglu, O., Corthals, G., Burkhard, P., Hochstrasser, D.F., and Sanchez, J.C. (2003) A panel of cerebrospinal fluid potential biomarkers for the diagnosis of Alzheimer's disease. *Proteomics*, **3**(8): p. 1486-94.

113. Selenica, M.L., Wang, X., Ostergaard-Pedersen, L., Westlind-Danielsson, A., and Grubb, A. (2007) Cystatin C reduces the in vitro formation of soluble Abeta1-42 oligomers and protofibrils. *Scand J Clin Lab Invest*, **67**(2): p. 179-90.

114. Vattemi, G., Engel, W.K., McFerrin, J., and Askanas, V. (2003) Cystatin C colocalizes with amyloid-beta and coimmunoprecipitates with amyloid-beta precursor protein in sporadic inclusion-body myositis muscles. *J Neurochem*, **85**(6): p. 1539-46.

115. Tizon, B., Ribe, E.M., Mi, W., Troy, C.M., and Levy, E. (2010) Cystatin C protects neuronal cells from amyloid-beta-induced toxicity. *J Alzheimers Dis*, **19**(3): p. 885-94.

116. Hudson, P.J. (1998) Recombinant antibody fragments. *Curr Opin Biotechnol*, **9**(4): p. 395-402.

117. Glennie, M.J. and Johnson, P.W. (2000) Clinical trials of antibody therapy. *Immunol Today*, **21**(8): p. 403-10.

118. Dumoulin, M., Conrath, K., Van Meirhaeghe, A., Meersman, F., Heremans, K., Frenken, L.G.J., Muyldermans, S., Wyns, L., and Matagne, A. (2002) Single-domain antibody fragments with high conformational stability. *Protein Science*, **11**(3): p. 500-515.

119. Desmyter, A., Decanniere, K., Muyldermans, S., and Wyns, L. (2001) Antigen specificity and high affinity binding provided by one single loop of a camel single-domain antibody. *J Biol Chem*, **276**(28): p. 26285-90.

120. Chothia, C., Lesk, A.M., Gherardi, E., Tomlinson, I.M., Walter, G., Marks, J.D., Llewelyn, M.B., and Winter, G. (1992) Structural repertoire of the human VH segments. *J Mol Biol*, **227**(3): p. 799-817.

121. Chothia, C., Lesk, A.M., Tramontano, A., Levitt, M., Smith-Gill, S.J., Air, G., Sheriff, S., Padlan, E.A., Davies, D., Tulip, W.R., and et al. (1989) Conformations of immunoglobulin hypervariable regions. *Nature*, **342**(6252): p. 877-83.

122. Decanniere, K., Transue, T.R., Desmyter, A., Maes, D., Muyldermans, S., and Wyns, L. (2001) Degenerate interfaces in antigen-antibody complexes. *J Mol Biol*, **313**(3): p. 473-8.

123. Kabat, E.A. and Wu, T.T. (1991) Identical V region amino acid sequences and segments of sequences in antibodies of different specificities. Relative contributions of VH and VL genes, minigenes, and complementarity-determining regions to binding of antibody-combining sites. *J Immunol*, **147**(5): p. 1709-19.

124. Muyldermans, S., Atarhouch, T., Saldanha, J., Barbosa, J.A., and Hamers, R. (1994) Sequence and structure of VH domain from naturally occurring camel heavy chain immunoglobulins lacking light chains. *Protein Eng*, **7**(9): p. 1129-35.

125. Transue, T.R., De Genst, E., Ghahroudi, M.A., Wyns, L., and Muyldermans, S. (1998) Camel single-domain antibody inhibits enzyme by mimicking carbohydrate substrate. *Proteins*, **32**(4): p. 515-22.

126. Webster, D.M., Henry, A.H., and Rees, A.R. (1994) Antibody-antigen interactions. *Current Opinion in Structural Biology*, **4**(1): p. 123-129.

127. Padlan, E.A. (1996) X-ray crystallography of antibodies. *Adv Protein Chem*, **49**: p. 57-133.

128. Nguyen, V.K., Hamers, R., Wyns, L., and Muyldermans, S. (2000) Camel heavy-chain antibodies: diverse germline V(H)H and specific mechanisms enlarge the antigen-binding repertoire. *EMBO J*, **19**(5): p. 921-30.

129. Papac, D.I., Hoyes, J., and Tomer, K.B. (1994) Epitope mapping of the gastrin-releasing peptide/anti-bombesin monoclonal antibody complex by proteolysis followed by matrix-assisted laser desorption ionization mass spectrometry. *Protein Sci*, **3**(9): p. 1485-92.

130. Parker, C.E., Papac, D.I., Trojak, S.K., and Tomer, K.B. (1996) Epitope mapping by mass spectrometry: determination of an epitope on HIV-1 IIIB p26 recognized by a monoclonal antibody. *J Immunol*, **157**(1): p. 198-206.

131. Hager-Braun, C., Hochleitner, E.O., Gorny, M.K., Zolla-Pazner, S., Bienstock, R.J., and Tomer, K.B. (2010) Characterization of a Discontinuous Epitope of the HIV Envelope Protein gp120 Recognized by a Human Monoclonal Antibody Using Chemical Modification and Mass Spectrometric Analysis. *Journal of the American Society for Mass Spectrometry*, **21**(10): p. 1687-1698.

132. Beg, J.M., Tymoczko, J.L., Stryer, L., ed. *Biochemistry* 6th ed. 2007, Freeman and Company: New York.
133. Lehninger, ed. *Principles of biochemistry*. 4th ed. 2004, W. H. Freeman: New York.
134. Dodson, G. and Wlodawer, A. (1998) Catalytic triads and their relatives. *Trends in Biochemical Sciences*, **23**(9): p. 347-352.
135. Lau, J.K.-C. and Cheng, Y.-K. (2006) SER-HIS-ASP catalytic triad in model non-aqueous solvent environment: A computational study. *Bioorganic & Medicinal Chemistry Letters*, **16**(22): p. 5797-5800.
136. Briand, L., Chobert, J.-M., Gantier, R., Declerck, N., Tran, V., Léonil, J., Mollé, D., and Haertlé, T. (1999) Impact of the lysine-188 and aspartic acid-189 inversion on activity of trypsin. *FEBS Letters*, **442**(1): p. 43-47.
137. Rüdiger, A.-H., Rüdiger, M., Carl, U.D., Chakraborty, T., Roepstorff, P., and Wehland, J. (1999) Affinity Mass Spectrometry-Based Approaches for the Analysis of Protein-Protein Interaction and Complex Mixtures of Peptide-Ligands. *Analytical Biochemistry*, **275**(2): p. 162-170.
138. Chou, P.H., Chen, S.H., Liao, H.K., Lin, P.C., Her, G.R., Lai, A.C., Chen, J.H., Lin, C.C., and Chen, Y.J. (2005) Nanoprobe-based affinity mass spectrometry for selected protein profiling in human plasma. *Anal Chem*, **77**(18): p. 5990-7.
139. Holtzhauer, M., ed. *Methoden in der Proteinanlytik*. 1996, Springer: Berlin.
140. Millar, A.L., Jackson, N.A., Dalton, H., Jennings, K.R., Levi, M., Wahren, B., and Dimmock, N.J. (1998) Rapid analysis of epitope-paratope interactions between HIV-1 and a 17-amino-acid neutralizing microantibody by electrospray ionization mass spectrometry. *Eur J Biochem*, **258**(1): p. 164-9.
141. Zhao, Y. and Chalt, B.T. (1994) Protein epitope mapping by mass spectrometry. *Anal Chem*, **66**(21): p. 3723-6.
142. Macht, M., Marquardt, A., Deininger, S.O., Damoc, E., Kohlmann, M., and Przybylski, M. (2004) "Affinity-proteomics": direct protein identification from biological material using mass spectrometric epitope mapping. *Anal Bioanal Chem*, **378**(4): p. 1102-11.
143. Yu, L., Gaskell, S.J., and Brookman, J.L. (1998) Epitope mapping of monoclonal antibodies by mass spectrometry: identification of protein antigens in complex biological systems. *J Am Soc Mass Spectrom*, **9**(3): p. 208-15.

144. Buck, M. (1998) Trifluoroethanol and colleagues: cosolvents come of age. Recent studies with peptides and proteins. *Q Rev Biophys*, **31**(3): p. 297-355.
145. Nelson, J.W. and Kallenbach, N.R. (1986) Stabilization of the ribonuclease S-peptide alpha-helix by trifluoroethanol. *Proteins*, **1**(3): p. 211-7.
146. Merutka, G., Lipton, W., Shalongo, W., Park, S.H., and Stellwagen, E. (1990) Effect of central-residue replacements on the helical stability of a monomeric peptide. *Biochemistry*, **29**(32): p. 7511-5.
147. Lazo, N.D. and Downing, D.T. (1997) Circular dichroism of model peptides emulating the amphipathic alpha-helical regions of intermediate filaments. *Biochemistry*, **36**(9): p. 2559-65.
148. Coles, M., Bicknell, W., Watson, A.A., Fairlie, D.P., and Craik, D.J. (1998) Solution structure of amyloid beta-peptide(1-40) in a water-micelle environment. Is the membrane-spanning domain where we think it is? *Biochemistry*, **37**(31): p. 11064-77.
149. Dragusanu, M., Petre, B.A., Slamnoiu, S., Vlad, C., Tu, T., and Przybylski, M. (2010) On-line bioaffinity-electrospray mass spectrometry for simultaneous detection, identification, and quantification of protein-ligand interactions. *J Am Soc Mass Spectrom*, **21**(10): p. 1643-8.
150. Liedberg, B., Nylander, C., and Lundstrom, I. (1995) Biosensing with surface plasmon resonance--how it all started. *Biosens Bioelectron*, **10**(8): p. i-ix.
151. Homola, J., Yee, S.S., and Gauglitz, G. (1999) Surface plasmon resonance sensors: review. *Sensors and Actuators B: Chemical*, **54**(1-2): p. 3-15.
152. Treitz, G., Gronewold, T.M., Quandt, E., and Zabe-Kuhn, M. (2008) Combination of a SAW-biosensor with MALDI mass spectrometric analysis. *Biosens Bioelectron*, **23**(10): p. 1496-502.
153. Gronewold, T.M.A. (2007) Surface acoustic wave sensors in the bioanalytical field: Recent trends and challenges. *Analytica Chimica Acta*, **603**(2): p. 119-128.
154. Malave, A.S., U.; Gronewold, T.M.A.; Perpeet, M.; Tewes, M.; (2006) Lithium Tantalate Surface Acoustic Wave Sensors for Bio-Analytical Applications in Sensors, 5th IEEE Conference on *Daegu* p. 604 - 607
155. Perpeet, M., Glass, S., Gronewold, T., Kiwitz, A., Malavé, A., Stoyanov, I., Tewes, M., and Quandt, E. (2006) SAW Sensor System for Marker-Free Molecular Interaction Analysis. *LANL*, **39**(8): p. 1747-1757.

156. Lange, K., Bender, F., Voigt, A., Gao, H., and Rappt, M. (2003) A surface acoustic wave biosensor concept with low flow cell volumes for label-free detection. *Anal Chem*, **75**(20): p. 5561-6.

157. Lee, D.S., Lee, J.H., Luo, J., Fu, Y., Milne, W.I., Maeng, S., Jung, M.Y., Park, S.H., and Yoon, H.C. (2009) A surface acoustic wave-based immunosensing device using a nanocrystalline ZnO film on Si. *J Nanosci Nanotechnol*, **9**(12): p. 7181-5.

158. Kao, K.S., Cheng, C.C., Chung, C.J., and Chen, Y.C. (2005) Surface acoustic wave properties of proton-exchanged LiNbO3 waveguides with SiO2 film. *IEEE Trans Ultrason Ferroelectr Freq Control*, **52**(3): p. 503-6.

159. Brown, W.M. and Dziegielewska, K.M. (1997) Friends and relations of the cystatin superfamily—new members and their evolution. *Protein Science*, **6**(1): p. 5-12.

160. Ochieng, J. and Chaudhuri, G. (2010) Cystatin superfamily. *J Health Care Poor Underserved*, **21**(1 Suppl): p. 51-70.

161. Fujihara, S., Shimode, K., Nakamura, M., Kobayashi, S., and Tsunematsu, T. (1989) Cerebral amyloid angiopathy with the deposition of cystatin C (gamma-trace) and beta-protein. *Prog Clin Biol Res*, **317**: p. 939-44.

162. Maruyama, K., Ikeda, S., Ishihara, T., Allsop, D., and Yanagisawa, N. (1990) Immunohistochemical characterization of cerebrovascular amyloid in 46 autopsied cases using antibodies to beta protein and cystatin C. *Stroke*, **21**(3): p. 397-403.

163. Grubb, A. and Lofberg, H. (1982) Human gamma-trace, a basic microprotein: amino acid sequence and presence in the adenohypophysis. *Proc Natl Acad Sci U S A*, **79**(9): p. 3024-7.

164. Clausen, J. (1961) Proteins in normal cerebrospinal fluid not found in serum. *Proc Soc Exp Biol Med*, **107**: p. 170-2.

165. Butler, E.A. and Flynn, F.V. (1961) The occurrence of post-gamma protein in urine: a new protein abnormality. *J Clin Pathol*, **14**: p. 172-8.

166. Colle, A., Guinet, R., Leclercq, M., and Manuel, Y. (1976) Occurrence of beta2-microglobulin and post-gamma globulin in human semen. *Clin Chim Acta*, **67**(1): p. 93-7.

167. Hochwald, G.M. and Thorbecke, G.J. (1963) Trace proteins in cerebrospinal fluid and other biological fluids. I. Effect of various fractionation procedures on

beta-trace and gamma-trace proteins and methods for isolation of both proteins. *Arch Biochem Biophys*, **101**: p. 325-34.

168. Seronie-Vivien, S., Delanaye, P., Pieroni, L., Mariat, C., Froissart, M., and Cristol, J.P. (2008) Cystatin C: current position and future prospects. *Clin Chem Lab Med*, **46**(12): p. 1664-86.
169. Jekel, P.A., Weijer, W.J., and Beintema, J.J. (1983) Use of endoproteinase Lys-C from Lysobacter enzymogenes in protein sequence analysis. *Anal Biochem*, **134**(2): p. 347-54.
170. Jung, G., Ueno, H., and Hayashi, R. (1999) Carboxypeptidase Y: structural basis for protein sorting and catalytic triad. *J Biochem*, **126**(1): p. 1-6.
171. Hayashi, R. (1976) Carboxypeptidase Y. *Methods Enzymol*, **45**: p. 568-87.
172. Jaskolski, M. (2001) 3D domain swapping, protein oligomerization, and amyloid formation. *Acta Biochim Pol*, **48**(4): p. 807-27.
173. Comeau, S.R., Gatchell, D.W., Vajda, S., and Camacho, C.J. (2004) ClusPro: a fully automated algorithm for protein-protein docking. *Nucleic Acids Res*, **32**(Web Server issue): p. W96-9.
174. Tovchigrechko, A. and Vakser, I.A. (2006) GRAMM-X public web server for protein-protein docking. *Nucleic Acids Res*, **34**(Web Server issue): p. W310-4.
175. Yu, Y., Kirkup, C.E., Pi, N., and Leary, J.A. (2004) Characterization of noncovalent protein-ligand complexes and associated enzyme intermediates of GlcNAc-6-O-sulfotransferase by electrospray ionization FT-ICR mass spectrometry. *J Am Soc Mass Spectrom*, **15**(10): p. 1400-7.
176. Fligge, T.A., Reinhard, C., Harter, C., Wieland, F.T., and Przybylski, M. (2000) Oligomerization of peptides analogous to the cytoplasmic domains of coatomer receptors revealed by mass spectrometry. *Biochemistry*, **39**(29): p. 8491-6.
177. Lecanu, L., Greeson, J., and Papadopoulos, V. (2006) Beta-amyloid and oxidative stress jointly induce neuronal death, amyloid deposits, gliosis, and memory impairment in the rat brain. *Pharmacology*, **76**(1): p. 19-33.
178. Janus, C., Pearson, J., McLaurin, J., Mathews, P.M., Jiang, Y., Schmidt, S.D., Chishti, M.A., Horne, P., Heslin, D., French, J., Mount, H.T., Nixon, R.A., Mercken, M., Bergeron, C., Fraser, P.E., St George-Hyslop, P., and Westaway, D. (2000) A beta peptide immunization reduces behavioural

impairment and plaques in a model of Alzheimer's disease. *Nature*, **408**(6815): p. 979-82.

179. Schenk, D., Barbour, R., Dunn, W., Gordon, G., Grajeda, H., Guido, T., Hu, K., Huang, J., Johnson-Wood, K., Khan, K., Kholodenko, D., Lee, M., Liao, Z., Lieberburg, I., Motter, R., Mutter, L., Soriano, F., Shopp, G., Vasquez, N., Vandevert, C., Walker, S., Wogulis, M., Yednock, T., Games, D., and Seubert, P. (1999) Immunization with amyloid-beta attenuates Alzheimer-disease-like pathology in the PDAPP mouse. *Nature*, **400**(6740): p. 173-7.
180. Alvarez, A., Opazo, C., Alarcon, R., Garrido, J., and Inestrosa, N.C. (1997) Acetylcholinesterase promotes the aggregation of amyloid-beta-peptide fragments by forming a complex with the growing fibrils, in J Mol Biol. p. 348-61.
181. Estus, S., Golde, T.E., Kunishita, T., Blades, D., Lowery, D., Eisen, M., Usiak, M., Qu, X.M., Tabira, T., Greenberg, B.D., and et al. (1992) Potentially amyloidogenic, carboxyl-terminal derivatives of the amyloid protein precursor. *Science*, **255**(5045): p. 726-8.
182. Esch, F.S., Keim, P.S., Beattie, E.C., Blacher, R.W., Culwell, A.R., Oltersdorf, T., McClure, D., and Ward, P.J. (1990) Cleavage of amyloid beta peptide during constitutive processing of its precursor. *Science*, **248**(4959): p. 1122-4.
183. Simonsen, A.H., Hansson, S.F., Ruetschi, U., McGuire, J., Podust, V.N., Davies, H.A., Mehta, P., Waldemar, G., Zetterberg, H., Andreasen, N., Wallin, A., and Blennow, K. (2007) Amyloid beta1-40 quantification in CSF: comparison between chromatographic and immunochemical methods. *Dement Geriatr Cogn Disord*, **23**(4): p. 246-50.
184. Lichtenthaler, S.F. and Haass, C. (2004) Amyloid at the cutting edge: activation of α-secretase prevents amyloidogenesis in an Alzheimer disease mouse model. *The Journal of Clinical Investigation*, **113**(10): p. 1384-1387.
185. Kumar, S. and Walter, J. (2011) Phosphorylation of amyloid beta (Abeta) peptides - a trigger for formation of toxic aggregates in Alzheimer's disease. *Aging (Albany NY)*, **3**(8): p. 803-12.
186. Manea, M. (2006) Design, Structural and Immuno-analytical Properties of Antigenic Polypeptides comprising a ß-Amyloid Plaque Specific Epitope, Konstanz.

187. Xue, W.-F., Homans, S.W., and Radford, S.E. (2008) Systematic analysis of nucleation-dependent polymerization reveals new insights into the mechanism of amyloid self-assembly. *Proceedings of the National Academy of Sciences*, **105**(26): p. 8926-8931.

188. Roychaudhuri, R., Yang, M., Hoshi, M.M., and Teplow, D.B. (2009) Amyloid β-Protein Assembly and Alzheimer Disease. *Journal of Biological Chemistry*, **284**(8): p. 4749-4753.

189. Walsh, D.M., Hartley, D.M., Kusumoto, Y., Fezoui, Y., Condron, M.M., Lomakin, A., Benedek, G.B., Selkoe, D.J., and Teplow, D.B. (1999) Amyloid beta-protein fibrillogenesis. Structure and biological activity of protofibrillar intermediates. *J Biol Chem*, **274**(36): p. 25945-52.

190. Kirkitadze, M.D., Condron, M.M., and Teplow, D.B. (2001) Identification and characterization of key kinetic intermediates in amyloid beta-protein fibrillogenesis. *J Mol Biol*, **312**(5): p. 1103-19.

191. Gong, Y., Chang, L., Viola, K.L., Lacor, P.N., Lambert, M.P., Finch, C.E., Krafft, G.A., and Klein, W.L. (2003) Alzheimer's disease-affected brain: presence of oligomeric A beta ligands (ADDLs) suggests a molecular basis for reversible memory loss. *Proc Natl Acad Sci U S A*, **100**(18): p. 10417-22.

192. Merz, P.A., Wisniewski, H.M., Somerville, R.A., Bobin, S.A., Masters, C.L., and Iqbal, K. (1983) Ultrastructural morphology of amyloid fibrils from neuritic and amyloid plaques. *Acta Neuropathol*, **60**(1-2): p. 113-24.

193. Fezoui, Y., Hartley, D.M., Harper, J.D., Khurana, R., Walsh, D.M., Condron, M.M., Selkoe, D.J., Lansbury, P.T., Jr., Fink, A.L., and Teplow, D.B. (2000) An improved method of preparing the amyloid beta-protein for fibrillogenesis and neurotoxicity experiments. *Amyloid*, **7**(3): p. 166-78.

194. Zagorski, M.G., Yang, J., Shao, H., Ma, K., Zeng, H., and Hong, A. (1999) Methodological and chemical factors affecting amyloid beta peptide amyloidogenicity. *Methods Enzymol*, **309**: p. 189-204.

195. Wood, S.J., Maleeff, B., Hart, T., and Wetzel, R. (1996) Physical, morphological and functional differences between ph 5.8 and 7.4 aggregates of the Alzheimer's amyloid peptide Abeta. *J Mol Biol*, **256**(5): p. 870-7.

196. Jan, A., Hartley, D.M., and Lashuel, H.A. (2010) Preparation and characterization of toxic Abeta aggregates for structural and functional studies in Alzheimer's disease research. *Nat Protoc*, **5**(6): p. 1186-209.

197. Teplow, D.B. (2006) Preparation of amyloid beta-protein for structural and functional studies. *Methods Enzymol*, **413**: p. 20-33.
198. Dahlgren, K.N., Manelli, A.M., Stine, W.B., Jr., Baker, L.K., Krafft, G.A., and LaDu, M.J. (2002) Oligomeric and fibrillar species of amyloid-beta peptides differentially affect neuronal viability. *J Biol Chem*, **277**(35): p. 32046-53.
199. Khurana, R., Coleman, C., Ionescu-Zanetti, C., Carter, S.A., Krishna, V., Grover, R.K., Roy, R., and Singh, S. (2005) Mechanism of thioflavin T binding to amyloid fibrils. *J Struct Biol*, **151**(3): p. 229-38.
200. LeVine, H., 3rd (1993) Thioflavine T interaction with synthetic Alzheimer's disease beta-amyloid peptides: detection of amyloid aggregation in solution. *Protein Sci*, **2**(3): p. 404-10.
201. Vassar, P.S. and Culling, C.F. (1959) Fluorescent stains, with special reference to amyloid and connective tissues. *Arch Pathol*, **68**: p. 487-98.
202. Biancalana, M. and Koide, S. (2010) Molecular mechanism of Thioflavin-T binding to amyloid fibrils, in Biochim Biophys Acta. p. 1405-12.
203. Groenning, M. (2009) Binding mode of Thioflavin T and other molecular probes in the context of amyloid fibrils-current status. *J Chem Biol*.
204. Naiki, H., Higuchi, K., Hosokawa, M., and Takeda, T. (1989) Fluorometric determination of amyloid fibrils in vitro using the fluorescent dye, thioflavin T1. *Anal Biochem*, **177**(2): p. 244-9.
205. Krchnãk, V., Vágner, J., àfár, P., Lebi, M. (1988) in Coil. Czech. Chern. Comm. p. 2542
206. Kaiser, E., Colescott, R.L., Bossinger, C.D., and Cook, P.I. (1970) Color test for detection of free terminal amino groups in the solid-phase synthesis of peptides. *Anal Biochem*, **34**(2): p. 595-8.
207. Vojkovsky, T. (1995) Detection of secondary amines on solid phase. *Pept Res*, **8**(4): p. 236-7.
208. Olsen, J.V., Ong, S.E., and Mann, M. (2004) Trypsin cleaves exclusively C-terminal to arginine and lysine residues. *Mol Cell Proteomics*, **3**(6): p. 608-14.
209. Bovaird, J.H., Ngo, T.T., and Lenhoff, H.M. (1982) Optimizing the o-phenylenediamine assay for horseradish peroxidase: effects of phosphate and pH, substrate and enzyme concentrations, and stopping reagents. *Clin Chem*, **28**(12): p. 2423-6.

210. Hempen, C., van Leeuwen, S.M., Luftmann, H., and Karst, U. (2005) Liquid chromatographic/mass spectrometric investigation on the reaction products in the peroxidase-catalyzed oxidation of o-phenylenediamine by hydrogen peroxide. *Anal Bioanal Chem*, **382**(1): p. 234-8.
211. Tarcha, P.J., Chu, V.P., and Whittern, D. (1987) 2,3-Diaminophenazine is the product from the horseradish peroxidase-catalyzed oxidation of o-phenylenediamine. *Anal Biochem*, **165**(1): p. 230-3.
212. Gronewold, T.M., Schlecht, U., and Quandt, E. (2007) Analysis of proteolytic degradation of a crude protein mixture using a surface acoustic wave sensor. *Biosens Bioelectron*, **22**(9-10): p. 2360-5.
213. Greenfield, N. and Fasman, G.D. (1969) Computed circular dichroism spectra for the evaluation of protein conformation. *Biochemistry*, **8**(10): p. 4108-16.
214. LeVine, H., 3rd (1999) Quantification of beta-sheet amyloid fibril structures with thioflavin T, in Methods Enzymol. p. 274-84.
215. Schagger, H. and von Jagow, G. (1987) Tricine-sodium dodecyl sulfate-polyacrylamide gel electrophoresis for the separation of proteins in the range from 1 to 100 kDa. *Anal Biochem*, **166**(2): p. 368-79.
216. Neuhoff, V., Arold, N., Taube, D., and Ehrhardt, W. (1988) Improved staining of proteins in polyacrylamide gels including isoelectric focusing gels with clear background at nanogram sensitivity using Coomassie Brilliant Blue G-250 and R-250, in Electrophoresis. p. 255-62.
217. Heukeshoven, J., and Dernick, R., (1985) Simplified method for silver staining of proteins in polyacrylamide gels and the mechanism of silver staining. *Electrophoresis*, **6**: p. 103-112.
218. www.gelifesciences.co.jp/tech_support/manual/pdf/rpn2105psaa.pdf.
219. Towbin, H., Staehelin, T., and Gordon, J. (1979) Electrophoretic transfer of proteins from polyacrylamide gels to nitrocellulose sheets: procedure and some applications, in Proc Natl Acad Sci U S A. p. 4350-4.
220. http://www.millipore.com.
221. Vertes, A., Gijbels, R., Levine, R. D. (1990) Homogeneous bottleneck model of matrix assisted UV laser desorption of large molecules. *Rapid Comm. Mass Spectrom.*, **4**: p. 228-233.
222. Dreisewerd, K., Schürenberg, M., M. Karas, M., Hillenkamp, F. (1995) Influence of the Laser Intensity and Spot Size on the Desorption of Molecules

and Ions in Matrix-Assisted Laser Desorption/Ionization with a Uniform Beam Profile. *Int. J. Mass Spetrom. Ion Proc.*, **14**: p. 127-148.

223. Holmes, J.L., Aubry, C., Mayer, P.M., ed. *Assigning structures to ions in mass spectrometry*. ed. C. Press2007: New York.
224. Peri, S., Steen, H., and Pandey, A. (2001) GPMAW--a software tool for analyzing proteins and peptides*. Trends Biochem Sci*, **26**(11): p. 687-9.
225. www.ballview.org.
226. Moll, A., Hildebrandt, A., Lenhof, H.P., and Kohlbacher, O. (2006) BALLView: a tool for research and education in molecular modeling*. Bioinformatics*, **22**(3): p. 365-6.
227. Essmann, U., Perera, L., Berkowitz, M.L., Darden, T., Lee, H., Pedersen, G. (1995) A smooth particle mesh Ewald method. *Melville, NY, ETATS-UNIS*: American Institute of Physics. **103**.
228. Koradi, R., Billeter, M., and Wuthrich, K. (1996) MOLMOL: a program for display and analysis of macromolecular structures*. J Mol Graph*, **14**(1): p. 51-5, 29-32.

7 Appendix

7.1 Appendix 1

Abbreviations:

ACN	Acetonitrile
AcOH	Acidic acid
Ab	Antibody
AD	Alzheimer's disease
APS	Ammonium persulfate
CDR	Complementary determining region
t-Boc	t-butoxycarbonyl
Da	Dalton
1-DE	one-dimensional gel electrophoresis
DHB	2,5-Dihydroxybenzoic acid
Δm	Mass difference
DMF	Dimethylformamide
DTT	Dithiothreitol
ELISA	Enzyme linked immunosorbent assay
ESI-MS	Electrospray ionisation- Mass spectrometry
Fab	Antigen-binding fragment
FAB-MS	Fast-atom-bombardment-mass spectrometry
Fmoc	9-Fluorenylmethoxycarbonyl-Rest
FT-ICR	Fourier transform-ion cyclotron resonance
HCCA	4-Hydroxy-α-cynamic acid
HPLC	High performance liquid chromatography
Hz	Hertz
IEF	Isoelectric focusing

IgG	Immunglobulin G
MALDI	Matrix-assisted laser desorption/ionisation
MS	Mass spectrometry
m/z	mass over charge ratio
NMM	N-methyl-morpholine
PBS	Phosphate buffer saline
pH	Negative logarithmus of H_3O^+ ion concentration
PMF	Peptide mass fingerprint
ppm	Part per million
PyBOP	Benzotriazol-1-yloxy-tris-pyrrolidinophosphonium-PF_6^-Salt
RP	Reverse phase
Rt	Retention time
SDS-PAGE	Sodium dodecyl sulphate-polyacrylamide gel electrophoresis
SPPS	Solid phase peptide synthesis
TEMED	N, N, N', N'- tetramethylethylenediamine
TFA	Trifluoroacetic acid
TCA	Trichloroacetic acid
TOF	Time-of-flight
Tween	Polyoxyethylen Sorbitan Monolaurat
UV	Ultraviolet
V	Volt
°C	Grad Celsius

7.2 Appendix 2

Amino acids abreviations

Name	One letter code	Three letter code	Mass increment
Alanine	A	Ala	71.037
Arginine	R	Arg	156.101
Asparagine	N	Asn	114.042
Aspartic acid	D	Asp	115.026
Cysteine	C	Cys	103.009
Glutamine	Q	Gln	128.058
Glutamic acid	E	Glu	129.042
Glycine	G	Gly	57.021
Histidine	H	His	137.058
Isoleucine	I	Ile	113.084
Leucine	L	Leu	113.084
Lysine	K	Lys	128.094
Methionine	M	Met	131.040
Phenylalanine	F	Phe	147.068
Proline	P	Pro	97.052
Serine	S	Ser	87.032
Threonine	T	Thr	101.047
Tryptophan	W	Trp	186.079
Tyrosine	Y	Tyr	163.063
Valine	V	Val	99.068

7.3 Appendix 3

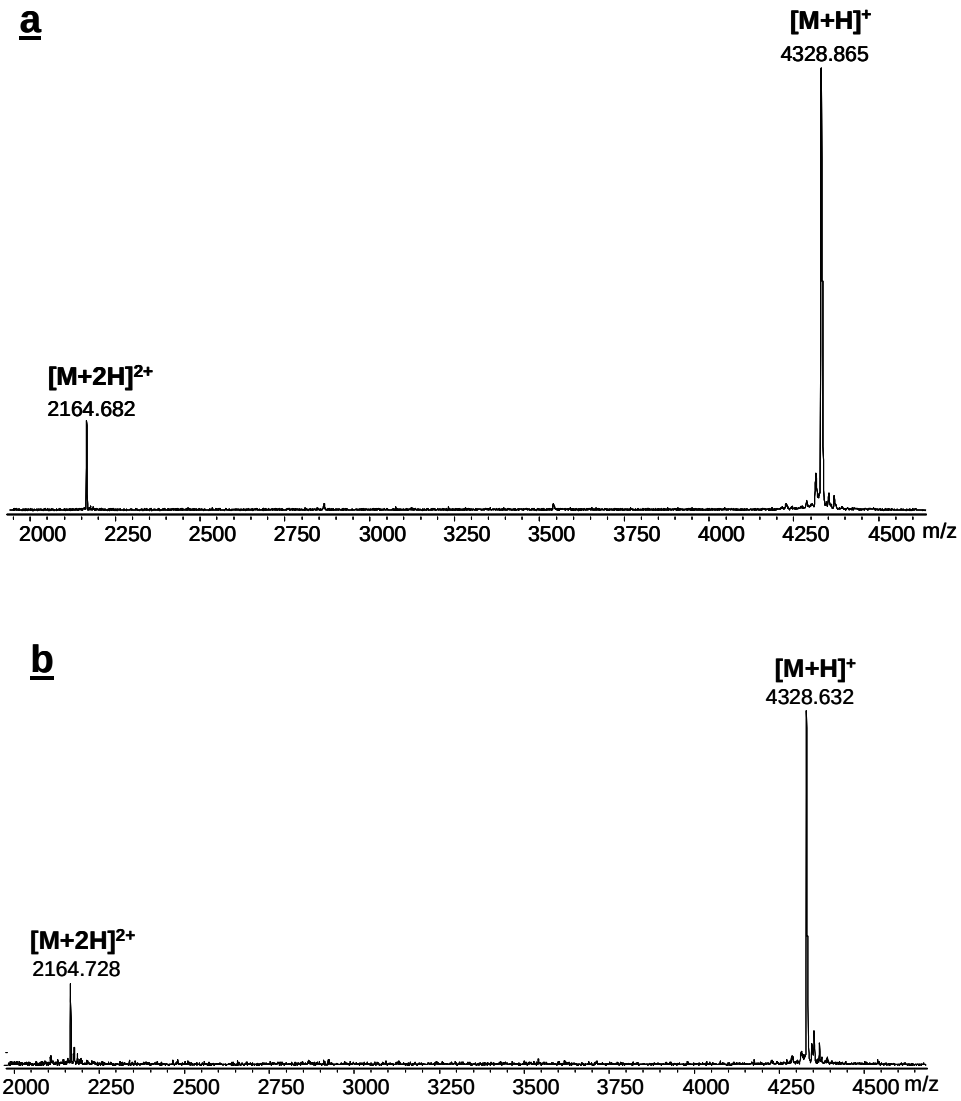

Figure 88: MALDI-TOF mass spectrum of **a** synthetic Aβ(1-40) and **b** recombinant Aβ(1-40) used for aggregation studies.

7.4 Appendix 4

Table 16: Aβ(1-40) peptide fragments obtained by tryptic digestion.

Fragment	Sequence	$[M+H]^+_{calc}$	$[M+H]^+_{exp.}$
[1-5]	DAEFR	637.6	637.5
[6-16]	HDSGYEVHHQK	1337.3	1337.4
[29-40]	GAIIGLMVGGVV	1085.3	1085.3
[17-28]	LVFFAEDVGSNK	1326.4	1326.4
[1-16]	DAEFRHDSGYEVHHQK	1956.0	1956.0
[6-28]	HDSGYEVHHQKLVFFAEDVGSNK	2644.8	2644.8
[1-28]	DAEFRHDSGYEVHHQKLVFFAEDVGSNK	3263.4	3263.4
[6-40]	HDSGYEVHHQKLVFFAEDVGSNKGAIIGLMVGGVV	3711.2	3711.5
[1-40]	DAEFRHDSGYEVHHQKLVFFAEDVGSNKGAIIGLMVGGVV	4329.8	4329.9

7.5 Appendix 5

Table 17: The corresponding Aβ(1-40) peptide fragments after digestion in solution with α-chymotrypsin.

Fragment	Sequence	$[M+H]^+_{calc}$	$[M+H]^+_{exp.}$
[20-35]	FAEDVGSNKGAIIGLM	1622.88	1623.05
[18-34]	VFFAEDVGSNKGAIIGL	1737.92	1737.63
[5-19]	RHDSGYEVHHQKLVF	1851.92	1852.89
[18-35]	VFFAEDVGSNKGAIIGLM	1868.18	1869.01
[21-40]	AEDVGSNKGAIIGLMVGGVV	1885.02	1885.53
[20-40]	FAEDVGSNKGAIIGLMVGGVV	2033.09	2033.07
[1-17]	DAEFRHDSGYEVHHQKL	2069.22	2069.19
[18-40]	VFFAEDVGSNKGAIIGLMVGGVV	2279.69	2279.72
[1-19]	DAEFRHDSGYEVHHQKLVF	2315.50	2316.66
[11-34]	EVHHQKLVFFAEDVGSNKGAIIGL	2609.98	2610.22
[11-35]	EVHHQKLVFFAEDVGSNKGAIIGLM	2741.16	2741.66
[11-40]	EVHHQKLVFFAEDVGSNKGAIIGLMVGGVV	3152.70	3152.92
[5-34]	RHDSGYEVHHQKLVFFAEDVGSNKGAIIGL	3325.70	3325.82
[5-35]	RHDSGYEVHHQKLVFFAEDVGSNKGAIIGLM	3456.90	3457.73
[5-40]	RHDSGYEVHHQKLVFFAEDVGSNKGAIIGLMVGGVV	3867.42	3868.07
[1-40]	DAEFRHDSGYEVHHQKLVFFAEDVGSNKGAIIGLMVGGVV	4329.81	4330.39

7.6 Appendix 6

Table 18: Summary of the Aβ(1-40) peptide fragment obtained by endoprotease GluC digestion in solution.

Fragment	Sequence	$[M+H]^+_{calc}$	$[M+H]^+_{exp.}$
[4-11]	FRHDSGYE	1011.03	1011.12
[1-11]	DAEFRHDSGYE	1326.32	1326.35
[12-22]	VHHQKLVFFAE	1355.58	1355.74
[12-40]	VHHQKLVFFAEDVGSNKGAIIGLMVGGVV	3022.58	3022.86
[4-40]	FRHDSGYEVHHQKLVFFAEDVGSNKGAIIGLMVGGVV	4014.60	4014.72
[1-40]	DAEFRHDSGYEVHHQKLVFFAEDVGSNKGAIIGLMVGGVV	4329.88	4330.02

7.7 Appendix 7

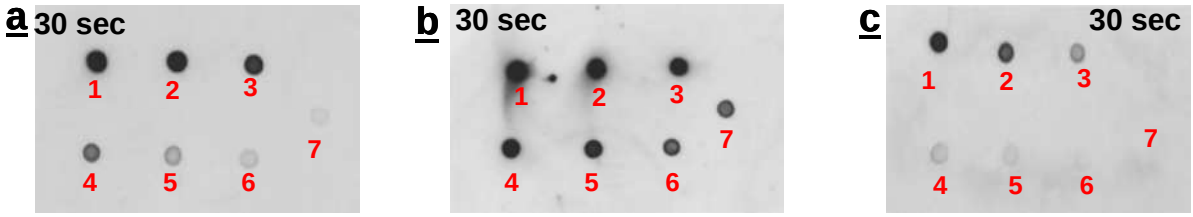

Figure 89: DOT-BLOT affinity experiments using different concentrations of Aβ(1-40): (1) 100 µM; (2) 50 µM; (3) 25 µM; (4) 12.5 µM; (5) 6.125 µM; (6) 3.125 µM; (7) 1.56 µM. As detection antibodies were used **a** anti-Aβ(1-16); **b** anti-Aβ(17-28) (4G8); **c** anti-APP antibodies.

7.8 Appendix 8

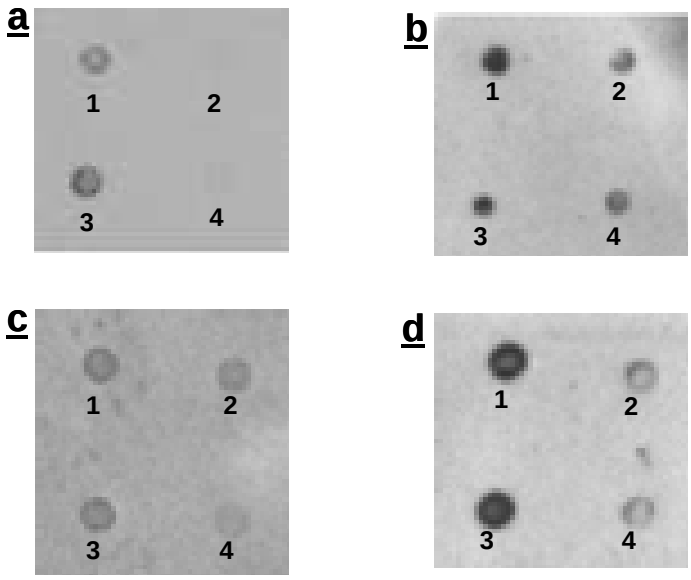

Figure 90: Dot blot analysis of a (1) and (3) Aβ(1-40) incubated 4 days in 20 mM PBS (2) Aβ(1-40) incubated with HCC(93-120) for 6 days (1:0.25 (mol)).